



Available online at www.sciencedirect.com

SciVerse ScienceDirect

Nuclear Data Sheets 113 (2012) 2841–2934

**Nuclear Data
Sheets**

www.elsevier.com/locate/nds

Modern Nuclear Data Evaluation with the TALYS Code System

A.J. Koning* and D. Rochman

Nuclear Research and Consultancy Group NRG, P.O. Box, 1755 ZG Petten, The Netherlands

(Received 13 July 2012; revised received 15 September 2012; accepted 24 September 2012)

This paper presents a general overview of nuclear data evaluation and its applications as developed at NRG, Petten. Based on concepts such as robustness, reproducibility and automation, modern calculation tools are exploited to produce original nuclear data libraries that meet the current demands on quality and completeness. This requires a system which comprises differential measurements, theory development, nuclear model codes, resonance analysis, evaluation, ENDF formatting, data processing and integral validation in one integrated approach. Software, built around the TALYS code, will be presented in which all these essential nuclear data components are seamlessly integrated. Besides the quality of the basic data and its extensive format testing, a second goal lies in the diversity of processing for different type of users. The implications of this scheme are unprecedented. The most important are:

1. Complete ENDF-6 nuclear data files, in the form of the TENDL library, including covariance matrices, for many isotopes, particles, energies, reaction channels and derived quantities. All isotopic data files are mutually consistent and are supposed to rival those of the major world libraries.
2. More exact uncertainty propagation from basic nuclear physics to applied (reactor) calculations based on a Monte Carlo approach: “Total” Monte Carlo (TMC), using random nuclear data libraries.
3. Automatic optimization in the form of systematic feedback from integral measurements back to the basic data.

This method of work also opens a new way of approaching the analysis of nuclear applications, with consequences in both applied nuclear physics and safety of nuclear installations, and several examples are given here. This applied experience and feedback is integrated in a final step to improve the quality of the nuclear data, to change the users vision and finally to orchestrate their integration into simulation codes.

* Corresponding author, electronic address: koning@nrg.eu

Editorial Note: All papers in the present issue, including this paper, are printed in black and white. Color version is available online at www.sciencedirect.com, see also www.elsevier.com/locate/nds.

Contents	
I. INTRODUCTION	2843
II. NUCLEAR MODEL CODE TALYS	2844
A. Optical Model	2845
1. Functional form	2847
2. Spherical dispersive OMP	2848
3. Coupled channels and direct reactions	2849
4. Semi-microscopic optical model (JLM)	2851
5. Complex particles	2853
6. Parameter uncertainties	2854
B. Level Density	2854
1. Constant temperature model	2854
2. Backshifted Fermi gas model	2856
3. Generalized superfluid model	2856
4. Collective effects in the level density	2857
5. Microscopic level densities	2858
6. Parameter uncertainties	2858
C. Gamma-ray Strength Functions	2859
1. Models for gamma-ray strength functions	2859
2. Renormalization of gamma-ray strength functions	2860
3. Photoabsorption cross section	2860
4. Parameter uncertainties	2860
D. Fission	2861
1. Fission transmission coefficients	2861
2. Fission barrier parameters	2863
3. Parameter uncertainties	2863
E. Compound Nucleus Reactions	2863
F. Pre-equilibrium Model	2866
1. Two-component exciton model	2866
2. Photon exciton model	2867
3. Continuum stripping, pick-up, break-up and knock-out reactions	2868
4. Pre-equilibrium angular distributions	2869
5. Parameter uncertainties	2870
G. Multiple Emission	2870
1. Multiple Hauser-Feshbach decay	2870
2. Multiple pre-equilibrium emission	2872
H. Nuclear Structure and Model Parameters	2872
I. Astrophysical Reaction Rates	2873
III. UNCERTAINTIES OF BASIC NUCLEAR DATA	2874
A. Uncertainties of Nuclear Model Parameters	2875
B. Sensitivity Analysis	2878
C. Practical Uncertainty Calculations	2878
IV. THE TALYS EVALUATION SYSTEM	2878
V. LIBRARY PRODUCTION: TENDL	2881
A. Neutron Sublibrary	2884
1. Resonance range	2884
2. Fast neutron range	2889
B. Other Sublibraries	2891
1. Proton, deuteron, triton, He-3, alpha and photon sublibrary	2891
2. Fission yields sublibraries	2893
C. ENDF-6 Formatting Procedures for TENDL	2894
1. MF1: General information	2895
2. MF2: Resonance parameters	2895
3. MF3: Reaction cross sections	2895
4. MF4: Angular distributions of secondary particles	2896
5. MF5: Energy distributions of secondary particles	2896
6. MF6: Product energy-angle distributions	2896
7. MF8/9/10: Production of radioactive nuclides	2897
8. MF12/14/15: Photon yields and secondary distributions	2897
9. MF31/32/33/34/35/40: Covariance data	2898
VI. TOTAL MONTE CARLO AND OTHER APPLICATIONS	2898
A. Uncertainty Propagation: TMC	2899
1. Criticality benchmarks	2901
2. Shielding benchmarks	2902
3. PWR burn-up	2903
4. Pseudo fission product	2905
5. GEN-IV example	2905
6. Non Gaussian distributions	2907
7. Future applications	2910
B. Covariances Versus TMC	2910
1. Perturbation vs. TMC	2911
2. Random pointwise/groupwise vs. TMC	2914
C. Polynomial Chaos and TMC	2915
D. TENDL Application for Heating Calculation	2916
E. Adjustment: The Petten Method	2916
1. Method	2917
2. How to adjust a library, method 1	2918
3. How to adjust a library, method 2	2918
4. Monte Carlo sensitivity	2919
F. Faster TMC	2923
VII. CONCLUSIONS	2926
Acknowledgments	2928
References	2928

I. INTRODUCTION

This paper describes a new way of providing basic experimental and theoretical nuclear reaction information in nuclear data libraries. The approach revolves around “old” ingredients such as nuclear model codes, an experimental database and nuclear data libraries, but the concept is new: Centered around the TALYS code[1], new approaches towards nuclear data library production/evaluation[2], validation and uncertainty propagation[3] are developed.

Nuclear data evaluation has a long history, dating back to the first nuclear data libraries of the 1950’s, when quantitative nuclear reaction analyses were based on only some scattered experimental data points. There simply was no method available to provide some form of completeness. Nevertheless, basic reactor physics codes of those days were able to predict the most essential characteristics of reactors and other criticality systems. On the nuclear modeling side, relatively simple optical models, level densities and compound nucleus models were used to estimate unmeasured cross sections on a channel-by-channel basis.

Also in nuclear science, times have changed. During the 1980’s and 1990’s, nuclear model codes like STAPRE [4], TNG [5], ALICE [6], GNASH [7] and EMPIRE [8] became available. The procedure for producing an evaluated library was the following: perform an evaluation of experimental data, and complement this with nuclear-model based predictions for important channels and energy ranges for which no experimental data are available. Many of the current isotopic data files are still from this era. Meanwhile, in the last decade the strong increase in computer speed and memory has had a significant effect on data evaluation. First of all, nuclear data evaluation relies much more on nuclear model calculations, which can now yield very complete data libraries. Sophisticated reaction theories have become amenable for implementation and even large-scale production of covariance data is now within reach. Also, automated processing scripts and versatile plotting software allows much quicker convergence to the best possible results. In spite of this evolution, nuclear data evaluation methodology has not changed as much as it should have. We still face the situation that all current nuclear reaction data libraries in the world are inconsistent in terms of contents and quality. This has to do with the commonly adopted incremental approach of nuclear data evaluation: Improvements to nuclear data libraries are usually performed on a nucleus-by-nucleus or even channel-by-channel basis, driven by a particular evaluation request. Moreover, a material is often evaluated using a certain version of a certain model code, using certain experimental data, at a certain time, filling only

certain parts of the data file, by a certain evaluator. All this leads to a collection of nuclear data files which may be partially very good and complete, but which originate from different eras and of which the quality is only known to the evaluator (who, especially in this branch of nuclear science, may be retired). The final product is well defined, like the ENDF/B-VII.1[9], JENDL-4.0[10], JEFF-3.1[11], CENDL-3.1[12] etc. library), but knowledge about the underlying process to create it is scattered over people and time. This poses problems when the library needs to be updated with new experimental or theoretical information. Very precise data, in line with a required target accuracy, may be added to a data file, but if the rest of that evaluated file is in bad shape (*e.g.* poor quality of competing channels or missing secondary distributions for angles or photons), the impact of such a high-precision measurement will be reduced.

With the help of the nuclear model code TALYS [1], which is now on the market for a decade or so, it is possible to adopt an entirely new strategy. TALYS aims to comprise important aspects such as physical quality, flexibility, robustness, completeness and efficiency into one software package. This opens the possibility to systematically produce nuclear data libraries for *all* nuclides and projectiles, complete in reaction channels, secondary distributions, and covariance data, and *overrule* these model-based data by experimental data for nuclide-channel-energy combinations for which TALYS can not deliver the required quality on its own. This leads to a much more consistent set of nuclear data libraries, since one isotopic evaluated file differs from the next *only* with regards to the availability, and hence the influence, of more or less experimental information, while all isotopic evaluations are equally complete, consistent and processable for applications. On top of that, randomization of all basic input parameters provides complete covariance information of the above, which opens new routes for uncertainty calculations in applied (reactor) physics.

This new method of nuclear data evaluation and validation, revolves completely around *reproducibility*: only the most essential components of an evaluation should be used and stored for future use: selected experimental data sets, a TALYS input file with adjusted parameters, and possible additional scripts for *e.g.* adoption of data from existing libraries. In fact, this collection of ingredients form the “data evaluation”, and not the ENDF-6 formatted data library that results from it. Sticking to this “rule” opens new possibilities and these will all be discussed in this paper.

The first spin-off of this new methodology is the TALYS Evaluated Nuclear data Library, TENDL. This library consists of a complete set of nuclear reaction data for incident neutrons, photons, protons, deuterons, tritons, Helium-3 and alpha particles, from 10^{-5} eV up to

200 MeV, for all 2430 isotopes from ^6Li to ^{281}Ds that are either stable or have a half-life longer than 1 second. All data are completely and consistently evaluated using a software system consisting of the TALYS nuclear reaction code, and other software to handle resonance data, experimental data, data from existing evaluations, and to provide the final ENDF-6 formatting, including covariance information. The result is a nuclear data library with mutually consistent reaction information for all isotopes and a quality that increases with yearly updates. For the TENDL library, but also for the other applications, we basically focus on three aspects of nuclear data libraries that we find equally important:

1. Realistic central values. In the early days of nuclear science this was, necessarily, the only issue under attention, since conditions 2. and 3. below could not yet be fulfilled. It still holds as the prime concern today: High-quality experimental data, complemented by powerful nuclear models, should be used to simulate reality as close as possible. Often there is a trade-off between differential and integral performance, while ideally these are excellent simultaneously.
2. Covariance data. Nuclear data uncertainty information and its propagation through applied reactor software is essential for an adequate safety and economy analysis of a nuclear device. The intrinsic quality of the central values mentioned under 1. is reflected by covariance data.
3. Completeness of the nuclear reaction description. This ensures that no phenomenon is neglected altogether in applied calculations. Important examples of omissions are unrealistic isotropy by leaving out angular distributions, incorrect gamma heating due to the absence of photon production data, *etc.* Omission of an entire class of secondary reaction information means also that the propagated effects of nuclear data uncertainties are underestimated.

To produce this library, TALYS input parameters are adjusted for many nuclides so that calculated cross sections agree with experimental data, while for important nuclides experimental or evaluated data are directly included. Also feedback from integral measurements is processed into the data libraries. For nuclides for which (almost) no experimental data exists, default TALYS calculations based on global models and parameters are used.

The second spin-off is uncertainty propagation. Above it was argued that a complete ENDF-formatted TENDL library can be produced out of a relatively compact set of basic information. If nuclear data library production is indeed so well automated, then the next step is to

produce hundreds or thousands of random ENDF files for the same isotope by perturbing this compact set of information, *i.e.* randomizing the nuclear model and resonance parameters. This enables exact and (equally important) easy propagation of nuclear data uncertainties through reactor calculations [3]. The technique was later coined Total Monte Carlo (TMC) by M. Herman. This can even be taken a step further [13] by automatically optimizing nuclear data libraries, through *e.g.* minimizing the total C/E of k-eff values for many integral benchmarks, and adopting the optimal random library. All these aspects will be discussed at length in this paper.

Whatever the application, TENDL, TMC or other future applications, the reproducibility condition allows nuclear data libraries to be easily improved when better ingredients become available in the future, or when *e.g.* shortcomings in TALYS or other software are repaired. As long as the evaluation input files per isotope are kept, this will lead to libraries with progressively increasing quality. The central message is that reproducibility allows to expand the notion of an isotopic nuclear data file drastically in two dimensions: (1) instead of one nuclide, one targets all nuclides simultaneously, (2) instead of one evaluated file, one targets hundreds to thousands of random data files for the same isotope.

In this paper, we will take you step-by-step through all stages of systematic nuclear data evaluation and validation. First, in Section II we describe the most important nuclear models and features of the TALYS code, which lies at the heart of our evaluation system. Next, in Section III the methodology to generate uncertainties of nuclear data from basic nuclear model parameters is explained. Section IV describes the structure of our total computational system, which includes all codes with nuclear mechanisms that are not covered by TALYS, ENDF-6 formatting software and covariance software. The first application of all this, the TENDL library, is outlined in Section V. Nuclear data uncertainty propagation in reactor and other applied calculations, by means of Total Monte Carlo, is discussed in Section VI. Finally, we end with conclusions in Section VII.

II. NUCLEAR MODEL CODE TALYS

The nuclear data evaluation and related validation methods outlined in this paper all revolve around TALYS. TALYS is software for the analysis and prediction of nuclear reactions that involve neutrons, photons, protons, deuterons, tritons, ^3He - and alpha-particles, in the 1 keV - 200 MeV energy range and for target nuclides of mass 5 and heavier. To achieve this, a suite of nuclear reaction models has been implemented into a single code system. This enables to evaluate nuclear reactions from the unresolved resonance range up to intermediate ener-

gies.

TALYS is extensively used for both basic and applied science. At the time of this writing, TALYS has been used in about 500 different publications since its initial release in 2004. Fig.1 shows a classification of these papers. In general, there are two main purposes of TALYS. First, it is a *nuclear physics* tool that can be used for the analysis of nuclear reaction experiments. The interplay between experiment and theory gives us insight in the fundamental interaction between particles and nuclei, and precise measurements enable us to constrain our models. In return, when the resulting nuclear models are believed to have sufficient predictive power, they can give an indication of the reliability of measurements.

After the nuclear physics stage comes the second function of TALYS, namely as a *nuclear data* tool: Either in a default mode, when no measurements are available, or after fine-tuning the adjustable parameters of the various reaction models using available experimental data, TALYS can *generate* nuclear data for all open reaction channels, on a user-defined energy and angle grid, beyond the resonance region. The nuclear data libraries that are constructed with these calculated and experimental results provide essential information for existing and new nuclear technologies. Important applications that rely directly or indirectly on data generated by nuclear reaction simulation codes like TALYS are: conventional and innovative nuclear power reactors (GEN-IV), transmutation of radioactive waste, fusion reactors, accelerator applications, homeland security, medical isotope production, radiotherapy, single-event upsets in microprocessors, oil-well logging, geophysics and astrophysics. Research programs in all of these fields have sponsored the development of TALYS.

Since TALYS plays such a central role in the entire evaluation system, it is appropriate to outline the various nuclear models implemented in TALYS in some detail. As a novelty for such a description, for each nuclear model we discuss and tabulate the uncertainties of the associated parameters. These a priori uncertainties have been determined on the basis of a global comparison of TALYS and experimental data, for the whole periodic table of elements and various reaction channels. Later, in Section III, we will explain how these parameter uncertainties are applied in our Monte Carlo uncertainty method.

Fig. 2 summarizes the nuclear models implemented in TALYS. Together they lead to the following output:

- Total, elastic and non-elastic cross sections,
- Elastic scattering angular distributions,
- Inelastic scattering cross sections and angular distributions to discrete states,

- Exclusive channel cross sections, *e.g.* (n,γ) , $(n,2n)$, (n,np) ..., energy and double-differential spectra,
- Photon production for discrete states and continuum,
- Isomeric and ground state cross sections,
- Fission cross sections, fragment and product yields,
- Residual production cross sections,
- Unresolved Resonance Range parameters,
- Total particle cross sections, *e.g.* (n,xn) , (n,xp) ..., energy double-differential spectra, and
- Astrophysical reaction rates.

The main mechanism where TALYS falls short is light-nuclide reactions, basically because the statistical model is not appropriate there. In Fig. 2, the label “Input” may give the obviously false impression that the maximal predictive quality can be obtained by simply specifying the nuclear reaction under consideration. Instead, usually various nuclear model parameters, fed to the code by means of keywords, need to be adjusted to produce the optimal results, although the four-line input file generally produces quite reasonable “blind” results, thanks to parameter trends that have been established over the years.

A. Optical Model

For any reaction analysis with TALYS, optical model calculations are performed first. The optical model represents the complicated interaction between an incident particle and a nucleus by a complex mean-field potential, which divides the reaction flux into a part covering shape elastic scattering and a part describing all competing reaction channels. By means of an optical model calculation we obtain the shape elastic angular distribution and polarisation, the reaction and total cross section and, for low energies, the s, p -wave strength functions and the potential scattering radius R' . The essential value of a good optical model is that it can reliably predict these quantities for energies and nuclides for which no measurements exist. Also, the quality of the not directly observable quantities that are provided by the optical model has an equally important impact on the evaluation of the various reaction channels. Well-known examples are transmission coefficients, for compound nucleus and multi-step compound decay, and the distorted wave functions that are used for direct inelastic reactions. Also, the reaction cross sections that are calculated with the optical model are crucial for the semi-classical pre-equilibrium models.

TALYS publications

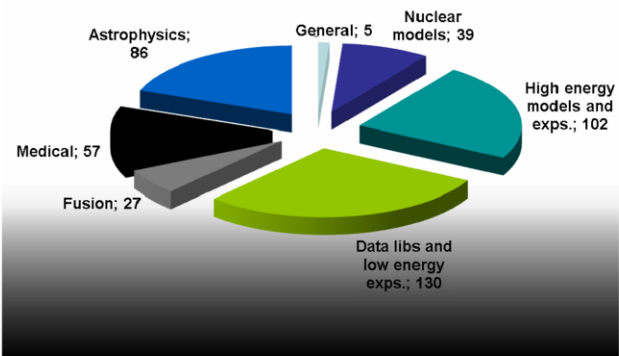
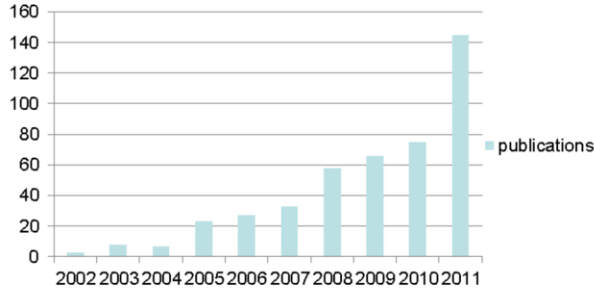


FIG. 1: Worldwide use of TALYS, divided over years and topics.

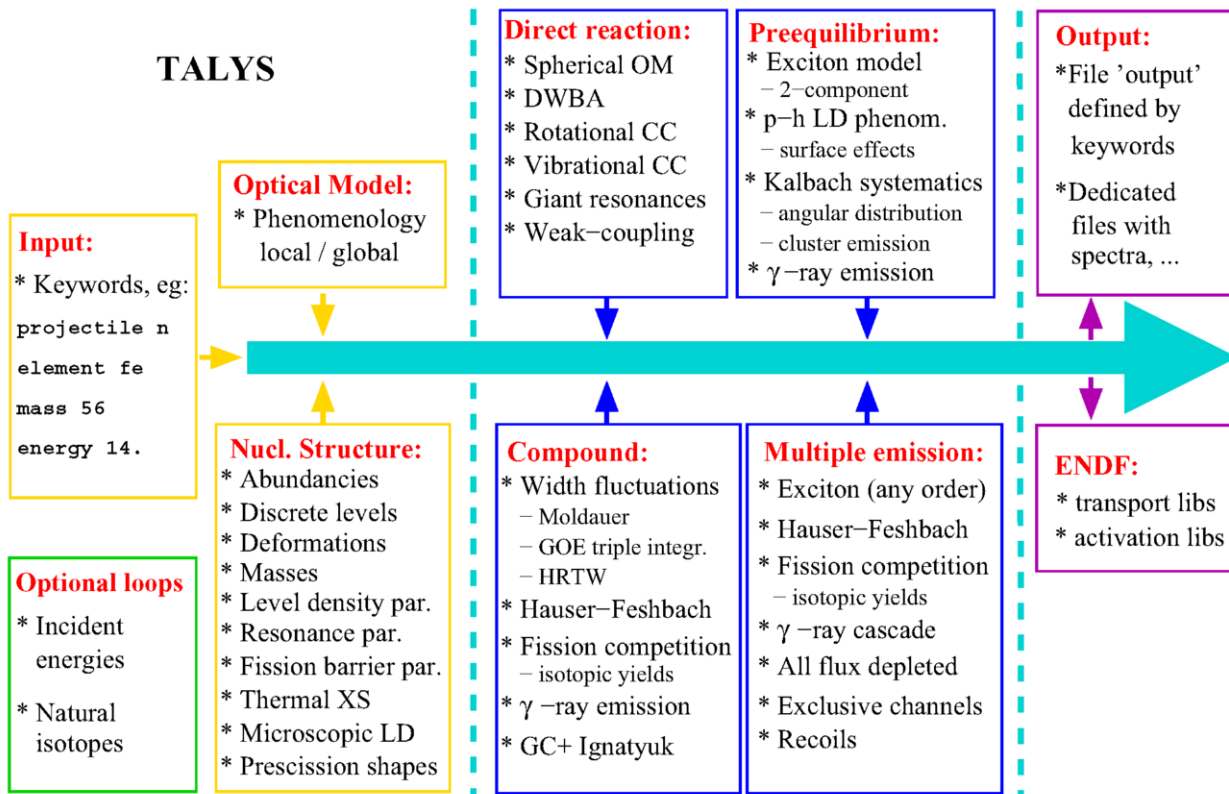


FIG. 2: Nuclear models in TALYS.

In TALYS, all optical model calculations are performed by ECIS-06 [14], which is implemented as a subroutine. They are first performed, and stored, for all possible outgoing particle channels and energies, so that the associated transmission coefficients can be used in pre-equilibrium and compound nucleus calculations. Next, a calculation is done for each user-defined incident energy.

We give an explicit outline of the parametrization here, so that the associated parameter uncertainties, which we provide later, can be understood.

1. Functional form

The default optical model potentials (OMP) used in TALYS are the local and global parametrization of Konig and Delaroche [15] (KD03). We generally only deviate from that parametrization in the case of deformed nuclides, or when reaction analyses performed with TALYS gives rise to adjustment of the KD03 parameters, in which case one may obtain a better compromise between basic OMP-related observables and non-elastic partial channels.

The phenomenological OMP for nucleon-nucleus scattering, \mathcal{U} , is defined as

$$\begin{aligned} \mathcal{U}(r, E) = & -\mathcal{V}_V(r, E) - i\mathcal{W}_V(r, E) - i\mathcal{W}_D(r, E) \\ & + \mathcal{V}_{SO}(r, E)\mathbf{l} \cdot \boldsymbol{\sigma} + i\mathcal{W}_{SO}(r, E)\mathbf{l} \cdot \boldsymbol{\sigma} \\ & + \mathcal{V}_C(r), \end{aligned} \quad (1)$$

where $\mathcal{V}_{V,SO}$ and $\mathcal{W}_{V,D,SO}$ are the real and imaginary components of the volume-central (V), surface-central (D) and spin-orbit (SO) potentials, respectively. E is the LAB energy of the incident particle in MeV. All components are separated in energy-dependent well depths, V_V, W_V, W_D, V_{SO} , and W_{SO} , and energy-independent radial parts f , namely

$$\begin{aligned} \mathcal{V}_V(r, E) &= V_V(E)f(r, R_V, a_V), \\ \mathcal{W}_V(r, E) &= W_V(E)f(r, R_V, a_V), \\ \mathcal{W}_D(r, E) &= -4a_D W_D(E) \frac{d}{dr} f(r, R_D, a_D), \\ \mathcal{V}_{SO}(r, E) &= V_{SO}(E) \left(\frac{\hbar}{m_\pi c} \right)^2 \frac{1}{r} \frac{d}{dr} f(r, R_{SO}, a_{SO}), \\ \mathcal{W}_{SO}(r, E) &= W_{SO}(E) \left(\frac{\hbar}{m_\pi c} \right)^2 \\ &\times \frac{1}{r} \frac{d}{dr} f(r, R_{SO}, a_{SO}). \end{aligned} \quad (2)$$

The form factor $f(r, R_i, a_i)$ is a Woods-Saxon shape

$$f(r, R_i, a_i) = (1 + \exp[(r - R_i)/a_i])^{-1}, \quad (3)$$

where the geometry parameters are the radius $R_i = r_i A^{1/3}$, with A being the atomic mass number, and the diffuseness parameters a_i . For charged projectiles, the Coulomb term \mathcal{V}_C , as usual, is given by that of a uniformly charged sphere

$$\begin{aligned} \mathcal{V}_C(r) &= \frac{Zze^2}{2R_C} \left(3 - \frac{r^2}{R_C^2} \right), \quad \text{for } r \leq R_C \\ &= \frac{Zze^2}{r}, \quad \text{for } r \geq R_C, \end{aligned} \quad (4)$$

with $Z(z)$ the charge of the target (projectile), and $R_C = r_C A^{1/3}$ the Coulomb radius.

The KD03 OMP parametrization for either incident neutrons or protons is

$$\begin{aligned} V_V(E) &= v_1[1 - v_2(E - E_f) + v_3(E - E_f)^2 \\ &\quad - v_4(E - E_f)^3] \\ W_V(E) &= w_1 \frac{(E - E_f)^2}{(E - E_f)^2 + (w_2)^2} \\ r_V &= \text{constant} \\ a_V &= \text{constant} \\ W_D(E) &= d_1 \frac{(E - E_f)^2}{(E - E_f)^2 + (d_3)^2} \exp[-d_2(E - E_f)] \\ r_D &= \text{constant} \\ a_D &= \text{constant} \\ V_{SO}(E) &= v_{so1} \exp[-v_{so2}(E - E_f)] \\ W_{SO}(E) &= w_{so1} \frac{(E - E_f)^2}{(E - E_f)^2 + (w_{so2})^2} \\ r_{SO} &= \text{constant} \\ a_{SO} &= \text{constant} \\ r_C &= \text{constant}, \end{aligned} \quad (5)$$

where $E_f = E_f^n$ for incident neutrons and $E_f = E_f^p$ for incident protons. Here, E_f is the Fermi energy, defined as the energy halfway between the last occupied and the first unoccupied shell of the nucleus. For incident neutrons,

$$E_f^n = -\frac{1}{2}[S_n(Z, N) + S_n(Z, N + 1)], \quad (6)$$

with S_n the neutron separation energy for a nucleus with proton number Z and neutron number N , while for incident protons

$$E_f^p = -\frac{1}{2}[S_p(Z, N) + S_p(Z + 1, N)], \quad (7)$$

with S_p the proton separation energy. We use the TALYS mass table to obtain the values of the separation energies.

In general, all parameters appearing in Eq. (5) differ from nucleus to nucleus. When enough experimental scattering data of a certain nucleus is available, a so called local OMP can be constructed. TALYS retrieves all the parameters v_1, v_2, \dots of these local OMPs automatically from its nuclear structure and model parameter database, which contains the same information as the various tables of Ref. [15]. If a local OMP parametrization is not available in the database, the built-in global optical models are automatically used, which can be applied for any Z, A combination. The global neutron OMP, validated for $0.001 \leq E \leq 200$ MeV and

$24 \leq A \leq 209$, is given by

$$\begin{aligned}
V_V(E) &= v_1^n [1 - v_2^n(E - E_f^n) + v_3^n(E - E_f^n)^2 \\
&\quad - v_4^n(E - E_f^n)^3] \\
W_V(E) &= w_1^n \frac{(E - E_f^n)^2}{(E - E_f^n)^2 + (w_2^n)^2} \\
r_V &= 1.3039 - 0.4054A^{-1/3} \\
a_V &= 0.6778 - 1.487 \cdot 10^{-4}A \\
W_D(E) &= d_1^n \frac{(E - E_f^n)^2}{(E - E_f^n)^2 + (d_3^n)^2} \exp[-d_2^n(E - E_f^n)] \\
r_D &= 1.3424 - 0.01585A^{1/3} \\
a_D &= 0.5446 - 1.656 \cdot 10^{-4}A \\
V_{SO}(E) &= v_{so1}^n \exp[-v_{so2}^n(E - E_f^n)] \\
W_{SO}(E) &= w_{so1}^n \frac{(E - E_f^n)^2}{(E - E_f^n)^2 + (w_{so2}^n)^2} \\
r_{SO} &= 1.1854 - 0.647A^{-1/3} \\
a_{SO} &= 0.59,
\end{aligned} \tag{8}$$

where the units are in fm and MeV and the parameters for the potential depths and E_f^n are given in Table I.

The global proton OMP is given by

$$\begin{aligned}
V_V(E) &= v_1^p [1 - v_2^p(E - E_f^p) + v_3^p(E - E_f^p)^2 \\
&\quad - v_4^p(E - E_f^p)^3] \\
&\quad + \bar{V}_C \cdot v_1^p \left[v_2^p - 2v_3^p(E - E_f^p) + 3v_4^p(E - E_f^p)^2 \right] \\
W_V(E) &= w_1^p \frac{(E - E_f^p)^2}{(E - E_f^p)^2 + (w_2^p)^2} \\
r_V &= 1.3039 - 0.4054A^{-1/3} \\
a_V &= 0.6778 - 1.487 \cdot 10^{-4}A \\
W_D(E) &= d_1^p \frac{(E - E_f^p)^2}{(E - E_f^p)^2 + (d_3^p)^2} \exp[-d_2^p(E - E_f^p)] \\
r_D &= 1.3424 - 0.01585A^{1/3} \\
a_D &= 0.5187 + 5.205 \cdot 10^{-4}A \\
V_{SO}(E) &= v_{so1}^p \exp[-v_{so2}^p(E - E_f^p)] \\
W_{SO}(E) &= w_{so1}^p \frac{(E - E_f^p)^2}{(E - E_f^p)^2 + (w_{so2}^p)^2} \\
r_{SO} &= 1.1854 - 0.647A^{-1/3} \\
a_{SO} &= 0.59 \\
r_C &= 1.198 + 0.697A^{-2/3} + 12.994A^{-5/3},
\end{aligned} \tag{9}$$

where the parameters for the potential depths, \bar{V}_C and E_f^p are given in Table II. The functional form of the proton global OMP differs from the neutron global OMP only by the Coulomb correction term in $V_V(E)$.

TABLE I: Potential depth parameters and Fermi energy for the neutron global OMP of Eq. (8).

v_1^n	$= 59.30 - 21.0(N - Z)/A - 0.024A$	MeV
v_2^n	$= 0.007228 - 1.48 \cdot 10^{-6}A$	MeV ⁻¹
v_3^n	$= 1.994 \cdot 10^{-5} - 2.0 \cdot 10^{-8}A$	MeV ⁻²
v_4^n	$= 7.10^{-9}$	MeV ⁻³
w_1^n	$= 12.195 + 0.0167A$	MeV
w_2^n	$= 73.55 + 0.0795A$	MeV
d_1^n	$= 16.0 - 16.0(N - Z)/A$	MeV
d_2^n	$= 0.0180 + 0.003802/(1 + \exp[(A - 156.)/8.])$	MeV ⁻¹
d_3^n	$= 11.5$	MeV
v_{so1}^n	$= 5.922 + 0.0030A$	MeV
v_{so2}^n	$= 0.0040$	MeV ⁻¹
w_{so1}^n	$= -3.1$	MeV
w_{so2}^n	$= 160.$	MeV
E_f^n	$= -11.2814 + 0.02646A$	MeV

TABLE II: Potential depth parameters and Fermi energy for the proton global OMP of Eq. (9). The parameter values for neutrons are given in Table I. \bar{V}_C appears in the Coulomb correction term $\Delta V_C(E)$, of the real central potential.

v_1^p	$= 59.30 + 21.0(N - Z)/A - 0.024A$	MeV
v_2^p	$= 0.007067 + 4.23 \cdot 10^{-6}A$	MeV ⁻¹
v_3^p	$= 1.729 \cdot 10^{-5} + 1.136 \cdot 10^{-8}A$	MeV ⁻²
v_4^p	$= v_4^n$	MeV ⁻³
w_1^p	$= 14.667 + 0.009629A$	MeV
w_2^p	$= w_2^n$	MeV
d_1^p	$= 16.0 + 16.0(N - Z)/A$	MeV
d_2^p	$= d_2^n$	MeV ⁻¹
d_3^p	$= d_3^n$	MeV
v_{so1}^p	$= v_{so1}^n$	MeV
v_{so2}^p	$= v_{so2}^n$	MeV ⁻¹
w_{so1}^p	$= w_{so1}^n$	MeV
w_{so2}^p	$= w_{so2}^n$	MeV
E_f^p	$= -8.4075 + 0.01378A$	MeV
\bar{V}_C	$= 1.73 \cdot Z \cdot A^{-1/3}/r_C$	MeV

2. Spherical dispersive OMP

The theory of the nuclear optical model can be reformulated in terms of dispersion relations that connect the real and imaginary parts of the optical potential, and an option is present in TALYS to take them into account. These dispersion relations are a natural result of the causality principle that a scattered wave cannot be emitted before the arrival of the incident wave. The dispersion component stems directly from the imaginary

part of the potential,

$$\Delta\mathcal{V}(r, E) = \frac{\mathcal{P}}{\pi} \int_{-\infty}^{\infty} \frac{\mathcal{W}(r, E')}{E' - E} dE', \quad (10)$$

where \mathcal{P} denotes the principal value. The total real central potential can be written as the sum of a Hartree-Fock term $\mathcal{V}_{HF}(r, E)$ and the the total dispersion potential $\Delta\mathcal{V}(r, E)$

$$\mathcal{V}(r, E) = \mathcal{V}_{HF}(r, E) + \Delta\mathcal{V}(r, E). \quad (11)$$

Since $\mathcal{W}(r, E)$ has a volume and a surface component, the dispersive addition is,

$$\begin{aligned} \Delta\mathcal{V}(r, E) &= \Delta\mathcal{V}_V(r, E) + \Delta\mathcal{V}_D(r, E) \\ &= \Delta\mathcal{V}_V(E)f(r, R_V, a_V) \\ &\quad - 4a_D\Delta\mathcal{V}_D(E)\frac{d}{dr}f(r, R_D, a_D), \end{aligned} \quad (12)$$

where the volume dispersion term is given by

$$\Delta\mathcal{V}_V(E) = \frac{\mathcal{P}}{\pi} \int_{-\infty}^{\infty} \frac{W_V(E')}{E' - E} dE', \quad (13)$$

and the surface dispersion term is given by

$$\Delta\mathcal{V}_D(E) = \frac{\mathcal{P}}{\pi} \int_{-\infty}^{\infty} \frac{W_D(E')}{E' - E} dE'. \quad (14)$$

Hence, the real volume well depth of Eq. (2) becomes

$$V_V(E) = V_{HF}(E) + \Delta\mathcal{V}_V(E), \quad (15)$$

and the real surface well depth is

$$V_D(E) = \Delta\mathcal{V}_D(E). \quad (16)$$

This term is thus added to the general definition of the optical model of Eq.(2). In general, Eqs. (13)-(14) cannot be solved analytically. However, under certain plausible conditions[16], analytical solutions exist. Under the assumption that the imaginary potential is symmetric with respect to the Fermi energy E_F ,

$$W(E_F - E) = W(E_F + E), \quad (17)$$

where W denotes either the volume or surface term, we can rewrite the dispersion relation as,

$$\Delta\mathcal{V}(E) = \frac{2}{\pi}(E - E_F)\mathcal{P} \int_{E_F}^{\infty} \frac{W(E')}{(E' - E_F)^2 - (E - E_F)^2} dE', \quad (18)$$

from which it easily follows that $\Delta\mathcal{V}(E)$ is skew-symmetric around E_F ,

$$\Delta\mathcal{V}(E + E_F) = -\Delta\mathcal{V}(E - E_F), \quad (19)$$

and hence $\Delta\mathcal{V}(E_F) = 0$. This can then be used to rewrite Eq. (10) as

$$\begin{aligned} \Delta\mathcal{V}(E) &= \Delta\mathcal{V}(E) - \Delta\mathcal{V}(E_F) \\ &= \frac{\mathcal{P}}{\pi} \int_{-\infty}^{\infty} W(E') \left(\frac{1}{E' - E} - \frac{1}{E' - E_F} \right) dE' \\ &= \frac{E - E_F}{\pi} \int_{-\infty}^{\infty} \frac{W(E')}{(E' - E)(E' - E_F)} dE'. \end{aligned} \quad (20)$$

For the Hartree-Fock term we adopt the usual form for $V_V(E)$ given in Eq. (5). The dispersion integrals for the functions of the imaginary part of the optical potential can be calculated analytically[16] and are included as options in ECIS-06. This makes the use of a dispersive optical model parametrization completely equivalent to that of a non-dispersive OMP: the dispersive contributions are calculated automatically once the OMP parameters are given. Upon comparison with a nondispersive parametrization, we find that v_1 is rather different (as expected) and that r_V , a_V , v_2 , v_3 , w_1 and w_2 are slightly different. Dispersive spherical neutron OMP parametrization are included for about 70 nuclides in the nuclear structure database.

3. Coupled channels and direct reactions

Various models for direct reactions are included in the program: DWBA for (near-)spherical nuclides, coupled-channels for deformed nuclides, the weak-coupling model for odd nuclei, and also a giant resonance contribution in the continuum. In all cases, TALYS drives the ECIS-06 code to perform the calculations. The results are presented as discrete state cross sections and angular distributions, or as contributions to the continuum.

The formalism outlined in the previous section works, theoretically, for nuclides which are spherical and, in practice, for nuclides which are not too strongly deformed. In general, however, the more general coupled-channels method should be invoked to describe simultaneously the elastic scattering channel and the low-lying states which are, due to their collective nature, strongly excited in inelastic scattering. These collective excitations can be described as the result of static or dynamic deformations, which cause the homogeneous neutron-proton fluid to rotate or vibrate. The deformation parameters can be predicted from (semi-)microscopic models or can be derived from an analysis of the experimental angular distributions.

The coupled-channels formalism for scattering and reaction studies is well known and will not be described here. For a detailed presentation, we refer to Ref. [17]. We will only state the main aspects here to put the formalism into practice. Refs. [18] and [19] have been used

as guidance. In general various different channels, usually the ground state and several inelastic states, are included in a coupling scheme while the associated coupled equations are solved. In ECIS-06, this is done in a so called sequential iterative approach [14]. Besides Ref. [14], Ref. [20] is also recommended for more insight in the use of the ECIS code.

Various collective models for deformed nuclei exist. Note that the spherical optical model of Eq. (2) is described in terms of the nuclear radius $R_i = r_i A^{1/3}$. For deformed nuclei, this expression is generalized to include collective motions. We will describe the ones that can be invoked by TALYS. The collective models are automatically applied upon reading the deformation parameter database of TALYS.

a. Symmetric rotational model In the symmetric rotational model, the radii of the different terms of the OMP are expressed as

$$R_i = r_i A^{1/3} \left[1 + \sum_{\lambda=2,4,\dots} \beta_\lambda Y_\lambda^0(\Omega) \right], \quad (21)$$

where the β_λ 's are permanent, static deformation parameters, and the Y functions are spherical harmonics. The quadrupole deformation β_2 plays a leading role in the interaction process. Higher order deformations β_λ (with $\lambda = 4, 6, \dots$) are systematically smaller in magnitude than β_2 . The inclusion of β_4 and β_6 deformations in coupled-channels calculations produces changes in the predicted observables, but in general, only β_2 and β_4 are important in describing inelastic scattering to the first few levels in a rotational band. For even-even nuclides like ^{184}W and ^{232}Th , the symmetric rotational model provides a good description of the lowest $0^+, 2^+, 4^+$ (and often $6^+, 8^+, \text{etc.}$) rotational band. The nuclear model and parameter database of TALYS specifies whether a rotational model can be used for a particular nucleus, together with the included levels and deformation parameters. Either a deformation parameter β_λ or a deformation length $\delta_\lambda = \beta_\lambda r_i A^{1/3}$ may be specified. The latter one is generally recommended since it has more physical meaning than β_λ and should not depend on incident energy (while r_i may, in some optical models, depend on energy). We take δ_λ equal for the three OMP components V_V , W_V and W_D and take the spin-orbit potential undeformed. The same holds for the vibrational and other collective models.

By default, TALYS uses the global optical model by Soukhovitskii et al. [21] for actinides. For rotational non-fissile nuclides, if no specific potential is specified through one of the various input methods, we take the KD03 local or global spherical potential and subtract 15% from the imaginary surface potential parameter d_1 , if rotational or vibrational levels are included in the coupling scheme.

b. Harmonic vibrational model A vibrational nucleus possesses a spherically symmetric ground state. Its excited states undergo shape oscillations about the spherical equilibrium model. In the harmonic vibrational model, the radii of the different terms of the OMP are expressed as

$$R_i = r_i A^{1/3} \left[1 + \sum_{\lambda\mu} \alpha_{\lambda\mu} Y_\lambda^\mu(\Omega) \right], \quad (22)$$

where the $\alpha_{\lambda\mu}$ operators can be related to the coupling strengths β_λ , describing the vibration amplitude with multipolarity λ . Expanding the OMP to first or second order with this radius gives the OMP expressions for the excitation of one-phonon (first order vibrational model) and two-phonon (second order vibrational model) states [14]. For vibrational nuclei, the minimum number of states to couple is two. For even-even nuclei, we generally use the $(0^+, 2^+)$ coupling, where the 2^+ level is a one-quadrupole phonon excitation. The level scheme of a vibrational nucleus (e.g. ^{110}Pd) often consists of a one-phonon state (2^+) followed by a $(0^+, 2^+, 4^+)$ triplet of two-phonon states. When this occurs, all levels are included in the coupling scheme with the associated deformation length δ_2 (or deformation parameter β_2). If the 3^- and 5^- states are strongly collective excitations, that is when β_3 and β_5 are larger than 0.1, these levels may also be included in the coupling scheme. An example is ^{120}Sn [22], where the low lying $(0^+, 2^+, 3^-, 4^+, 5^-)$ states can all be included as one-phonon states in a single coupling scheme.

Again, if no specific potential is specified through one of the various input methods, we take the KD03 local or global spherical potential and subtract 15% from the imaginary surface potential parameter d_1 .

c. Vibration-rotational model For certain nuclides, the level scheme consists not only of one or more rotational bands, but also of one or more vibrational bands that can be included in the coupling scheme. An example is ^{238}U , where many vibrational bands can be coupled. Such calculations are automatically performed by TALYS. Depending on the number of levels included, the calculations can be time-consuming.

d. Asymmetric rotational model In the asymmetric rotational model, in addition to the spheroidal equilibrium deformation, the nucleus can oscillate such that ellipsoidal shapes are produced. In this model the nucleus has rotational bands built on the statically deformed ground state and on the γ -vibrational state. The radius is now angular dependent,

$$\begin{aligned} R_i(\Theta) = & r_i A^{1/3} (1 + \beta_2 \cos \gamma Y_2^0(\Omega) + \sqrt{\frac{1}{2}} \beta_2 \sin \gamma (Y_2^2(\Omega) \\ & + Y_2^{-2}(\Omega)) + \beta_4 Y_4^0(\Omega)), \end{aligned} \quad (23)$$

where we restrict ourselves to a few terms. The deformation parameters β_2 , β_4 and γ need to be specified. ^{24}Mg is an example of a nucleus that can be analyzed with the asymmetric rotational model. Mixing between bands is not yet automated in TALYS.

e. Distorted Wave Born Approximation The Distorted Wave Born Approximation (DWBA) is only valid for small deformations. Until the advent of the more general coupled-channels formalism, it was the commonly used method to describe inelastic scattering, for both weakly and strongly coupled levels. Nowadays, we see DWBA as a first order vibrational model for small deformation, with only a single iteration to be performed for the coupled-channels solution. (See, however Satchler [23] for the exact difference between this so called distorted wave method and DWBA). The interaction between the projectile and the target nucleus is modeled by the derivative of the OMP for elastic scattering times a strength parameter. The latter, the deformation parameter β_λ , is then often used to vary the overall magnitude of the cross section (which is proportional to β_λ^2).

In TALYS, we use DWBA

- (a) if a deformed OMP is not available. This applies for the spherical OMPs mentioned before, which are all based on elastic scattering observables only. Hence, if we have not constructed a coupled-channels potential, TALYS will automatically use (tabulated or systematical) deformation parameters for DWBA calculations.
- (b) if a deformed OMP is used for the first excited states only. For the levels that do not belong to that basic coupling scheme, *e.g.* for the many states at somewhat higher excitation energy, we use DWBA with (very) small deformation parameters.

f. Odd nuclei: Weak coupling Direct inelastic scattering off odd- A nuclei can be described by the weak-coupling model [24], which assumes that a valence particle or hole interacts only weakly with a collective core excitation. Hence the model implies that the nucleon inelastic scattering by the odd- A nucleus is very similar to that by the even core alone, *i.e.* the angular distributions have a similar shape. Let L be the spin of the even core state, and J_0 and J the spin of the ground and excited state, respectively, of the odd- A nucleus, resulting from the angular momentum coupling. Then, the spins J of the multiplet states in the odd- A nucleus range from $|L - J_0|$ to $L + J_0$. If the strength of the inelastic scattering is characterized by the square of the deformation parameters $\beta_{L,J}^2$, then the sum of all $\beta_{L,J}^2$ or $\sigma(E)$ for the transitions in the odd- A nucleus should be equal to the value β_L^2 or $\sigma(E)$ for the single transition in the even

core nucleus

$$\sum_J \beta_{L,J}^2 = \beta_L^2, \quad \sum_J \sigma_{J_0 \rightarrow J} = \sigma_{0 \rightarrow L}, \quad (24)$$

where the symbol $0 \rightarrow L$ indicates a transition between the ground state to the excited state with spin L in the even core nucleus. The deformation parameters $\beta_{L,J}^2$ are now given by

$$\beta_{L,J}^2 = \frac{2J+1}{(2J_0+1)(2L+1)} \beta_L^2. \quad (25)$$

In practice, the DWBA cross sections are calculated for the real mass of the target nucleus and at the exact excitation energies of the odd- A states, but for the even-core spin L and with deformation parameters $\beta_{L,J}$.

We stress that such a weak-coupling model is not full-proof. First of all, there are always two choices for the even-even core. The default in TALYS is to use the even-even core obtained by subtracting a nucleon, but the other choice, to obtain the even-even core by adding a nucleon, may sometimes be more appropriate. The next uncertainty is the choice of levels in the odd- A core. We select the levels that are closest to the excitation energy of the even-spin state of the even-even core. Again, this may not always be the most appropriate choice.

4. Semi-microscopic optical model (JLM)

Besides the phenomenological OMP, it is also possible to perform TALYS calculations with the semi-microscopic nucleon-nucleus spherical optical model potential as described in [25]. E. Bauge's MOM code [26] has been implemented as a subroutine to perform so called Jeukenne-Lejeune-Mahaux (JLM) OMP calculations. The optical model potential of [25] and its extension to deformed and unstable nuclei has been widely tested [25]-[30] and produces predictions from $A = 30$ to 240 and for energies ranging from 10 keV up to 200 MeV. In this version of TALYS, only spherical JLM OMP's are included.

The MOM module reads the radial matter densities from the nuclear structure database and performs the folding of the Nuclear Matter (NM) optical model potential described in [25] with the densities to obtain a local OMP. This is then put in the ECIS-06 routine to compute observables by solving the Schrödinger equation for the interaction of the projectile with the aforementioned OMP. The OMP's are calculated by folding the target radial matter density with an OMP in nuclear matter based on the Brückner-Hartree-Fock work of Jeukenne, Lejeune and Mahaux [31]-[34]. This NM OMP was then phenomenologically altered in [25, 35] in order to improve the agreement of predicted finite

nuclei observables with a large set of experimental data. These improvements consist in unifying the low and high energy parameterizations of the NM interaction in [35], and in studying the energy variations of the potential depth normalization factors in [25]. These factors now include non-negligible normalizations of isovector components [25] that are needed in order to account simultaneously for (p,p) and (n,n) elastic scattering as well as (p,n) isobaric analogue state quasi-elastic scattering. The final NM potential for a given nuclear matter density $\rho = \rho_n - \rho_p$ and asymmetry $\alpha = (\rho_n + \rho_p)/\rho$ reads

$$\begin{aligned} U_{NM}(E)_{\rho,\alpha} &= \lambda_V(E) \left[V_0(\tilde{E}) \pm \lambda_{V1}(E)\alpha V_1(\tilde{E}) \right] \\ &+ i\lambda_W(E) \left[W_0(\tilde{E}) \pm \lambda_{W1}(E)\alpha W_1(\tilde{E}) \right], \end{aligned} \quad (26)$$

with E the incident nucleon energy, $\tilde{E} = E - V_c$ (where V_c is the Coulomb field), V_0 , V_1 , W_0 , and W_1 the real isoscalar, real isovector, imaginary isoscalar, and imaginary isovector NM OMP components respectively, and λ_V , λ_{V1} , λ_W , and λ_{W1} the real (isoscalar+isovector), real isovector, imaginary, and imaginary isovector normalization factors respectively. The values of λ_V , λ_{V1} , λ_W , and λ_{W1} given in [25] read

$$\lambda_V(E) = 0.951 + 0.0008 \ln(1000E) + 0.00018 [\ln(1000E)]^2 \quad (27)$$

$$\begin{aligned} \lambda_W(E) &= \left[1.24 - \left[1 + e^{(\frac{E-4.5}{2.9})} \right]^{-1} \right] \\ &\times \left[1 + 0.06 e^{-(\frac{E-14}{3.7})^2} \right] \left[1 - 0.09 e^{-(\frac{E-80}{78})^2} \right] \\ &\times \left[1 + \left(\frac{E-80}{400} \right) \Theta(E-80) \right], \end{aligned} \quad (28)$$

$$\lambda_{V1}(E) = 1.5 - 0.65 \left[1 + e^{\frac{E-1.3}{3}} \right]^{-1}, \quad (29)$$

$$\begin{aligned} \lambda_{W1}(E) &= \left[1.1 + 0.44 \left[1 + \left(e^{\frac{E-40}{50.9}} \right)^4 \right]^{-1} \right] \\ &\times \left[1 - 0.065 e^{-(\frac{E-40}{13})^2} \right] \left[1 - 0.083 e^{-(\frac{E-200}{80})^2} \right] \end{aligned} \quad (30)$$

with the energy E expressed in MeV. As stated in [25], in the 20 to 50 MeV range, the uncertainties related to λ_V , λ_{V1} , λ_W , and λ_{W1} are estimated to be 1.5%, 10%, 10%, and 10%, respectively. Outside this energy range, uncertainties are estimated to be 1.5 times larger. In order to apply the NM OMP to finite nuclei an approximation had to be performed. This is the Local Density Approximation (LDA) where the local value of the finite nucleus OMP is taken to be the NM OMP value for

the local finite nucleus density: $U_{FN}(r) = U_{NM}(\rho(r))$. Since this LDA produces potentials with too small rms radii, the improved LDA, which broadens the OMP with a Gaussian form factor (31), is introduced. In [25, 35] different prescriptions for the improved Local Density approximation are compared and LDA range parameters are optimized,

$$\begin{aligned} U_{FN}(r, E) &= (t\sqrt{\pi})^{-3} \int \frac{U_{NM}(\rho(r'), E)}{\rho(r')} \\ &\exp(-|\vec{r} - \vec{r}'|^2/t_r^2)\rho(r')d\vec{r}', \end{aligned} \quad (31)$$

with t the range of the Gaussian form factor. The $t_r = 1.25$ fm and $t_i = 1.35$ fm values were found [25] to be global optimal values for the real and imaginary ranges, respectively.

Finally, since no spin-orbit (SO) potential exists between a nucleon and NM, the Scheerbaum [36] prescription was selected in [35], coupled with the phenomenological complex potential depths $\lambda_{v_{so}}$, and $\lambda_{w_{so}}$. The SO potential reads

$$U_{n(p)}^{so}(r) = (\lambda_{v_{so}}(E) + i\lambda_{w_{so}}(E)) \frac{1}{r} \frac{d}{dr} \left(\frac{2}{3} \rho_{p(n)} + \frac{1}{3} \rho_{n(p)} \right), \quad (32)$$

with

$$\lambda_{v_{so}} = 130 \exp(-0.013 E) + 40, \quad (33)$$

and

$$\lambda_{w_{so}} = -0.2(E - 20), \quad (34)$$

where E is in MeV. Various variations of the JLM potential are possible, such as that of Goriely and Delaroche [37], which contains a different normalization for the imaginary potential, appropriate for astrophysics calculations.

a. Giant resonances The high-energy part of the continuum spectra are generally described by pre-equilibrium models. These models are essentially of a single-particle nature. Upon inspection of continuum spectra, some structure in the high-energy tail is observed that can not be accounted for by the smooth background of the single-particle pre-equilibrium model. For example, many 14 MeV inelastic neutron spectra show a little hump at excitation energies around 6-10 MeV. This structure is due to collective excitations of the nucleus that are known as giant resonances [38, 39]. We use a macroscopic, phenomenological model to describe giant resonances in the inelastic channel. For each multipolarity, an energy weighted sum rule (EWSR) S_ℓ applies,

$$S_\ell = \sum_i E_{\ell,i} \beta_{\ell,i}^2 = 57.5 A^{-5/3} l(2l+1) \text{ MeV}, \quad (35)$$

where $E_{\ell,i}$ is the excitation energy of the i -th state with multipolarity ℓ . The summation includes all the low-lying collective states, for each ℓ , that have already been included in the coupled-channels or DWBA formalism. The EWSR thus determines the remaining collective strength that is spread over the continuum. Our treatment is phenomenological in the sense that we perform a DWBA calculation with ECIS-06 for each giant resonance state and spread the cross section over the continuum with a Gaussian distribution. The central excitation energy for these states and the spreading width is different for each multipolarity and has been empirically determined. For the giant monopole resonance (GMR) EWSR we have

$$S_0 = 23A^{-5/3} \text{ MeV}, \quad (36)$$

with excitation energy and width

$$E_{0,GMR} = 18.7 - 0.025A \text{ MeV}, \quad \Gamma_{GMR} = 3 \text{ MeV}. \quad (37)$$

The EWSR for the giant quadrupole resonance (GQR) is

$$S_2 = 575A^{-5/3} \text{ MeV}, \quad (38)$$

with

$$E_{0,GQR} = 65A^{-1/3} \text{ MeV}, \quad \Gamma_{GQR} = 85A^{-2/3} \text{ MeV}. \quad (39)$$

The EWSR for the giant octupole resonance is

$$S_3 = 1208A^{-5/3} \text{ MeV}, \quad (40)$$

which has a low-energy (LEOR) and a high-energy (HEOR) component. Following Kalbach [39], we assume

$$S_{3,LEOR} = 0.3S_3, \quad S_{3,HEOR} = 0.7S_3, \quad (41)$$

with excitation energy and width

$$E_{0,LEOR} = 31A^{-1/3} \text{ MeV}, \quad \Gamma_{LEOR} = 5 \text{ MeV}, \quad (42)$$

and

$$E_{0,HEOR} = 115A^{-1/3} \text{ MeV}, \quad \Gamma_{HEOR} = 9.3 - A/48 \text{ MeV} \quad (43)$$

respectively. We also take as width for the actual Gaussian distribution $\Gamma_{Gauss} = 0.42\Gamma_\ell$.

The contribution from giant resonances is automatically included in the total inelastic cross section, and the effect is most noticeable in the single- and double-differential energy spectra. In the future, it may be possible to extend the current GDR implementation by other multipolarities as well.

5. Complex particles

For deuterons, tritons, Helium-3 and alpha particles, we use a simplification of the folding approach of Watanabe [40], see Ref. [41]. We take the nucleon OMPs described in the previous section, either local or global, as the basis for these complex particle potentials.

For deuterons, the real central potential depth at incident energy E is

$$V_V^{deuteron}(E) = V_V^{neutron}(E/2) + V_V^{proton}(E/2), \quad (44)$$

and similarly for W_V and W_D . For the spin-orbit potential depth we have

$$V_{SO}^{deuteron}(E) = (V_{SO}^{neutron}(E) + V_{SO}^{proton}(E))/2, \quad (45)$$

and similarly for W_{SO} . For the radius and diffuseness parameter of the real central potential we have

$$\begin{aligned} r_V^{deuteron} &= (r_V^{neutron} + r_V^{proton})/2, \\ a_V^{deuteron} &= (a_V^{neutron} + a_V^{proton})/2, \end{aligned} \quad (46)$$

and similarly for the geometry parameters of the other potentials. Note that several of these formulae are somewhat more general than necessary, since the nucleon potentials mostly have geometry parameters, and also potential depths such as V_{SO} , which are equal for neutrons and protons (a_D is an exception). The general formulae above have been implemented to also account for other potentials, if necessary. Various alternative deuteron OMP's have been constructed, among which a few recent ones, and these models [42]-[45] are include as options.

For tritons, the real central potential depth at incident energy E is

$$V_V^{triton}(E) = 2V_V^{neutron}(E/3) + V_V^{proton}(E/3), \quad (47)$$

and similarly for W_V and W_D . For the spin-orbit potential depth we have

$$V_{SO}^{triton}(E) = (V_{SO}^{neutron}(E) + V_{SO}^{proton}(E))/6, \quad (48)$$

and similarly for W_{SO} . For the radius and diffuseness parameter of the real central potential we have

$$\begin{aligned} r_V^{triton} &= (2r_V^{neutron} + r_V^{proton})/3, \\ a_V^{triton} &= (2a_V^{neutron} + a_V^{proton})/3, \end{aligned} \quad (49)$$

and similarly for the geometry parameters of the other potentials.

For Helium-3, the real central potential depth at incident energy E is

$$V_V^{Helium-3}(E) = V_V^{neutron}(E/3) + 2V_V^{proton}(E/3), \quad (50)$$

and similarly for W_V and W_D . For the spin-orbit potential depth we have

$$V_{SO}^{He-3}(E) = (V_{SO}^{neutron}(E) + V_{SO}^{proton}(E))/6, \quad (51)$$

and similarly for W_{SO} . For the radius and diffuseness parameter of the real central potential we have

$$\begin{aligned} r_V^{He-3} &= (r_V^{neutron} + 2r_V^{proton})/3, \\ a_V^{He-3} &= (a_V^{neutron} + 2a_V^{proton})/3, \end{aligned} \quad (52)$$

and similarly for the geometry parameters of the other potentials.

For alpha's, the real central potential depth at incident energy E is

$$V_V^{alphas}(E) = 2V_V^{neutron}(E/4) + 2V_V^{proton}(E/4), \quad (53)$$

and similarly for W_V and W_D . For the spin-orbit potential depth we have

$$V_{SO}^{alphas}(E) = W_{SO}^{alphas}(E) = 0. \quad (54)$$

For the radius and diffuseness parameter of the real central potential we have

$$\begin{aligned} r_V^{alphas} &= (r_V^{neutron} + r_V^{proton})/2, \\ a_V^{alphas} &= (a_V^{neutron} + a_V^{proton})/2, \end{aligned} \quad (55)$$

and similarly for the geometry parameters of the other potentials.

Often, we find that the double folding potential of Demetriou, Grama and Goriely [46] presents a good alternative to the simple phenomenological folding models, so that is included as an option too.

In general, what is missing is a systematic study of the quality of complex particle optical models, when compared with available experimental data.

6. Parameter uncertainties

In the quest for a universal set of uncertainties for nuclear model parameters, assessing the uncertainty of optical model potential (OMP) parameters is a natural first step. Therefore, we first investigate to what extent a random parameter variation method, to be outlined in the next Section, can reproduce the deviation between the global OMP and experimental data.

TALYS has been set in a mode in which only the optical model related observables are calculated, and 1000 runs with random optical model parameters have been performed. The global uncertainties were then basically obtained using trial and error: they were adjusted until for total cross sections and angular distributions, the

collection of random curves overlaps as much as possible the data and their uncertainties or discrepant data sets. The range for which this was done consists of a significant subset, covering all masses and energies of interest, of the experimental database that was used for the construction of KD03. An example for neutrons incident on ^{93}Nb is shown in Fig. 3. We note that for some cases it is difficult to obtain a satisfactory central value fit, such as for the neutron total cross section of ^{56}Fe below a few MeV. In those cases, either the parameter uncertainties need to be wider in that energy range, or (unphysical) energy-dependent parameters would have to be invoked.

The resulting parameter uncertainties for neutrons are given in Table III. Of course, the global uncertainty of each parameter can be overruled in specific cases, when more (precise) experimental data is available. On average, the uncertainty bands are large enough to cover the deviation between the global results and experimental data. However, for a few cases we are slightly too optimistic, and sometimes the resulting uncertainties are a bit too conservative, *e.g.* for total cross sections above 20 MeV.

Because of the amount of experimental data, the parameters for the neutron OMP are more constrained than those for protons. This is clear from Table III. For complex particles, the folding procedure to construct the OMP introduces a further uncertainty. Therefore, the default uncertainties for incident protons (r_V^p , etc.) of Table III are multiplied by a factor of 1.5 for deuterons, tritons and alpha particles, and by a factor of 2 for Helium-3 particles.

B. Level Density

The level density models implemented in TALYS have been discussed extensively in Refs. [47] and [48] so we will restrict ourselves to the essential formulae here and will again focus on the uncertainty ranges of the level density parameters.

1. Constant temperature model

For the level density the standard option is to take a combination of the Constant Temperature Model (CTM) at low energies and the Fermi gas model at high energies. The Fermi gas level density for spin J , parity Π and excitation energy E_x is

$$\rho_F(E_x, J, \Pi) = \frac{1}{2} \frac{R_F(E_x, J)}{\sqrt{2\pi}} \frac{\sqrt{\pi}}{12} \frac{\exp\left(2\sqrt{aU}\right)}{a^{1/4} U^{5/4}}, \quad (56)$$

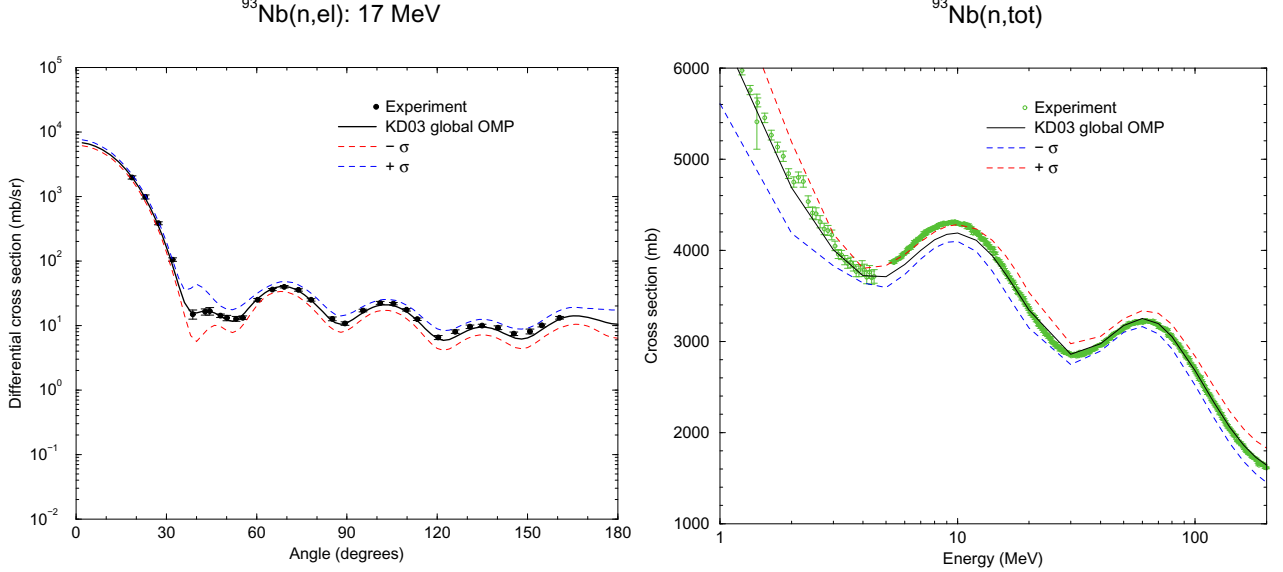


FIG. 3: Comparison of experimental angular distributions (left) and total cross sections (right) and calculated results including uncertainty for $n + {}^{93}\text{Nb}$.

where the first factor $\frac{1}{2}$ indicates an equiparity distribution, and the Fermi gas spin distribution is given by

$$R_F(E_x, J) = \frac{2J+1}{2\sigma^2} \exp\left[-\frac{(J+\frac{1}{2})^2}{2\sigma^2}\right]. \quad (57)$$

The trends for the various parameters in this formula have been studied in Ref. [47]. First, $U = E_x - \Delta$, with Δ the pairing energy, which has a systematic value given by

$$\Delta = \chi \frac{12}{\sqrt{A}}, \quad (58)$$

where $\chi = 0, 1$ or 2 for odd-odd, odd or even-even nuclei, respectively.

The level density parameter a is energy-dependent and takes into account the damping of shell effects at high excitation energy [49],

$$a(E_x) = \tilde{a} \left[1 + \delta W \frac{1 - \exp(-\gamma U)}{U} \right]. \quad (59)$$

Here, δW is the shell correction energy in MeV which we take as the difference between the real mass of the nucleus and the mass according to the spherical liquid drop model as given by Myers and Swiatecki [50]. The asymptotic level density value \tilde{a} is given by

$$\tilde{a} = \alpha A + \beta A^{2/3}, \quad (60)$$

in which we generally use the parameters

$$\alpha = 0.0666, \beta = 0.2587, \quad (61)$$

which we have obtained from a simultaneous fit of the associated level density of Eq. (56) to all average resonance spacing parameters D_0 of the Reference Input Parameter Library [26], at the neutron separation energy S_n , *i.e.*

$$\frac{1}{D_0} = \sum_{J=|I-\frac{1}{2}|}^{J=I+\frac{1}{2}} \rho_F(S_n, J, \Pi), \quad (62)$$

where I is the spin of the target nucleus.

From the same fit, the following systematical formula for the shell damping parameter γ is obtained,

$$\gamma = \frac{0.459}{A^{\frac{1}{3}}} \text{ MeV}^{-1}, \quad (63)$$

The spin cut-off factor σ^2 is given by

$$\sigma_F^2(E_x) = R_\sigma \frac{A^{5/3}}{\tilde{a}} \sqrt{aU}. \quad (64)$$

with $R_\sigma = 0.01389$. On average, the \sqrt{aU}/\tilde{a} has the same energy- and mass-dependent behaviour as the temperature $\sqrt{U/a}$. The differences occur in the regions with large shell effects. Hence, all parameters to compute Eq. (59) and thus Eq. (56) are determined.

There are various variations of the above Fermi Gas equations which have been implemented in TALYS. First of all, in the CTM the Fermi Gas model only holds above a matching energy E_M , while below E_M the so-called

TABLE III: Uncertainties of nuclear model parameters, given as fraction (%) of the absolute value. The uncertainty of a_π , g_ν is in terms of the mass number A

Parameter	uncertainty (%)	Parameter	uncertainty (%)
Optical model			
r_V^n	2	d_1^n	10
a_V^n	2	d_2^n	10
v_1^n	2	d_3^n	10
v_2^n	3	r_{SO}^n	10
v_3^n	3	a_{SO}^n	10
v_4^n	5	v_{so1}^n	5
w_1^n	10	v_{so2}^n	10
w_2^n	10	w_{so1}^n	20
r_D^n	3	w_{so2}^n	20
a_D^n	4		
r_V^p	4	d_1^p	20
a_V^p	4	d_2^p	20
v_1^p	4	d_3^p	20
v_2^p	6	r_{SO}^p	20
v_3^p	6	a_{SO}^p	20
v_4^p	10	v_{so1}^p	10
w_1^p	20	v_{so2}^p	20
w_2^p	20	w_{so1}^p	40
r_D^p	6	w_{so2}^p	40
a_D^p	8	r_C^p	10
λ_V	5	λ_{V1}	5
λ_W	5	λ_{W1}	5
λ_{Vso}	5	λ_{Wso}	5
Level density			
a	11.25-0.03125.A	σ^2	30
γ	30	δW	± 1 MeV
α	30	β	30
R_σ	30	γ	30
E_0	20	E_M	20
T	10	δ	± 2 MeV
K_{rot}	80		
C_{HFM}	30	δ_{HFM}	30
Gamma-ray strength			
Γ_γ	20	$\sigma_{E\ell}$	20
$\Gamma_{E\ell}$	20	$E_{E\ell}$	10
E_{nor}	20	E_{shift}	± 0.8 MeV
Fission			
B_f	10	$\hbar\omega_f$	10
Pre-equilibrium			
M^2	30	$R_{\pi\pi}$	30
$R_{\nu\pi}$	30	$R_{\pi\nu}$	30
$R_{\nu\nu}$	30	R_γ	50
g_ν	11.25-0.03125.A	E_{surf}	20
g_π	11.25-0.03125.A	C_{break}	80
C_{knock}	80	C_{strip}	80

constant temperature law applies. Hence, in the CTM we have for the total level density

$$\begin{aligned}\rho^{tot}(E_x) &= \rho_T^{tot}(E_x), & \text{if } E_x \leq E_M, \\ &= \rho_F^{tot}(E_x), & \text{if } E_x \geq E_M,\end{aligned}\quad (65)$$

and similarly for the level density

$$\begin{aligned}\rho(E_x, J, \Pi) &= \frac{1}{2} R_F(E_x, J) \rho_T^{tot}(E_x), & \text{if } E_x \leq E_M, \\ &= \rho_F(E_x, J, \Pi), & \text{if } E_x \geq E_M\end{aligned}\quad (66)$$

Note that the spin distribution of Eq. (56) is also used in the constant temperature region.

The constant temperature part of the total level density reads

$$\rho_T^{tot}(E_x) = \frac{dN(E_x)}{dE_x} = \frac{1}{T} \exp\left(\frac{E_x - E_0}{T}\right). \quad (67)$$

Approaches to solve the matching equations between the two regions, and related systematic formulae for the parameters, can be found in Ref. [47]

2. Backshifted Fermi gas model

A different, often used, model in TALYS is the Backshifted Fermi Gas level density. It consists again of the general Fermi Gas formalism of Eqs. (56-64) with only one essential deviation: instead of a constant temperature part, the model is expressed in terms of an effective excitation energy $U = E_x - \Delta^{BFM}$, where the energy shift is given by

$$\Delta^{BFM} = \chi \frac{12}{\sqrt{A}} + \delta, \quad (68)$$

with

$$\begin{aligned}\chi &= -1, \text{ for odd - odd,} \\ &= 0, \text{ for odd - even,} \\ &= 1, \text{ for even - even,}\end{aligned}\quad (69)$$

and δ an adjustable parameter to fit experimental data per nucleus. This model has its own asymptotic level density parameters α and β .

3. Generalized superfluid model

The Generalized Superfluid Model (GSM) takes superconductive pairing correlations into account according to the Bardeen-Cooper-Schrieffer theory. The phenomenological version of the model [51, 52] is characterized by a phase transition from a superfluid behaviour at low

energy, where pairing correlations strongly influence the level density, to a high energy region which is described by the FGM. The GSM thus resembles the CTM to the extent that it distinguishes between a low energy and a high energy region, although for the GSM this distinction follows naturally from the theory and does not depend on specific discrete levels that determine a matching energy. Instead, the model automatically provides a constant temperature-like behaviour at low energies. For the full set of equations we refer to Ref. [47]. In general, we find the GSM to be performing less in cross section calculations than the other level density models.

4. Collective effects in the level density

All the previously described models do not explicitly account for collective effects. However, it is well known that generally the first excited levels of nuclei result from coherent excitations of the fermions it contains. The Fermi gas model is not appropriate to describe such levels. Nevertheless, the models presented so far can still be applied successfully in most cases since they incorporate collectivity in the level density in an effective way through a proper choice of the energy-dependent level density parameter values.

In some calculations, especially if the disappearance of collective effects with excitation energy plays a role (*e.g.* in the case of fission), one would like to model the collective effects in more detail. It can be shown that the collective effects may be accounted for explicitly by introducing collective enhancement factors on top of an intrinsic level density $\rho_{F,\text{int}}(E_x, J, \Pi)$. Then the deformed Fermi gas level density $\rho_{F,\text{def}}(E_x, J, \Pi)$ reads

$$\rho_{F,\text{def}}(E_x, J, \Pi) = K_{\text{rot}}(E_x)K_{\text{vib}}(E_x)\rho_{F,\text{int}}(E_x, J, \Pi), \quad (70)$$

while the total level densities $\rho_{F,\text{def}}^{\text{tot}}$ and $\rho_{F,\text{int}}^{\text{tot}}$ are related in the same way. K_{rot} and K_{vib} are called the rotational and vibrational enhancement factors, respectively. If K_{rot} and K_{vib} are explicitly accounted for, $\rho_{F,\text{int}}(E_x, J, \Pi)$ should now describe purely single-particle excitations, and can be determined again by using the Fermi gas formula. Obviously, the level density parameter a of $\rho_{F,\text{int}}$ will be different from that of the effective level density described before.

The vibrational enhancement of the level density is approximated [26] by

$$K_{\text{vib}} = \exp[\delta S - (\delta U/t)], \quad (71)$$

where δS and δU are changes in the entropy and excitation energy, respectively, resulting from the vibrational modes and T is the nuclear temperature. These changes

are described by the Bose gas relationships, i.e.

$$\begin{aligned} \delta S &= \sum_i (2\lambda_i + 1) \left[(1 + n_i) \ln(1 + n_i) - n_i \ln n_i \right], \\ \delta U &= \sum_i (2\lambda_i + 1) \omega_i n_i, \end{aligned} \quad (72)$$

where ω_i are the energies, λ_i the multipolarities, and n_i the occupation numbers for vibrational excitations at a given temperature. The disappearance of collective enhancement of the level density at high temperatures can be taken into account by defining the occupation numbers in terms of the equation

$$n_i = \frac{\exp(-\gamma_i/2\omega_i)}{\exp(\omega_i/T) - 1}, \quad (73)$$

where γ_i are the spreading widths of the vibrational excitations. This spreading of collective excitations in nuclei should be similar to the zero-sound damping in a Fermi liquid, and the corresponding width can be written as

$$\gamma_i = C(\omega_i^2 + 4\pi^2 T^2). \quad (74)$$

The value of $C = 0.0075 A^{1/3}$ was obtained from the systematics of the neutron resonance densities of medium-weight nuclei [53]. We use a modified systematics [26] which includes shell effects to estimate the phonon energies (in MeV), namely

$$\omega_2 = 65 A^{-5/6} / (1 + 0.05\delta W), \quad (75)$$

for the quadrupole vibrations and

$$\omega_3 = 100 A^{-5/6} / (1 + 0.05\delta W), \quad (76)$$

for the octupole excitations.

An alternative, liquid drop model, estimation of the vibrational collective enhancement factor is given by [54]

$$K_{\text{vib}}(E_x) = \exp \left(0.0555 A^{\frac{2}{3}} t^{\frac{4}{3}} \right). \quad (77)$$

A more important contribution to the collective enhancement of the level density originates from rotational excitations. Its effect is not only much stronger ($K_{\text{rot}} \sim 10 - 100$ whereas $K_{\text{vib}} \sim 3$), but the form for the rotational enhancement depends on the nuclear shape as well. This makes it crucial, among others, for the description of fission cross sections. The expression for the rotational enhancement factor depends on the deformation [26, 55]. Basically, K_{rot} is equal to the perpendicular spin cut-off parameter σ_{\perp}^2 ,

$$\sigma_{\perp}^2 = I_{\perp} t, \quad (78)$$

with the rigid-body moment of inertia perpendicular to the symmetry axis given by

$$I_{\perp} = I_0 \left(1 + \frac{\beta_2}{3} \right) = 0.01389 A^{5/3} \left(1 + \frac{\beta_2}{3} \right), \quad (79)$$

where β_2 is the ground-state quadrupole deformation, which we take from the nuclear structure database. Hence,

$$\sigma_{\perp}^2 = 0.01389 A^{5/3} \left(1 + \frac{\beta_2}{3}\right) \sqrt{\frac{U}{a}}. \quad (80)$$

For high excitation energies, it is known that the rotational behavior vanishes. To take this into account, it is customary to introduce a phenomenological damping function $f(E_x)$ which is equal to 1 in the purely deformed case and 0 in the spherical case. The expression for the level density is then

$$\begin{aligned} \rho(E_x, J, \Pi) &= [1 - f(E_x)] K_{\text{vib}}(E_x) \rho_{F,\text{int}}(E_x, J, \Pi), \\ &\quad + f(E_x) \rho_{F,\text{def}}(E_x, J, \Pi) \\ &= K_{\text{rot}}(E_x) K_{\text{vib}}(E_x) \rho_{F,\text{int}}(E_x, J, \Pi) \end{aligned} \quad (81)$$

where

$$K_{\text{rot}}(E_x) = \max(1 + [\sigma_{\perp}^2 - 1]f(E_x), 1). \quad (82)$$

The function $f(E_x)$ is taken as a combination of Fermi functions,

$$f(E_x) = \frac{1}{1 + \exp(\frac{E_x - E_{\text{col}}^{g.s.}}{d_{\text{col}}^{g.s.}})}, \quad (83)$$

which yields the desired property of K_{rot} going to 1 for high excitation energy. Little is known about the parameters that govern this damping, although attempts have been made (see *e.g.* [56]). In TALYS, the values $E_{\text{col}}^{g.s.} = 30$ MeV, $d_{\text{col}}^{g.s.} = 5$ MeV are taken.

Finally, these collective enhancement expressions can be applied to the various phenomenological level density models. The CTM formalism can be extended with explicit collective enhancement, *i.e.* the total level density reads

$$\begin{aligned} \rho^{\text{tot}}(E_x) &= \rho_T^{\text{tot}}(E_x) \quad \text{if } E_x \leq E_M, \\ &= K_{\text{rot}}(E_x) K_{\text{vib}}(E_x) \rho_{F,\text{int}}^{\text{tot}}(E_x), \quad \text{if } E_x \geq E_M, \end{aligned} \quad (84)$$

and similarly for the level density $\rho(E_x, J, \Pi)$. Note that the collective enhancement is not applied to the constant temperature region, since collectivity is assumed to be already implicitly included in the discrete levels. This means that for fission barriers, the temperature may deviate considerably from its effective, non-collective counterpart. The matching problem is completely analogous to that described before, although the resulting parameters E_M , E_0 and T will of course be different. The BFM can also be extended with explicit collective enhancement.

5. Microscopic level densities

Besides the phenomenological models that are used in TALYS, there is also an option to employ more microscopic approaches. For the RIPL database, Goriely has calculated level densities from drip line to drip line on the basis of Hartree-Fock calculations [57] for excitation energies up to 150 MeV and for spin values up to $I = 30$. In addition, new energy-, spin- and parity-dependent nuclear level densities based on the microscopic combinatorial model have been proposed by Hilaire and Goriely [48]. The combinatorial model includes a detailed microscopic calculation of the intrinsic state density and a collective enhancement is added to this. The only phenomenological aspect of the model is a simple damping function for the rotational effects. The calculations make coherent use of nuclear structure properties determined within the deformed Skyrme-Hartree-Fock-Bogolyubov framework. Level densities for more than 8500 nuclei are made available in tabular form at, for excitation energies up to 200 MeV and for spin values up to $J = 49$.

Since these microscopical level densities, which we will call ρ_{HFM} , have not been adjusted to experimental data, adjustment flexibility is added through a scaling function, *i.e.*

$$\begin{aligned} \rho(E_x, J, \pi) &= \exp(C_{\text{HFM}} \sqrt{E_x - \delta_{\text{HFM}}}) \\ &\cdot \rho_{\text{HFM}}(E_x - \delta_{\text{HFM}}, J, \pi), \end{aligned} \quad (85)$$

where by default $C_{\text{HFM}} = 0$ and $\delta_{\text{HFM}} = 0$ (*i.e.* unaltered values from the tables). The “pairing shift” δ_{HFM} simply implies obtaining the level density from the table at a different energy. The constant C_{HFM} plays a role similar to that of the level density parameter a of phenomenological models. Adjusting C_{HFM} and δ_{HFM} together gives adjustment flexibility at both low and higher energies.

6. Parameter uncertainties

The global uncertainties we assign to the level density parameters discussed above are given in Table III. Again, we have validated these global uncertainties by means of visual comparison of scattered random TALYS curves with experimental data for the whole nuclide chart. Two aspects of Table III deserve special mention. First, there is a mass dependence in the *uncertainty* of the level density parameter a . At the moment, we consider this trend as effective: for heavy nuclides, the reaction flux is divided over less channels ((n, γ), (n,n') and (n,2n)) than for light nuclides which have significant proton and alpha emission channels. For light nuclides, the model predictions for the various partial cross sections

are therefore more uncertain, which is reflected in the functional form for a in Table III. With the mass dependent formula of Table III, we find that we can globally cover experimental data with our random TALYS results. Second, note that also in the low-energy part of the level density the CTM parameters have default uncertainties. All but one (usually the matching energy E_M) of the CTM level density parameters can be randomly varied after which the matching problem between the constant temperature part and the Fermi gas part is numerically solved.

C. Gamma-ray Strength Functions

Gamma-ray transmission coefficients are important for the description of the gamma emission channel in nuclear reactions. This is an almost universal channel since gamma rays, in general, may accompany emission of any other emitted particle. Like the particle transmission coefficients that emerge from the optical model, gamma-ray transmission coefficients enter the Hauser-Feshbach model for the calculation of the competition of photons with other particles.

The gamma-ray transmission coefficient for multipolarity ℓ of type X (where $X = M$ or E) is given by

$$T_{X\ell}(E_\gamma) = 2\pi f_{X\ell}(E_\gamma) E_\gamma^{2\ell+1}, \quad (86)$$

where E_γ denotes the gamma energy and $f_{X\ell}(E_\gamma)$ is the energy-dependent gamma-ray strength function.

1. Models for gamma-ray strength functions

In TALYS four models for the gamma-ray strength function are implemented. The first is the so-called Brink-Axel option [58], in which a standard Lorentzian form describes the giant dipole resonance shape, *i.e.*

$$f_{X\ell}(E_\gamma) = K_{X\ell} \frac{\sigma_{X\ell} E_\gamma \Gamma_{X\ell}^2}{(E_\gamma^2 - E_{X\ell}^2)^2 + E_\gamma^2 \Gamma_{X\ell}^2}, \quad (87)$$

where $\sigma_{X\ell}$, $E_{X\ell}$ and $\Gamma_{X\ell}$ are the strength, energy and width of the giant resonance, respectively, and

$$K_{X\ell} = \frac{1}{(2\ell+1)\pi^2 \hbar^2 c^2}. \quad (88)$$

At present, we use the Brink-Axel option for all transition types other than $E1$. For $E1$ radiation, the default option used in TALYS is the generalized Lorentzian form of Kopecky and Uhl [59],

$$\begin{aligned} f_{E1}(E_\gamma, T) &= K_{E1} \left(\frac{E_\gamma \tilde{\Gamma}_{E1}(E_\gamma)}{(E_\gamma^2 - E_{E1}^2)^2 + E_\gamma^2 \tilde{\Gamma}_{E1}(E_\gamma)^2} \right. \\ &\quad \left. + \frac{0.7 \Gamma_{E1} 4\pi^2 T^2}{E_{E1}^3} \right) \sigma_{E1} \Gamma_{E1}, \end{aligned} \quad (89)$$

where the energy-dependent damping width $\tilde{\Gamma}_{E1}(E_\gamma)$ is given by

$$\tilde{\Gamma}_{E1}(E_\gamma) = \Gamma_{E1} \frac{E_\gamma^2 + 4\pi^2 T^2}{E_{E1}^2}, \quad (90)$$

and T is the nuclear temperature given by [60]

$$T = \sqrt{\frac{E_n + S_n - \Delta - E_\gamma}{a(S_n)}}, \quad (91)$$

where S_n is the neutron separation energy, E_n the incident neutron energy, Δ the pairing correction (see the Section on level densities) and a the level density parameter at S_n .

For $E1$ -transitions, GDR parameters for various individual nuclides exist, and these are stored in the nuclear structure database of TALYS. Some nuclides have a split GDR, *i.e.* a second set of Lorentzian parameters. For these cases, the incoherent sum of two strength functions is taken. For all transitions other than $E1$, systematic formulae compiled by Kopecky [26], for the resonance parameters are used. For $E1$ transitions for which no tabulated data exist, we use

$$\begin{aligned} \sigma_{E1} &= 1.2 \times 120 N Z / (A \pi \Gamma_{E1}) \text{ mb}, \\ E_{E1} &= 31.2 A^{-1/3} + 20.6 A^{-1/6} \text{ MeV}, \\ \Gamma_{E1} &= 0.026 E_{E1}^{1.91} \text{ MeV}. \end{aligned} \quad (92)$$

For $E2$ transitions we use

$$\begin{aligned} \sigma_{E2} &= 0.00014 Z^2 E_{E2} / (A^{1/3} \Gamma_{E2}) \text{ mb}, \\ E_{E2} &= 63. A^{-1/3} \text{ MeV}, \\ \Gamma_{E2} &= 6.11 - 0.012 A \text{ MeV}. \end{aligned} \quad (93)$$

For multipole radiation higher than $E2$, we use

$$\begin{aligned} \sigma_{E\ell} &= 8.10^{-4} \sigma_{E(\ell-1)}, \\ E_{E\ell} &= E_{E(\ell-1)} \\ \Gamma_{E\ell} &= \Gamma_{E(\ell-1)}. \end{aligned} \quad (94)$$

For $M1$ transitions we use

$$\begin{aligned} f_{M1} &= 1.58 A^{0.47} \text{ at } 7 \text{ MeV}, \\ E_{M1} &= 41. A^{-1/3} \text{ MeV}, \\ \Gamma_{M1} &= 4 \text{ MeV}, \end{aligned} \quad (95)$$

where Eq. (87) thus needs to be applied at 7 MeV to obtain the σ_{M1} value. For multipole radiation higher than $M1$, we use

$$\sigma_{M\ell} = 8.10^{-4} \sigma_{M(\ell-1)}, \quad E_{M\ell} = E_{M(\ell-1)} \quad \Gamma_{M\ell} = \Gamma_{M(\ell-1)}. \quad (96)$$

For all cases, the systematics can be overruled with user-defined input parameters.

In addition to the GDR contribution above, pygmy resonances can be included by adding another contribution of the form (87) to the strength function.

TALYS also provides two microscopic options for $E1$ radiation, with gamma-ray strength functions calculated according to the Hartree-Fock BCS model and the Hartree-Fock-Bogolyubov model, see Ref. [26]. Since these microscopical strength functions, f_{HFM} , have not been adjusted to experimental data, we add adjustment flexibility through a scaling function, *i.e.*

$$f_{E1}(E_\gamma) = f^{nor} f_{HFM}(E_\gamma + E_{\text{shift}}), \quad (97)$$

where by default $f^{nor} = 1$ and $E_{\text{shift}} = 0$ (*i.e.* unaltered values from the tables). The energy shift E_{shift} simply implies obtaining the level density from the table at a different energy. Adjusting f^{nor} and E_{shift} together gives enough adjustment flexibility.

2. Renormalization of gamma-ray strength functions

At sufficiently low incident neutron energies, the average radiative capture width Γ_γ is due entirely to the s -wave interaction, and it is Γ_γ at the neutron separation energy S_n that is often used to normalize gamma-ray transmission coefficients [61]. The Γ_γ values are, when available, read from our nuclear structure database. For nuclides for which no experimental value is available, we use an interpolation table by Kopecky [62] for $40 < A < 250$, the simple form

$$\Gamma_\gamma = 1593/A^2 \text{ eV}, \quad (98)$$

for $A > 250$, while we apply no gamma normalization for $A < 40$.

The s -wave radiation width may be obtained by integrating the gamma-ray transmission coefficients over the density of final states that may be reached in the first step of the gamma-ray cascade. The normalization is then carried out as follows

$$\frac{2\pi\Gamma_\gamma}{D_0} = G_{\text{norm}} \sum_J \sum_\Pi \sum_{X\ell} \sum_{I'=\lvert J-\ell \rvert}^{J+\ell} \sum_{\Pi'} \int_0^{S_n} dE_\gamma T_{X\ell}(E_\gamma) \rho(S_n - E_\gamma, I', \Pi') f(X, \Pi', \ell), \quad (99)$$

where D_0 is the average resonance spacing and ρ is the level density. The J, Π sum is over the compound nucleus states with spin J and parity Π that can be formed with s -wave incident particles, and I', Π' denote the spin and parity of the final states. The multipole selection rules are $f(E, \Pi', \ell) = 1$ if $\Pi = \Pi'(-1)^\ell$, $f(M, \Pi', \ell) = 1$ if $\Pi = \Pi'(-1)^{\ell+1}$, and 0 otherwise. It is understood that the integral over E_γ includes a summation over discrete states. G_{norm} is the normalization factor that ensures

the equality (99). In practice, the transmission coefficients (86) can thus optionally be multiplied by G_{norm} before they enter the nuclear reaction calculation, with as default the value returned by Eq. (99).

3. Photoabsorption cross section

TALYS requires photo-absorption cross sections for photo-nuclear reactions and for pre-equilibrium gamma-ray emission. Following Chadwick et al. [63], the photo-absorption cross section is given by

$$\sigma_{\text{abs}}(E_\gamma) = \sigma_{\text{GDR}}(E_\gamma) + \sigma_{\text{QD}}(E_\gamma). \quad (100)$$

The GDR component is related to the strength functions outlined above. It is given by

$$\sigma_{\text{GDR}}(E_\gamma) = \sum_i \sigma_{E1,i} \frac{(E_\gamma \Gamma_{E1,i})^2}{(E_\gamma^2 - E_{E1,i}^2)^2 + E_\gamma^2 \Gamma_{E1,i}^2}, \quad (101)$$

where the parameters are specified in the previous subsection. The sum over i is over the number of parts into which the GDR is split.

The quasi-deuteron component σ_{QD} is given by

$$\sigma_{\text{QD}}(E_\gamma) = L \frac{NZ}{A} \sigma_d(E_\gamma) f(E_\gamma). \quad (102)$$

Here, $\sigma_d(E_\gamma)$ is the experimental deuteron photo-disintegration cross section, parametrized as

$$\sigma_d(E_\gamma) = 61.2 \frac{(E_\gamma - 2.224)^{3/2}}{E_\gamma^3}, \quad (103)$$

for $E_\gamma > 2.224$ MeV and zero otherwise. The so-called Levinger parameter is $L = 6.5$ and the Pauli-blocking function is approximated by the polynomial expression

$$f(E_\gamma) = 8.3714 \cdot 10^{-2} - 9.8343 \cdot 10^{-3} E_\gamma + 4.1222 \cdot 10^{-4} E_\gamma^2 - 3.4762 \cdot 10^{-6} E_\gamma^3 + 9.3537 \cdot 10^{-9} E_\gamma^4, \quad (104)$$

for $20 < E_\gamma < 140$ MeV,

$$f(E_\gamma) = \exp(-73.3/E_\gamma), \quad (105)$$

for $E_\gamma < 20$ MeV, and

$$f(E_\gamma) = \exp(-24.2348/E_\gamma), \quad (106)$$

for $E_\gamma > 140$ MeV.

4. Parameter uncertainties

The global uncertainties we assign to gamma-ray strength function parameters are given in Table III. In

practical evaluation work, the uncertainties of the GDR parameters $\sigma_{E\ell}$, $\Gamma_{E\ell}$ and $E_{E\ell}$ are generally kept at their global values. The uncertainty of the average radiative width Γ_γ is often adjusted to let the TALYS uncertainty band cover the scattered experimental data of neutron capture data. Fig.4 shows the uncertainty of the $^{86}\text{Sr}(\text{n},\gamma)$ cross section using a 15 % uncertainty of Γ_γ .

D. Fission

The probability that a nucleus fissions can be estimated by TALYS on both phenomenological and microscopic grounds. Cross sections for (multi-chance) fission can be calculated. For this, various nuclear quantities are required.

1. Fission transmission coefficients

For fission, the default model implemented in TALYS is based on the transition state hypothesis of Bohr and the Hill-Wheeler expression. This yields transmission coefficients that enter the Hauser-Feshbach model to compete with the particle and photon transmission coefficients.

a. Transmission coefficient for one fission barrier
The Hill-Wheeler expression gives the probability of tunneling through a barrier with height B_f and width $\hbar\omega_f$ for a compound nucleus with excitation energy E_x . It reads

$$T_f(E_x) = \frac{1}{1 + \exp\left[-2\pi\frac{(E_x - B_f)}{\hbar\omega_f}\right]}, \quad (107)$$

For a transition state with excitation energy ε_i above the top of the same barrier, one has

$$T_f(E_x, \varepsilon_i) = \frac{1}{1 + \exp\left[-2\pi\frac{(E_x - B_f - \varepsilon_i)}{\hbar\omega_f}\right]}, \quad (108)$$

which means that the barrier is simply shifted up by ε_i .

For a compound nucleus with excitation energy E_x , spin J , and parity Π , the total fission transmission coefficient is the sum of the individual transmissions coefficients for each barrier through which the nucleus may tunnel, and thus reads in terms of the previously introduced $T_f(E_x, \varepsilon_i)$

$$T_f^{J,\Pi}(E_x) = \sum_i T_f(E_x, \varepsilon_i) f(i, J, \Pi) + \int_{E_{th}}^{E_x} \rho(\varepsilon, J, \Pi) T_f(E_x, \varepsilon) d\varepsilon, \quad (109)$$

The summation runs over all discrete transition states on top of the barrier and E_{th} marks the beginning of the continuum. In this equation, $f(i, J, \Pi) = 1$ if the spin and parity of the transition state equal that of the compound nucleus and 0 otherwise. Moreover, $\rho(\varepsilon, J, \Pi)$ is the level density of fission channels with spin J and parity Π for an excitation energy ε . The main difference with the usually employed expressions is that the upper limit in the integration is finite. This expression also enables to define the number of fission channels by replacing $T_f(E_x, \varepsilon_i)$ by 1 in Eq. (109). This is needed for width fluctuation calculations where the fission transmission coefficient is treated as a continuum transmission coefficient.

b. Transmission coefficient for multi-humped barriers
For double humped barriers, the generally employed expression is based on an effective transmission coefficient T_{eff} defined by

$$T_{eff} = \frac{T_A T_B}{T_A + T_B}, \quad (110)$$

where T_A and T_B are the transmission coefficients for barrier A and B respectively, calculated with Eq. (109).

If a triple humped barrier needs to be considered, the expression for T_{eff} reads

$$T_{eff} = \frac{T_{AB} T_C}{T_{AB} + T_C}, \quad (111)$$

where T_{AB} is given by Eq. (110). Consequently, the expression used in TALYS reads

$$T_{eff} = \frac{T_A T_B T_C}{T_A T_B + T_A T_C + T_B T_C}, \quad (112)$$

For any number of barrier, the effective number of fission channels is calculated as in the case for one barrier [64].

c. Class II/III states
Class II (resp. III) states may be introduced when double (resp. triple) humped barriers are considered. In the particular situation where the excitation energy E_{CN} of the compound nucleus is lower than the barrier heights, fission transmission coefficients display resonant structures which are due to the presence of nuclear excited levels (Class II) in the second, or in the third (Class III) well of the potential energy surface. When such resonant structures occur, the expression for the effective fission transmission coefficient has to be modified (generally enhanced).

The way this resonant effect is determined depends on the number of barriers that are considered.

In the case where two barriers occur, the effective fission transmission coefficient T_{eff} can be written as

$$T_{eff} = \frac{T_A T_B}{T_A + T_B} \times F_{AB}(E_{CN}), \quad (113)$$

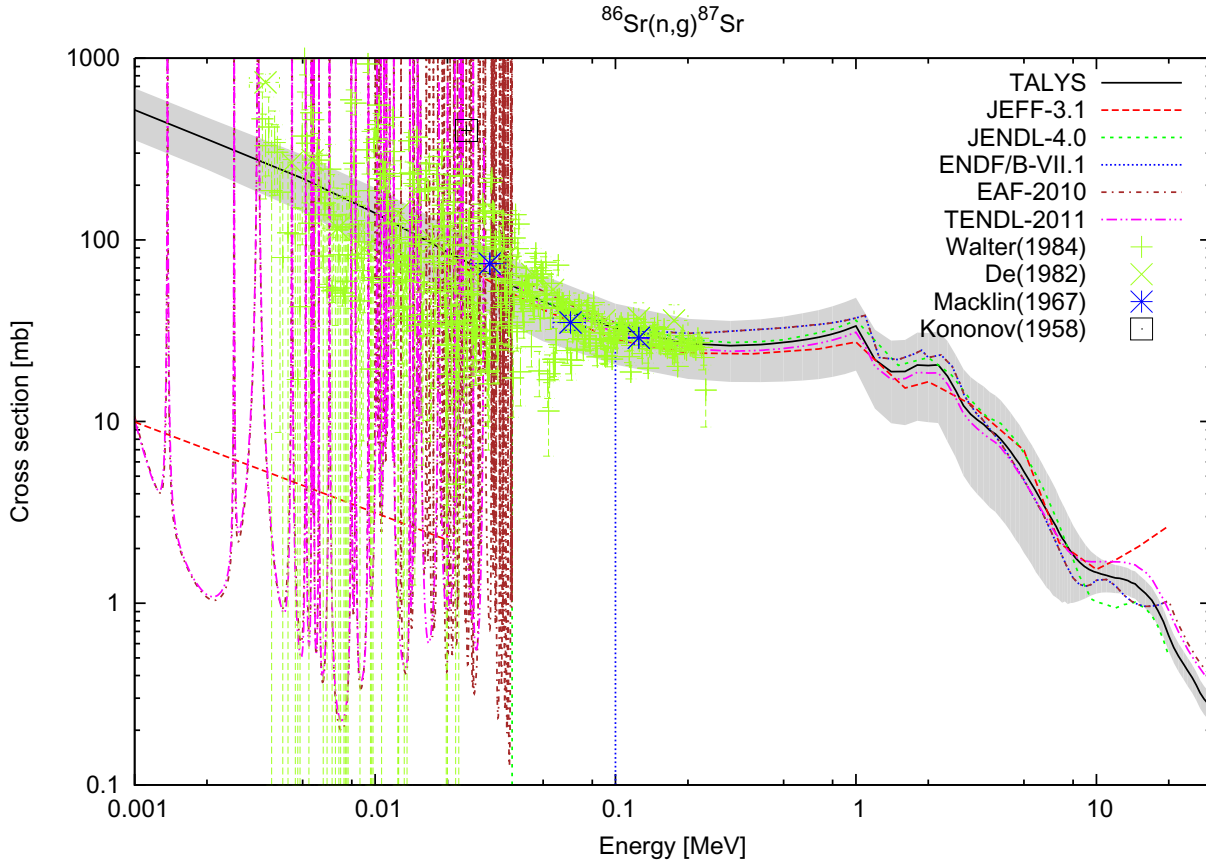


FIG. 4: TALYS uncertainty band of ^{86}Sr capture cross section due to uncertainty of gamma-ray parameters, compared with experimental data and nuclear data libraries.

where $F_{AB}(E_{CN})$ is a factor whose value depends on the energy difference between the excitation energy of the nucleus and that of a class II state located in the well between barrier A and B . It has been shown [65] that the maximum value of $F_{AB}(E)$ reaches $\frac{4}{T_A+T_B}$ and gradually decreases over an energy interval defined as the width Γ_{II} of the class II state with excitation energy E_{II} . This is accounted for using the empirical quadratic expression

$$F_{AB}(E) = \frac{4}{T_A + T_B} + \left(\frac{E - E_{II}}{0.5\Gamma_{II}} \right)^2 \times \left(1 - \frac{4}{T_A + T_B} \right), \quad (114)$$

if $E_{II} - 0.5\Gamma_{II} \leq E \leq E_{II} + 0.5\Gamma_{II}$ and $F_{AB} = 1$ otherwise.

Theoretically, this expression is valid for the tunneling through a single double humped barrier whereas in realistic situations, both T_A and T_B are obtained from a summation over several transition states. One may thus have large T_A and T_B values so that Eq. (114) may give $F_{AB}(E) \leq 1$. Such a situation can only occur for

high enough excitation energies for which the individual Hill-Wheeler contributions in Eq. (109) are large enough. However, in TALYS, we only consider class II states with excitation energies lower than the height of the first barrier. Consequently, the resonant effect can only occur if the compound nucleus energy E_{CN} is (i) lower than the top of the first barrier and (ii) close to a resonant class II state ($E_{II} - 0.5\Gamma_{II} \leq E_{CN} \leq E_{II} + 0.5\Gamma_{II}$). With such requirements, the individual Hill-Wheeler terms are clearly small, and $T_A + T_B \ll 1$.

If three barriers A , B and C are considered, the situation is more complicated. In this case, three situations can occur depending on the positions of the class II and class III states. Indeed the enhancement can be due either to a class II state or to a class III state, but on top of that, a double resonant effect can also occur if both a class II and a class III state have an excitation energy close to the compound nucleus energy. For any situation, the enhancement is first calculated for the first and the

second barrier giving the transmission coefficient

$$T_{eff}^{AB} = T_{AB} \times F_{AB}, \quad (115)$$

with F_{AB} given by Eq. (114) as in the previous case.

Next, the eventual coupling with a class III state with energy E_{III} of width Γ_{III} is accounted for by generalizing Eq. (113) writing

$$T_{eff}^{ABC} = \frac{T_{eff}^{AB} T_C}{T_{eff}^{AB} + T_C} \times F_{ABC}(E_{CN}), \quad (116)$$

where $F_{ABC}(E_{CN})$ is given by generalizing Eq. (114) writing

$$F_{ABC}(E) = \frac{4}{T_{eff}^{AB} + T_C} + \left(\frac{E - E_{III}}{0.5\Gamma_{III}} \right)^2 \times \left(1 - \frac{4}{T_{eff}^{AB} + T_C} \right) \quad (117)$$

if $E_{III} - 0.5\Gamma_{III} \leq E \leq E_{III} + 0.5\Gamma_{III}$ and $F_{ABC} = 1$ otherwise.

2. Fission barrier parameters

In TALYS several options are included for the choice of the fission barrier parameters:

1. Experimental parameters from the RIPL database [26]: collection of a large set of actinide fission barrier heights and curvatures for both the inner and outer barrier based on a fit to experimental data, compiled by V. Maslov. Moreover, this compilation contains head band transition states. This is generally our first choice.
2. Mamdouh parameters [66]: set of double-humped fission barrier heights for numerous isotopes derived from Extended Thomas-Fermi plus Strutinsky Integral calculations.
3. Rotating-Finite-Range Model (RFRM) by Sierk [67]: single-humped fission barrier heights are determined within a rotating liquid drop model, extended with finite-range effects in the nuclear surface energy and finite surface-diffuseness effects in the Coulomb energy.
4. Rotating-Liquid-Drop Model (RLDM) by Cohen *et al* [68].
5. WKB approximation: As an alternative to the Hill-Wheeler approach, it is also possible to use the WKB approximation to calculate fission transmission coefficients. We use an implementation by Sin and Capote and refer to Ref. [69] for the full details of this method.

In the current version of TALYS, the dependence on angular momentum of the fission barriers is discarded. If LDM barriers are employed in the calculation, they are corrected for the difference between the ground-state and fission barrier shell correction energy

$$B_f^{LDM}(T) = B_f^{LDM}(0) - (\delta W_{groundstate} - \delta W_{barrier}) * g(T), \quad (118)$$

This correction gradually disappears with temperature due to the washing out of the shell effects [70]

$$g(T) = \begin{cases} 1 & \text{for } T < 1.65 \text{ MeV}, \\ 5.809 \exp(-1.066 T) & \text{for } T \geq 1.65 \text{ MeV}. \end{cases} \quad (119)$$

Shell corrections on top of the fission barrier are generally unknown. They obviously play an important role for the level density as well. Default values are adopted: for subactinides $\delta W_{barrier} = 0$ MeV, for actinides $\delta W_{barrier,inner} = 2.5$ MeV and $\delta W_{barrier,outer} = 0.6$ MeV [26].

3. Parameter uncertainties

The global uncertainties we assign to fission parameters are given in Table III. For fission, the difference between global and 'adjusted' parameter uncertainties is the largest. There is still a lot of development required in fission theory, and the sensitivity of fission transmission coefficients, as they appear in the Hauser-Feshbach formula, on the associated parameters is huge. Hence, the global uncertainties given in Table III give large uncertainties in the fission cross section. At the same time, if a fission cross section is experimentally well known, the associated 'adjusted' fission parameter uncertainty is small, in fact much smaller than can be expected on theoretical grounds. Examples are given in Fig. 5 where the uncertainties of the fission barriers and widths have been reduced to a few percent for the experimentally known nuclides ^{231}Pa , ^{243}Am and ^{245}Cm , while the default uncertainties of Table III have been applied to ^{254}Es .

E. Compound Nucleus Reactions

With the optical model, level density, gamma-ray strength function and fission transmissions coefficient as ingredients, the compound nucleus model can be used to describe low-energy reactions. Actually, the term compound nucleus reaction is commonly used for two different processes: (i) capture of the projectile in the target nucleus to form a compound nucleus, which subsequently emits a particle or gamma, (ii) multiple emission from the chain of excited residual nuclides following the

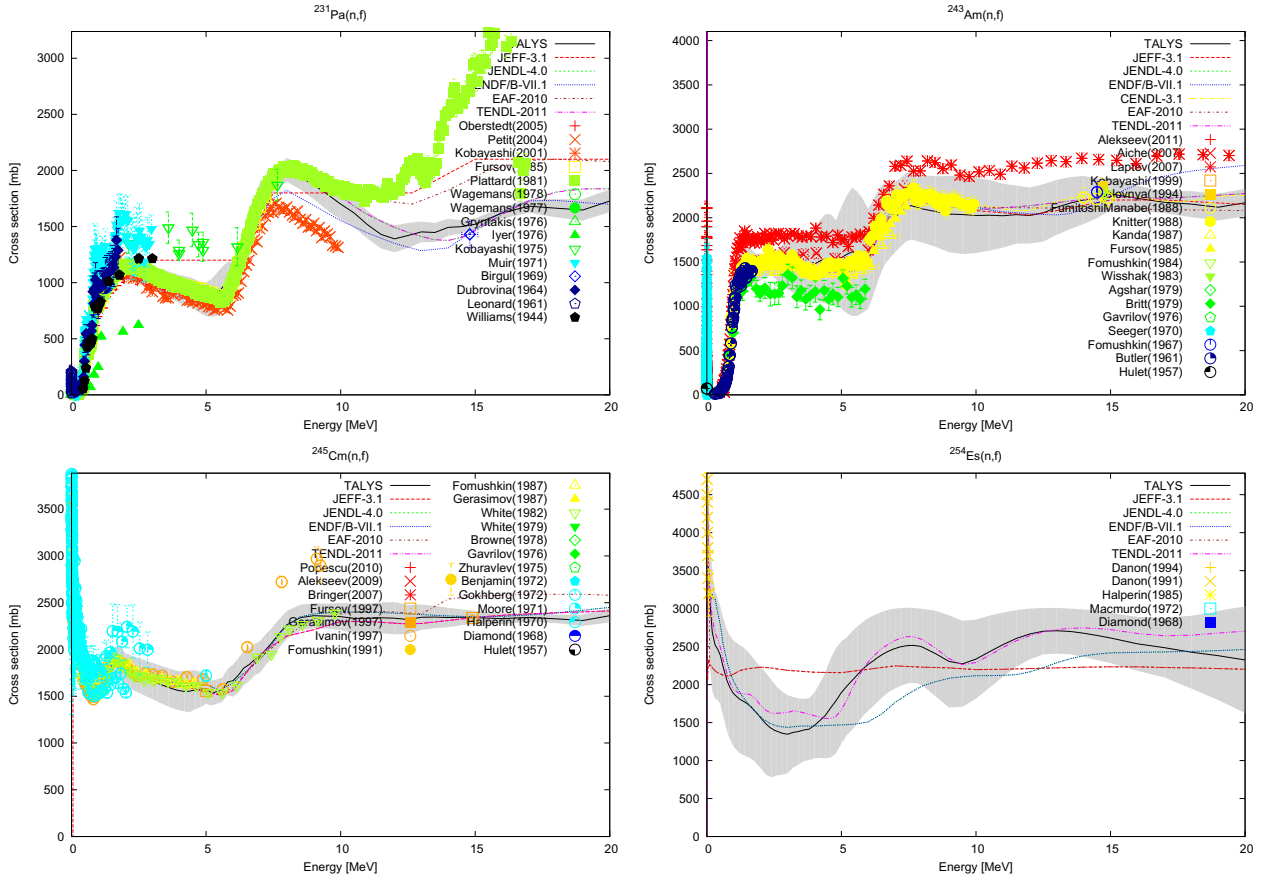


FIG. 5: TALYS uncertainty band of ^{231}Pa , ^{243}Am , ^{245}Cm , and ^{254}Es neutron-induced fission cross section due to uncertainty of fission barrier parameters, compared with experimental data and nuclear data libraries. Only the fission barrier parameters of ^{254}Es have been kept at their default values.

binary reaction. Both are needed for a complete nuclear reaction description and are thus implemented in TALYS. At low incident energy (i) plays an important role. It differs from (ii) (which we will discuss later) at two important points: (a) the presence of width fluctuation corrections in the compound nucleus expression and (b) non-isotropic, though still symmetric, angular distributions. In the compound nucleus picture, the projectile and the target nucleus form a compound nucleus with a total energy E^{tot} and a range of values for the total spin J and parity Π . The following energy, angular momentum and parity conservation laws need to be obeyed,

$$\begin{aligned} E_a + S_a &= E_{a'} + E_x + S_{a'} = E^{tot} \\ s + I + l &= s' + I' + l' = J \\ \pi_0 \Pi_0 (-1)^l &= \pi_f \Pi_f (-1)^{l'} = \Pi, \end{aligned} \quad (120)$$

while the compound nucleus formula for the binary cross section is given by

$$\begin{aligned} \sigma_{\alpha\alpha'}^{comp} &= D^{comp} \frac{\pi}{k^2} \sum_{J=mod(I+s,1)}^{l_{max}+I+s} \sum_{\Pi=-1}^1 \frac{2J+1}{(2I+1)(2s+1)} \\ &\sum_{j=|J-I|}^{J+I} \sum_{l=|j-s|}^{j+s} \sum_{j'=|J-I'|}^{J+I'} \sum_{l'=|j'-s'|}^{j'+s'} \delta_\pi(\alpha) \delta_\pi(\alpha') \\ &\frac{T_{\alpha l j}^J(E_a) \langle T_{\alpha' l' j'}^J(E_{a'}) \rangle}{\sum_{\alpha'', l'', j''} \delta_\pi(\alpha'') \langle T_{\alpha'' l'' j''}^J(E_{a''}) \rangle} W_{\alpha l j \alpha' l' j'}^J. \end{aligned} \quad (121)$$

In the above equations, the projectile a is characterized by energy E_a , spin s , parity π_0 , orbital angular momentum l , total angular momentum j , and a general channel index $\alpha = \{a, s, E_a, E_x^0, I, \Pi_0\}$, where I is the spin, Π_0 the parity and E_x^0 the excitation energy (usually zero) of the target nucleus. The quantities with a prime re-

fer to the ejectile. Further, S_a is the separation energy, l_{max} the maximal l -value for the projectile (dependent on incident energy), J the total angular momentum of the compound system, D^{comp} the depletion factor to account for direct and pre-equilibrium effects, k the wave number of relative motion, T the transmission coefficient and W the width fluctuation correction (WFC) factor. Finally, $\delta_\pi(\alpha') = 1$, if $(-1)^{l'} \pi_f \Pi_f = \Pi$ and 0 otherwise.

In order to let Eq. (121) represent the general case, we have denoted the outgoing transmission coefficient by $\langle T_{\alpha' l' j'}^J(E_{a'}) \rangle$. For this, two cases can be distinguished. If the excitation energy E_x , that is implicit in the definition of channel α' , corresponds to a discrete state of the final nucleus, then we simply have

$$\langle T_{\alpha' l' j'}^J(E_{a'}) \rangle = T_{\alpha' l' j'}^J(E_{a'}), \quad (122)$$

and $E'_{a'}$ is exactly determined by Eq. (120). For α' channels for which E_x is in the continuum, we have an effective transmission coefficient for an excitation energy bin with width ΔE_x ,

$$\langle T_{\alpha' l' j'}^J(E_{a'}) \rangle = \int_{E_x - \frac{1}{2}\Delta E_x}^{E_x + \frac{1}{2}\Delta E_x} dE_{x'} \rho(E_{x'}, J, \Pi) T_{\alpha' l' j'}^J(E_{a'}), \quad (123)$$

where ρ is the level density and T is evaluated at an emission energy $E_{a'}$ that corresponds to the middle of the excitation energy bin, *i.e.* $E_{a'} = E^{tot} - E_x - S_{a'}$. Hence, both transitions to discrete states and transitions to the whole accessible continuum are covered by the sum over α' in Eq. (121). The normalization factor D^{comp}

$$D^{comp} = [\sigma_{CF} - \sigma^{disc,direct} - \sigma^{PE}] / \sigma_{CF}, \quad (124)$$

with σ_{CF} the compound nucleus formation cross section, $\sigma^{disc,direct}$ the direct reaction contribution for weakly coupled discrete levels and σ^{PE} the pre-equilibrium cross section. This indicates that in TALYS we adopt the common assumption that direct, pre-equilibrium and compound contributions can be added incoherently. This formula for D^{comp} is only applied for weakly coupled channels that deplete the flux, such as contributions from the Distorted Wave Born Approximation (DWBA) or pre-equilibrium reactions. Strongly coupled levels are taken into account in the estimation of σ_{reac} from coupled channels calculations.

The compound nucleus formula (121) *without* the WFC factor W is commonly known as the Hauser-Feshbach formula. The WFC factor W accounts for the correlations that exist between the incident and outgoing waves. From a qualitative point of view, these correlations enhance the elastic channel and accordingly decrease the other open channels. Above a few MeV of projectile energy, when many competing channels are

open, the WFC factors go to 1 and the resulting Hauser-Feshbach model is then adequate to describe the compound nucleus decay. Various models for the WFC factor exist, and a comparison among them [64, 71] revealed that the best choice for practical calculations is that of Moldauer [72]. Moldauer's expression for the WFC factor is based on the assumption that a χ^2 law with ν degrees of freedom applies for the partial decay widths, which can be calculated from a Porter-Thomas distribution, which is a χ^2 distribution with $\nu = 1$. Switching to a more compact notation in which we leave out J and define $a = \{\alpha, l, j\}$ and $b = \{\alpha', l', j'\}$, the compound nucleus cross section can be written

$$\sigma_{ab} = \frac{\pi}{k_a^2} \frac{T_a T_b}{\sum_c T_c} W_{ab}, \quad (125)$$

for each combination of a and b .

Then, W_{ab} reads

$$W_{ab} = (1 + \frac{2\delta_{ab}}{\nu_a}) \int_0^\infty dx \prod_c \left(1 + \frac{2T_c x}{\nu_c \sum_i T_i} \right)^{-(\delta_{ac} + \delta_{bc} + \nu_c/2)}. \quad (126)$$

Moldauer has parametrized ν using Monte Carlo calculations, giving

$$\nu_a = 1.78 + (T_a^{1.212} - 0.78) \exp \left(-0.228 \sum_c T_c \right). \quad (127)$$

Consult Ref. [64] for a generalization of this formula to take into account photons, continuum channels and fission. The application of the WFC factor in the compound nucleus formula is crucial for an adequate description of, among others, the excitation function for inelastic scattering.

We also require the compound nucleus formula for the angular distribution. The differential cross section is

$$\frac{d\sigma_{\alpha\alpha'}^{comp}(\theta)}{d\Omega} = \sum_L C_L^{comp} P_L(\cos \Theta), \quad (128)$$

where P_L are Legendre polynomials. The Legendre coefficients C_L^{comp} are given by

$$C_L^{comp} = D^{comp} \frac{\pi}{k^2} \sum_{J,\Pi} \frac{2J+1}{(2I+1)(2s+1)} \sum_{j=|J-I|}^{J+I} \sum_{l=|j-s|}^{j+s} \sum_{j'=|J-I'|}^{J+I'} \sum_{l'=|j'-s'|}^{j'+s'} \delta_\pi(\alpha) \delta_\pi(\alpha') W_{\alpha l j \alpha' l' j'}^J A_{Ilj I' l' j'; L}^J \times \frac{T_{\alpha l j}^J(E_a) \langle T_{\alpha' l' j'}^J(E_{a'}) \rangle}{\sum_{\alpha'', l'', j''} \delta_\pi(\alpha'') \langle T_{\alpha'' l'' j''}^J(E_{a''}) \rangle}, \quad (129)$$

where the Blatt-Biedenharn factor A is given by

$$\begin{aligned} A_{IljI'l'j';L}^J &= \frac{(-1)^{I'-s'-I+s}}{4\pi} (2J+1)(2j+1)(2l+1) \\ &\times (2j'+1)(2l'+1) \langle ll00|L0 \rangle \mathcal{W}(Jjj;IL) \mathcal{W}(jll;Ls) \\ &\times \langle l'l'00|L0 \rangle \mathcal{W}(Jj'Jj';I'L) \mathcal{W}(j'j'l'l';Ls'), \end{aligned} \quad (130)$$

where $(|)$ are Clebsch-Gordan coefficients and \mathcal{W} are Racah coefficients. The compound elastic scattering angular distributions are added to their direct counterparts, that are obtained from the optical model calculation. Eqs. (121) and (128-130) show that the WFC factors and the angular distribution factors depend on all the angular momentum quantum numbers involved, and thus have to be re-evaluated each time inside all the summations. We generally need these formulae for relatively low incident energy, where the WFC has a significant impact and where the compound nucleus cross section to each individual discrete state is large enough to make its angular distribution of interest. For projectile energies above several MeV (we generally take the neutron separation energy as a safe upper limit), the width fluctuations have disappeared, meaning that $W_{\alpha l j \alpha' l' j'}^J = 1$ for all channels. Then, instead of performing the full calculation for the angle-integrated compound cross section, Eq. (121) can be decoupled into two parts that represent the incoming and outgoing reaction flux, respectively. It simplifies to

$$\sigma_{\alpha \alpha'}^{comp} = \sum_{J=mod(I+s,1)}^{l_{max}+I+s} \sum_{\Pi=-1}^1 \sigma_{J\Pi}^{CF}(E^{tot}) \frac{\Gamma_{\alpha'}(E^{tot}, J, \Pi \rightarrow E_x, I', \Pi_f)}{\Gamma^{tot}(E^{tot}, J, \Pi)}, \quad (131)$$

where $\sigma_{J\Pi}^{CF}$ is the compound formation cross section per spin and parity

$$\begin{aligned} \sigma_{J\Pi}^{CF}(E^{tot}) &= D^{comp} \frac{\pi}{k^2} \frac{2J+1}{(2I+1)(2s+1)} \\ &\times \sum_{j=|J-I|}^{J+I} \sum_{l=|j-s|}^{j+s} T_{\alpha l j}^J(E_a) \delta_\pi(\alpha), \end{aligned} \quad (132)$$

which itself obeys

$$\sum_{J=mod(I+s,1)}^{l_{max}+I+s} \sum_{\Pi=-1}^1 \sigma_{J\Pi}^{CF}(E^{tot}) = D^{comp} \sigma_{reac}. \quad (133)$$

The partial decay widths are

$$\begin{aligned} \Gamma_{\alpha'}(E^{tot}, J, \Pi \rightarrow E_x, I', \Pi_f) &\frac{1}{2\pi\rho(E^{tot}, J, \Pi)} \\ &\times \sum_{j'=|J-I'|}^{J+I'} \sum_{l'=|j'-s'|}^{j'+s'} \delta_\pi(\alpha') \langle T_{\alpha' l' j'}^J(E'_a) \rangle, \end{aligned} \quad (134)$$

and the total decay width is

$$\Gamma^{tot}(E^{tot}, J, \Pi) = \sum_{\alpha''} \Gamma_{\alpha''}(E^{tot}, J, \Pi \rightarrow E_x, I'', \Pi_f), \quad (135)$$

where we sum over all possible states in the residual nuclides through the sum over α'' . Note that the term with the compound nucleus level density, $2\pi\rho$, is present in both Eq. (134) and Eq. (135) and therefore does not need to be calculated in practice for Eq. (131). A formula similar to Eq. (131) will be presented later for multiple compound emission.

F. Pre-equilibrium Model

At incident energies above about 10 MeV, a significant part of the reaction flux is emitted in the pre-equilibrium stage, *i.e.* it takes place after the first stage of the reaction but long before statistical equilibrium of the compound nucleus is attained. It is imagined that the incident particle step-by-step creates more complex states in the compound system and gradually loses its memory of the initial energy and direction. The default pre-equilibrium model of TALYS is the two-component exciton model [73, 74] which has been tested against basically all available experimental nucleon spectra for $A > 24$ [73].

1. Two-component exciton model

The basic formula for the exciton model cross section is,

$$\begin{aligned} \frac{d\sigma_k^{EM}}{dE_k} &= \sigma^{CF} \sum_{p_\pi=p_\pi^0}^{p_\pi^{eq}} \sum_{p_\nu=p_\nu^0}^{p_\nu^{eq}} W_k(p_\pi, h_\pi, p_\nu, h_\nu, E_k) \\ &\times S_{pre}(p_\pi, h_\pi, p_\nu, h_\nu), \end{aligned} \quad (136)$$

where $p_\pi(p_\nu)$ is the proton (neutron) particle number and $h_\pi(h_\nu)$ the proton (neutron) hole number, σ^{CF} is the compound formation cross section, calculated with the optical models of Section II A, and S_{pre} the time-integrated strength which determines how long the system remains in a certain exciton configuration. The initial proton and neutron particle numbers are denoted $p_\pi^0 = Z_p$, and $p_\nu^0 = N_p$ with $Z_p(N_p)$ being the proton (neutron) number of the projectile. In general, $h_\pi = p_\pi - p_\pi^0$ and $h_\nu = p_\nu - p_\nu^0$, so that the initial hole numbers are zero, *i.e.* $h_\pi^0 = h_\nu^0 = 0$, for primary pre-equilibrium emission. In Eq. (136) the equilibrium particle numbers are $p_\pi^{eq} = p_\nu^{eq} = 6$, whereas the remainder of the reaction flux is distributed through the Hauser-Feshbach model for compound nucleus reactions.

The full reaction dynamics that leads to Eq. (136) is described in [73]. We here restrict ourselves to the formulae that contain the model- and parameter-dependent quantities.

The emission rate W_k for ejectile k with spin s_k is given by

$$W_k(p_\pi, h_\pi, p_\nu, h_\nu, E_k) = \frac{2s_k + 1}{\pi^2 \hbar^3} \mu_k E_k \sigma_{k,inv}(E_k) \times \frac{\omega(p_\pi - Z_k, h_\pi, p_\nu - N_k, h_\nu, E_x)}{\omega(p_\pi, h_\pi, p_\nu, h_\nu, E^{tot})}, \quad (137)$$

where $\sigma_{k,inv}(E_k)$ is the inverse reaction cross section as calculated from the optical model and ω is the two-component particle-hole state density, for which we use the expression by Dobeš and Běták [75]

$$\omega(p_\pi, h_\pi, p_\nu, h_\nu, E_x) = \frac{g_\pi^{n_\pi} g_\nu^{n_\nu}}{p_\pi! h_\pi! p_\nu! h_\nu! (n-1)!} \times (U - A(p_\pi, h_\pi, p_\nu, h_\nu))^{n-1} f(p, h, U, V), \quad (138)$$

The finite well function $f(p, h, E_x, V)$ accounts for the fact that a hole cannot have an energy below that of the bottom of the potential well depth V . It is given by

$$f(p, h, E_x, V) = 1 + \sum_{i=1}^h (-1)^i \binom{h}{i} \left[\frac{E_x - iV}{E_x} \right]^{n-1} \times \Theta(E_x - iV), \quad (139)$$

where Θ is the unit step function. Note that f is different from 1 only for excitation energies greater than V . In the original version of Dobeš and Běták, V is given by the depth E_f of the Fermi well. This was generalized by Kalbach [39, 76] to obtain an effective method to include surface effects in the first stage of the interaction, leading to a harder pre-equilibrium spectrum. For the first stage the maximum depth of the hole should be significantly reduced, since in the surface region the potential is shallower than in the interior. This automatically leaves more energy to be adopted by the excited particle, yielding more emission at the highest outgoing energies. We use the following functional form for V in terms of the projectile energy E_p and the mass A ,

$$V = 22 + 16 \frac{E_p^4}{E_p^4 + (450/A^{1/3})^4} \text{ MeV}$$

for $h = 1$ and incident protons,

$$V = 12 + 26 \frac{E_p^4}{E_p^4 + (245/A^{1/3})^4} \text{ MeV}$$

for $h = 1$ and incident neutrons,

$$V = E_f = 38 \text{ MeV for } h > 1. \quad (140)$$

See Ref. [73] for a further justification of this parametrization. Finally, we use partial level density parameters $g_\pi = Z/15$ and $g_\nu = N/15 \text{ MeV}^{-1}$.

The (complicated) expression for S_{pre} contains the adjustable transition matrix element M^2 for each possible transition between neutron-proton exciton configurations.

We use the following expression for the matrix element,

$$M^2 = \frac{1}{A^3} \left[6.8 + \frac{4.2 \times 10^5}{(\frac{E^{tot}}{n} + 10.7)^3} \right] \text{ MeV}^2, \quad (141)$$

where the total exciton number is given by $n = p_\pi + h_\pi + p_\nu + h_\nu$.

For the two-component dynamics, the following proton-neutron ratio for the squared internal transition matrix elements was adopted to give the best overall agreement with experiment,

$$\begin{aligned} M_{\pi\pi}^2 &= R_{\pi\pi} M^2, & R_{\pi\pi} &= 1 \\ M_{\nu\nu}^2 &= R_{\nu\nu} M^2, & R_{\nu\nu} &= 1.5 \\ M_{\pi\nu}^2 &= R_{\pi\nu} M^2, & R_{\pi\nu} &= 1 \\ M_{\nu\pi}^2 &= R_{\nu\pi} M^2, & R_{\nu\pi} &= 1. \end{aligned} \quad (142)$$

2. Photon exciton model

For pre-equilibrium photon emission, we have implemented the model of Akkermans and Gruppelaar [77]. This model gives a simple but powerful simulation of the direct-semidirect capture process within the framework of the exciton model. Analogous to the particle emission rates, the continuum γ -ray emission rates may be derived from the principle of detailed balance or microscopic reversibility, assuming that only $E1$ -transitions contribute. In a two-component picture, this yields

$$\begin{aligned} W_\gamma(p_\pi, h_\pi, p_\nu, h_\nu, E_\gamma) &= R_\gamma \frac{E_\gamma^2}{\pi^2 \hbar^3 c^2} \\ &\times \frac{\sigma_{\gamma,abs}(E_\gamma)}{\omega(p_\pi, h_\pi, p_\nu, h_\nu, E^{tot})} \\ &\times \left(\frac{g^2 E_\gamma \frac{1}{2} \omega(p_\pi - 1, h_\pi - 1, p_\nu, h_\nu, E_x - E_\gamma)}{g(n-2) + g^2 E_\gamma} \right. \\ &+ \frac{g^2 E_\gamma \frac{1}{2} \omega(p_\pi, h_\pi, p_\nu - 1, h_\nu - 1, E_x - E_\gamma)}{g(n-2) + g^2 E_\gamma} \\ &\left. + \frac{gn\omega(p_\pi, h_\pi, p_\nu, h_\nu, E_x - E_\gamma)}{gn + g^2 E_\gamma} \right), \quad (143) \end{aligned}$$

where $\sigma_{\gamma,abs}(E_\gamma)$ is the photon absorption cross section and R_γ is an adjustable parameter.

3. Continuum stripping, pick-up, break-up and knock-out reactions

For pre-equilibrium reactions involving deuterons, tritons, Helium-3 and alpha particles, a contribution from the exciton model is automatically calculated with the formalism of the previous subsections. It is however well-known that for nuclear reactions involving projectiles and ejectiles with different particle numbers, mechanisms like stripping, pick-up, break-up and knock-out play an important role and these direct-like reactions are not covered by the exciton model. Therefore, Kalbach [78] developed a phenomenological contribution for these mechanisms, which we have included in TALYS. In total, the pre-equilibrium cross section for these reactions is given by the sum of an exciton model (EM), nucleon transfer (NT), knock-out (KO), and break-up (BU) contribution

$$\frac{d\sigma_k^{\text{PE}}}{dE_k} = \frac{d\sigma_k^{\text{EM}}}{dE_k} + \frac{d\sigma_k^{\text{NT}}}{dE_k} + \frac{d\sigma_k^{\text{KO}}}{dE_k} + \frac{d\sigma_k^{\text{BU}}}{dE_k}, \quad (144)$$

where the contribution from the exciton model was outlined in the previous subsection. It should be mentioned that the predictive power of these phenomenological models is not as good as that for nucleons. A lot of parameter-specific adjustment is often necessary to fit available experimental data. In the empirical expressions below, all energies are in MeV.

a. Transfer reactions The general differential cross section formula for a nucleon transfer reaction of the type $A(a,b)B$ is

$$\begin{aligned} \frac{d\sigma_{a,b}^{\text{NT}}}{dE_b} &= C_{\text{strip}} \frac{2s_b + 1}{2s_a + 1} \frac{A_b}{A_a} \frac{E_b \sigma_{b,\text{inv}}(E_b)}{A_a} K \\ &\times \left(\frac{A_a}{E_a + V_a} \right)^{2n} \left(\frac{C_a}{A_B} \right)^n N_a \left(\frac{2Z_A}{A_A} \right)^{2(Z_a+2)h_\pi+2p_\nu} \\ &\times \omega_{\text{NT}}(p_\pi, h_\pi, p_\nu, h_\nu, U), \end{aligned} \quad (145)$$

where

$$\begin{aligned} C_a &= 5500 \text{ for incident neutrons,} \\ &= 3800 \text{ for incident charged particles,} \end{aligned} \quad (146)$$

$$\begin{aligned} N_a &= \frac{1}{80E_a} \text{ for pickup,} \\ &= \frac{1}{580\sqrt{E_a}} \text{ for stripping,} \\ &= \frac{1}{1160\sqrt{E_a}} \text{ for exchange.} \end{aligned} \quad (147)$$

K is an enhancement factor taking into account the fact that d , t and ${}^3\text{He}$ are loosely bound

$$\begin{aligned} K &= 12 \text{ for } (N, \alpha), \\ &= 12 - 11 \frac{E_a - 20}{E_a} \text{ for } (\alpha, N) \text{ and } E_a > 20, \\ &= 1 \text{ otherwise,} \end{aligned} \quad (148)$$

where N stands for either neutron or proton. The well depth V_a is set at

$$V_a = 12.5A_a \text{ MeV,} \quad (149)$$

and represents the average potential drop seen by the projectile between infinity and the Fermi level. The possible degrees of freedom for the reaction are all included in the residual state density $\omega_{\text{NT}}(p_\pi, h_\pi, p_\nu, h_\nu, U)$. Since we do not use this model to describe exchange reactions in inelastic scattering, there is no need to sum the various terms of Eq. (145) over p_π , as in Ref. [78]. The exciton numbers are automatically determined by the transfer reaction, *i.e.* $n = |A_a - A_b|$, $n_\pi = h_\pi = |Z_a - Z_b|$, $n_\nu = h_\nu = |N_a - N_b|$, $p_\pi = p_\nu = 0$. The accessible state density that is directly determined by the reaction is $\omega(p_\pi, h_\pi, p_\nu, h_\nu, U)$, given by Eq. (138). The total residual state density however also takes into account more complex configurations that can be excited by the transfer reaction. It is given by

$$\begin{aligned} \omega_{\text{NT}}(p_\pi, h_\pi, p_\nu, h_\nu, U) &= \\ &\sum_{i=0}^3 \sum_{j=0}^{3-i} (X_{\text{NT}})^{i+j} \omega(p_\pi + i, h_\pi + i, p_\nu + j, h_\nu + j, U) \\ &+ \sum_{i=0}^{p_\pi} \sum_{j=0}^{h_\pi} \sum_{k=0}^{p_\nu} \sum_{l=0}^{h_\nu} \omega(p_\pi - i, h_\pi - j, p_\nu - k, h_\nu - l, U) \\ &\times \Theta(i + j + k + l - \frac{1}{2}), \end{aligned} \quad (150)$$

The first term allows that up to three particle-hole pairs can be excited in a transfer reaction. The factor X_{NT} represents the probability for exciting such a pair and is given by

$$X_{\text{NT}} = \frac{7\sqrt{E_a/A_a}}{V_1 A_A^2} (p_\nu^2 + p_\pi^2 + h_\nu^2 + 1.5h_\pi^2). \quad (151)$$

For neutrons and protons we adopt for V_1 the value given by Eq.(140), for deuterons and tritons we take $V_1=17$ MeV, and for Helium-3 and alpha particles we take $V_1=25$ MeV. The finite well depth correction for Eq. (150) are made using a well depth of

$$\begin{aligned} V &= V_1 \left(\frac{2Z}{A} \right) \text{ if } n_\pi = 0 \\ &= V_1 \text{ otherwise.} \end{aligned} \quad (152)$$

The second term of Eq. (150) allows for transfer of nucleons at the Fermi level. Here, the Heaviside function is merely used to avoid double counting of $\omega(p_\pi, h_\pi, p_\nu, h_\nu, U)$.

b. *Knockout reactions* For $(\text{nucleon}, \alpha)$ reactions a knockout contribution is added. The general differential cross section formula for a knockout reaction of the type $A(a, b)B$ is

$$\frac{d\sigma_{a,b}^{KO}}{dE_b} = C_{knock} \frac{\sigma_{a,inv}(E_a)}{14} (2s_b + 1) A_b E_b \sigma_{b,inv}(E_b) \times \frac{P_b g_a g_b [U - A_{KO}(p_a, h_b)]}{\sum_{c=a,b} (2s_c + 1) A_c \langle \sigma_c \rangle (E_m + 2B_c)(E_m - B_c)^2 \frac{g_a g_b^2}{6g_c}}, \quad (153)$$

where P_b is the probability of exciting a b -type particle-hole pair, E_m is the maximum emission energy, and B_c is the Coulomb barrier for a particle c . The average inverse cross section $\langle \sigma_c \rangle$ is given by

$$\langle \sigma_c \rangle = \int_{B_{coul,c}}^{E_{max}} dE \sigma_c(E). \quad (154)$$

For the knockout model, the single-particle state density parameters for the cluster degrees of freedom g represent the number of cluster states per unit energy. The relevant values are given by

$$g_n = N/13, \quad g_p = Z/13, \quad g_\alpha = A/208 \text{ MeV}^{-1}. \quad (155)$$

The Pauli correction factor A_{KO} is given by

$$A_{KO}(p_a, h_b) = \frac{1}{2g_a^2} - \frac{1}{2g_b^2}. \quad (156)$$

The probabilities for exciting the various particle-hole pairs are

$$\begin{aligned} P_n &= \frac{N_A - \phi Z_A}{A_A - 2\phi Z_A + \phi Z_A/2} \\ P_p &= \frac{Z_A - \phi Z_A}{A_A - 2\phi Z_A + \phi Z_A/2} \\ P_\alpha &= \frac{\phi Z_A/2}{A_A - 2\phi Z_A + \phi Z_A/2}. \end{aligned} \quad (157)$$

The factors ϕ are a kind of pre-formation parameters [78]. The following values are adopted

$$\begin{aligned} N_A \leq 116 : \phi &= 0.08 \\ 116 \leq N_A < 126 : \phi &= 0.02 + 0.06(126 - N_A)/10 \\ 126 \leq N_A < 129 : \phi &= 0.02 + 0.06(N_A - 126)/3 \\ 129 \leq N_A : \phi &= 0.08. \end{aligned} \quad (158)$$

c. *Break-up reactions* For reactions induced by complex particles, break-up may play an important role. This holds especially for weakly bound projectiles like deuterons. Break-up is here defined as having a projectile fragment emerge from the reaction in a relatively narrow peak centered close to the beam velocity and strongly directed toward forward angles. For deuterons only, a simple model by Kalbach has been included [79]. This leads to an extra contribution in the (d,n) and (d,p) channels.

The centroid energy of the breakup peak, in MeV, is given by

$$\epsilon_0 = \frac{A_b}{A_a} \left(\epsilon_a - B_{a,b} - \frac{Z_a Z_A}{9.5} \right) + \frac{Z_b Z_B}{9.5}, \quad (159)$$

where ϵ_a represents the channel energy (the energy of both the emitted particle and the recoiling nucleus in the center of mass), and $B_{a,b}$ is the binding energy in the projectile for the indicated breakup channel (2.224 MeV for deuterons). The peak is assumed to be described by a Gaussian line shape with a width parameter of

$$\Gamma = 1.15 + 0.12 E_a - \frac{A_A}{140}, \quad (160)$$

where E_a is the laboratory energy of the incident deuteron, and the width parameter is given in MeV. The break-up cross section is assumed to be

$$\sigma_{BU} = K_{d,b} \frac{(A_A^{1/3} + 0.8)^2}{1 + \exp(\frac{13-E_a}{6})}, \quad (161)$$

where the normalization factors are

$$\begin{aligned} K_{d,n} &= 18, \\ K_{d,p} &= 21. \end{aligned} \quad (162)$$

Finally, the differential break-up cross section is given by

$$\frac{d\sigma_{a,b}^{BU}}{dE_b} = C_{break} \sigma_{BU} \frac{1}{\Gamma \sqrt{2\pi}} \exp\left(-\frac{(\epsilon_0 - E_b)^2}{\Gamma^2}\right). \quad (163)$$

The stripping/pick-up, break-up and knock-out contributions can be adjusted with the C_{strip} , C_{break} and C_{knock} parameters, (default 1) respectively, see also Table III.

4. Pre-equilibrium angular distributions

Semi-classical models, such as the exciton model, have always had some problems to describe angular distributions (essentially because it is based on a compound-like concept instead of a direct one). A powerful phenomenological method is given by Kalbach [80]. It is

based on experimental information only and the insight that in general, a pre-equilibrium process consists of a forward peaked part (multi-step direct) and an isotropic part (multi-step compound), and that the angular distributions are fairly structureless and all look alike. The Kalbach formula for the double-differential cross section for a projectile a and an ejectile b is

$$\frac{d^2\sigma_{a,xb}}{dE_b d\Omega} = \frac{1}{4\pi} \left[\frac{d\sigma^{\text{PE}}}{dE_b} + \frac{d\sigma^{\text{comp}}}{dE_b} \right] \frac{a}{\sinh(a)} \\ \times [\cosh(a \cos \Theta) + f_{MSD}(E_b) \sinh(a \cos \Theta)], \quad (164)$$

where $\frac{d\sigma^{\text{PE}}}{dE_b}$ and $\frac{d\sigma^{\text{comp}}}{dE_b}$ are the angle-integrated pre-equilibrium and compound spectra, respectively, and f_{MSD} is the so-called multi-step direct or pre-equilibrium ratio

$$f_{MSD}(E_b) = \frac{d\sigma^{\text{PE}}}{dE_b} / \left[\frac{d\sigma^{\text{PE}}}{dE_b} + \frac{d\sigma^{\text{comp}}}{dE_b} \right], \quad (165)$$

which thus increases from practically 0 at very low emission energy to 1 at the highest emission energies. Hence, once the angle-integrated spectra are known, the parameter a determines the angular distribution. The parametrization of a is given in [80].

Since we calculate the pre-equilibrium and compound cross sections explicitly (and actually only use f_{MSD} for ENDF-6 data libraries), Eq. (164) can be reduced to a formula for the double-differential pre-equilibrium cross section

$$\frac{d^2\sigma_{a,xb}^{\text{PE}}}{dE_b d\Omega} = \frac{1}{4\pi} \frac{d\sigma^{\text{PE}}}{dE_b} \frac{a}{\sinh(a)} \exp(a \cos \Theta), \quad (166)$$

to which the isotropic compound angular distribution can be added. In sum, given the angle-integrated spectrum $\frac{d\sigma^{\text{PE}}}{dE_b}$ by some physics model, the double-differential cross section is returned quite simply and reasonably accurate by Eq. (166).

5. Parameter uncertainties

The global uncertainties we assign to pre-equilibrium parameters are given in Table III. Also here, these global uncertainties stem from a comparison of scattered random TALYS curves with experimental data for the whole nuclide chart. Note that for the partial level density parameters the same mass-dependent trend as for the total level density parameter a is adopted. The complex-particle parameters C_{strip} , C_{break} and C_{knock} , have rather large uncertainties, which is an effective way to take the shortcomings of the corresponding models into account. This can be seen in Fig. 6 where the resulting (n, α) uncertainty band is rather wide.

G. Multiple Emission

At incident energies above approximately 7-10 MeV (the neutron separation energy), the residual nuclides formed after the first binary reaction are left with enough excitation energy to enable further decay by particle emission. This is called multiple emission. We distinguish between two mechanisms: multiple Hauser-Feshbach (compound) decay and multiple pre-equilibrium decay.

1. Multiple Hauser-Feshbach decay

This is the conventional way, and for incident energies up to several tens of MeV sufficient, to treat multiple emission. For these energies, it can be assumed that pre-equilibrium processes only take place in the binary reaction and that secondary and further particles are emitted by compound emission.

After the binary reaction, the residual nucleus may be left in an excited discrete state i' or an excited state within a bin i' which is characterized by excitation energy $E'_x(i')$, spin I' and parity Π' . The population of this state or set of states is given by a probability distribution for Hauser-Feshbach decay P^{HF} that is completely determined by the binary reaction mechanism. For a binary neutron-induced reaction to a discrete state i' , i.e. when $E'_x(i')$, I' and Π' have unique values, the residual population is given by

$$P^{\text{HF}}(Z', N', E'_x(i'), I', \Pi') = \\ \sigma_{n,k'}^{i'}(E'^{\text{tot}}, I, \Pi \rightarrow E'_x(i'), I', \Pi'), \quad (167)$$

where $\sigma_{n,k'}^{i'}$ is the neutron-induced non-elastic reaction cross section for a discrete state, and where the ejectile k' connects the initial compound nucleus (Z_C, N_C) and the residual nucleus (Z', N') . For binary reactions to the continuum, the residual population of states characterized by (I', Π') per $E'_x(i')$ bin is given by the sum of a pre-equilibrium and a compound contribution

$$P^{\text{HF}}(Z', N', E'_x(i'), I', \Pi') = \int dE_{k'} \frac{d\sigma^{\text{comp,cont}}}{dE_{k'}} \\ (E'^{\text{tot}}, I, \Pi \rightarrow E'_x(i'), I', \Pi') + \mathcal{P}^{\text{pre}}(Z', N', p_{\pi}^{\max} + 1, \\ h_{\pi}^{\max} + 1, p_{\nu}^{\max} + 1, h_{\nu}^{\max} + 1, E'_x(i')), \quad (168)$$

where the integration range over $dE_{k'}$ corresponds exactly with the bin width of $E'_x(i')$, $d\sigma^{\text{comp,cont}}/dE_{k'}$ is the binary compound cross section to the continuum, and \mathcal{P}^{pre} denotes the population entering the compound stage after primary preequilibrium emission. The expression for \mathcal{P}^{pre} will be given by Eq. (172) below.

Once the first generation of residual nuclides/states has been filled, the picture can be generalized to tertiary

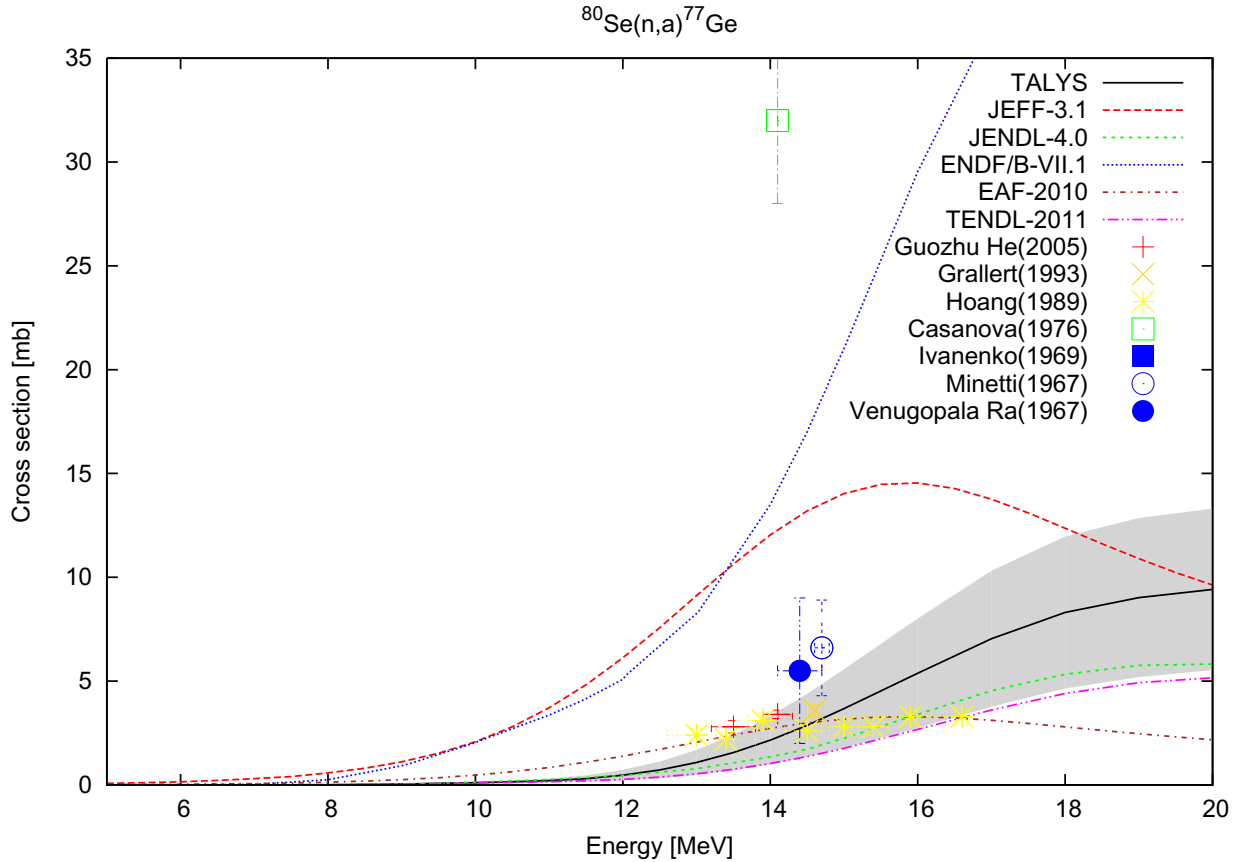


FIG. 6: TALYS uncertainty band of $^{80}\text{Se}(n,\alpha)$ cross section due to uncertainty of stripping and knockout parameters, compared with experimental data and nuclear data libraries.

and higher order multiple emission. In general, the population P^{HF} before decay of a level i' or a set of states $(I', \Pi', E_{x'}(i'))$ in bin i' of a nucleus (Z', N') in the reaction chain is proportional to the feeding, through the ejectiles k' , from all possible mother bins i with an energy $E_x(i)$ in the (Z, N) nuclides, *i.e.*

$$\begin{aligned} P^{\text{HF}}(Z', N', E_{x'}(i'), I', \Pi') &= \sum_{I, \Pi} \sum_{k'} \sum_i \\ &[P^{\text{HF}}(Z, N, E_x(i), I, \Pi) \\ &+ \mathcal{P}^{\text{pre}}(Z, N, p_\pi^{\max} + 1, h_\pi^{\max} + 1, p_\nu^{\max} + 1, \\ &h_\nu^{\max} + 1, E_x(i))] \frac{\Gamma_{k'}(E_x(i), I, \Pi \rightarrow E_{x'}(i'), I', \Pi')}{\Gamma^{\text{tot}}(E_x(i), I, \Pi)}. \end{aligned} \quad (169)$$

The appearance of the indices p_π^{\max} indicates that only the reaction population that has not been emitted via the (multiple) pre-equilibrium mechanism propagates to the multiple compound stage. Similar to Eq. (134) the

decay widths are given by

$$\begin{aligned} \Gamma_{k'}(E_x(i), I, \Pi \rightarrow E_{x'}(i'), I', \Pi') &= \frac{1}{2\pi\rho(E_x(i), I, \Pi)} \\ &\sum_{j'=|J-I'|}^{J+I'} \sum_{l'=|j'-s'|}^{j'+s'} \delta_\pi(\alpha') \langle T_{\alpha' l' j'}^J(E_{a'}') \rangle. \end{aligned} \quad (170)$$

The total decay width is

$$\begin{aligned} \Gamma^{\text{tot}}(E_x(i), I, \Pi) &= \sum_{k''} \sum_{I''=\text{mod}(J+s, 1)}^{J+l_{\max}} \sum_{\Pi''=-1}^1 \sum_{i''} \\ &\Gamma_{k''}(E_x(i), I, \Pi \rightarrow E_{x''}(i''), I'', \Pi''). \end{aligned} \quad (171)$$

Similar to the formula for binary emission, the term $2\pi\rho$ (compound nucleus level density) of the decay width of Eq.(170) falls out of the multiple emission expression of Eq.(169) and therefore does not need to be calculated in practice. In sum, the only differences between binary and multiple compound emission are that width fluctuations and angular distributions do not enter the model

and that the initial compound nucleus energy, E^{tot} , is replaced by an excitation energy bin E_x of the mother nucleus. With this scheme, TALYS follows all reaction chains until all emission channels are closed, while the spectra of all emitted particles that are produced along the chain are recorded in the appropriate arrays.

2. Multiple pre-equilibrium emission

If the residual nucleus has a high excitation energy, resulting from a binary reaction with a high incident energy, this nucleus is far from equilibrated and it should be described by more degrees of freedom than just E_x , J and Π . In general, we need to keep track of the particle-hole configurations that are excited throughout the reaction chain and thereby calculate multiple pre-equilibrium emission up to any order within the exciton model. The mechanism for multiple pre-equilibrium emission up to the second order has been outlined in various papers [81]-[84].

We introduce the pre-equilibrium population $\mathcal{P}^{pre}(Z, N, p_\pi, h_\pi, p_\nu, h_\nu, E_x(i))$ which holds the amount of the reaction population present in a unique (Z, N) nucleus, $(p_\pi, h_\pi, p_\nu, h_\nu)$ exciton state and excitation energy bin $E_x(i)$. A special case is the pre-equilibrium population for a particular exciton state after binary emission, which can be written as

$$\begin{aligned} \mathcal{P}^{pre}(Z', N', p_\pi - Z_{k'}, h_\pi, p_\nu - N_{k'}, h_\nu, E_{x'}(i')) = \\ \sigma^{CF}(Z_C, N_C, E^{tot}) W_{k'}(Z_C, N_C, E^{tot}, p_\pi, h_\pi, p_\nu, h_\nu, E_{k'}) \\ \times S^{pre}(Z_C, N_C, E^{tot}, p_\pi, h_\pi, p_\nu, h_\nu), \end{aligned} \quad (172)$$

where $Z_{k'}$ ($N_{k'}$) corresponds to the ejectile charge (neutron) number. The residual excitation energy $E_{x'}(i')$ is linked to the total energy E^{tot} , the ejectile energy $E_{k'}$, and its separation energy $S(k')$ by $E_{x'}(i') = E^{tot} - E_{k'} - S(k')$. This \mathcal{P}^{pre} represents the feeding term for secondary pre-equilibrium emission. Note that for several particle-hole configurations this population is equal to zero.

In general, the pre-equilibrium population can be expressed in terms of the mother nucleus, excitation energy bins, and particle-hole configurations from which it is fed. The residual population is given by a generalization of Eq. (136), in which $\sigma^{CF}(Z_C, N_C, E^{tot})$ is replaced by the population of the particle-hole states left after the previous emission stage $\mathcal{P}^{pre}(Z, N, p_\pi^0, h_\pi^0, p_\nu^0, h_\nu^0, E_x(i))$. Since several combinations of emission and internal transitions may lead to the same configuration, a summation is applied over the ejectiles treated in multiple pre-equilibrium (neutrons and protons), over the $(p_\pi^0, h_\pi^0, p_\nu^0, h_\nu^0)$ configurations with which the next step

is started and over the mother excitation energy bins

$$\begin{aligned} \mathcal{P}^{pre}(Z', N', p'_\pi, h'_\pi, p'_\nu, h'_\nu, E_{x'}(i')) = & \sum_{k'=n,p} \sum_{p_\pi^0=1}^{p_\pi^{\max}} \sum_{h_\pi^0=1}^{h_\pi^{\max}} \\ & \sum_{p_\nu^0=1}^{p_\nu^{\max}} \sum_{h_\nu^0=1}^{h_\nu^{\max}} \sum_i \mathcal{P}^{pre}(Z, N, p_\pi^0, h_\pi^0, p_\nu^0, h_\nu^0, E_x(i)) \\ & \times W_k(Z, N, p_\pi, h_\pi, p_\nu, h_\nu, E_x(i), E_{k'}) \\ & \times S^{pre}(Z, N, p_\pi, h_\pi, p_\nu, h_\nu, E_x(i)), \end{aligned} \quad (173)$$

where the mother and daughter quantities are related by

$$\begin{aligned} Z &= Z' + Z_{k'}, \\ N &= N' + N_{k'}, \\ p_\pi &= p'_\pi + Z_{k'}, \\ h_\pi &= h'_\pi, \\ p_\nu &= p'_\nu + N_{k'}, \\ h_\nu &= h'_\nu, \\ E_x &= E_{x'}(i') + E_{k'} + S_{k'}. \end{aligned} \quad (174)$$

We thus need to keep track of every possible $(Z', N', p'_\pi, h'_\pi, p'_\nu, h'_\nu, E_{x'}(i'))$ configuration, which is uniquely linked to $(Z, N, p_\pi, h_\pi, p_\nu, h_\nu, E_x(i))$ mother exciton state through the ejectile characterized by $(Z_{k'}, N_{k'}, E_{k'})$. The term $P(Z, N, p_\pi, h_\pi, p_\nu, h_\nu, E_x(i))$ represents the part of the pre-equilibrium cross section that starts in $(Z, N, p_\pi^0, h_\pi^0, p_\nu^0, h_\nu^0, E_x(i))$ and survives emission up to a new particle-hole state $(Z, N, p_\pi, h_\pi, p_\nu, h_\nu, E_x(i))$.

The part of \mathcal{P}^{pre} that does not feed a new multiple pre-equilibrium population automatically goes to the multiple Hauser-Feshbach chain of Eq. (169).

The final expression for the multiple pre-equilibrium spectrum is

$$\begin{aligned} \frac{d\sigma_k^{MPE}}{dE_{k'}} = & \sum_{p_\pi^0=1}^{p_\pi^{\max}} \sum_{h_\pi^0=1}^{h_\pi^{\max}} \sum_{p_\nu^0=1}^{p_\nu^{\max}} \sum_{h_\nu^0=1}^{h_\nu^{\max}} \\ & \sum_i \mathcal{P}^{pre}(Z, N, p_\pi^0, h_\pi^0, p_\nu^0, h_\nu^0, E_x(i)) \sum_{p_\pi=p_\pi^0}^{p_\pi^{\max}} \sum_{h_\pi=h_\pi^0}^{h_\pi^{\max}} \\ & \sum_{p_\nu=p_\nu^0}^{p_\nu^{\max}} \sum_{h_\nu=h_\nu^0}^{h_\nu^{\max}} W_k(Z, N, p_\pi, h_\pi, p_\nu, h_\nu, E_x(i), E_{k'}) \\ & \times S^{pre}(Z, N, p_\pi, h_\pi, p_\nu, h_\nu, E_x(i)). \end{aligned} \quad (175)$$

H. Nuclear Structure and Model Parameters

The nuclear structure and model parameter database in TALYS comes for a large part of the Reference Input

Parameter Library RIPL [26]. The RIPL database, a result of various IAEA Coordinated Research Programs, gives nuclear model developers a tremendous head start. They can mostly focus on the implementation of reaction mechanisms, while the input parameters for this have been made available through RIPL in a easily accessible format.

First of all, TALYS uses the experimental values of the Audi Wapstra table (2003) [85] for nuclear masses by default. When no experimental values are available, Goriely's mass table based on HFB calculations with the Skyrme force [86] is adopted. The latter table also provides the ground state deformation parameters β_2 and β_4 . We note that for reaction Q-values one needs the masses of two nuclides. If for only one of them the experimental mass is known, we take the two *theoretical* mass excesses to calculate the Q-value, for consistency. This only occurs for nuclides far from the line of stability.

The discrete level file is based on that of Belgya, as produced for the RIPL database. For exotic nuclides, the ground state properties as determined from HFB calculations have been added. Also, missing spins, parities and branching ratios have been estimated from simple spin distribution principles, to avoid any flux conservation problems in gamma decay.

A unique feature of the database of TALYS is that it includes coupling schemes for coupled channels calculations for all nuclides. Together with the deformation parameters of the mass database, this enables automatic direct reaction calculations for deformed nuclides. The level of complexity of rotational or vibrational-rotational calculations can be specified by the user. For example, the vibration-rotational model is thus invoked if within the rotational model also states belonging to a vibrational band are specified (for ^{238}U this may add up to a coupling scheme of 23 levels).

Level density parameters are provided for the Constant Temperature model, the Fermi Gas model, the Generalized Superfluid model, as well as for tabulated microscopic level densities. All parameters have been adjusted simultaneously to the discrete level database and average neutron resonance spacings, and are equal to those reported in Ref. [47]. For the microscopic level densities, also level densities for fission barriers are tabulated. The average neutron resonance spacings, strength functions and experimental total radiative widths come directly from the RIPL database.

The Giant Dipole Resonance (GDR) parameters, needed for gamma-ray strength functions, come directly from RIPL database. In addition, tabulated microscopic gamma ray strength functions [87] are stored for thousands of nuclides, calculated according to Hartree-Fock BCS and QRPA theory.

Neutron and proton optical model parameters are stored for the KD03 potential, as well as a disper-

sive variant of KD03. For the calculation of the JLM OMP, both Goriely and Hilaire have provided radial matter densities from the proton dripline to the neutron dripline.

For fission, the various options for fission barriers and widths have already been discussed in Section II D. In addition, head band transition and class II states for even-even, even-odd, odd-odd, and odd-even nuclides are stored in tables. For fission transmission coefficients calculated with the WKB approximation, potential energy curves are stored. Finally, for the calculation of fission yields with the Brosa model, parameters that fix the precession shape of the nucleus in each fission mode are provided, as well as temperature-dependent fission barrier parameters per fission mode.

I. Astrophysical Reaction Rates

All nuclear models described so far are important for technological applications, and the rest of this paper will concern those applications. However, for completeness we wish to mention that a complete calculation of astrophysical reaction rates is also possible with TALYS. Moreover, astro-relevant capture measurements, at *e.g.* 30 keV, are also important for nuclear model and parameter validation: the same cross sections are often important in *e.g.* analyses on inventories of fission products.

In stellar interiors, nuclides not only exist in their ground states but also in different thermally excited states and a thermodynamic equilibrium holds locally to a very good approximation. Therefore, most of nuclear astrophysics calculations have made use of nuclear reaction rates evaluated within the statistical model [89]. The assumption of a thermodynamic equilibrium combined with the compound nucleus cross sections for the various excited states then allows to produce Maxwellian-averaged reaction rates, which is important input for stellar evolution models. Calculation of stellar reaction rates is obviously not new, but TALYS provides some features which automatically makes the extension to reaction rate calculations very worthwhile. In contrast with existing dedicated astrophysical reaction rate codes, TALYS provides the inclusion of the pre-equilibrium reaction mechanism (which even for low energies may be significant for nuclides far from stability[88]), the detailed competition between all open channels, the inclusion of multi-particle emission (neglected in most astrophysics codes), the inclusion of detailed width fluctuation corrections, the inclusion of parity-dependent level densities, the inclusion of coupled channel description for deformed nuclei, and the coherent inclusion of fission channel. Different prescriptions are also used when normalizing nuclear models on available experimental data, such as level densities on s-wave spacings or E1 resonance

strength on photoabsorption data.

The energies of both the targets and projectiles, as well as their relative energies E , obey Maxwell-Boltzmann distributions corresponding to the temperature T at that location (or a black-body Planck spectrum for photons). The astrophysical rate is obtained by integrating the cross section given by Eq. (121) over a Maxwell-Boltzmann distribution of energies E at the given temperature T . In addition, in hot astrophysical plasmas, a target nucleus exists in its ground as well as excited states. In a thermodynamic equilibrium situation, the relative populations of the various levels of nucleus with spins I^μ and excitation energies E_x^μ obey a Maxwell-Boltzmann distribution. Hence, in the formulae to follow, it is understood that the definition of the incident α channel, see below Eq. (121), now includes an explicit superscript μ to distinguish between the excited states. The effective stellar rate of $\alpha \rightarrow \alpha'$ in the entrance channel at temperature T taking due account of the contributions of the various target excited states is finally expressed as

$$N_A \langle \sigma v \rangle_{\alpha\alpha'}^*(T) = \left(\frac{8}{\pi m} \right)^{1/2} \frac{N_A}{(kT)^{3/2} G(T)} \int_0^\infty dE \sum_\mu \frac{(2I^\mu + 1)}{(2I^0 + 1)} \sigma_{\alpha\alpha'}^\mu(E) E \exp\left(-\frac{E + E_x^\mu}{kT}\right), \quad (176)$$

where k is the Boltzmann constant, m the reduced mass of the α channel, N_A the Avogadro number, and

$$G(T) = \sum_\mu (2I^\mu + 1)/(2I^0 + 1) \exp(-E_x^\mu/kT), \quad (177)$$

the T -dependent normalized partition function. Inverse reactions can also be estimated making use of the reciprocity theorem [89]. In particular, the stellar photodissociation rates are classically derived from the radiative capture rates by

$$\lambda_{(\gamma,\alpha)}^*(T) = \frac{(2I + 1)(2j + 1)}{(2I' + 1)} \frac{G_I(T)}{G_{I'}(T)} \left(\frac{AA_a}{A'} \right)^{3/2} \times \left(\frac{kT}{2\pi\hbar^2 N_A} \right)^{3/2} N_A \langle \sigma v \rangle_{(\alpha,\gamma)}^* e^{-Q_{\alpha\gamma}/kT}, \quad (178)$$

where $Q_{\alpha\gamma}$ is the Q-value of the $I^0(\alpha, \gamma)I'^0$ capture channel. Note that, in stellar conditions, the reaction rates for targets in thermal equilibrium are usually believed to obey reciprocity since the forward and inverse channels are symmetrical, in contrast to the situation which would be encountered for targets in their ground states only [89]. In TALYS, the total stellar photodissociation

rate is determined from

$$\lambda_{(\gamma,j)}^*(T) = \frac{\sum_\mu (2J^\mu + 1) \lambda_{(\gamma,\alpha)}^\mu(T) \exp(-E_x^\mu/kT)}{\sum_\mu (2J^\mu + 1) \exp(-E_x^\mu/kT)}, \quad (179)$$

where the photodissociation rate $\lambda_{(\gamma,\alpha)}^\mu$ of state μ with excitation energy E_x^μ is given by

$$\lambda_{(\gamma,\alpha)}^\mu(T) = \int_0^\infty c n_\gamma(E, T) \sigma_{(\gamma,\alpha)}^\mu(E) dE, \quad (180)$$

where c is the speed of light, $\sigma_{(\gamma,j)}^\mu(E)$ the photodisintegration cross section at energy E , and n_γ the stellar γ -ray distribution well described by the back-body Planck spectrum at the given temperature T .

III. UNCERTAINTIES OF BASIC NUCLEAR DATA

The assessment of uncertainties in nuclear reaction data is important for both basic physics and technological applications. First, it defines the current quality of both experimental and theoretical nuclear reaction physics. Experimental uncertainties represent a sort of limit of the current-day precision with which we can measure a particular observable (the fact that these uncertainties have a systematical and a statistical component requires a discussion on its own). Theoretical uncertainties would represent the extent to which we are (un)able to cast nature into models and their associated parameters. Second, nuclear reaction data, such as cross sections, resonance parameters, energy spectra and angular distributions are of prime importance to the computational simulation of nuclear installations. A reliable assessment of the uncertainties in calculated integral reactor parameters depends directly on the uncertainties of the underlying nuclear data. To make the most impact for design calculations, nuclear data libraries should include uncertainty information. Starting from the covariance matrices of the basic nuclear data, error propagation in transport, reactor, activation,*etc.* codes enables to estimate the uncertainties of calculated design parameters, which has a profound impact on issues of general concern such as safety and economy.

An often heard complaint is that covariance nuclear data are scarce, and also that the covariance evaluation process can be rather complex and time-consuming. While the good habit of delivering error bars is followed by almost all experimental nuclear physicists, theoreticians seldom provide uncertainties, let alone a full covariance matrix, with their results. There is actually no excuse for that: as long as: (a) an exact description of the strong interaction, and (b) the exact solution for the many-body problem, have not been developed

we know that model-predicted nuclear data have only one certainty: they are imprecise. The first step is thus to quantify such limitations into numerical uncertainties. With the help of the TALYS nuclear model code and the current-day computer power, it is now possible to do something about this. We note that the basic ideas of our approach have first been outlined by Smith [90], and we have implemented his ideas in a code called TASMAN, which is part of the total evaluation system that we discuss in the next Section, to show that the method is actually feasible. The essential idea is to assume that each nuclear model parameter has its own uncertainty. TALYS is run many times, whereby each time all elements of the input parameter vector are *randomly* sampled from a normal or uniform distribution, centered around either a default value or a value adjusted to experiment, with a specific width for each parameter. This provides a lot of statistical information, such as exact uncertainty distributions, and after averaging the results also variances and a full covariance matrix, see the formalism below. It should be noted that uncertainties, or rather defects, of the nuclear models themselves are not (yet) included in this approach. This method can directly be applied to all non-elastic channels and their associated nuclear model parameters such as total and partial level density parameters, fission barrier parameters, gamma-ray strength functions and pre-equilibrium parameters. The basic objective behind the construction of TASMAN is to facilitate all this. The *default* uncertainties used for the nuclear model parameters of TALYS have already been discussed in the previous Section and are given in Table III.

A. Uncertainties of Nuclear Model Parameters

A short, simple mathematical formalism will suffice to explain the method of covariance generation from random model parameters. Often, a nuclear model calculation is performed with various model parameters p_1, p_2, \dots , of which some are adjusted to obtain the optimal description of experimental data. An input file may for example contain the optical model parameters $p_1 = r_v$ (real central radius), $p_2 = a_v$ (real central diffuseness), etc., followed by the level density parameters and so on. Let \mathbf{p} be the vector of the L adjustable nuclear model parameters that are relevant to the problem under consideration, *i.e.*

$$\mathbf{p} = \{p_1, \dots, p_l, \dots, p_L\}. \quad (181)$$

In practice L may take on values from one up to several tens, or even hundreds. The case of many adjustable parameters occurs *e.g.* for complete optical model studies or when many residual nuclides, each characterized

by their own set of parameters (level density, *etc.*), are involved in a calculation. Next, let $\boldsymbol{\sigma}$ be a vector of N calculated quantities,

$$\boldsymbol{\sigma} = \{\sigma_1, \dots, \sigma_i, \dots, \sigma_N\}. \quad (182)$$

The obvious choice for the elements of $\boldsymbol{\sigma}$ are cross sections, and we will indeed generally use the term “cross sections” for $\boldsymbol{\sigma}$. It should however be understood that $\boldsymbol{\sigma}$ may contain all other quantities of interest as well, such as angular distributions, differential energy spectra, *etc.* For example, for a statistical study on parameters of the optical model and the associated observables, $\boldsymbol{\sigma}$ may contain total cross sections σ^{tot} and elastic angular distributions $d\sigma^{\text{el}}/d\Omega$ at various incident energies and outgoing angles. As another example, if we are interested in a covariance matrix for applied purposes (evaluated nuclear data file), $\boldsymbol{\sigma}$ may contain the total and partial cross sections for all open reaction channels at various incident energies. Whatever the objective, it is obvious that $\boldsymbol{\sigma}$ may contain a very large number of elements. The vector $\boldsymbol{\sigma}$ is a function T of the vector \mathbf{p} ,

$$\boldsymbol{\sigma} = T(\mathbf{p}), \quad (183)$$

where here T stands for the entire TALYS nuclear model code. The basis of our method is to let TALYS perform many calculations for the same projectile + target combination, whereby each time all L elements of the \mathbf{p} vector are randomly sampled from a normal distribution with a specific width Δp_l for each parameter p_l , *i.e.*

$$p_l^{(k)} = p_l^{(0)} \pm \Delta p_l, \quad l = 1, L, \quad (184)$$

where we have added a superscript (k) to denote the k -th TALYS run, *i.e.*

$$\boldsymbol{\sigma}^{(k)} = T(\mathbf{p}^{(k)}). \quad (185)$$

Note that a more general probability distribution can be used for the sampling, but so far we have not found any reason to deviate from a uniform or a normal distribution. Another extension would be to perform correlated sampling, on the basis of knowledge of cross-correlations between parameters. This is however done on the basis of a rejection mechanism as explained later in this section. The initial set of input parameters, the central values, is denoted as $\mathbf{p}^{(0)}$ and the corresponding initial calculated cross section vector as $\boldsymbol{\sigma}^{(0)}$, obtained from the initial TALYS calculation. This initial set represents generally one of the following two cases: (a) the best possible parameter set, adjusted to experimental data, obtained from a numerical and/or visual optimization procedure, or (b) a so-called global nuclear model calculation with all parameters equal to their default values. After the initial calculation, the first set of random parameters

$\mathbf{p}^{(1)}$ will lead to a set of cross sections $\sigma^{(1)}$ that is different from $\sigma^{(0)}$. From the results, we can obtain the single covariance matrix element $(\sigma_i^{(1)} - \bar{\sigma}_i^{(0)})(\sigma_j^{(1)} - \bar{\sigma}_j^{(0)})$, which is a measure of the change of σ_j relative to the change of σ_i . In a Monte Carlo approach, such a single covariance matrix element alone is rather meaningless, since all parameters are simultaneously sampled from a random distribution, and no significant information can be available after one run. However, after performing many calculations, all statistical information like average values, uncertainties and covariance matrices will gradually become available. An average element of the covariance matrix for cross sections is given by

$$V_{ij} = \frac{1}{K} \sum_{k=1}^K (\sigma_i^{(k)} - \bar{\sigma}_i)(\sigma_j^{(k)} - \bar{\sigma}_j), \quad i, j = 1, N, \quad (186)$$

where K is the total number of TALYS runs needed for statistical convergence, and the average calculated cross sections are

$$\bar{\sigma}_i = \frac{1}{K} \sum_{k=1}^K \sigma_i^{(k)}, \quad i = 1, N, \quad (187)$$

for which one would expect that $\bar{\sigma}_i \approx \sigma_i^{(0)}$ for all elements i , if the non-linearities are not too strong. Similarly, an average element of the *relative* covariance matrix for cross sections can be obtained,

$$R_{ij} = V_{ij}/(\bar{\sigma}_i \bar{\sigma}_j), \quad i, j = 1, N. \quad (188)$$

The extent to which the calculated results co-vary is most clearly represented by the average element of the *correlation* matrix for cross sections

$$C_{ij} = V_{ij}/\sqrt{V_{ii}V_{jj}}, \quad i, j = 1, N, \quad (189)$$

whose elements take on values between -1 (complete anti-correlation), 0 (no correlation) and 1 (complete correlation). As an example, if by changing model parameters the central value of the total neutron non-elastic cross section at a certain incident energy remains equal, while the central value of the $(n,2n)$ cross section increases, we expect the central value of the (n,n') cross section to decrease to compensate for this, and this anti-correlation between two cross sections will be reflected by a negative value of the C_{ij} element of the covariance matrix that relates $\sigma_{n,n'}$ and $\sigma_{n,2n}$ uncertainties at that particular energy. The diagonal elements of the relative covariance matrix R represent the variance and its square root the uncertainty. Hence, the final calculated cross sections together with their relative errors (square-root of the diagonal elements of the relative covariance matrix) can be expressed as

$$\sigma_i^{\text{final}} = \bar{\sigma}_i(1 \pm \sqrt{R_{ii}}), \quad i = 1, N. \quad (190)$$

Actually, the values of Eqs. (186)-(190) can be updated, and inspected, after every TALYS run, and statistical convergence is reached when the running index k approaches K . For K , an appropriate value needs to be determined, and we usually continue until the average values for the statistical quantities (average, variance, skewness) no longer vary outside a small range.

We can construct similar statistical quantities for the L input parameters that we use in every run, such as the average covariance matrix element for model parameters,

$$P_{lm} = \frac{1}{K} \sum_{k=1}^K (p_l^{(k)} - \bar{p}_l)(p_m^{(k)} - \bar{p}_m), \quad l, m = 1, L, \quad (191)$$

where the average model parameters are,

$$\bar{p}_l = \frac{1}{K} \sum_{k=1}^K p_l^{(k)}, \quad l = 1, L, \quad (192)$$

where we should obtain $\bar{p}_l \approx p_l^{(0)}$. Similarly, we have the relative covariance matrix element for model parameters,

$$R_{lm}^P = P_{lm}/(p_l^{(0)} p_m^{(0)}), \quad l, m = 1, L, \quad (193)$$

and the correlation matrix element for model parameters,

$$C_{lm}^P = P_{lm}/\sqrt{P_{ll}P_{mm}}, \quad l, m = 1, L. \quad (194)$$

The final model parameters with their relative errors are

$$p_l^{\text{final}} = \bar{p}_l(1 \pm \sqrt{R_{ll}^P}), \quad l = 1, L. \quad (195)$$

Of course, Eqs. (191)-(195) are meaningless when we take uncorrelated, randomly sampled parameters as starting point: after enough iterations, we will simply obtain as a result what we put in, provided the random generator is reliable. The parameter covariance matrix will be $P_{lm} = 0$ for $l \neq m$, since in that case we assume to have no a priori knowledge of the correlation of the model parameters. Also, Eq.(195) becomes equal to Eq. (184). The statistical expressions for the model parameters do however become meaningful when parameter correlations are obtained on the basis of included experimental data. There exist various mathematical rigorous methods for automatic parameter/cross section optimization, mostly based on Bayesian statistics. These methods include experimental data, with or without proper covariance matrices, directly in the optimization procedure, which yields both a parameter correlation matrix and a set of the optimized cross sections [91]. Alternatively, correlated sampling using multivariate Gaussian distributions could be performed, if one wishes to pursue Monte Carlo covariance methods. Similar techniques are used in the backward-forward Monte

Carlo methods [92]. Both methods have shown their strength in particular cases, but often, the experimental data needs to be “pre-conditioned” to avoid unrealistic results. At the moment, we take the point of view that mathematical rigor is welcome once both the experimental uncertainties and the uncertainties in the theoretical nuclear models are well under control. Until this has been accomplished, we are in some sense less ambitious: As a first step, we find it safer to use the collection of experimental data as a visual guide to obtain realistic results, *i.e.* we do not literally include them in the optimization scheme. We are however ambitious in the final objective, namely to establish a universal set of nuclear model parameters, their uncertainties, as well as the resulting cross sections and uncertainties, that can safely be used as realistic prior in covariance studies. We think that Table III represents a first good step into this. Once this is established, one can zoom in on a particular nuclide, use its available experimental data, possibly make use of the optimization methods mentioned above and demand that the final results do not deviate completely from the universal set. The latter condition is important, if a covariance technique leads to unrealistic uncertainties in the parameters or final cross sections, something is wrong somewhere. To obtain the final cross section uncertainties and the parameter correlations, we use a simple binary reject/accept method: we put an uncertainty band around the best, or global, data set $\sigma^{(0)}$, such that the available scattered experimental data falls more or less inside this uncertainty band. Next we make sure that our initial parameter uncertainties produce cross section uncertainty bands that are somewhat larger than those indicated by the experimental data. If the calculated cross sections fall inside the experimentally determined uncertainty band we accept the input parameter set, otherwise we reject it. We generally aim for an accept/reject ratio of 1:2. After enough iterations, a full parameter covariance matrix is obtained, which now includes off-diagonal correlations since only certain combinations of nuclear model parameters led to results that were accepted. This procedure can be followed for one particular reaction channel or for all open channels simultaneously.

The method sketched above, although seemingly successful in practical calculations, definitely needs to be improved and extended, to ensure that all available physical knowledge is taken into account. Among the present shortcomings are:

- Neglect of model defects. At the moment, the shortcomings of the model itself are attempted to be covered by enlarging the parameter uncertainties used in the TALYS sampling. However, as shown by Neudecker et al[93], including model defects in the scheme may alter the final uncertainties and cross-correlations. Especially for models like pre-equilibrium cluster emission and fission, which are known to lack good predictive power, there may be a significant effect.
- No mathematical unified method to include both experimental and theoretical uncertainties, as argued in Ref.[157]. In the present Monte Carlo method, global uncertainties for the parameters have been obtained by comparing TALYS uncertainty bands with the spread of different experimental data sets over the whole nuclide chart. Next, for a specific nuclide, TALYS parameter uncertainties are squeezed to obtain shallower uncertainty bands in accordance with the fitted results for the nuclide under study. This is thus not a ‘mathematical evaluation’ based on generalized least squares or anything similar, which is often seen as the only “true” route towards a nuclear data library. In view of the problems of such mathematical evaluation, this step forward can only be taken by an implementation of so-called Unified Monte Carlo[157] in the current method. This is possible, and has in fact been accomplished in Ref[157], but needs to be combined with Total Monte Carlo, to be detailed later, to become really successful. This has not yet been accomplished. Until that time, the shortcomings of the current Monte Carlo method will have to be taken into account in an effective way: uncertainty methods without direct, mathematical, inclusion of experimental uncertainties will lead to too strong, positively correlated uncertainties. For a correct impact on design parameters, this could effectively be covered by changing the diagonal terms of the covariance matrix. In sum, the current method is not at all related to generalized-least-square method, is not Bayesian and is not used for updating information. It simply provides a statistical ensemble of results which may be directly used in Monte Carlo calculations. The method is entirely based on visual guidance and, very important, expertise on whether the generated results are reasonable, *i.e.* not adopting what comes literally out of a mathematical Bayesian approach. However, an exact method, going beyond Unified Monte Carlo, including all available information without any approximation, is under development. As a final resort, one could always use model-derived data, as present in *e.g.* the TENDL data library, as prior for a Bayesian approach including experimental data.
- As experimental data are not mathematically, but only in an average sense, included in this approach, cross-correlations between experimental data are

also not taken into account. This approximation corresponds to the use of normal chi-square instead of generalized chi-square in the uncertainty approach.

B. Sensitivity Analysis

We can relate the variation of the cross sections to the variation of the model parameters. This can be done through the relative sensitivity matrix S . There are two ways to calculate the sensitivity matrix with TASMAN. The first is by means of the classical relation

$$S_{il} = \frac{(\sigma_i^{(1)} - \sigma_i^{(0)}) p_l^{(0)}}{(p_l^{(1)} - p_l^{(0)}) \sigma_i^{(0)}}, \quad i = 1, N, \quad l = 1, L, \quad (196)$$

where $\sigma_i^{(1)}$ is the cross section obtained using parameter $p_l^{(1)}$. In practice, for this option we keep all TALYS input parameters at their default values and move the parameters one by one to obtain the S_{il} elements. This quantity sheds light on the relative importance of the various model parameters. S is dimensionless and directly reflects the dependence of a cross section σ_i on the model parameter p_l . For example, a value of -3.5 for the element S_{il} means that if the model parameter p_l is increased by 10%, the cross section σ_i decreases by 35%. Care should be taken that the samples are not taken around the minimum, so that the sensitivity is underestimated. A different way is to build up the sensitivity matrix during the random runs, *i.e.* similar to obtaining the average covariance matrix of Eq. (186),

$$S_{il} = \frac{\sum_{k=1}^K (p_l^{(k)} - \bar{p}_l)(\sigma_i^{(k)} - \bar{\sigma}_i) \bar{p}_l}{\sum_{k=1}^K (p_l^{(k)} - \bar{p}_l)^2 \bar{\sigma}_i}, \quad i = 1, N, \quad l = 1, L. \quad (197)$$

Again, S will converge to its final value after many calculations. Actually, it is the statistical convergence of S that determines the appropriate value for K . Note however that this approach will only work for the most sensitive parameters, the S values for insensitive parameters are unreliable since they drown in the Monte Carlo noise. One advantage of the Monte Carlo approach is that each σ_i generally does not depend on all parameters. This means that in one and the same run we contribute to the statistical convergence of uncorrelated σ_i simultaneously. If a particular cross section depends on only 1 or 2 parameters, then the average of the associated covariance matrix elements will be obtained quicker than for a cross section that depends on many parameters. This information is contained in S . We thus have to wait for the convergence of the cross section that depends on the most parameters, until we can adopt Eqs. (186)-(195) as the final results.

C. Practical Uncertainty Calculations

All parameters of the models built in TALYS have what we call “default uncertainties,” as listed in Table III. It means that when these uncertainties are applied to the parameters in Eq. (184), the resulting cross sections, angular distributions, *etc.* display uncertainty bands which on average overlap different experimental data sets. In other words, the default uncertainties have been set to simulate the current discrepancy between measurements and between models and measurements. Two comments are directly in order: (1) of course, this can never be full-proof, since certain reaction channels are measured better than others, (2) it is clear that when zooming in on a particular nucleus, the various parameter uncertainties need to be altered. For practical evaluation work, we then proceed with uncertainties just as with the central values: they are fitted, and the more precise the experimental data is, the smaller the resulting parameter uncertainties. The particular parameters for which this holds are identified using the sensitivity analysis explained above. Fig. 7 shows examples for neutrons incident on ^{88}Sr : random parameter variations lead to a set of random curves, which can be averaged to obtain the standard deviation. Clearly, not always all experimental data are covered. Physical judgment and statistical behavior of the entire collection of data often lead to the identification of some outliers which are not necessarily covered by the uncertainty bands.

IV. THE TALYS EVALUATION SYSTEM

The full nuclear data file production relies on a small number of codes and programs, automatically linked together. The output of this system is either one ENDF-6 formatted file, including covariances if needed, or a large number of random ENDF-6 files. The central evaluation tool is the TALYS code. A few other satellite programs are used to complete missing information and randomize input files. At the end of the calculation scheme, the formatting code TEFAL produces the ENDF files. The following programs are used:

- The TALYS code

The nuclear reaction code TALYS has been extensively described in Section II. In the entire evaluation system, it is basically used as a black box.

- The TASMAN code

TASMAN is a computer code for the production of covariance data using results of the nuclear model code TALYS, and for automatic optimization of the TALYS results with respect to experimental data. The essential idea is to assume that each

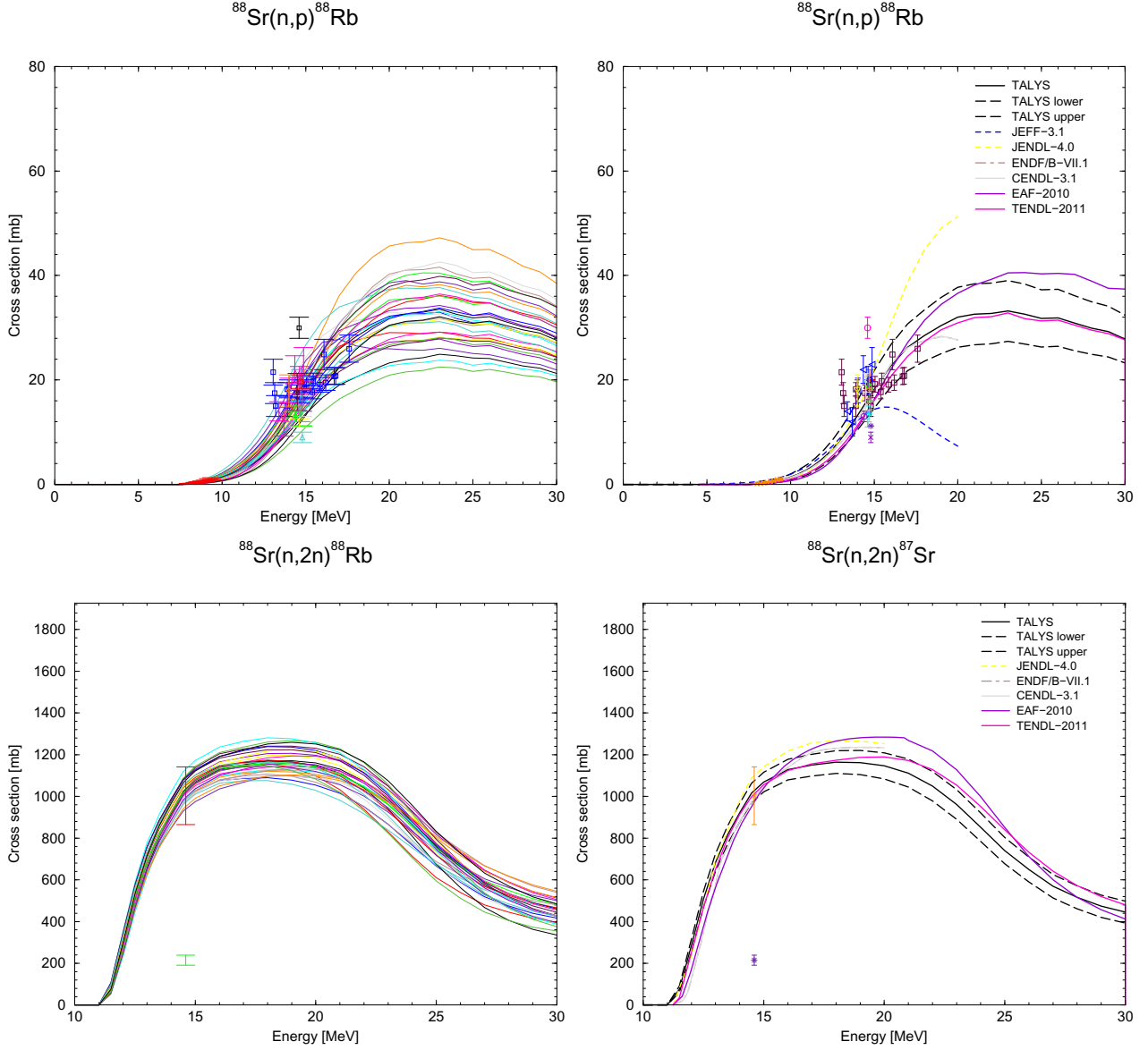


FIG. 7: Random cross sections and related uncertainty bands for $^{88}\text{Sr}(n,\text{p})^{88}\text{Rb}$ and $^{88}\text{Sr}(n,2\text{n})$.

nuclear model (*i.e.* TALYS input) parameter has its own uncertainty, where often the uncertainty distribution is assumed to have either a Gaussian or uniform shape. Running TALYS many times, whereby each time all elements of the input parameter vector are *randomly* sampled from a distribution with a specific width for each parameter, provides all needed statistical information to produce a full covariance matrix. The basic objective behind the construction of TASMAN is to facilitate all this.

TASMAN is using central value parameters, as well as a probability distribution function. The central values were chosen to globally obtain the best fit to experimental cross sections and angular distributions (see for instance Ref. [15]). The uncertainties on parameters (or widths of the distributions) are also obtained by comparison with experimental data, directly taken as “raw data” (*i.e.* not adjusted for new standard information *etc.*) from the EXFOR database [94]. The distribution probability can then be chosen between, equiprobable,

Normal or other. In principle, with the least information available (no measurement, no theoretical information), the equiprobable probability distribution should be chosen. Otherwise, the Normal distribution is considered.

An important quantity to obtain rapid statistical convergence in the Monte Carlo process is the selection of random numbers. Several tests were performed using pseudo-random numbers, quasi-random numbers (Sobol sequence), Latin Hypercube random numbers or Centroidal Voronoi Tessellations random numbers. As the considered dimension (number of parameters for a TALYS calculation) is rather high (from 50 to 80), not all random number generators perform as required (covering as fast as possible the full parameter space, without repeating very similar configurations and avoiding correlations). For the time being, the random data files are produced using the Sobol quasi-random number generator.

- **The TEFAL code**

TEFAL is a computer code for the translation of the nuclear reaction results of TALYS, and data from other sources if TALYS is not adequate, into ENDF-6 formatted nuclear data libraries. The basic objective behind the construction of TEFAL is to create nuclear data files without error-prone human interference. Hence, the idea is to first run TALYS for a projectile-target combination and a range of incident energies, and to obtain a ready to use nuclear data library from the TEFAL code through processing of the TALYS results, possibly in combination with experimental data or data from existing data libraries. This procedure is completely automated, so that the chance of *ad hoc* human errors is minimized.

- **The TARES program**

This is a code to generate resonance information in the ENDF-6 format, including covariance information. It makes use of resonance parameter databases such as the EXFOR database [94], resonance parameters from other libraries (ENDF/B-VII.0 [95]) or compilations (Ref. [96]). ENDF-6 procedures can be selected, for different R-matrix approximations, such as the Multi-level Breit Wigner or Reich Moore formalism. The covariance information is stored either in the “regular” covariance format or in the compact format. For short range correlation between resonance parameters, simple formulas as presented in Ref. [97] are used, based on the capture kernel. No long-range correlations are considered for now.

In the case of major actinides, resonance param-

eters are taken from evaluated libraries, such as ENDF/B-VII.0 or JEFF-3.1. These values are almost never given with uncertainties. In this case, uncertainties from compilations or measurements are assigned to the evaluated resonance parameters. Although not the best alternative, it nevertheless allows to combine central values with uncertainties.

For the unresolved resonance range, an alternative solution to the average parameters from TALYS is to adopt parameters from existing evaluations. In the following, this solution is followed. The output of this program is a resonance file with central values (MF2), a resonance file with random resonance parameters (MF2) and two covariance files (MF32 standard and compact).

- **The TANES program**

TANES is a simple program to calculate fission neutron spectrum based on the Los Alamos model [98]. The original Madland-Nix [99] or Los Alamos model for the calculation of prompt fission neutrons characteristics (spectra and multiplicity) has been implemented in a stand-alone module. The TANES code is using this stand-alone module, combined with parameter uncertainties (on the total kinetic energy, released energy and multichance fission probabilities) to reproduce and randomize the fission neutron spectrum. The output of this program is the central and random values for the fission neutron spectra at different incident energies (MF5) and their covariances (MF35).

- **The TAFIS program**

TAFIS is used to calculate fission yields, prompt neutron emission from fission and other necessary fission quantities (kinetic energy of the fission products, kinetic energy of the prompt and delayed fission neutrons, total energy released by prompt and delayed gamma rays). For fission yields, it is using the systematics of fission-product yields from A.C. Wahl [100], combined with *ad hoc* uncertainties. It calculates the independent and cumulative fission yields at any incident energy up to 200 MeV and for different incident particles (spontaneous, neutrons, protons, deuterons, etc.). Empirical equations representing systematics of fission-product yields are derived from experimental data. The systematics give some insight into nuclear-structure effects on yields, and the equations allow estimation of yields from fission of any nuclide ($Z = 90$ to 98 and $A = 230$ to 252). For neutron emission, different models are used depending on the energy range and are presented in Ref. [100]. The output of this program is

a fission yield file with uncertainties, prompt neutron emission files for central and random values (MF1 MT452), a list of central and random fission quantities (MF1 MT458) and prompt neutron covariances (MF31).

- Autotalys

Autotalys is a script which takes care of the communication between all software and packages described above and runs the complete sequence of codes, if necessary for the whole nuclide chart. Many options regarding TALYS and all other codes can be set, and it makes the library production straightforward.

Up to this point, the system for performing an entire nuclear reaction simulation, including its storage in a complete ENDF-6 data library, has been defined. The principle of reproducibility that we advertised before now allows us to loop this over:

1. Many random input parameter sets. This lies at the basis of Total Monte Carlo and will be discussed in Section VI.
2. Many nuclides, leading to the central value evaluation of the TENDL library, to be discussed in the next Section.
3. Many nuclides *and* many input parameter sets, leading to TENDL + covariance data, also discussed in the next Section.

V. LIBRARY PRODUCTION: TENDL

The concept of the TALYS Evaluated Nuclear Data Library, TENDL, is based on principles which have already been embraced by many other industries: quality, automation, reproducibility, completeness and consistency. It relies on robust open source (*i.e.* traceable) nuclear model software and on the two simple ideas that any information used to create an evaluation is kept “forever” to be re-used as necessary, and that manual intervention *during* the library production is strictly forbidden. It is even possible to “clone” an existing library and start further development from that point, *e.g.* adopt the entire ENDF/B-VII.0 [95] library and fill all missing sections, high-energy data, covariance data using TALYS. We will not detail in this paper all the specifics of the TENDL libraries, but will show several examples of its contents. A preliminary description of TENDL has been given in [101].

To get better insight in how to divide the effort to produce something like a TENDL library, we wish to focus your attention on Table IV, which represents an

attempt to classify all nuclides in groups of importance, “averaged over applications”. This classification is based on subjective experience, amount of literature, data user requests,*etc.* The list applies to fission, fusion and accelerator (such as medical) applications, although fusion and accelerator scientists would probably leave out the actinides from this list, and each of the three communities is generally interested in a different energy range (which is left out of Table IV for simplicity).

Not surprisingly, the Material column is highly correlated with the Experimental data column. A statistical analysis of the EXFOR database will confirm that the importance of a material or isotope in applications, as categorized in decreasing order from (1) to (12), is in general reflected by the amount of available experimental data. The only exception to this rule is isotopes which are important, but at the same time suffer from experimental difficulties (target enrichment, target activity,*etc.*) such as certain fission products, minor actinides or some low-abundance isotopes.

For the Nuclear model column of Table IV, the situation is different. In principle, complete nuclear model calculations can be performed for *all* nuclides, reaction channels and energies, important or not. In fact, the basis for TENDL is formed by complete nuclear data libraries, all with essentially the same structure, for all material categories (1) to (12). The first version of the library, TENDL-2008, was actually just that: the isotopic nuclear data libraries were made by global TALYS calculations only, without any further adjustment of any model parameters or inclusion of experimental data. In more recent versions of TENDL, progressively more effort is invested in nuclide specific parameters and experimental data as we move up the list from category (12) to (1), until for the most important channels, *e.g.* $^{238}\text{U}(\text{n},\gamma)$, nuclear model calculations are completely normalized by experimental data, existing evaluated data, or differential data inferred from integral measurements, in certain energy ranges. Note that even for such nuclides, TALYS is still used for all other energy ranges and reaction channels. One can thus *not* state that nuclear models become less important if we move higher on the list, we always need them for completeness. In sum, TENDL-2011 contains all cases present in Table IV, *i.e.* it ranges from detailed channel-by-channel evaluation work to completely “blind” libraries.

Another new feature in large scale data evaluations is that for the production of TENDL we include integral data evaluation as much as possible in the process. In this way, we largely bypass the usual decay, of one or more years, of feedback from reactor analyses. Again, this is possible by adopting a more disciplined and quality assured working method. Basically it means that the ENDF-6 data file should not be touched manually, and is rather seen as a helpful by-product of an evaluation pro-

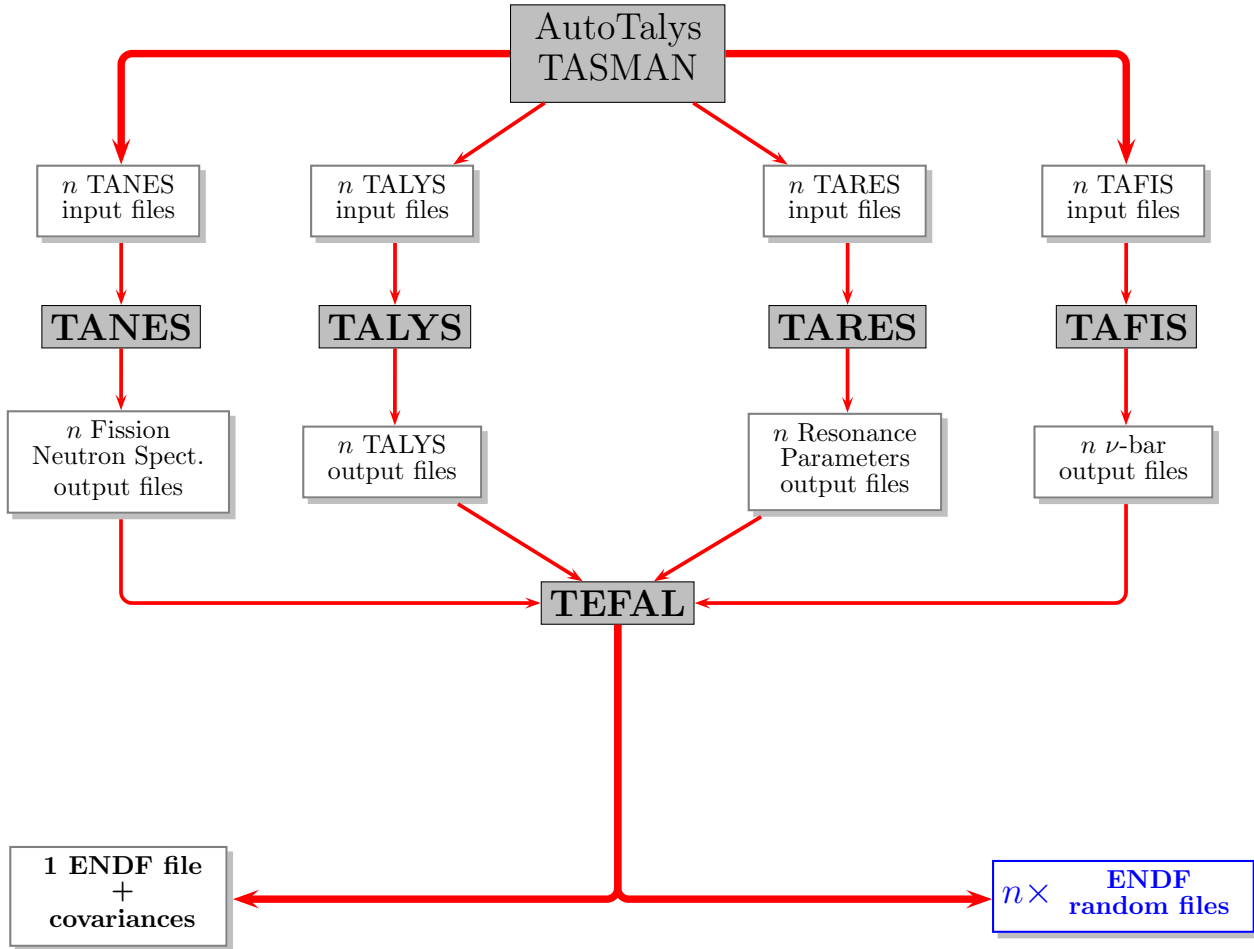


FIG. 8: Flowchart of the nuclear data file evaluation and production with the TALYS system.

cess. Fig. 9 summarizes the approach. Once the nuclear model code and ENDF formatting code used in the evaluation process are well verified and validated, the 3 left boxes contain the essential information that produces a nuclear data file. All relevant experimental data for the nucleus under consideration should be readily available, as well as a file with deduced resonance parameters (and uncertainties). An input file for the nuclear model code with parameters (and uncertainties) adjusted to reproduce the available experimental data produces a complete set of nuclear reaction results. Finally, a formatting code produces the ENDF-6 data file, which is driven by a script that performs any additional actions such as copy-paste from existing data libraries or, if necessary, scientifically dubious adjustments for the sake of good performance of the data file in applications.

The TENDL-2011 library, available from www.talys.eu, comes in various different representations:

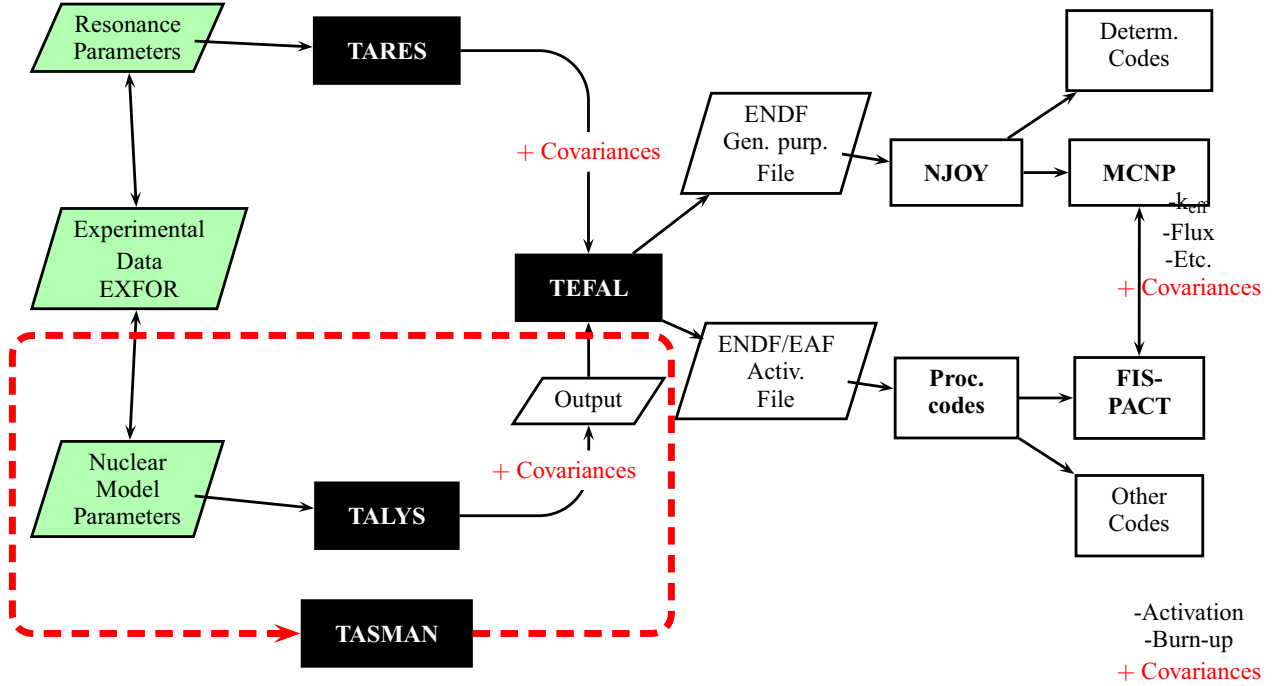
- For nuclear physicists: all data stored in human-readable x-y tables, categorized per projectile-target-channel-reaction quantity, enabling easy plotting and processing. There are Tabulated files for total, partial, and residual cross sections, gamma-ray intensities, spectra and angular distributions.
- For nuclear data evaluators: Evaluated data libraries in ENDF-6 format. Besides the usual sections MF1-15, also complete covariance date files for fission quantities, resonance parameters, cross sections, angular distributions and isomer production are stored in MF31-40.
- For nuclear data users: all libraries are available in applied formats for use in reactor codes, such as multi-group covariance matrices, the AMPX format and the ACE format for MCNP(X).

TABLE IV: Classes of materials and related evaluation aspects, in decreasing order of technological importance. The boundaries between classes have been left vague on purpose.

Material	Experimental data	Nuclear models	Evaluation/Validation
(1) The Big Three: $^{235,238}\text{U}$, ^{239}Pu	High-quality measurements (uncertainty < 2 % for important channels), directly (cor)related with neutron standards Often more than 10-20 exp. data sets in same energy range	Models overruled by experimental data for important channels: complete normalization of model results	Need for reliable experiment-based covariance data Direct feedback from integral measurements: criticality, reactor systems, inventory, etc.
(2) Important coolants and structural materials: H, C, O, Fe	Many experimental data sets for many channels uncertainty < 10% (dosimetry reactions < 3 %)	Precise nuclear model calculations with many parameters to interpolate between measurements. Light nuclides difficult	Sometimes differential data overruled by data with better integral performance
(3) Other coolants and structural materials: N, Na, Al, Si, Ti, V, Cr, Mn, Ni, Cu, Zr, Mo, W, Pb, Bi,...	Many experimental data sets for only the most important channels	Parameter adjustment for well-measured channels	
(4) Other important actinides: ^{232}Th , ^{233}U , $^{240-242}\text{Pu}$	Many experimental data sets for almost all secondary distributions (angles, spectra, photons, etc.)	Models used for almost all secondary distributions (angles, spectra, photons, etc.)	Isolated benchmarks available for transport or activation analyses
(5) Important fission products: ^{99}Tc , ^{103}Rh , ^{129}I ,...			
(6) Breeding materials and reflectors: Li, Be,...		Model calculations with a few parameters adjusted to the few exp. data sets	
(7) Absorbers: Gd, Hf,...	Experimental data only available for (low energy) total, elastic, capture (resonance parameters) and a few other channels		Global covariance estimates
(8) Minor actinides: $^{241,242m,243}\text{Am}$, ^{237}Np ,...			Automatic production of data libraries
(9) Remaining materials (natural isotopes): P, S, Cl, Ca,....			
(10) Remaining long-lived nuclides ($\tau > 1$ year)	(Almost) no experimental data		(Almost) no integral experimental data
(11) Medium long-lived nuclides (1000 sec. $< \tau < 1$ year)		Complete reliance on nuclear models, preferably microscopic	
(12) Short-lived nuclides ($\tau < 1000$ sec.)			Astrophysics

The TENDL-2011 library contains sub-libraries for incident neutrons, protons, deuterons, tritons, helium-3's, alphas, photons and a fission yield sublibrary. For all types of incident particles, nuclear data libraries for 2430 isotopic targets are produced. These are all isotopes, in either ground or metastable state, with a half-life longer than 1 sec. from $Z = 3$ (Li) to $Z = 110$ (Ds), see

Fig. 10. This is about a factor of 8 more nuclides than in any other world library. All libraries extend up to 200 MeV.



Monte Carlo: 1000 TALYS runs

FIG. 9: Flowchart of automated, reproducible evaluation process used for the production of TENDL-2008-2012.

A. Neutron Sublibrary

As explained above, one consistent production method for the TENDL nuclear data libraries is used, and they are all complete in terms of reaction information. However, in line with Table IV, progressively more effort was invested when moving from the exotic nuclides to the most important nuclides. This holds especially for incident neutrons. Hence,

1. For important nuclides, specific TALYS parameter adjustment and inclusion of experimental data is required. Also more and better resonance information is generally available.
2. For more important nuclides, a larger number of random TALYS runs to construct a covariance matrix was used. This number ranges from 3 random runs for the most exotic nuclides to several hundred for the most important ones. This was explained in more detail in Section III. Here, it suffices to state that more random runs leads to a more statistically converged covariance matrix.

With this categorization it is possible to produce TENDL in two months on a 200 processor-cluster. Obvi-

ously, with future increase of computer speed the number of random TALYS runs per isotope can easily be increased.

1. Resonance range

Resonance parameters are extracted from the latest measurements (such as from the EXFOR database [94]), and from compilations (*i.e.* The Atlas of Neutron Resonances [96]). These two sources of information cover the vast majority of experimental data used for the isotopes in TENDL. Alternatively, for major actinides and other important structural materials, resonance parameters are imported from existing evaluations. As often uncertainties are not included in other libraries, resonance parameter uncertainties are then obtained from other sources (such as EXFOR). For the remaining ones, hypothetical resonance levels are used and the technique to describe those is explained in the next paragraph.

Particular effort has been invested in the adjustment of resonance parameters to obtain consistency between measured thermal elastic, capture and if relevant fission cross sections for all stable and known long-lived isotopes. In practice, resonance parameters for the negative

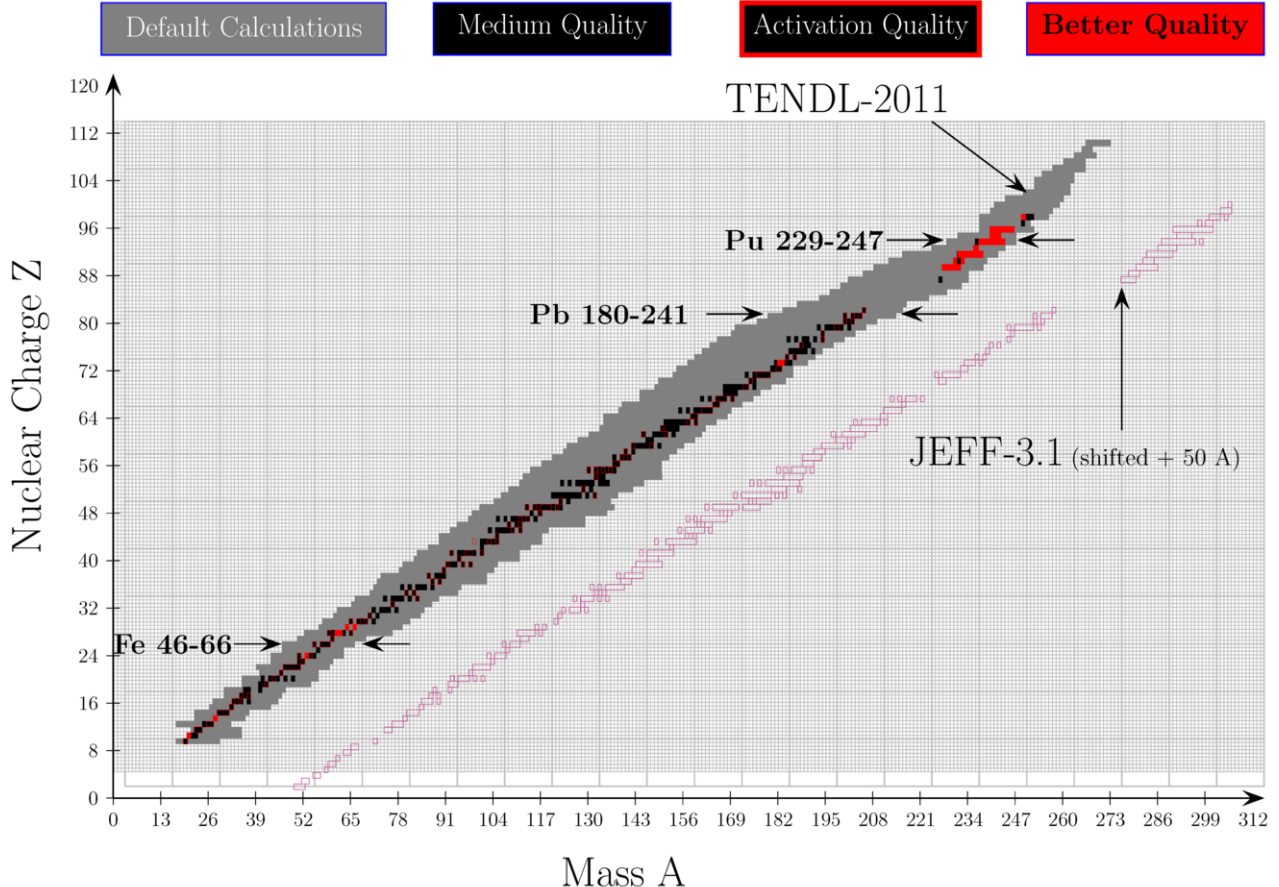


FIG. 10: Table of all nuclides included in the neutron sub-library of TENDL-2011. Colors represent quality of the evaluation. For comparison, nuclides evaluated in JEFF-3.1 are also presented, shifted in mass. Here, “activation quality” means a level of quality equal to that found in activation libraries such as EAF-2010.

and first positive resonances together with the scattering radius are adjusted. Examples of resolved resonance ranges are presented in Fig. 11.

In general, the TENDL-2011 thermal cross sections are in good agreement with those of other evaluations, as presented in Figures 12, 13 and 14.

For the unresolved resonance range (URR), TENDL-2011 generally includes URR parameters as calculated by TALYS, though sometimes the URR parameters are imported from ENDF/B-VII.0, JEFF-3.1.1 or JENDL-4.0.

a. Resolving the URR One of the worrying aspects of the current nuclear data libraries that was mentioned before is the completeness of information that is varying so much from isotope to isotope. This holds also, in fact especially, for the resonance range. Inspection of *e.g.* the Atlas of Neutron Resonances [96]) reveals that there are nuclides with very well measured resonance ranges, nuclides with only a few measured resonances, and nuclides

with no measurements at all. In TENDL, an attempt is made to remedy this, without jeopardizing the quality of existing experimental information: resonance parameters are guessed. The idea to obtain approximate cross sections in the resonance range when no measurements exist is not new. The first and easiest solution is to extend the optical model calculation to low energy or to use a $1/v$ function and calculate smooth cross sections from 10^{-5} eV to the MeV region. No structure can be obtained, but this approximation allows to obtain the experimental, or systematical, thermal cross section if the parameters of the optical model and the level densities are adjusted. An example of such an approach is presented in Fig. 15 for the $^{90}\text{Sr}(n,\gamma)$ cross section.

A drawback of this method can be seen from Fig. 15: there is a clear separation between the “pseudo-resonance range” and the fast neutron region. Additionally, it is also difficult to adjust the resonance integral I_γ if measured values existed (see C/E values in Fig. 15).

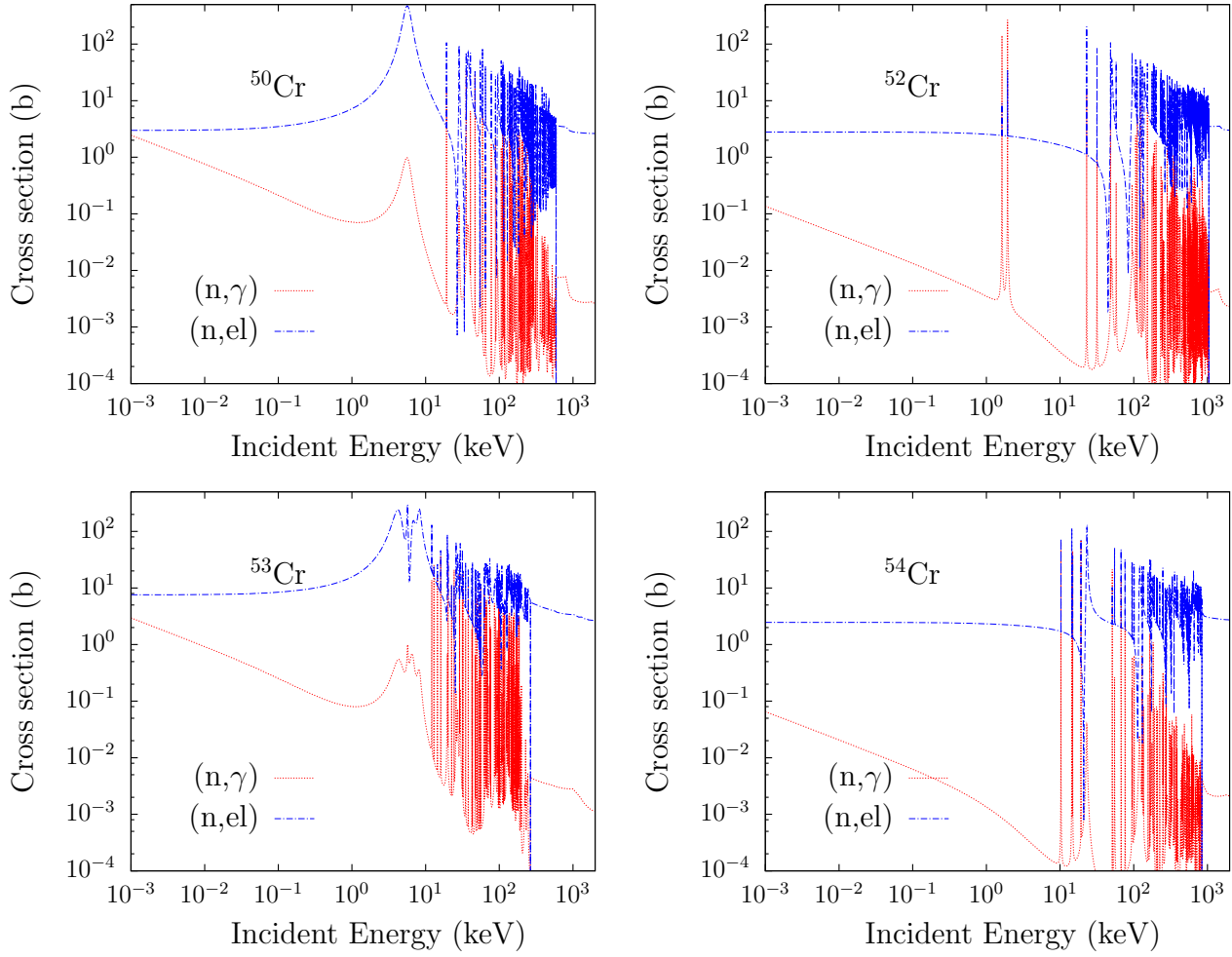


FIG. 11: Neutron elastic and capture cross section for chromium isotopes in the resonance range at 300°K.

The proposed method, which is often called the picket-fence model, consists to expand the region of overlap (unresolved resonance range) and “*resolve*” it (or reconstruct it), down to low energy, virtually to 10^{-5} eV in the case of isotopes without known resonances, and up to the first excited level in general. Depending on the degree of knowledge for a given isotope, the above proposition can be implemented with different degrees of difficulty. It is then convenient to introduce a classification depending on the amount of knowledge for a given isotope. In the following, we will only consider the usual set of isotopes with half-lives longer than one second, including stable isotopes, representing ≈ 2430 nuclides.

- At the first extreme, isotopes without any experimental reaction information (about 1600 isotopes). In this case, as no specific information can be used to adjust calculations, we fully rely on systematics, as defined in TALYS from Ref. [102] or the

underlying optical model potential and level density model [102, 103].

- In between the two extremes, isotopes with scarce experimental data such as thermal cross sections, resonance integrals, average cross sections at high energy (about 400 isotopes). The model parameters are adjusted to reproduce the existing data (such as cross sections or existing resonances).
- At the other end of the spectrum, isotopes with measured pointwise cross sections, resonances, integral measurements, and resolved resonance parameters (about 400 isotopes). The resonance estimation method can still be applied, but great care should be taken that the modifications do not deteriorate their performances.

As a starting point for resonance estimation, energy-dependent statistical parameters as well as specific cross

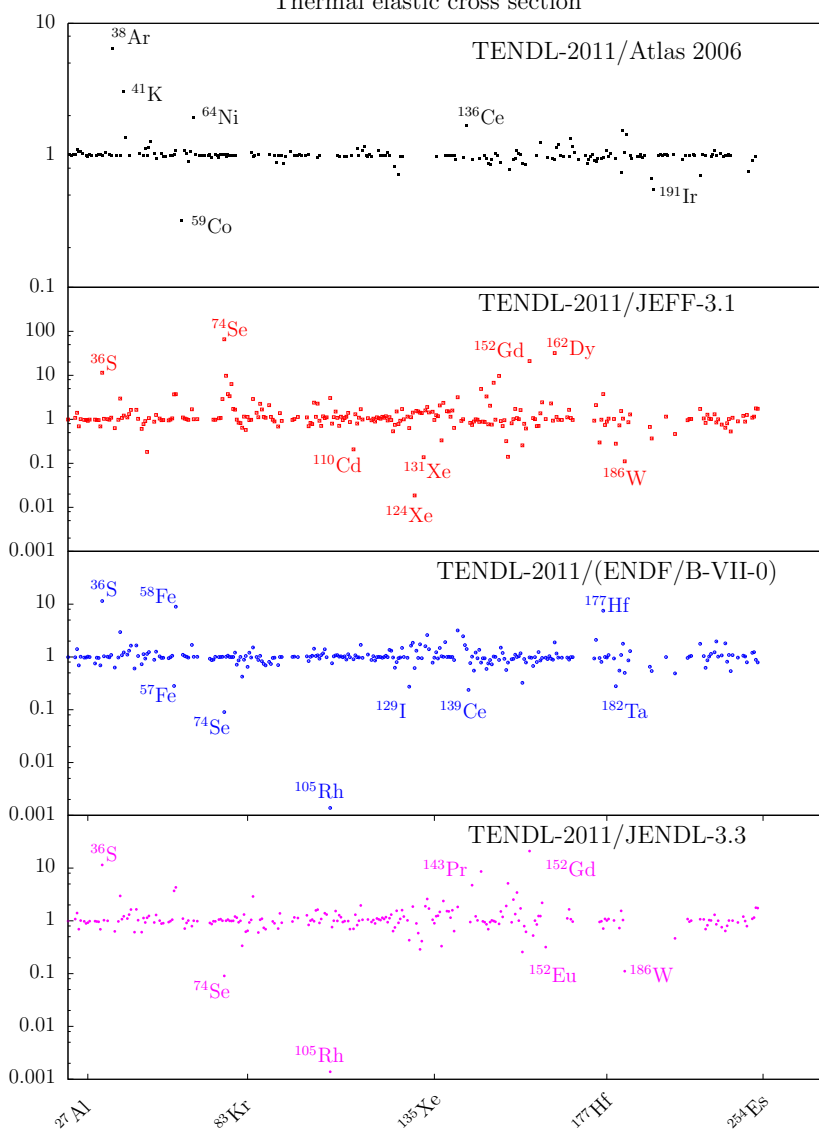


FIG. 12: Ratios of thermal elastic cross sections between different libraries and compilations.

sections are needed in the whole energy range. These parameters are for each orbital angular momentum l and spin of the resonance state j :

- the scattering radius r ,
- the average level spacing D_0 ,
- the average reduced neutron width Γ_n^0 ,
- the average radiation width Γ_γ ,
- and if relevant the average fission width Γ_f .

The necessary cross sections, consistent with the above parameters are the elastic, capture, inelastic and fission

cross sections. These pointwise cross sections can be kept as is above an arbitrary energy limit, usually lower than the first inelastic level. Below this energy limit the average parameters can be converted into statistical resonance structures. This energy limit can be arbitrary chosen, but in practice, it defines the number of resolved resonances and should therefore not be too high.

The basic idea is to generate random ladders of resonances using the statistical properties of the unresolved resonance range [104, 105]. Ladders can be generated at an energy E by randomly selecting a starting resonance energy for one (l, j) sequence, and also randomly selecting a set of widths for that resonance using the appropriate average widths and χ^2 distribution functions. The

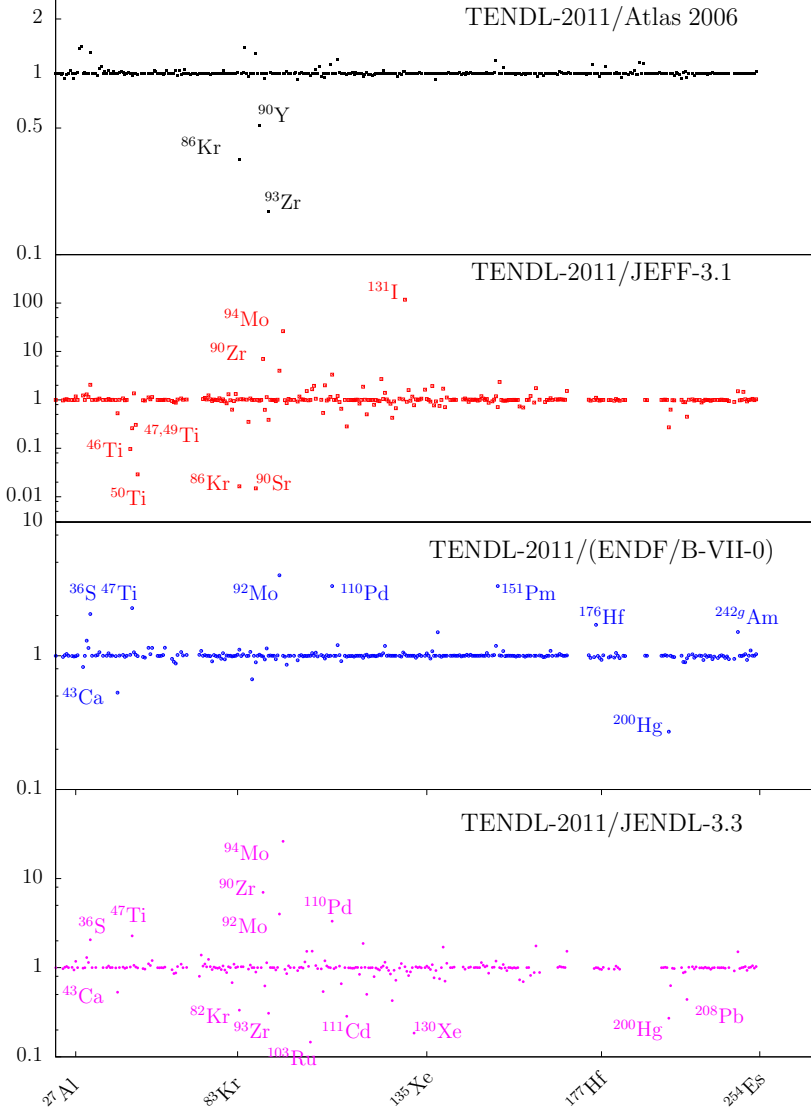


FIG. 13: Ratios of thermal capture cross sections between different libraries and compilations.

next higher resonance energy can be selected by sampling from the Wigner distribution for resonance spacings, and a new set of widths for that resonance can be chosen. The process is continued until a long ladder of resonances for that (l, j) is obtained. The process for the other (l, j) sequences is then repeated, each such sequence being uncorrelated in positions from the others. In the current implementation of CALENDF, for each (l, j) couple, a GOE random matrix (Gaussian Orthogonal Ensemble) [106] is used to generate resonance energies. This allows to follow the Wigner law and to include correlations between two successive resonances. Following the average parameters obtained in the unresolved

resonance range, CALENDF determines “segments”, in which a few tens of s-wave resonances are included. Using stratified random numbers, the widths of the resonances are obtained. The evolution from a simple “no resonance” approach to a full-blown GOE-based resonance range can be seen in Fig. 15. In TENDL-2011, resonances were estimated in a (too) regular pattern from level density estimates (which at least was more realistic than *no* resonance), while the TENDL-2012 curve is more physically based and shows irregular structure.

Fig. 16 presents a few advantages of the method: no unphysical cut-off between the resonance and the fast neutron ranges, no constant cross sections at low neu-

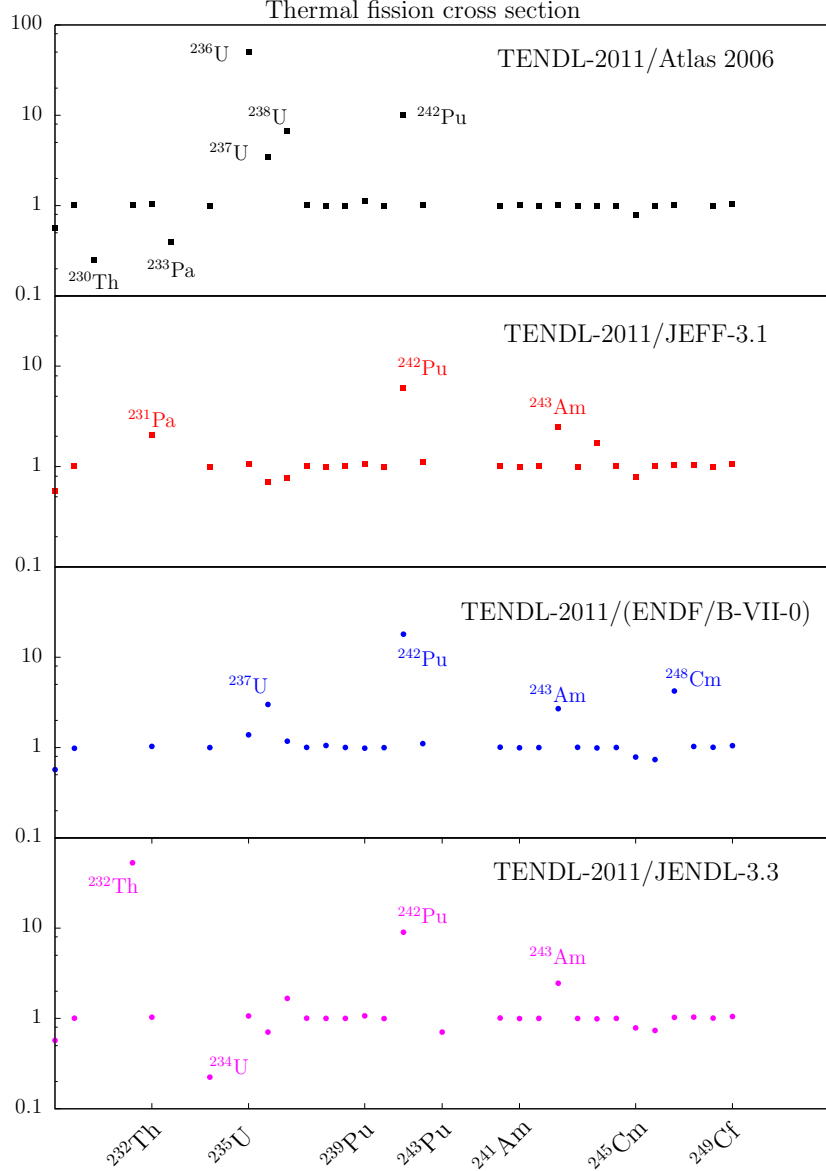


FIG. 14: Ratios of thermal fission cross sections between different libraries and compilations.

tron energy and better agreement with integral data. The method has been applied successfully, since it has been tested for well-measured cases, to all isotopes living longer than one second, and the results will be part of the TENDL libraries starting in 2012.

2. Fast neutron range

The quality of the evaluations in the fast neutron range can be classified in three categories, depending on the amount of “knowledge” (*e.g.* experimental data) which is included in the calculation scheme. For the vast

majority of unstable nuclei except the actinides, in the absence of experimental information, default TALYS calculations were performed to obtain cross sections, angular distributions and differential data. These results were directly formatted to the ENDF-6 format. These evaluations are labeled “default calculations” (as presented in Fig. 10). Default model parameters were then applied, which follows systematics globally adjusted for stable isotopes.

For stable isotopes, actinides and long-lived nuclei for which experimental data are available, adjusted TALYS parameters were used to reproduce experimental information. These evaluations are then labeled “medium

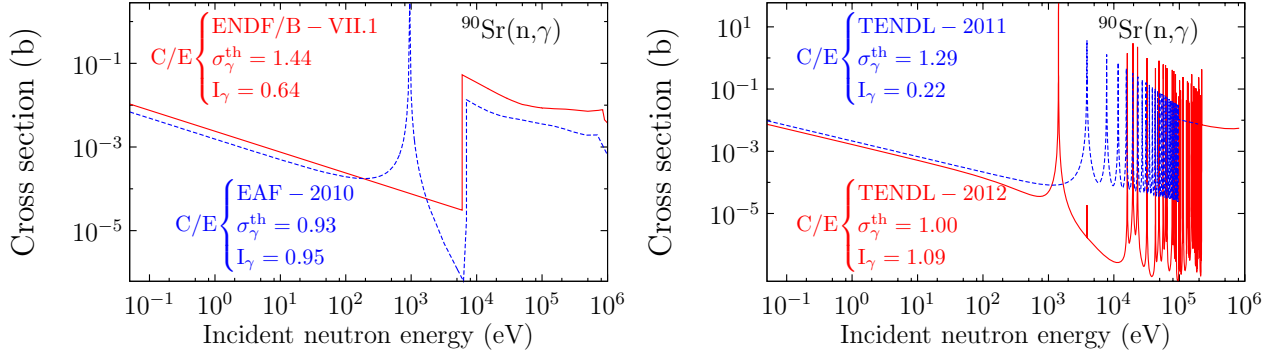


FIG. 15: Examples of different approaches for ^{90}Sr ($t_{1/2} = 28$ years) in the low energy region. Left: basic optical model calculation for ENDF/B-VII.1 and Single Resonance Approximation (SRA) for EAF-2010. Right: multi-SRA for TENDL-2011 and the present methodology for TENDL-2012.

quality” (in black in Fig. 10).

In the case of some particularly important isotopes (such as ^{235}U or ^{238}U), an extra step in the evaluation procedure is made, applying minor adjustments to cross sections to obtain good k_{eff} benchmark results. These evaluations are called “better quality” and appear in red in Fig. 10.

In the mass range $19 < A < 210$, default and adjusted TALYS calculations were performed. For TENDL-2011, TALYS parameters were adjusted to obtain good agreement between calculated total and partial cross sections and experimental data. For each target nuclide, typically 10-20 TALYS input parameters are adjusted and stored in a database. The most often changed parameters are the real volume radius and diffuseness of the optical model, the particle-hole state density parameters for the pre-equilibrium process, the total level density parameters a of the compound and residual nuclides, and the knockout and stripping parameters to adjust the (n,α) cross sections. In Table V such an optimal input file for neutrons incident on ^{80}Se is displayed. This has been done for hundreds of nuclides.

Fig. 17 shows some results of preliminary TENDL-2012 data (the curve labeled TALYS + uncertainty band) for several nuclides compared with other libraries and experimental data.

Actinide evaluations were performed up to the nuclear charge 110 and mass 281. For the less important ones (presented in gray in Fig. 10), no particular adjustments were made, a default TALYS calculation was performed. For the main ones (presented in black and red in Fig. 10), important cross sections (such as capture, fission, inelastic, elastic and $(n,2n)$) were adjusted to experimental data and to other evaluations such as from the ENDF/B-VII.0 library.

More efforts were made in the case of $^{235},^{238}\text{U}$ and ^{239}Pu . A combination of TALYS calculations and Monte Carlo

TABLE V: Optimal TALYS input file for neutrons on ^{80}Se .

projectile n
element Se
mass 80
energy energies
rvadjust n 1. 0.01 1. 0.5 0.99
rvadjust n 1. 10. 5.5 1.02
gamgamadjust 34 81 0.45
gnadjust 34 81 0.90
gpadjust 34 81 0.90
m2constant 0.9
rvadjust p 1.04
avadjust p 1.04
rvadjust a 1.15
avadjust a 1.15
aadjust 32 77 1.10
Cstrip a 2.40
Cknock a 2.40
tadjust 34 80 1.15
branch 34 81 7 1 1 1.
branch 34 81 10 1 1 1.
branch 34 81 14 1 1 1.

search was used to obtain evaluations which gives best results for a limited number of k_{eff} benchmarks. For these actinides, the following method was used:

- In the fast neutron range, the main cross sections were adjusted in the TALYS runs to be as close as possible to the measurements and to the evaluations.
- For ^{235}U , ^{238}U and ^{239}Pu , a few benchmarks were used to finalize adjustments on different cross sections to obtain a C/E close to one.
- In a second step, a larger number k_{eff} benchmarks

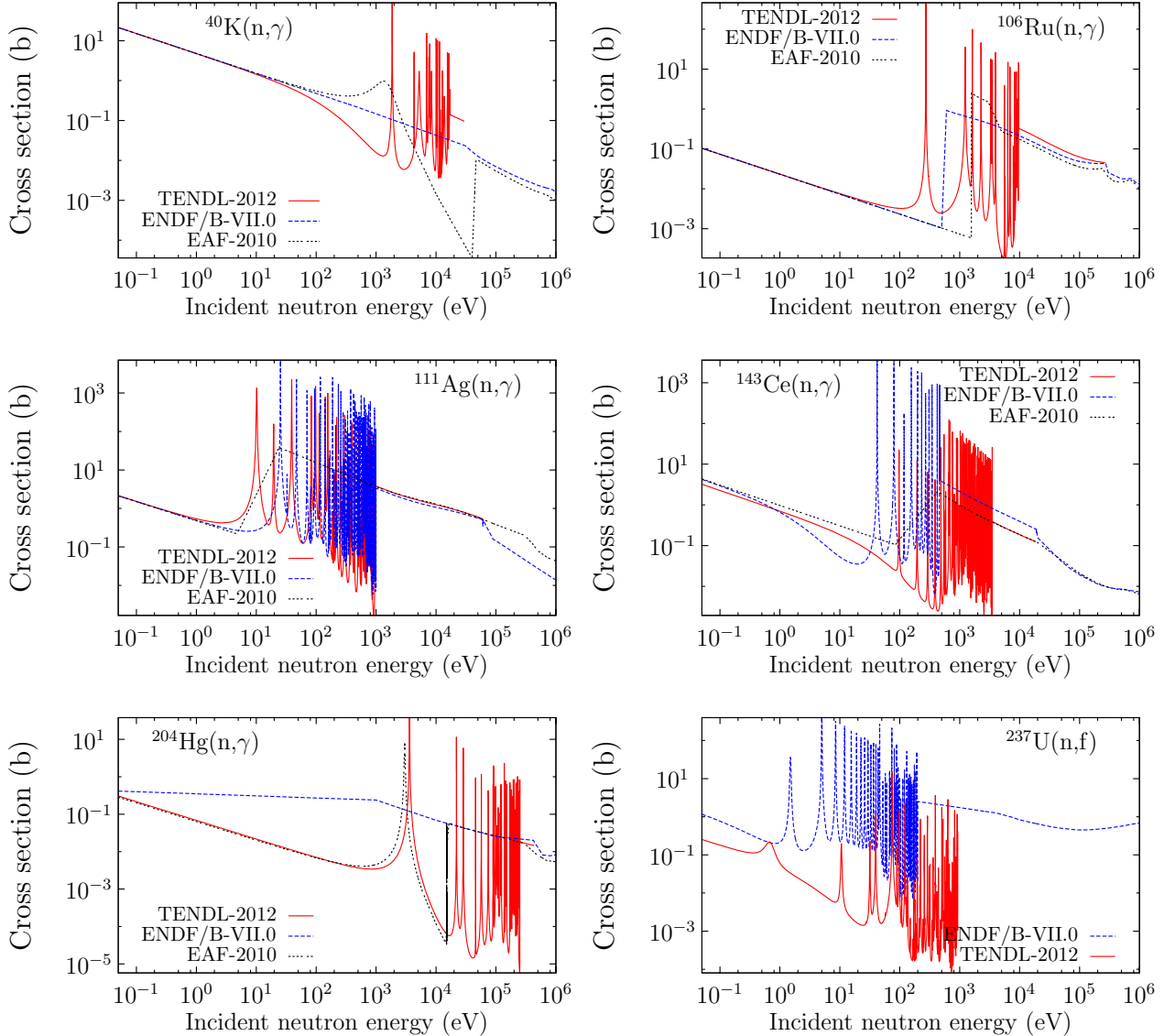


FIG. 16: Example of reconstructed resolved resonances based on the TALYS unresolved resonance range and CALENDF for 6 short-lived and low abundance isotopes, compared to other evaluations.

were analyzed, and TALYS model parameters were slightly modified to improve results.

B. Other Sublibraries

1. Proton, deuteron, triton, He-3, alpha and photon sublibrary

Complete proton data libraries for 2430 isotopes, *i.e.* all targets with half life longer than 1 second, with energies from 1 to 200 MeV, have been produced. All cal-

culations are performed with default parameters, even though we are well aware that better fits to experimental data can be obtained for several nuclides. The poor excuse is that sensitivity analyses for proton applications such as accelerator shielding and medical isotope production are to our knowledge non-existent, *i.e.* there is little guidance to what level of quality proton libraries should be evaluated for each material. The proton data libraries are thus simply an alternative to the intranuclear cascade codes used at high energies, in which also no adjustment to experimental data takes place. A stronger excuse is that it takes time to collect experimental data, and to

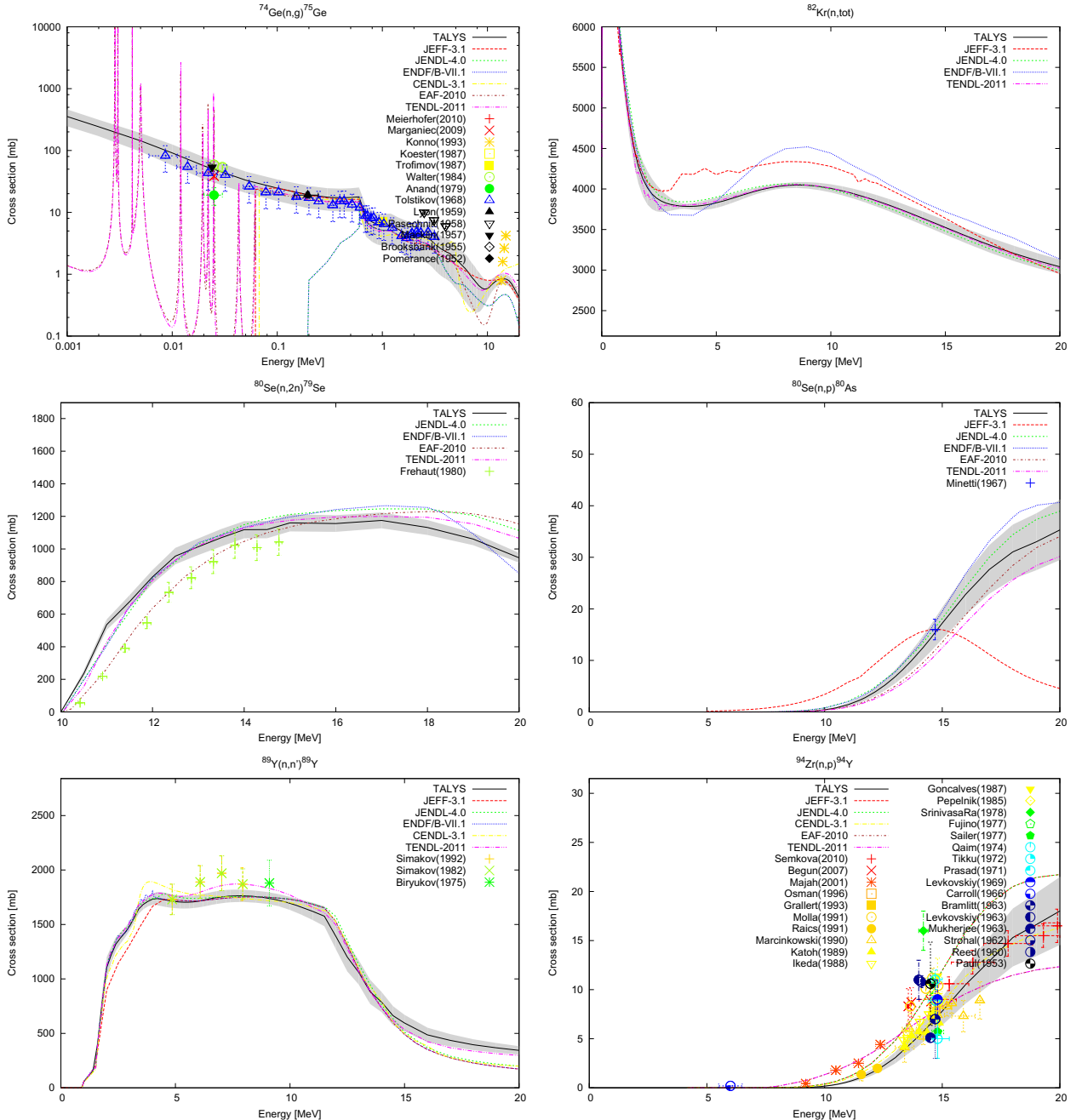


FIG. 17: Some examples of the TENDL-2012 beta library (curves labeled TALYS), compared with other libraries and experimental data for some nuclides.

adjust TALYS input parameters to obtain the optimal description for each isotope. The latter effort has been done for the NRG-2004 library [107], consisting of 26 isotopic evaluations, and in other libraries such as LA-150 [111] and JENDL-HE [108]. As the evaluation effort is relatively simpler than for neutrons, we expect to be able

to zoom in on experimental proton-induced data in the coming years for all materials, like we did for incident neutrons. We note that it is our experience that the difference between a global and a parameter-adjusted evaluation is larger for neutrons than for protons, *i.e.* for protons there is less to be gained, and libraries produced

by default TALYS calculations already perform reasonably well.

For incident protons, the most important, and most measured, observables are elastic scattering angular distributions, total non-elastic cross sections, double-differential particle emission spectra and residual production cross sections. Even though TENDL-2011 is, for incident protons and other charged particles a global non-adjusted library, its quality can directly be related to existing global predictions for the first 3 of the 4 above mentioned classes of data. In Ref. [15], local and global optical proton models were constructed which provide a satisfactory description of a large collection of experimental elastic scattering angular distributions and total non-elastic cross sections. Next, a similar effort was done for the pre-equilibrium exciton model [73] to enable reliable predictions for nucleon emission spectra. As can be inferred from these two papers, a rather good description can already be obtained without nuclide-by-nuclide adjustment. A subclass which is not yet sufficiently well under control is formed by proton-induced deuteron, triton, Helium-3 and alpha spectra, although TALYS now includes more powerful systematics for pick-up and stripping reactions. For the fourth category, residual production cross sections, such a global modeling adjustment exercise has not yet been undertaken with TALYS although there are indications that it outperforms other codes for this. Table VI shows the results of a global comparison by Konobeyev et al. [109], who compared TENDL and various different intranuclear cascade models as implemented in MCNPX, with all proton-induced experimental cross sections that could be found in EXFOR, for energies up to 150 MeV. The definition of all goodness-of-fit estimators in that table can be found in [109]. Here, it suffices to state that with the exception of the last three 'P' parameters, a lower value means better performance. It is clear that up to 150 MeV TENDL gives the best agreement with, at least, differential data, which may not be surprising since the competing INC codes were initially designed for higher energies than that. For the moment we expect that the above mentioned constrained optical and pre-equilibrium models, combined with newly parametrized level density models [47], automatically produce satisfactory predictions for residual production cross sections. We realize that this is not always the case, and observed deviations up to a factor of 2 suggest the need for further improvements in nuclear models and their parameters. Finally, for recoil information, which are calculated by TALYS with a deterministic approach, we can compare them with the more exact Monte Carlo calculation of [110]. Again, results are usually comparable within a factor of 2.

a. Deuteron, triton, He-3 and alpha sublibrary Also for composite particles, a total number of 2430 isotopes nuclear data libraries are produced. For complex

charged-particles, the models used in TALYS are for a large part the same as that for protons. There are a few notable differences however. The first is that a complex-particle optical model potential is now also used for the incident channel to generate transmission coefficients. The compound, direct and pre-equilibrium models implemented in TALYS are also applicable for incident complex particles. The pick-up and stripping models used for incident nucleons also apply here, though obviously with different parameters [78] than for incident neutrons. An extra contribution is given by a break-up peak in the emission spectrum for some particle-transfer reactions like (d,p) and (d,n). For this, a recent model by Kalbach [79] has been implemented.

b. Photon sublibrary A total number of 2430 isotopes are evaluated for incident photons up to 200 MeV in TENDL-2011. An example of gamma-induced fission on ^{235}U is presented in Fig. 18.

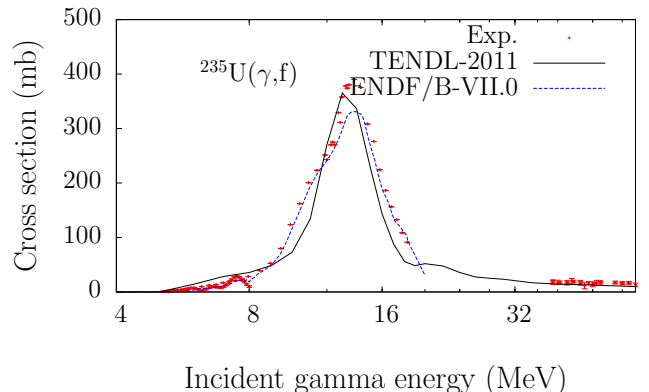


FIG. 18: Gamma induced fission on ^{235}U for ENDF/B-VII.0 and TENDL-2011.

2. Fission yields sublibraries

Independent and cumulative fission yields are provided for a large number of actinides, incident particle energies (and for spontaneous fission) and incident particles. Files for the following cases are included in TENDL-2011:

- Isotopes: $^{223-226}\text{Ra}$, $^{225-227}\text{Ac}$, $^{227-234}\text{Th}$, $^{227-233}\text{Pa}$, $^{230-239}\text{U}$, $^{235-239}\text{Np}$, $^{236-244}\text{Pu}$, $^{240,241,243,244}\text{Am}$, $^{240-249}\text{Cm}$, $^{245-249}\text{Bk}$, $^{248-253}\text{Cf}$, $^{252-255}\text{Es}$ and $^{253,255,257}\text{Fm}$
- Incident particles: spontaneous fission, neutron, proton, deuteron, triton, ^3He and alpha
- Incident energies: (0.0253 eV, 1 eV, 100 eV,

TABLE VI: Comparison of TENDL and intranuclear cascade models for experimental data (EXFOR) for incident protons up to 150 MeV, by means of various goodness-of-fit factors. For the P factors holds, the larger the better, for the other factors the opposite holds.

Factors	Bertini/ Dresner	Bertini/ ABLA	ISABEL Dresner	ISABEL/ ABLA	CEM03	MPM	TENDL ABLA
H	24.	43.	23.	39.	19.	43.	12.
C_H	1.5	2.6	1.2	1.8	1.1	2.7	1.1
D_{CE}	0.6	0.93	0.72	0.97	0.64	0.96	0.45
D_{EC}	3.5	1.7	5.4	3.8	13.	3.6	0.91
R_{CE}	1.1	1.6	1.2	1.6	1.2	1.5	1.1
R_{EC}	4.2	2.2	6.1	4.3	14.	4.2	1.7
F_M	1.4	0.96	1.3	0.99	1.2	1.1	1.1
$\langle F \rangle$	2.9	2.5	3.3	2.8	3.0	2.7	1.9
L	0.6	0.84	0.47	0.66	0.39	0.83	0.28
S	1.8	1.7	1.7	1.6	1.6	1.5	1.3
C_S	1.0	1.0	1.1	1.0	1.1	1.0	1.0
$P_{1.3}$	0.36	0.34	0.31	0.30	0.35	0.31	0.46
$P_{2.0}$	0.70	0.70	0.65	0.60	0.70	0.68	0.84
$P_{10.0}$	0.95	0.97	0.93	0.96	0.96	0.96	0.99

500 keV, 1 MeV, 14 MeV) for neutrons and 20 MeV for others.

The underlying approach is as follows. All independent and cumulative fission yields are calculated with the Wahl systematics [100]. If a fission yield happens to be already evaluated in another library, the evaluated fission yield is imported if it is larger than 0.001 %. In the case of independent fission yields, the whole distribution is renormalized to 2. In this manner, previously evaluated quantities are conserved and missing information is added from mass $A = 60$ to $A = 180$.

C. ENDF-6 Formatting Procedures for TENDL

The data files which are created for TENDL are generally a combination of output results from TALYS, data from other software and existing data tables or libraries (non-TALYS data are usually neutron resonance data, low-energy neutron total, elastic, capture or fission cross sections, average number of fission neutrons, and fission neutron spectra, but other parts of existing libraries can be added too), all processed into an ENDF-6 file. The full ENDF-6 format for storing nuclear data is documented in the ENDF-6 manual [112]. Here, we restrict ourselves to those ENDF-6 procedures that we find the most appropriate for the production of modern, complete and processable nuclear data libraries. As outlined in Ref. [112], see also [113] for a less formal introduction, classes of quantities such as cross sections, angular distributions, covariance data, etc. are represented by so-called MF-numbers, whereas different reaction chan-

nels such as (n,tot), (n,2n), etc. are represented by MT-numbers. Together, the MF/MT combinations allow for a complete representation of a nuclear reaction. For every reaction channel TEFAL writes all cross sections, energy spectra, angular distributions, associated photon production, etc. that are provided by TALYS, or other sources, to the appropriate MF/MT section in the ENDF-6 format.

Most effort of both TALYS and TEFAL has gone into the simulation and formatting of low energy neutron data, not only because this is the most important energy range for applications, but this is also the energy region where both nuclear modeling and data formatting is the most complicated. However, one difference with many traditional nuclear data libraries is that TEFAL can produce data files that extend up to 200 MeV, and also for incident particles other than neutrons, provided of course that such data have been calculated with TALYS first.

We will first describe for each MF section the various options that have been programmed into TEFAL to fill these sections, first for the central values and then for covariance data. In principle, this is always done with incident neutrons in mind, but we will make special mention for incident photons and charged particles, when appropriate. This may be regarded as a first “filtering” action on the ENDF manual, leaving only the procedures that should survive in modern evaluations. We realize that this is subjective, but our experience is that the procedures chosen here are the most robust for the various processing codes. Again, a complete description of all these options can be found in the ENDF manual [112].

Depending on the projectile, purpose, and type of li-

brary, each evaluated file may contain the following data:

1. MF1: General information

Each data file starts with the usual header information like author, type of library, maximum energy, name of institute,*etc.* Next, a textual description of the evaluation methods, experimental data used,*etc.* is included. Also, the full directory of used MF/MT sections is given.

In neutron libraries for actinides, MF1 also contains the average number of neutrons from fission. In the current version of TEFAL, these are adopted from existing data libraries or, if not available, from systematics. The best combination of these two sources is often sorted out by the TAFIS code [114], whose output can be directly used by TEFAL. The total number of neutrons is given in MT452, the delayed neutron data in MT455 and the prompt neutron data in MT456. The components of energy release from fission are given in MT458.

2. MF2: Resonance parameters

MF2 is only used, and allowed, for incident neutrons. Resonance parameters are adopted from the best possible data set, where “best” denotes a combination of most recent and completeness of the resonances. In the majority of cases, MF2 is generated by the TARES code [115], which extracts resonance parameters from the latest measurements (as obtained from the EXFOR database), from compilations (*i.e.* The Atlas of Neutron Resonances [96]), or existing data libraries and turns that into ENDF-6 format. The first two of these sources of information cover the vast majority of experimental data used in TEFAL. The data are generally stored in Reich-Moore format for non-actinides and Multi-Level Breit-Wigner format for actinides. In case of adoption of resonance data from other libraries, TEFAL also “beautifies” the resonance data, *i.e.* all data is rewritten using the e11.6 format, without leading zeroes or leading blanksetc.

3. MF3: Reaction cross sections

By default, all cross section data come from TALYS, while sometimes we also take a small part of the data from other sources. All data calculated by TALYS are stored by TALYS in separate output files and are written to separate MT-sections of MF3. A summarized classification of these cross sections is as follows:

- Total (MT1), elastic (MT2) and non-elastic (MT3) cross sections.

- Inelastic cross sections to discrete states (MT51-90) and other binary cross section to discrete levels such as (n,p) (MT600-640).
- Continuum inelastic cross sections (MT91) and other continuum cross sections such as (n,p) (MT649).
- Exclusive channel cross sections, *e.g.* (n, γ) (MT102), (n,2n) (MT16), (n,p) (MT103), (n,no) (MT22),*etc.*
- For fissionable nuclides, fission cross sections (MT18-21,38).

If the user requests so, a complete description of all open channels (and associated MT-numbers) is included, provided the maximal cross section in an excitation function over the whole energy range exceeds 10^{-9} b. In each MT section, enough incident energies are used to provide a realistic representation of the energy-dependent cross sections.

In general, the elastic scattering cross section is obtained by subtracting the non-elastic cross section from the total cross section. If low energy cross sections are adopted from an existing data library or experiment, the elastic cross section is thus derived from evaluated, usually experiment-based, total cross sections and optical model based non-elastic cross sections. All experimentally observed structure in the data, which would not be predicted by an optical model, is thus automatically retained.

For the construction of a high energy data file, say up to 200 MeV, procedures different from those used in the low energy files have to be employed, since it is no longer possible to store all reactions that describe different sequential particle emissions in separate MT-numbers. There are two possibilities to solve this. The first is to keep the detailed representation of neutron cross sections into several MT sections below 20 MeV, and after the introduction of new MT numbers in 2010 a limit of 60 MeV is now also proposed. Next, one can switch to a more lumped description above 20 or 60 MeV [97, 111, 116, 117]. Most high-energy libraries follow this procedure. For energies above 20(60) MeV, MT5 then contains the total non-elastic cross section, *i.e.* it is equal to MT3. By itself, this quantity is not very interesting, since it is too inclusive, *i.e.* it comprises all the partial cross sections. It can however be combined with the particle yields and relative energy-angle distributions of MF6/MT5 to obtain the particle production cross sections and double-differential cross sections. The total non-elastic cross section thus serves as an important normalization of all the non-elastic partial processes that take place. Of course, one would have to make sure that the actual cross section excitation

curves remain continuous at 20(60) MeV after reconstruction. For example, the $(n,2n)$ cross section is given in MT16 up to 20(60) MeV and as a residual production yield, for the nuclide reached after an $(n,2n)$ reaction, in MF6/MT5. At 20(60) MeV, the same cross section value should emerge at these two different locations.

It is also possible to adopt a different procedure [118], in which there is no abrupt switch at 20(60) MeV. Instead, the MT sections which are used at low energies are used all the way up to the upper energy, *e.g.* 200 MeV, of the data file, and MT5 is only used for the *remaining* cross section. *i.e.* the sum of cross sections which are not stored in the MT numbers for exclusive reactions. The cross section in MT5 thus gradually increases with energy as more channels can not be represented by a pre-defined MT number. This has the advantage that the cross sections for a particular reaction channel remain inside one and the same MT number. Also, it is possible to make use of more exclusive secondary information, such as covariance information in MF33 up to 200 MeV, instead of giving this information only up to 20(60) MeV. A difficulty in creating such data files is that at higher energies the lumped particle production yields and spectra of MF6/MT5 need to be corrected for the channels that have been taken into account explicitly in the other MT sections. This is challenging from a numerical point of view. At the moment, for TENDL we prefer to put an abrupt switch at 20 MeV.

For incident charged particles, in principle the same possibilities exist to store data. There are however a few deviations from the neutron case. First of all the total cross section (MT1) is undefined, since it is infinite. This is a result of the charged-particle elastic scattering cross section which is the square of the sum of a nuclear amplitude and a Coulomb amplitude. This means that the charged-particle elastic scattering cross section is infinite since the associated angular distribution is dominated by the Rutherford formula for Coulomb scattering, which diverges at zero degrees. The ENDF-6 format allows to circumvent this and to store only the nuclear and the Coulomb-nuclear interference cross section in MT2, so that it can be recombined with the Coulomb term afterwards. This quantity is obtained by integrating the associated angular distributions. Note that because of the interference effect, the tabulations can be negative at some energies.

In most proton, or other charged-particle, evaluations the only other section in MF3 is MT5, which contains the total non-elastic cross section, with which the information of MF6/MT5 can be combined to obtain particle production cross sections and (double-)differential cross sections, similar to neutrons. It is however also possible to use specific MT numbers as for neutrons. In that case it is easier to read directly *e.g.* the $(p,2n)$ cross section from MT16, instead of deriving it from the MF3-

MF6/MT5 combination. There are indications however, that the processing route for this option is not (yet) stable enough. Hence, for applied calculations we often use the lumped presentation.

For incident photons, the same choice between specific MT numbers and a lumped MT5 representation can be made. This time however, there is no MT2 (elastic scattering). Similar to charged particles, we generally used the lumped MT5 representation for applied calculations

4. MF4: Angular distributions of secondary particles

The versatility of MF6 (explained below) for the storage of almost any secondary distribution entails that one may choose to use MF4 for the neutron elastic scattering distribution only, while all other secondary angular distributions are stored in MF6. For (in)elastic scattering at incident energies below 20(60) MeV, Legendre coefficients are given on a sufficiently precise energy grid. They are the sum of calculated Legendre coefficients for compound nucleus and shape-elastic scattering. For incident energies above 20(60) MeV, relative angular distributions are tabulated. TEFAL contains options to use either MF4 or MF6 for inelastic (MT51-90) or non-elastic (MT600-) scattering to discrete states. The choice between either MF4 or MF6 is often correlated with the choices for other secondary data (such as gamma production and covariance data).

5. MF5: Energy distributions of secondary particles

For modern evaluations, MF5 has almost completely been replaced by MF6, since the latter can take into account coupled energy-angle distributions. The only reason to still use MF5 is for the very important secondary fission neutron spectra. Indeed, we use MF5/MT18 for this. The fission neutron spectrum may be produced by the TANES code [119]. If we adopt the fission neutron spectra from other libraries, we obviously adopt all associated ENDF-6 parameters as well.

6. MF6: Product energy-angle distributions

In MF6 we store all secondary distributions and relative particle and photon yields. The following data can be included:

- Angular distributions to discrete states for (n,n') (MT51-90), (n,p) (MT600-640), \dots (n,α) (MT800-840), if they are not already included in MF4.

- Double-differential spectra for exclusive channels (all MT-numbers for continuum channels) and recoil data.
- Exclusive gamma yields for discrete states and continuum (all MT-numbers) if they are not stored in MF12,14 and 15.
- Residual production yields ($E > 20(60)$ MeV, MT5).
- Total particle multiplicity, for (n,xn) , (n,xp) , ..., $(n,x\alpha)$ ($E > 20(60)$ MeV, MT5).
- Total particle energy and double-differential spectra ($E > 20(60)$ MeV, MT5).

If MF4 is not already used for this, the angular distribution for inelastic scattering to each discrete state may be given with Legendre coefficients up to 20(60) MeV. Next, for each discrete state the exclusive yields for all the discrete gamma rays that originate from all other levels may be given. Similarly, the angular distribution and gamma rays for the (n,p) etc. reactions to discrete levels may be stored.

For continuum channels like $(n,2n)$, etc., on a sufficiently dense incident energy grid the secondary energy-angle distributions for each ejectile are specified by means of the relative emission spectra and the parameters for the Kalbach systematics for angular distributions [80]. Next, if MF12,14 and 15 are not already used, the photon yield is tabulated as a function of incident energy. For each incident energy, the photon production is given for all discrete gamma lines present in the final nucleus. A continuum photon distribution is added to this. We assume isotropy for all produced gamma rays. Note that we thus do not need MF12-15 for the photon production that accompanies each reaction. As a final subsection, recoil data are given.

For energies above 20(60) MeV, MT5 may contain the production yields of particles and residual products. It also contains the secondary energy-angle distributions for all particles and photons. First, the yields for neutrons are given for the whole energy range. Next, on a secondary energy grid the relative emission spectra are given together with the parameters for the Kalbach systematics for angular distributions. Inelastic scattering cross sections for discrete states have been broadened and are added to the continuum spectra. This procedure is repeated for emitted protons, deuterons, tritons, Helium-3, alpha particles and photons. Finally, the residual production yields are given per final product and, if appropriate, separated for ground state and isomers. All these relative yields and distributions can be multiplied with the cross sections given in MF3/MT5

to get the production cross sections, single- and double-differential cross sections. In the subsections per residual product, the recoils are also given.

For incident charged particles, in MF6/MT2 the relative angular distributions for the nuclear and Coulomb-nuclear interference terms of elastic scattering are tabulated on an angular grid. Next, in MT5 the production yields of particles and residual products are stored, similar to neutrons but now for all energies, i.e. also below 20(60) MeV. The last paragraph of the section above for neutrons applies here too.

For incident photons, we usually take the lumped MF6/MT5 presentation, and discard angular information. Complete energy spectra and residual cross sections are provided however.

7. MF8/9/10: Production of radioactive nuclides

For reactions to nuclides with isomers, MF8 designates where the information for isomeric versus ground state production can be found. On the basis of the pointer set in MF8, isomeric production data are put in either MF9 or MF10. If the reaction channel has no threshold or has low energy resonances (such as (n,γ) , (n,α) , etc. with $Q > 0$), the branching ratios are put in MF9, which can then be combined with the cross sections in MF3 to create the final isomeric cross sections. For threshold reactions, the cross sections are stored directly in MF10, see also Ref. [120] for more details on these choices. By default, TALYS (and thus TEFAL also) treats final states with a lifetime that exceeds 1 second as isomer, but this can be set to another value in the TALYS input.

8. MF12/14/15: Photon yields and secondary distributions

If MF6 is not already used for this, MF12 can be used to store the photon production multiplicities or transition probability arrays. The latter is a simple representation in which the branching ratios for discrete levels are written to the data file, after which a processing code can combine this with the partial cross sections in MF3. We generally use this for discrete level reactions (MT51, etc.) Alternatively, the calculate relative photon yields can be given for partial cross sections. These result from the ratio of the photon production cross section and the (MF3) cross section. Total gamma ray yields and yields per discrete transition can be given.

As for photon angular distributions (MF14), we generally assume that they are isotropic, even though this is generally not true. There are a few reasons for taking isotropy: TALYS can currently not produce photon angular distributions and the applied relevance is, as far as we know, not very large.

If not already stored in MF6, continuum photon spectra can be given in MF15 for partial cross sections other than those to discrete levels.

9. *MF31/32/33/34/35/40: Covariance data*

The representation of uncertainty, or more general, covariance data in the ENDF-6 format is both limited and complex. Nevertheless, we generally try to incorporate a large amount of covariance data in our library. Even though we can apply this for any type of library, we do this for incident neutrons only, as we are not aware of any initiative to study uncertainty propagation for incident charged particles.

The covariance data for the number of fission neutrons, in MF31, are provided by the TAFIS code [114]. On the basis of rather simple assumptions a full covariance file for the total $\bar{\nu}$ is delivered.

In MF32, we store the covariance data of resonance parameters, considering variations in the resonance energy and the neutron, radiative and fission widths. The uncertainties of these parameters are mainly based on the Atlas of Neutron Resonances, 5th edition [96], although other sources are used as well. For each isotope, the bound level resonance parameters, scattering radius and uncertainties have been adjusted to match the microscopic uncertainties (thermal elastic and capture cross sections as well as the capture integral), as given in the Atlas, or as extracted from evaluated libraries. No long-range correlations between uncertainties of Γ_n and Γ_γ are considered for the time being. For correlation of uncertainties between parameters of the same resonance, the method described in Ref. [97] is used. Uncertainties on cross sections have been checked and are partially presented in Refs. [121] and [3]. It should be noted that until recently the scattering radius could not be varied in the existing format for MF32, (which would underestimate the correlations of uncertainties of different resonances in elastic and total cross sections) however we have added its uncertainty in a vacant field in the header of each subsection. This is now part of the official ENDF-6 format. The covariance data of MF32 are all produced by the TARES code [115], although we also have the flexibility to read in data from existing libraries.

In MF33, we store the covariance data of most, but not all, reaction channels that are given in MF3. All covariance data are generated with the TASMAN code, which generates TALYS runs using a Monte Carlo parameter sampling method. In principle, for each MT-number, the stored information may consist of:

1. Covariance matrix element for MT₁, E₁ and MT₁, E₁ (variances).

2. Covariance matrix element for MT₁, E₁ and MT₁, E₂ (correlations of uncertainties for the same reaction channel between different energies).
3. Covariance matrix element for MT₁, E₁ and MT₂, E₁ (correlations of uncertainties of different reaction channels for the same energy).
4. Covariance matrix element for MT₁, E₁ and MT₂, E₂ (correlations between different reaction channels for different energies).

but the latter completeness of inter-channel uncertainty correlations is only used for very important channels. Classes 1 and 2 are covered by NI-type subsubsections with the flag LB=5, followed by an LB=8 section which contains the cross section variances multiplied by 0.001 (a suggestion taken over from S. Tagesen and used, for example, in the JEFF-3.0 Fe-56 file). There are indications that the LB=8 section is no longer necessary in contemporary processing codes but we still include it. These are the covariance data TEFAL writes by default. Classes 3 and 4 can also be covered by the flag LB=6 to account for the different energy grids that two correlated MT-sections may have. Since the total correlation matrix is fully symmetric, we only need to include the correlation elements between different MT-numbers once, and we do that in the subsection with the lowest of the two MT-numbers. Usually, we include covariance information for all the total cross sections, the most important lumped partial cross sections and a few individual inelastic cross sections per level (MT51-54). We generally do not include covariance data for MT-numbers 600 and higher.

In MF34, we store the covariance data of the angular distributions that are given in MF4. All covariance data are generated with the TASMAN code, which generates TALYS runs using a Monte Carlo parameter method. We generally use MF34 only for elastic scattering (MT2), in which case covariance data are given for the first 6 Legendre coefficients. Both intra- and inter-correlations of the uncertainties of the various Legendre coefficients are given. As in MF33, the LB=5 representation is used.

The covariance data for fission neutron spectra are provided by the TANES code [119]. The contents of MF35 are covariance data between different outgoing energies of the neutron spectra.

Finally, in MF40 we give the covariances for isomeric production, *i.e.* the covariance data belonging to MF10.

VI. TOTAL MONTE CARLO AND OTHER APPLICATIONS

For the TENDL library described above, a single ENDF-6 covariance data file is created by averaging the

hundreds to thousands of complete nuclear data sets coming from TALYS or other codes, see the box at the lower left hand side of Fig. 9. An alternative approach [3] is to take the effect of a single random sampling of nuclear model parameters all the way to the end, *i.e.* to create one ENDF-6 file per random set of input parameters, process it and perform an applied calculation. This process is depicted in Fig. 19.

In other words, every random curve is stored in a different ENDF-6 file, while every ENDF-6 file is complete for all quantities, *i.e.* MF1-15 are used. This approach has later been coined (by M. Herman) “Total” Monte Carlo (TMC) and makes uncertainty propagation a lot easier (apart from the calculation time) than when using perturbation and covariance software.

A. Uncertainty Propagation: TMC

The complete control of the production of nuclear data can thus be used to repeat the same applied calculation a large number of times, whereby each time the input parameters are changed from one iteration to the next one, leading to slightly different results. Since 2008, several TMC applications have been published: on criticality-safety benchmarks [121, 122], fusion-related benchmarks [123, 124], uncertainty propagation for a Sodium Fast Reactor [125, 126, 127], evaluation and applications overview [2, 128], comparison between TMC and perturbation methods [129, 130, 131], and uncertainty propagation for burn-up of PWR fuel cell elements [132]. In these references, the propagation of nuclear data uncertainties to nuclear systems are realized by means of Monte Carlo calculations, by repeating a large number of times the same calculation/simulation, each time using a different nuclear data file for the isotope of interest. The necessary step, being automation of the production of random libraries for the simulations, is now under control for different codes such as MCNP [133], SERPENT [134] or DRAGON [135]. The procedure to generate random ENDF files together with an ENDF file containing the average cross sections and the covariance information was detailed in Ref. [3]. In summary, 20 to 30 theoretical parameters are all varied together within pre-determined ranges to create TALYS inputs, (see for instance Table III). With the addition of a large number of random resonance parameters, nuclear reactions from thermal energy up to 20 MeV are covered. The TALYS system creates random ENDF nuclear data files based on these random inputs. To simultaneously enable uncertainty calculations with the conventional perturbation method, at the end of the generation of all the random files the covariance information (average, uncertainties and correlations), which is automatically available, is also extracted and formatted into

an ENDF file.

After the generation of random nuclear data files, a few codes and programs are used: a transport (plus burn-up) code and NJOY [136, 137]. We emphasize again that automation and a disciplined, quality assured working method (with emphasis on reproducibility) are imperative to accomplish this. First of all, TALYS, NJOY and the transport code(s) need to be very robust and secured against relatively large variations in input parameters. Next, all detailed knowledge about the material/benchmark in question should be present in the input files of these codes. It is clear that manual intervention must be completely excluded in the sequence of code calculations. Once all that is assured, the rest is relatively simple: if we can do a full calculation loop once, we can also do it 1000 times.

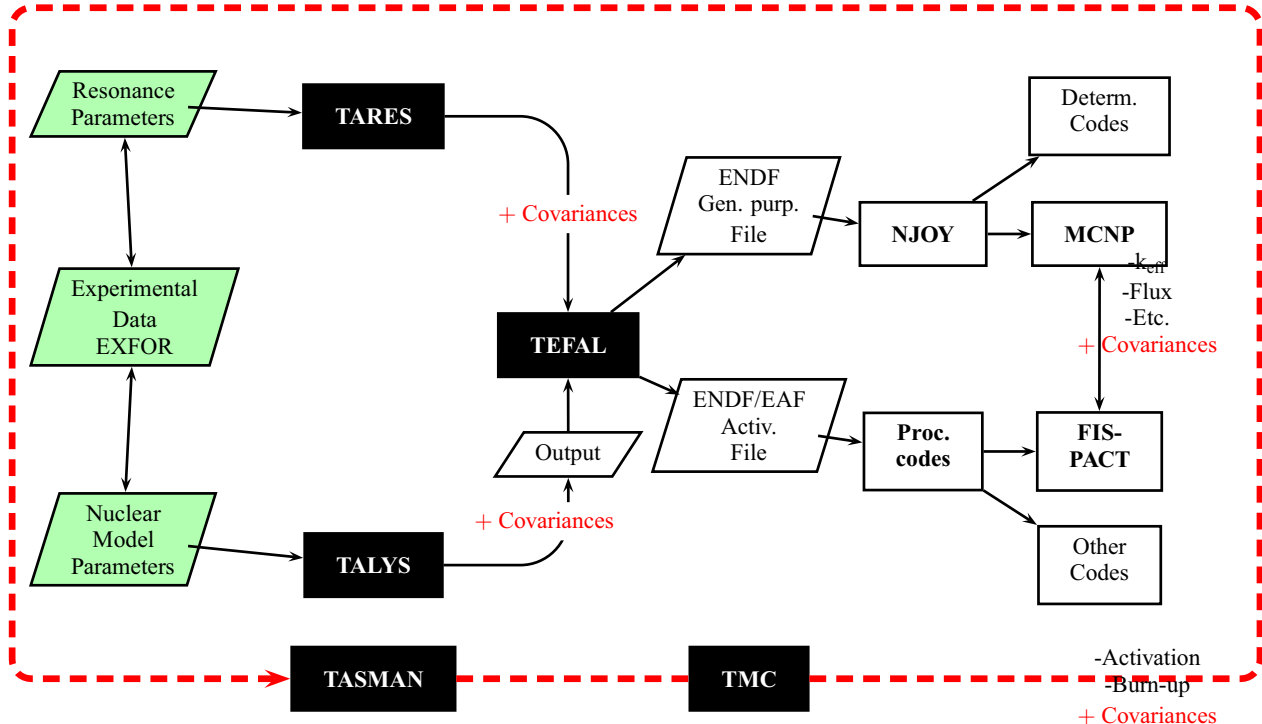
The input files for this method are a geometry input file and n random ENDF files. Each random ENDF file is produced by the TALYS system (see Fig. 8), is fully reproducible and consists of a unique set of nuclear data. Each random file is completely different from another one: $\bar{\nu}$ and energy released per fission (MF1 in ENDF language), resonance parameters (MF2), cross sections (MF3), angular distributions (MF4), fission neutron spectrum (MF5), double differential data (MF6), isomeric data (MF8-10) and gamma production data (MF12-15) are varied.

Examples of random cross sections for important actinides are presented in Fig. 20.

From the n different nuclear data files, n different values of a design parameter are calculated with an application code, such as n different k_{eff} values. If a Monte Carlo transport code is used (as MCNP or SERPENT), a reactor parameter can be obtained with its statistical uncertainty. In the case of deterministic codes, the statistical uncertainty does not exist. From the calculated probability distribution of k_{eff} , the total standard deviation σ_{total} reflects two different effects

$$\sigma_{\text{total}}^2 = \sigma_{\text{statistics}}^2 + \sigma_{\text{nuclear data}}^2. \quad (198)$$

The first one ($\sigma_{\text{statistics}}$) is from the statistical uncertainty. Depending on the calculated parameters, the statistical uncertainty can be provided by the simulation code. In the case of k_{eff} , reaction rates and macroscopic cross sections calculations, it is derived from the number of histories (neutrons) used in the Monte Carlo code. It typically varies as $1/\sqrt{N}$, N being the number of considered histories, is known in advance and in principle can be minimized by investing enough computer time. In other cases, such as for the calculation of the number densities obtained during burn-up calculations (with a transport code followed by a depletion code), $\sigma_{\text{statistics}}$ is not provided. In this case, an estimation of the statistical uncertainty can be realized as follows:



Monte Carlo: 1000 runs of all codes

FIG. 19: Total Monte Carlo: Loop over all basic physics and application software.

- the benchmark parameters are fixed to their nominal values (as defined in the benchmark description),
- the nuclear data are also fixed to a given library,
- the seed defining the sequence of the pseudo random numbers used during the simulation is randomly changed and new calculations are realized. After a large number of calculations, the obtained results (distributions) for the reaction rates and other quantities can be used to extract a standard deviation, equal to as $\sigma_{\text{statistics}}$.

This method is tested by comparing the statistical uncertainty given by the Monte Carlo code for k_{eff} and the one obtained by varying the seed of the pseudo random numbers. In the case of k_{eff} , both uncertainties agree. It should nevertheless be noted that this method provides small “statistical” uncertainties for the number densities, regardless of the absolute number densities (if a nucleus is produced in a large number or not). For instance, the “statistical” uncertainty on ^{233}U is about 0.8 %, and 0.02 % for ^{236}U , with ^{236}U being produced 10^6 times more than ^{233}U . In Ref. [138] similar results

are found: standard deviations are almost the same during the burn-up for a given element, and the statistical uncertainties are rather small (from 0.01 to 0.1 % for actinides). The last quantity in Eq. (198) ($\sigma_{\text{nuclear data}}$) lies in the use of different random nuclear data files from one simulation to the next one. They induce a spread in the k_{eff} distribution, which can unequivocally be assigned to the spread of cross sections, angular distributions and so on. This spread is not known and is to be derived from the present Monte Carlo approach. The quadratic sum of the two distinct spreads is equal to the total observed standard deviation. If the observed spread is of the order of the statistical uncertainty (first effect), only a maximum value can be attributed to the spread due to nuclear data. An alternative approach, presented in the last section of this paper and called “fast TMC”, is making use of short calculations, where the statistical uncertainties are larger than the effect of nuclear data. But by randomly changing seeds, the statistical effect can be evaluated and removed.

As mentioned before, the TMC method allows to vary much more information than included in the covariance files used by the perturbation methods, which considers resonance parameters (MF2) and cross sections (MF3)

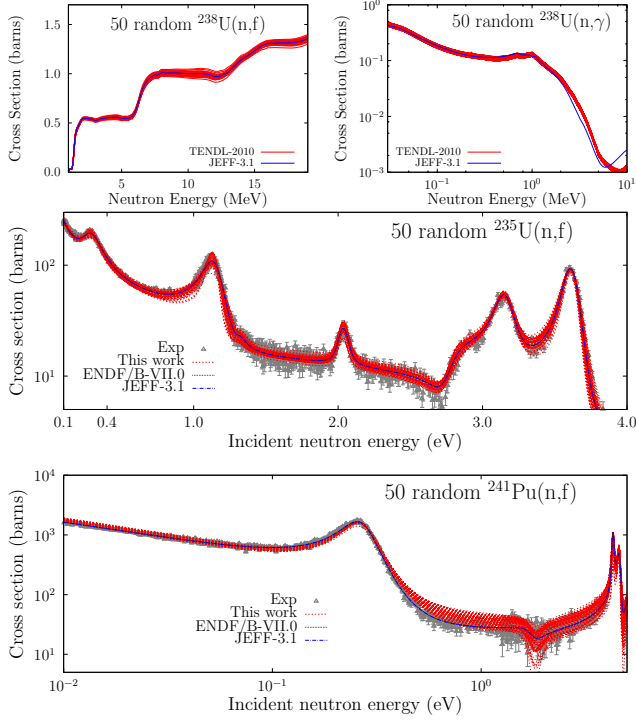


FIG. 20: Random capture and fission cross sections for $^{235,238}\text{U}$ and ^{241}Pu used in the TMC method.

uncertainties, with a limited amount of cross correlations. An example of a k_{eff} calculation for a typical PWR pin cell at 0 GWd/tHM is presented in Fig. 21 for 300 random calculations [139].

The two first moments of the distribution are presented as a function of random sampling. It can be seen that the probability distribution is still fluctuating, but the impact on the average k_{eff} and the standard deviation (uncertainty) is small. A necessary preliminary step before applying this method is to adjust the important nuclear data uncertainties (mainly cross sections and $\bar{\nu}$) to accepted levels, such as defined by experimental differential data. The obtained simulated quantities on reactors and other nuclear systems will depend on the nuclear data uncertainties. In the following a few examples of the application of the TMC method will be presented.

1. Criticality benchmarks

The application of the TMC method to criticality-safety benchmarks was historically the first one realized. The k_{eff} benchmarks are extracted from the ICSBEP list [140] and can easily be used with MCNP. As mentioned, the production of MCNP libraries (ACE files) is also automated with NJOY. The TMC method was

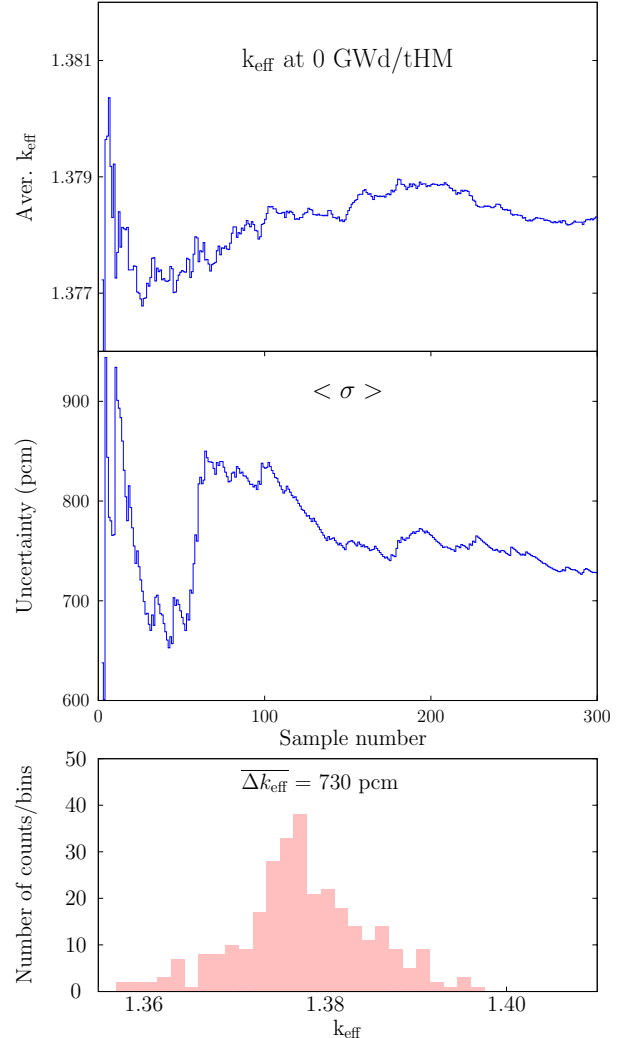


FIG. 21: Top and middle: Example of convergence for the k_{eff} distribution at 0 GWd/tHM in the case of changing ^{238}U nuclear data. Two moments of the distribution are presented: the average and the standard deviation. See Ref. [139] for details. Bottom: Histogram of the k_{eff} distribution.

tested on hundreds of benchmarks, from fast to thermal systems, highly uranium enriched or full plutonium systems. An example of criticality benchmarks is presented in Fig. 22 (see Ref. [121] for details). In this figure, only two elements were randomly varied: ^{19}F and Mo. By selecting the benchmarks where these two elements are abundant, their effect can be noticed. For benchmarks where Mo is present in small quantities or far from

the reacting area, the k_{eff} will be slightly affected. An interesting case is the study of variations of important actinides and their impact on criticality benchmarks. Uranium 235 and 238 as well as ^{239}Pu , being present

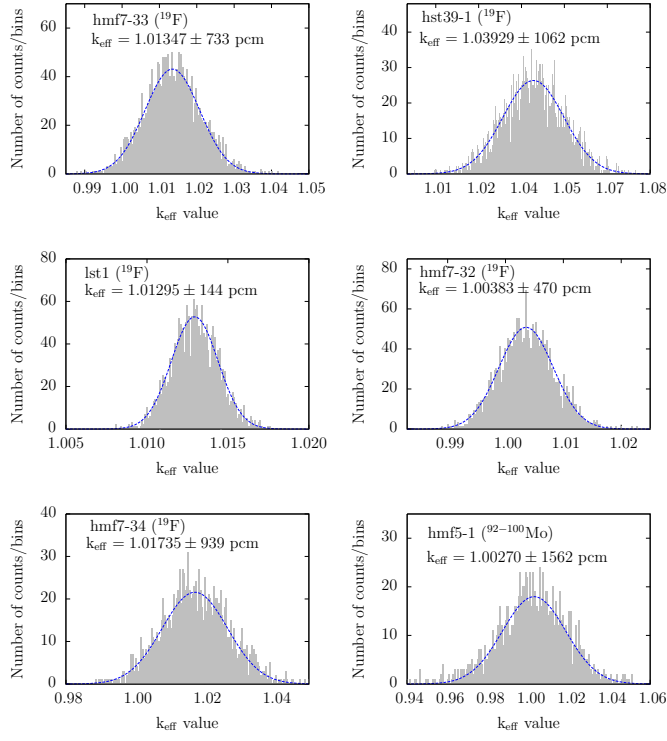


FIG. 22: k_{eff} distribution for criticality-safety benchmarks containing ^{19}F and $^{92-100}\text{Mo}$. Nuclear data for the isotopes in brackets are randomly varied.

in large amount in the benchmarks will have a major effect. Other types of nuclear data can also be predominant in the sense of uncertainties. Not only the amount of a given material is important, but also the knowledge of its nuclear data. For instance, the fission cross section of ^{235}U is a key-player in these benchmarks, but as it is well known, it will have a limited impact. It is then a trade-off between the sensitivity and the degree of knowledge which will determine the importance of a nuclear reaction for uncertainty propagation. A recent question is related to other nuclear data such as thermal scattering data or nuclear data for light elements. What is their global impact on benchmarks? Is the thermal scattering data of H in H_2O as important as the thermal fission cross section of ^{235}U ? To partially answer this kind of questions, Table VII presents the uncertainties for a selected number of benchmarks, varying different nuclear data. Additional results and explanations can be found in Refs. [121, 141, 142].

Additionally to the impact of a complete ENDF file, it is possible to study the effect of a part of the nuclear data file, such as the resonance range, the angular distribution, or the fission neutron spectrum. To realize that, the same procedure is applied, but instead of

TABLE VII: Examples of uncertainties on k_{eff} for criticality-safety benchmarks, varying specific nuclear data. Each criticality benchmark name consists of three letters: the first one defining the degree of enrichment (h for high, i for intermediate, l for low enriched ^{235}U , p for a plutonium benchmark), the second one defining the physical form (m for metal, s for solution, c for compound) and the last one defining the neutron spectrum (f for fast, t for thermal and i for intermediate)

Benchmark	Variied Nuclear data	Impact on k_{eff} (pcm)
hst42-1	H in H_2O therm. scat.	200
lct7-1	H in H_2O therm. scat.	120
pst1-1	H in H_2O therm. scat.	350
pst12-14	H in H_2O therm. scat.	620
hct21-21	H	10
lct5-9	H	30
pst25-19	H	50
lct4-17	H	80
hst42-5	H	150
lct60-1	^{16}O	15
mst5-63	^{16}O	50
lct12-3	^{16}O	80
pst25-2	^{16}O	110
pst22-9	^{16}O	210
hst39-1	^{19}F	$\simeq 800$
pmf12	$^{54-58}\text{Fe}$	$\simeq 100$
hmf27	$^{204-208}\text{Pb}$	$\simeq 300$
mcf1	^{238}U	750
pmf1	^{239}Pu	800
pmf1	^{240}Pu	150

varying the complete ENDF file, only sections are randomly changed. Then the simulations can be performed and uncertainties are obtained due to $\bar{\nu}$, the fission cross section in the fast neutron range, or the capture cross section: see Table VIII.

2. Shielding benchmarks

Another domain of application of the TMC method is the shielding calculation [123, 124]. Similar to criticality-safety benchmarks, the propagation of nuclear data uncertainties to fusion-related benchmarks can be realized by means of Monte Carlo calculations, by repeating a large number of times the same shielding MCNP calculation (typically a thousand times), each time using a different nuclear data file for the isotope of interest. As for the criticality benchmarks, this collection of random nuclear data files is produced by running the TALYS system many times and contains cross sections, resonance parameters, single- and double-differential distributions. All these quantities are thus randomly varied from one

TABLE VIII: Examples of uncertainties on k_{eff} and reaction rates due to ^{235}U for a typical PWR pin cell. For details, see Ref. [143]. Uncertainties are presented in %. “rr” stands for reaction rates.

Nuclear data	Quantity	burn-up (GWd/MTU)	
		0	50
All	k_{∞}	0.50	0.28
MF1		0.19	0.06
MF2		0.39	0.20
MF3		0.06	0.04
MF4		0.05	-
MF5		0.27	0.16
All	rr $^{235}\text{U}(n,\gamma)$	2.05	2.28
MF1		-	-
MF2		1.90	2.17
MF3		0.39	0.30
MF4		0.03	0.02
MF5		0.43	0.36

benchmark calculation to another. The NJOY processing code processes all these nuclear data libraries into ACE files which are then used by the Monte Carlo code MCNP. Finally, for every random nuclear data library an entire MCNP calculation is performed. With TMC, for the first time a complete set of fusion shielding benchmark calculations can be presented with the inclusion of their uncertainties, using a method without linearization, and implicitly taking into account cross section correlations, cross correlation between reactions and the uncertainties of single- and double-differential distributions.

Fusion shielding benchmarks are generally used to test design codes and nuclear data for fusion devices. A new nuclear data library is usually validated with a large number of these benchmarks by comparing calculation results (using the library and *e.g.* a Monte Carlo code such as MCNP) with integral measurements. In general, the nuclear data file for a given isotope or element is created on the basis of theoretical nuclear model calculations and microscopic measurements, with eventually some adjustments due to a restricted number of integral measurements. As the collection of integral experiments used in the TALYS system is heavily fission-dominated, such adjusted data files usually produce good agreement with *e.g.* criticality-safety or fission reactor benchmarks, but as the energy range of interest is generally in the thermal and resonance range, the same data files may perform poorly for 14-MeV spectra coming from (d,t) reactions. In the fast neutron range, a number of nuclear model parameters is varied and is entered into TALYS.

Examples of random angular distributions are pre-

sented in Fig. 23. The basic approach used for shielding benchmarks is very close to the one for criticality benchmarks (see Ref. [3]) and can be summarized as follows:

1. Because of the small number of available shielding benchmarks, a restricted number of isotopes can be considered. They range from silicon to tungsten (for instance Al, Co, Cr, Fe, Zr, Ti, W).
2. For the selected isotope, a large number of different ENDF-6 nuclear data libraries are created (1000 to 2000) using random model and resonance parameters included in the TALYS system (as the shielding benchmarks use 14 MeV neutron source, the resonance range is much less relevant than the fast neutron range).
3. All ENDF-6 files are processed with the NJOY code to produce ACE libraries for the Monte Carlo code MCNP.
4. For each shielding benchmark [144, 145, 146], calculations are performed using each time a different set of ACE files (for each isotope of a given element).

These calculations provide a large number of leakage fluxes for each benchmark, from which statistical quantities can be extracted (such as means, widths, skewness, convergence behavior). This type of procedure was already applied for numerous shielding benchmarks, as presented in Ref. [123]. To illustrate one case, Fig. 24 presents the case of the Oktavian benchmark (in this case, a copper sphere with at its center a 14 MeV d-T neutron source) for which the $^{63,65}\text{Cu}$ nuclear data were randomly changed. The shadow below the curve represents the $1-\sigma$ uncertainty coming from the variation of Cu isotopes.

3. PWR burn-up

An application where the TMC method presents some advantages compared to traditional methods is the uncertainty propagation for burn-up and isotope inventory. By using a transport code and a depletion code where the same nuclear data are used (such as the Monte Carlo SERPENT code, which uses ACE libraries for both transport *and* burn-up), it is straightforward to repeat identical burn-up calculations with random nuclear data. This was applied to the OECD benchmark for Uncertainty Analysis in Best-Estimate Modelling (UAM) for Design, Operation and Safety Analysis of LWRs [147]. The description of the geometry of the benchmark is given in Ref. [147] and is not repeated in the following.

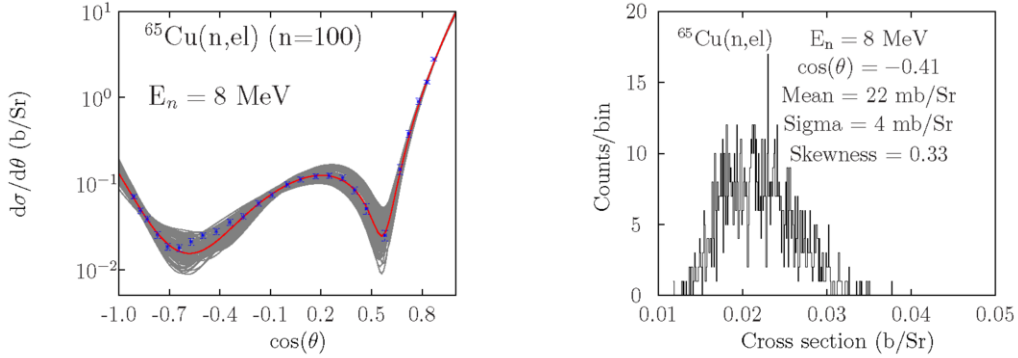


FIG. 23: Random calculations in the fast neutron range for the angular distribution of $^{65}\text{Cu}(n,\text{el})$ at 8 MeV. The left panel presents the 100 first calculations and the right panel presents a projection at $\cos(\theta) = -0.41$.

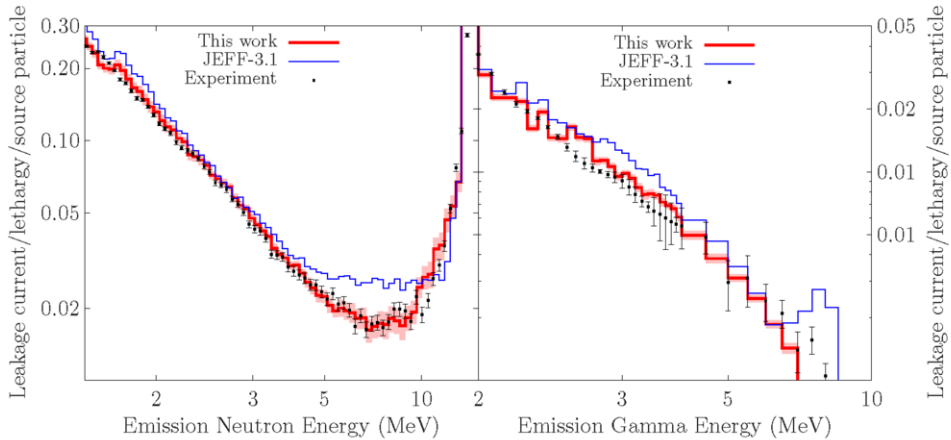


FIG. 24: Oktavian benchmark results with the copper data being random, compared to the results with the JEFF-3.1 library.

The fuel test is a typical fuel rod from a TMI-1 PWR, 15x15 assembly design.

Because of the different stages of the reactor calculations (transport, depletion and radiotoxicity), the nuclear data have been historically divided in different categories. The underlying quantities are nevertheless the same. For instance, because different codes calculate separately the transport of neutrons and the depletion of fuel, different nuclear data (namely transport and activation data) happened to be used for the same reactions. With SERPENT, it is now possible to specify a unique source of nuclear data for the whole chain of calculations, from the first irradiation time to centuries of decay.

For convenience, some parts of the nuclear data are still separated because of the type of physics they represent: fission yields, decay data (half-lives, Q-values, gamma decay scheme...) and reactions of a nucleus with an incident neutron (cross sections, emitted particles, emission spectra, angular distributions...). These three types of data are also measured and evaluated by different communities with different knowledge:

1. *Transport data*: associated with cross sections, angular distributions, single and double differential data, emission spectra. These quantities are used in the transport calculations as well as with the depletion code. The uncertainties on these quantities were verified in many different calculations and references (see for instance Refs. [3, 13, 97, 121, 123, 126, 127, 148]).

2. *Fission yields*: In the depletion calculations, the fission products produced from the fission of actinides are based on the fission yields taken from separated evaluated files. In the present case, they are obtained from the TAFIS code and normalized to the ENDF/B-VII.1 yields and uncertainties. If a yield (and its uncertainty) is present in ENDF/B-VII.1, its value is adopted, and if not, the Wahl systematics is used [100]. For the present calculations, yield uncertainties are limited to a maximum of 100 %.

3. The *decay data* are the decay properties of an excited or unstable nucleus (half-lives, Q-values, decay scheme).

A complete list of results can be found in Ref. [143]. It was found that for burn-up applications, the decay data have a very limited impact (which might be different in decay heat calculation). An example of the impact of the nuclear data and engineering quantities is presented in Fig. 25 for the number densities of ^{237}Np . Depending on the quantity which is considered (k_{eff} , 1-group cross sections, reaction rates, or number densities for actinides or fission products), each of the above nuclear data “types” will have a different impact. For instance, fission yields do not induce large uncertainties except for inventories of fission products.

4. Pseudo fission product

Another advantage of the TMC method is the possibility to account for a “pseudo fission product (PFP)”. The notion of PFP comes from the time when all fission products could not be simulated in a separated way and a PFP was created in order to concentrate in a single product the effects of many. This PFP is still used nowadays in many reactor calculations. By randomizing at the same time nuclear data for a selection of fission products, it is possible to simulate this PFP. The combined effect is presented in Ref. [143] and Fig. 25. For this exercise, a total of 138 fission products from ^{72}Ge to ^{167}Er was considered. Their impact on a burn-up calculation for a typical PWR pin-cell is also summarized in Table IX.

TABLE IX: Examples of uncertainties on k_{eff} , reaction rates and number densities due to lumped fission products for a typical PWR pin cell. For details, see Ref. [143]. Uncertainties are presented in %. “rr” stands for reaction rates, “Nd” for number densities.

	Burn-up (GWd/MTU)			Cooling time		
	0	20	40	60	10y	100y
k_{∞}	0.05	0.36	0.31	0.28		
rr $^{235}\text{U}(n,\gamma)$	0.03	0.03	0.09	0.19		
rr $^{239}\text{Pu}(n,f)$	0.00	0.21	0.28	0.40		
rr $^{239}\text{Pu}(n,\gamma)$	0.00	0.23	0.30	0.40		
Nd ^{239}Pu	0.00	0.37	0.44	0.54	0.54	
Nd ^{240}Pu	0.00	0.10	0.10	0.19	0.19	0.18
Nd ^{137}Cs	0.00	0.00	0.01	0.02	0.02	0.02
Nd ^{142}Nd	0.00	12.6	12.8	12.7	12.7	12.7
Nd ^{153}Eu	0.00	5.03	8.10	10.4	10.4	10.4

5. GEN-IV example

The TMC method was recently applied to one of the Generation-IV systems: the Kalimer-600 Sodium Fast Reactor [126]. The impact of nuclear data uncertainties on many reactor quantities (sodium void coefficient, k_{eff} and the delayed neutron fraction β_{eff}), burn-up and radiotoxicity due to a large number of isotopes (actinides and structural and coolant materials such as Na, Fe, Zr) was assessed. A detailed description of the model can be found in Ref. [126] and will not be repeated here. The MCNP code was used for the transport part of the simulation together with FISPACT for the depletion steps [149]. The sodium void reactivity (SVR) in units of dollars (\$) can be obtained with the following equation

$$\text{SVR} = \frac{k_2 - k_1}{k_1 k_2} \frac{1}{\beta_{\text{eff}}} \times 10^5, \quad (199)$$

where the number of delayed neutrons β_{eff} (in units of pcm) and the k_{eff} values are obtained from the MCNP calculations, following the calculation method presented in Ref. [150]. k_1 corresponds to the core flooded with Na coolant, and k_2 to the same core voided of Na coolant. In both cases the Na coolant present in the axial and radial reflectors is supposed to remain unchanged. The SVR is a difficult case for a Monte Carlo code because it is obtained from the difference of two values (k_{eff} with and without sodium) close to each other. The small difference of k_{eff} can easily be smaller than the statistical uncertainty and (very) long calculations are needed. Results on the void coefficient, k_{eff} and β_{eff} are presented in Table X. The statistical uncertainty distribution of the

TABLE X: Uncertainties on the sodium void coefficient (SVR) due to different nuclear data uncertainties.

Isotope	Varied Nuclear data	Uncertainty on		
		SVR	k_{eff}	β_{eff}
^{23}Na	all	$\simeq 6\%$	130 pcm	<1 %
^{238}U	all	$\simeq 6\%$		2.5 %
^{239}Pu	all	$\simeq 2.5\%$	800 pcm	1 %
^{56}Fe	all		110 pcm	<1 %

SVR is presented in Fig. 26 for more than 800 MCNP calculations.

This study of reactor coefficients could point out some shortcoming of uncertainty propagation methods, not specifically linked to the TMC method, but related to the method of production of covariance files or of random nuclear data:

- Strong correlation of calculated nuclear data covariances

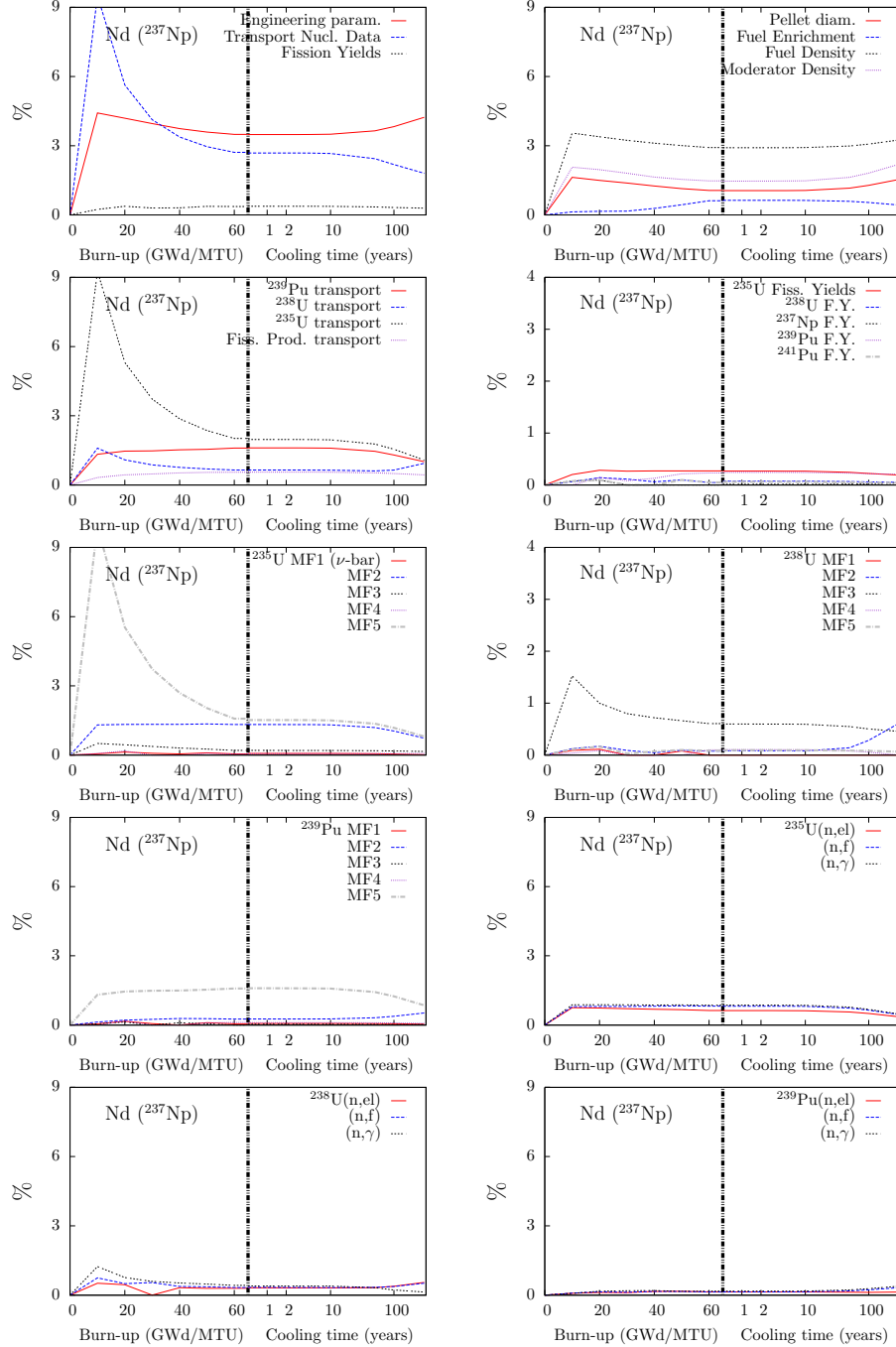


FIG. 25: Uncertainties on ^{237}Np atomic densities for different reactions and nuclear data quantities in the case of the burn-up of a typical PWR fuel rod (see Ref. [143] for details).

As a result of the use of the TALYS system and theoretical models, energy-energy correlations for a given cross section are quite strong (without the mathematical inclusion of differential experimental

data, energy-energy correlations are above 50 %). It affects the benchmark results in the sense that, for instance, the capture cross section in the fast range will move up or down from one random eval-

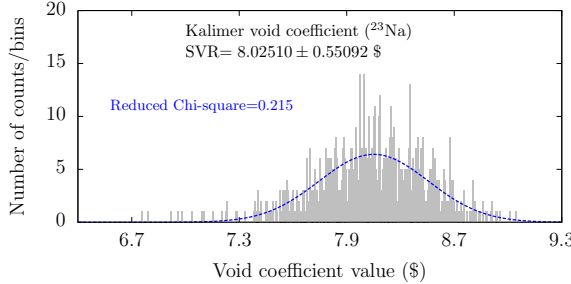


FIG. 26: Calculated sodium void coefficient (SVR) for the Kalimer-600 design, varying the ^{23}Na nuclear data file [126].

uation to another, keeping a rigid shape. Even if correlations are not basic physical quantities like cross sections, reflecting only the method used to obtain cross sections, it is generally believed that differential experimental data should be mathematically included in the process and therefore correlations will be weaker. As a consequence the shape of cross sections should become less rigid and the benchmark results could vary more. We are currently studying solutions to that problem, as for instance using the “Unified Monte Carlo” presented in Ref. [151].

- Correlations between isotopes

Covariance files do not in general contain cross correlation between isotopes. This is a common issue in nuclear data evaluation, and it is not restricted to the TMC method. Cross correlations between isotope come from experimental measurements. When a reaction rate is measured, this is performed together with a standard reaction (often a fission chamber containing ^{238}U). The standard reaction is used to normalize the data of interest and to obtain a convenient unit (such as barns). This manipulation brings a strong correlation between the reaction for the isotope of interest and the standard reaction. Cross correlations between isotopes can also come from similar experimental methods used to obtain a nuclear quantity. This deficiency to disregard them in nuclear data evaluation is important when trying to combine uncertainties due to different isotopes. Finally, measurements done on natural elements automatically induce correlations between isotopes.

Most of these drawbacks are also related to perturbation methods using covariance matrices, or find their origins in the nuclear data evaluation procedure which implies limitations for all methods using nuclear data. The TMC method is nevertheless the most general one and contains the least amount of approximations, especially when ex-

perimental covariance data are properly taken into account. Extension of this method with ideas as exposed in Ref. [157] are thus required.

Similar to the previous study for the void coefficient, k_{eff} and β_{eff} , random nuclear data files are used to calculate inventories at the end of the fuel cycle and radiotoxicities up to 10^7 years after irradiation. Each set of random nuclear data files provides a different inventory and radiotoxicity. This is an application of the TMC method to burn-up calculations. As mentioned before, a large number of similar calculations are performed, randomly changing each time the transport nuclear data files. An example of calculated inventories for a few actinides as a function of irradiation time is presented in Fig. 27. The time for one burn-up calculation, and thus for each random set of nuclear data, is rather long (about 5 days on a single 3 GHz CPU), and a total of 250 burn-up calculations were performed. This number is significantly smaller than in the previous sections, but considering the amount of computational power at our disposal, it gives a reasonably precise estimate of the uncertainties. From previous studies with the TMC method (see Refs. [126] or [123]), we can estimate that the uncertainties are known to about 10 % after 250 samples. It can be noted that the impact of transport nuclear data is not the same for all actinides. Globally, the nuclear data uncertainties are larger for small quantities of specific actinides.

6. Non Gaussian distributions

One of the unexpected outcomes of the TMC method is to obtain non-Normal probability distributions for a given system quantity. Up to now, the non-symmetric distributions were seen for k_{eff} in Refs. [3, 121] for zirconium, tungsten and lead (*hmf-64* benchmark series), for the ADS and other systems. It was shown in these references that the k_{eff} distributions can be well represented by the so-called “extreme value theory” or EVT, see Fig. 28. The corresponding benchmarks are mostly defined as fast systems, meaning that over 50 % of the fissions occur at energies over 100 keV. Nevertheless, the EVT behavior is also noticed in two thermal systems (over 50 % of the fissions occur at energies less than 0.625 eV), *ict3-132* and *ict3-133* for $^{90-96}\text{Zr}$, and one intermediate system (over 50 % of the fissions occur at energies between 0.625 eV and 100 keV), *hci5-5* for $^{90-96}\text{Zr}$. However, not all systems where zirconium isotopes are varied present the EVT behavior. In the case of *mmf11-2* and *mmf11-3*, k_{eff} distributions are close to Normal, whereas in the case of tungsten and lead, all studied benchmarks show an EVT behavior. In the case of lead isotopes, the asymmetric k_{eff} distribution was related to the shape of the inelastic and capture cross section distributions at a few MeV where a deviation from a Gaussian

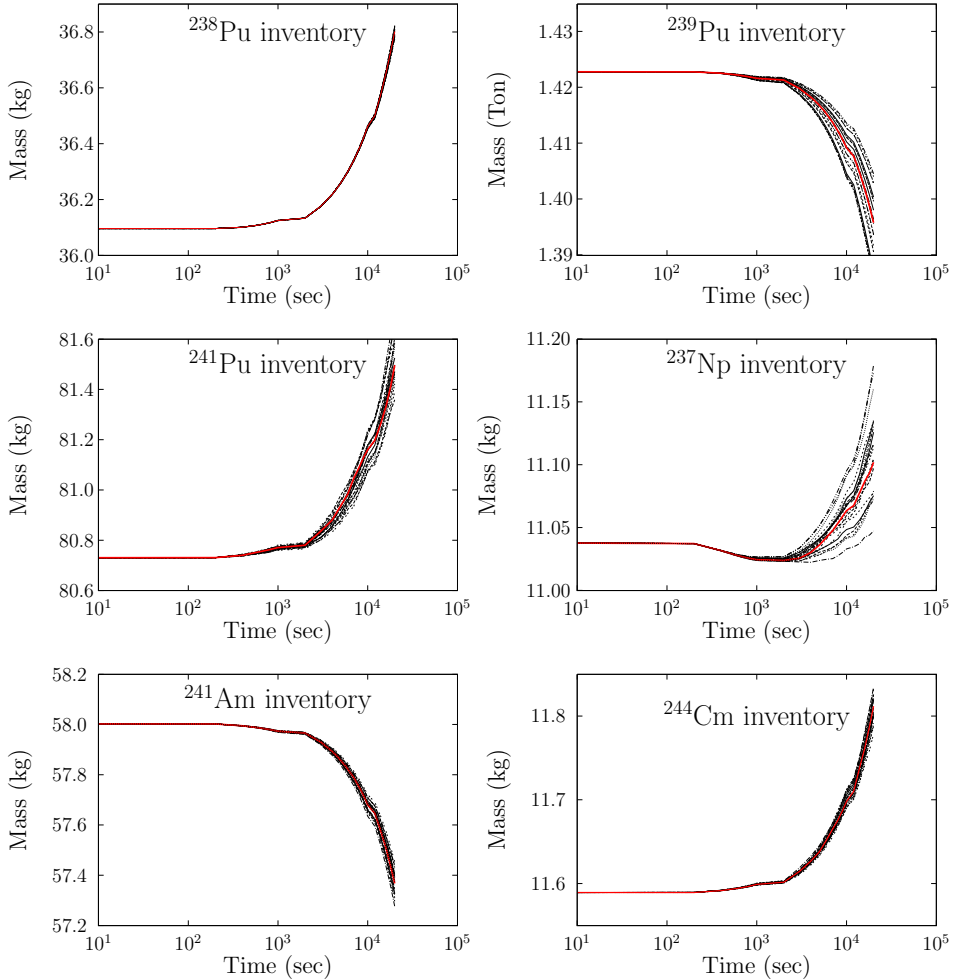


FIG. 27: Examples of calculated inventories for $^{238},^{239},^{241}\text{Pu}$, ^{237}Np , ^{241}Am and ^{244}Cm for the KALIMER-600 Sodium Fast Reactor (see Ref. [126]). The spread between the curves are due to variations in ^{238}U nuclear data.

was observed.

In the case of zirconium isotopes, asymmetric distributions appear for systems where zirconium is used as a reflector (*hci5-5*) but also in the core with graphite reflector (*ict3*). Nevertheless in the case of *mmf-11* (with Zr in the core and graphite as reflector), the distribution is symmetric. The main difference between these systems is the neutron spectrum, maximum at thermal energy for the *ict3* benchmark, and above thermal energy for the *hci5-5* and *mmf-11* benchmarks.

If one looks at the nuclear data files which were used to produce very small k_{eff} values for the *hci5-5* benchmark ($k_{\text{eff}} < 0.85$), it can be noticed that they also induce low k_{eff} values for the *ict3* and *mmf-11* benchmarks. Alternatively, nuclear data files which were used to produce very large k_{eff} values for the *hci5-5* benchmark ($k_{\text{eff}} > 1.00$) also induce large k_{eff} for the other

systems. It was demonstrated in Ref. [121] that the EVT behavior is obtained from large uncertainties on specific cross sections. In the case of the *hci5-5* benchmark where the EVT behavior was observed, the capture cross section of ^{94}Zr is inducing this effect. This cross section is presented in Fig. 29.

From this figure, it is apparent that the run with the *extremely* high capture cross section produces an extreme k_{eff} . Nevertheless, the “case 433” ^{94}Zr file only produces a k_{eff} value of 0.85 and the remaining 0.07 (to reach a k_{eff} of 0.78) comes from the contribution of the other zirconium isotopes. As seen in the bottom of Fig. 29, the cross section distribution at 1 MeV is strongly asymmetric (with a skewness of 2.8), with an important tail towards high values. We note again that such an asymmetric distribution can not be represented in conventional ENDF-6 covariance matrices.

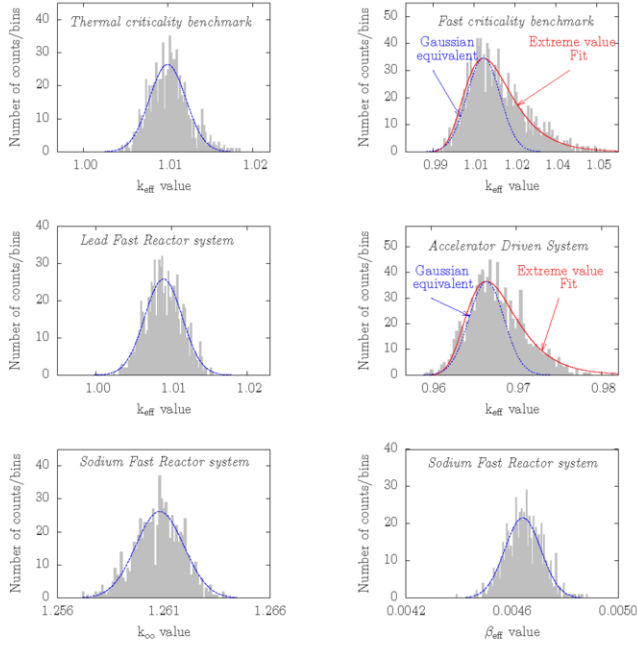


FIG. 28: Distribution of k_{eff} , k_{∞} and β_{eff} in thermal and fast systems [3].

Because of using default values for our initial uncertainties, the knowledge of the capture cross section of ^{94}Zr seems rather poor. It can be expected that the EVT behavior is directly caused by this insufficient knowledge of the capture cross section. It could be argued that a smaller uncertainty on the $^{94}\text{Zr}(n,\gamma)$ cross section would make the EVT behavior disappear, because the extreme values above 40 mb at 1 MeV (for instance) would disappear. Contrary to this consideration, it can be advocated that a better knowledge of the cross section would only decrease the dispersion (or standard deviation), and not change the shape of the cross section distribution (as in the case of lead isotopes in Ref. [3]). We believe that the EVT behavior will still be present in the case of smaller cross section uncertainties obtained from nuclear model, but the non-Gaussian distribution would be narrower than in the present case (if the cross-sections and uncertainties are determined by measurement, rather than from nuclear model calculations, the EVT behavior might disappear).

The non-Gaussian probability distribution can also be obtained from the variation of thermal scattering data [141]. Examples of such k_{eff} distributions are presented in Fig. 30. As shown, the probability distributions for the k_{eff} are significantly changing from the benchmarks with low sensitivities to thermal scattering data to the ones with high sensitivities. Single or double Normal distributions are indicated as eye-guide. The

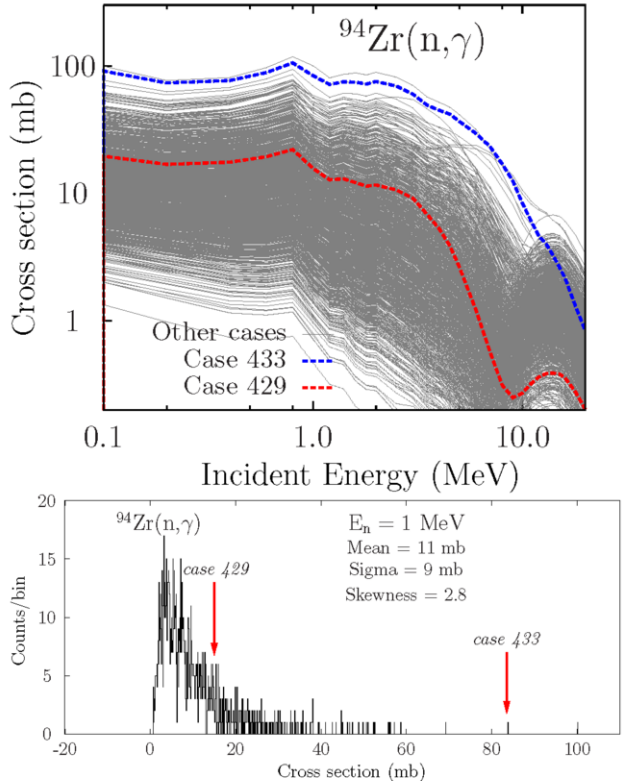


FIG. 29: Random capture cross sections for ^{94}Zr used in our benchmark calculations (top: as a function of neutron energy; bottom: at the neutron energy of 1 MeV. The red dotted curve corresponds to the “case 429” (within the Gaussian part of the k_{eff} distribution) and the blue dotted curve to the “case 433” (in the high k_{eff} part, or EVT tail, of the distribution.)

deviation from a Normal distribution for some of the benchmarks can be related to the results presented in Ref. [3], where deviations were also found in the case of high k_{eff} uncertainties. In Ref. [3], the non-Normal distributions were obtained from non-Normal cross section distributions. Here again, the present distributions are related to the uniform probability distributions used for the model parameters, as shown in Fig. 31. Two kinds of parameter distributions are presented in this figure: uniform (as in Fig. 30) and a Normal distribution for the model parameters ω_t , ω_j , σ_1 , σ_2 , $\rho(\beta)$, α and β (see Ref. [141] for the definition of these parameters). In the case of the ps12-14 benchmark, which has a high sensitivity to the scattering data, the shapes of the k_{eff} distributions are different, depending on the type of distributions for model parameters. This indicates that not only the mean and the standard deviation of a probability distribution are important, but also its shape. It should be noted that only normally distributed

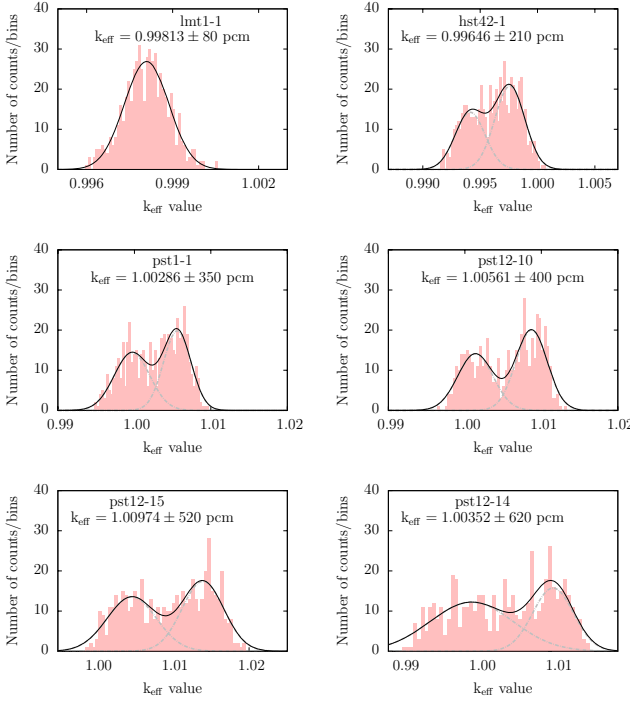


FIG. 30: Calculated k_{eff} values for 6 benchmarks, varying the thermal scattering data for H in H_2O . Note that the total standard deviation is increasing from the top left figure to the right bottom figure. The fits by one or two Gaussians are not used to extract the standard deviations.

parameters guarantee consistency between Monte Carlo and least-squares calculated results. Additional studies comparing the impact of non-normal parameter distributions on covariance calculations[152] found anomalies if uniform distributions are used in data evaluation.

7. Future applications

All the above examples are dealing with steady-state physics of nuclear systems, with or without burn-up calculations. A possible continuation of the TMC method is in the thermo-hydraulic and transient calculations. This domain of reactor physics is rather separated from the above mentioned examples and it is worth investing efforts to demonstrate the advantages of the TMC method. The first steps are currently being taken.

Completely uncharted is the land of uncertainty propagation for charged-particle nuclear data. Accelerator-shielding (for dose and activation), medical isotope production and other applications can all be extended with uncertainty analyses using TMC, and this extension is probably simpler than for reactor physics.

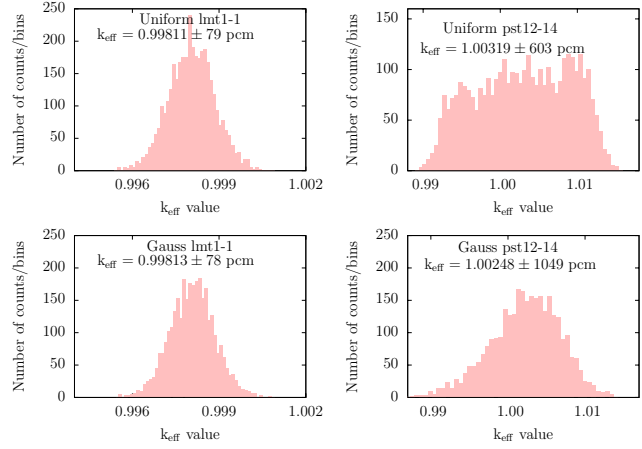


FIG. 31: Calculated k_{eff} values for 2 benchmarks varying the thermal scattering data for H in H_2O : pst12-14 and lmt1 for two different distributions of the random model parameters: uniform (top plots) and normal (bottom plots). The non-normal distributions in Fig. 30 can be attributed to the uniform distributions for the model parameters.

B. Covariances Versus TMC

A very natural question is “how does TMC compare with uncertainty propagation using covariance matrices ?”. This subject can be very extensively studied, depending on the type of covariance uncertainty propagation which is used. As of today, four variants can be found, which can be seen as approximate variants of TMC:

1. Direct perturbation method.
2. Generation of random pointwise cross sections based on covariance files, followed by a “TMC-light”, *i.e.* random data libraries are not generated from scratch (using TALYS + resonance data) but rather by applying available covariance data files.
3. Very close to the previous one, generation of random grouped cross sections based on covariance files, followed by a “TMC-light”.
4. Modification of the ACE files based on given covariances.

Connected with all this, one should realize that contrary to TMC, ENDF-6 formatting of covariances is not comprehensive. For example, there are no covariances defined for secondary distributions in MF6 and many cross-correlations are not taken into account. Therefore, TMC results will never be equivalent to the traditional covariance approach based on ENDF-6 formatted covariance files.

1. Perturbation vs. TMC

The first method involves a full deterministic approach using sensitivity calculations together with a sandwich formula. This method has been extensively used for the past decades, and a variant based on the MCNP code can be found in Refs. [153, 154]. The global flowchart of steps for each of the methods is presented in Fig. 32.

Of course, for consistency the same MCNP model for each of the selected criticality-safety benchmarks is used in the TMC and perturbation methods. Similarly, the same versions of the processing tools NJOY and SUSD [155] are used for the entire study. In order to compare results from these methods, the starting points need to be similar. A necessary step is to obtain equivalent nuclear data files to be used by both methods. On one side, the TMC method is using a large number of random ENDF files (nuclear data files, containing all necessary information to be used by MCNP after processing), and alternatively, the perturbation method is using a single ENDF file containing covariance information. For a consistent comparison, the cross sections from the single ENDF file used in the perturbation approach need to correspond to the average of the large number of random files. Additionally, the covariance information (uncertainties and correlations) has to represent the set of random ENDF files used in the TMC approach. To ensure this, the technique applied in this study is to generate these ENDF files from the same set of runs using the TALYS code.

The procedure to generate random ENDF files together with an ENDF file containing the average cross sections and the covariance information was detailed in Ref. [47]. In total, 20 to 30 theoretical parameters are all varied together within pre-determined ranges to create TALYS inputs. These parameters are randomly independently varied, implying slow convergence for calculated quantities. More efficient sampling have been presented in Refs. [156] and [157]. This method allows to cover to top part of Fig. 32, from the “ n TALYS input files”, to the boxes labeled “1 ENDF file + covariances” and “ $n \times$ ENDF random files”.

The perturbation approach relies in principle on a unique “NJOY+MCNP+SUSD” calculation. The inputs are the geometry MCNP input file (common to the TMC approach) and an ENDF file containing covariances. As shown in Fig. 32, an ENDF file is processed by NJOY to produce processed cross sections (used by MCNP) and processed covariances (used by SUSD). The “Add perturbation”, “MCNP input file + perturbation card” and “MCNP” boxes in Fig. 32 present the essential part of the sensitivity calculation. The sensitivity profile S is defined as the relative change in a response parameter R due to a relative change in a cross section

in a particular energy group g

$$S = \frac{(\delta R)/R}{(\delta \sigma_g)/\sigma_g}. \quad (200)$$

In this case, the response parameter is a scalar quantity, which is a function of the incident neutron energy. The sensitivity profile S is obtained using the perturbation option of MCNP, which corresponds to the “PERT”-card:

1. A cross section is selected for which the profile is to be generated. In the following, four cross sections will be considered: elastic, inelastic, fission and capture cross sections. Only one specific isotope is varied each time.
2. A material card is created in which the atomic density for the relevant isotope is increased by 1 %.
3. a “PERT”-card is created specifying that the relevant material is replaced by the perturbed material in each of the cells in which the material is present. Perturbation cards are given for all energy groups. In this paper, the 33-energy group structure (from thermal energy to 20 MeV) is adopted.
4. Finally, MCNP is run with these modifications in the input. In the MCNP output, a table is given with the results of the perturbations with statistical uncertainties and, in case of criticality benchmarks, k_{eff} values with statistical uncertainties.

This method can then applied to criticality-safety benchmarks as defined in the ICSBEP list [140]. Combining sensitivity and covariances is represented in Fig. 32 by the “SUSD” box. The sensitivity results and the processed covariances are combined together with the SUSD code. Sensitivity and covariance matrices are produced in a similar energy group. Sensitivities are calculated for cross sections only (resonance region and fast neutron range), as the perturbation option in MCNP can not be used for other quantities. Thus, the effects of angular distributions, double differential data and, in the case of actinides $\bar{\nu}$ and fission neutron spectrum, are not included in this approach. The calculated quantity is an uncertainty on k_{eff} due to nuclear data.

An important condition to fulfill is that both methods use the same nuclear data. In other words, cross sections in the unique ENDF file used by the perturbation method should be equal to the average of the cross sections from the n random ENDF files used by the TMC method. Furthermore, the probability distribution of the cross sections from the n random ENDF files should correspond to the covariance information included in the unique ENDF file used by the perturbation method. What applies for cross sections applies also for

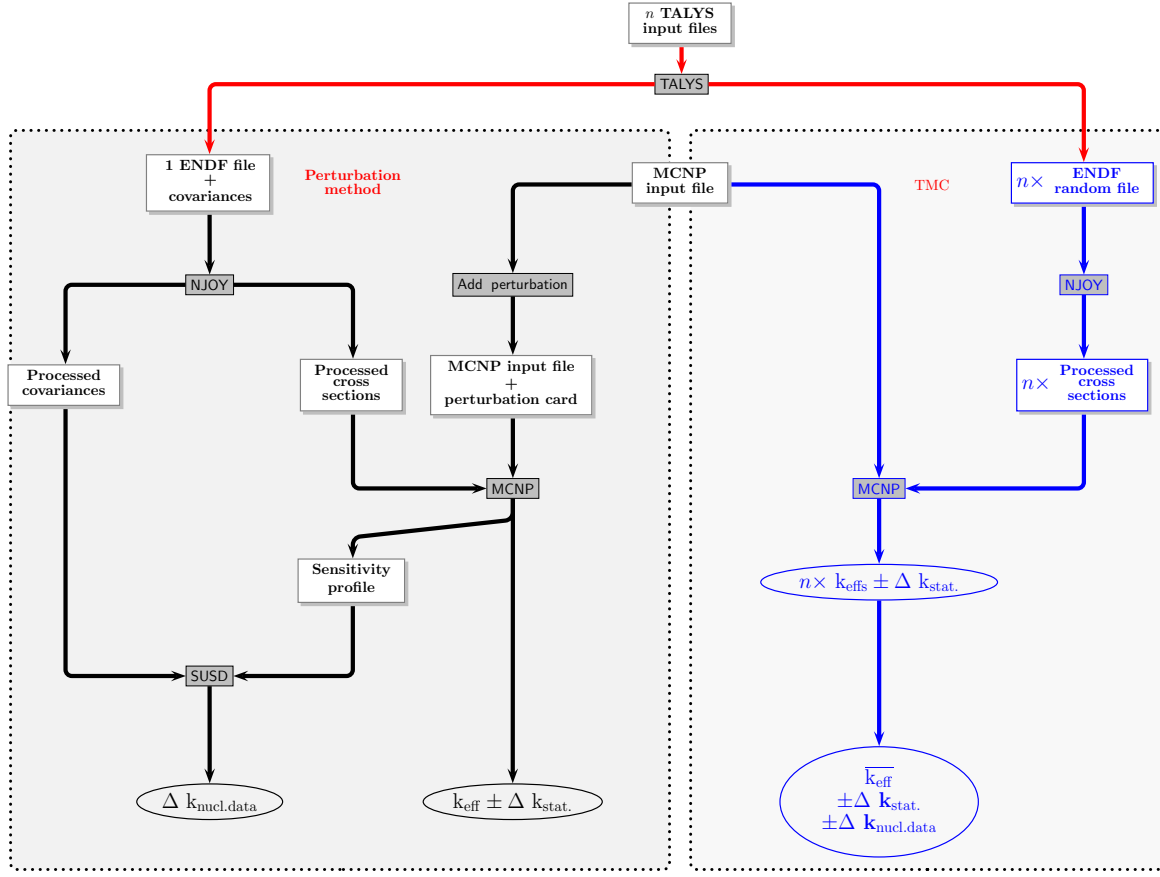


FIG. 32: Flowchart of the uncertainty propagation for TMC and perturbation method as presented in Refs. [153, 154].

resonance parameters, $\bar{\nu}$, single and double-differential data, even if the perturbation method is not using the three latter quantities.

Independent of these requirements, the ENDF format for the covariance storage assumes that any probability distribution can be represented by its first and second moments, and it is assumed by covariance processing codes that a normal probability distribution should be used. This assumption, inherent to the ENDF format and its processing, does not apply in the case of TMC calculations. In these examples, a normal probability distribution is chosen for the generation of random parameters used in the TMC method. Once the probability distributions are the same, enough samples need to be considered to ensure that the random parameters of the TMC method converge to the values used in the perturbation method (and included in MF32 and MF33). In the case of a larger uncertainty, see Fig. 33, the probability distribution has a non-negligible contribution in the domain of negative random parameters, which is not physical. Fig. 33 presents an extreme case where the

uncertainty on the radiative width is 50 %. A different distribution could be chosen for the TMC method in order to avoid such negative numbers (such as a log-normal distribution), but not for the perturbation approach. Many different solutions exist for this problem of negative random parameters:

- When a negative number (or outlier) is drawn from a normal probability distribution, a new number can be redrawn until it is positive. This example is presented in the left part of Fig. 33. The distribution is no longer symmetric: a smaller standard deviation and a higher mean value are obtained. In Fig. 33, differences of 3 % for the average $\bar{\Gamma}_\gamma^{(2)}$ and 6 % for the uncertainty on $\bar{\Gamma}_\gamma^{(2)}$ are obtained with the expectation values.
- Outliers can be redrawn from a uniform distribution. This solution adds noise to the distribution, and modifies the original distribution to a *watered down* normal distribution.

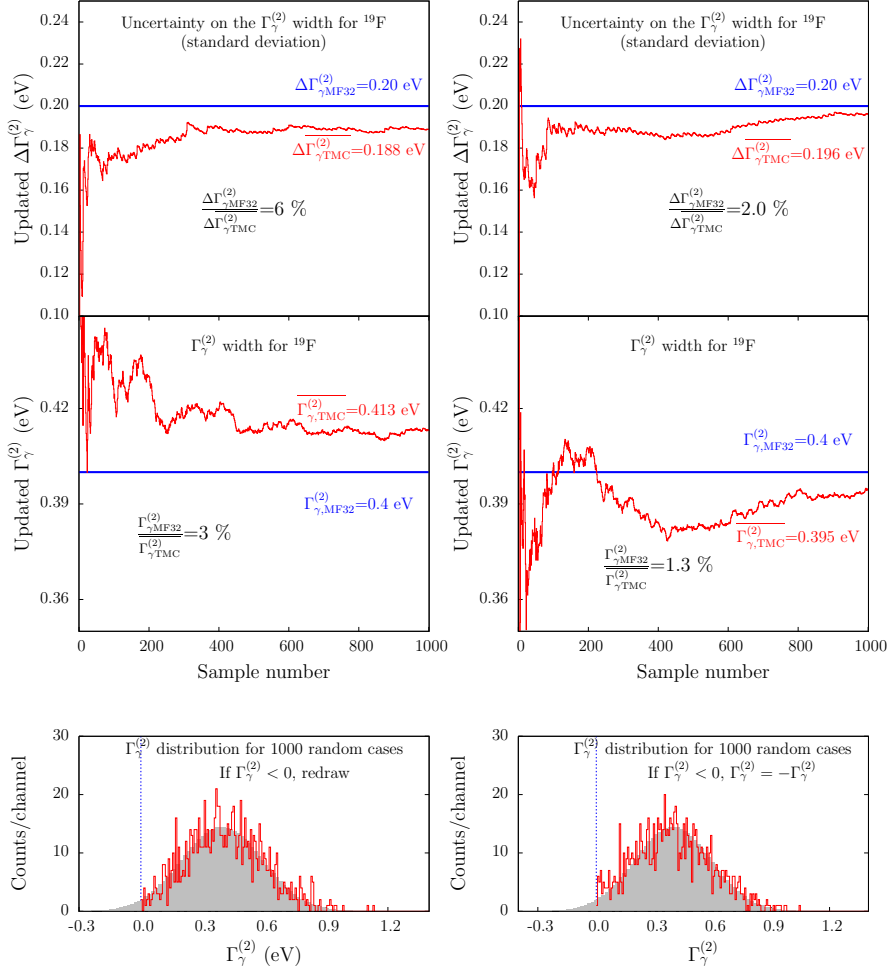


FIG. 33: Convergence and probability distribution for the radiative width $\Gamma_{\gamma}^{(2)}$ of the second resonance of ^{19}F . Two parameters are presented: the average width and its standard deviation for 1000 samples. The bottom plot is the probability distribution for $\Gamma_{\gamma}^{(2)}$ (second resonance of ^{19}F). Left: if the random $\Gamma_{\gamma}^{(2)} < 0$, it is excluded and a new random $\Gamma_{\gamma}^{(2)}$ is generated. Right: if the random $\Gamma_{\gamma}^{(2)} < 0$, then $\Gamma_{\gamma}^{(2)} = -\Gamma_{\gamma}^{(2)}$.

- Outliers are set to the original mean of the distribution. This solution causes a peak at the center of the distribution.
- Outliers are set to its closest threshold, but this solution also induces peaks in the distribution.
- Absolute values of the outliers are kept. This solution is presented in the right part of Fig. 33. The original probability distribution is then modified around the zero value, but it allows to obtain an average and a standard deviation closer to the expected ones, compared to the first solution.

For this study, we adopt the last solution (absolute values of negative random numbers). This issue points out a

difference between the TMC and perturbation methods. Probability distributions for resonance parameters are not identical for both methods, and differences for the average are increasing with increasing parameter uncertainties.

It should be mentioned that the main resonances are usually also the best known, which implies that the above differences are not expected to have a large effect on cross sections. Comparisons of benchmark uncertainties are presented in Table XI for benchmarks and isotopes with high sensitivity are selected. Even though the majority of benchmarks is highly sensitive to ^{235}U and ^{238}U , other isotopes were also selected to cover a wide range of masses and nuclear charges. A direct comparison between the TMC and perturbation methods is pre-

sented in Table XI, for 33 criticality-safety benchmarks. Ratios of the k_{eff} uncertainties for the two methods are calculated.

TABLE XI: Comparison between the TMC and the perturbation method for a few criticality-safety benchmarks. PERT means MCNP perturbation card.

Benchmark	Isotopes	k_{eff} (Stat.)	Uncertainty (pcm)		
		TMC	PERT	$\frac{\text{PERT}}{\text{TMC}}$	
hmt9-s	^{24}Mg	1.00384(48)	77	19	0.25
hmt13-625	^{56}Fe	1.00998(85)	910	884	0.97
lct10-1	^{208}Pb	1.00109(25)	131	113	0.86
u3ct1-1	^{232}Th	0.99670(50)	189	193	1.02
ict3-132	^{90}Zr	1.00190(43)	139	129	0.93
pmm1-1	^{28}Si	1.00055(42)	535	451	0.84
hci5-5	^{90}Zr	0.92720(42)	431	480	1.11
hcm3-5	^{90}Zr	0.99503(44)	90	104	1.15
hmf7-34	^{19}F	1.02172(35)	306	231	0.75
mcf1-1	^{23}Na	0.98586(16)	54	18	0.33
u3mf1	^{233}U	1.00035(38)	974	960	0.98

A few different cases can be observed, but an overall comparison between the results from the perturbation method and the TMC method shows a global agreement. The cases are classified as follows:

1. A good agreement is obtained between both methods. Four benchmarks are in this category. Both results from NJOY and PUFF processing are in good agreement, and are within 7 % of the TMC results. For these four cases, the most sensitive reaction is the capture cross section, being at least three times more important than the other cross sections. Furthermore, the isotope of interest is not part of the reflector of these systems.
2. The agreement is not as good as for the four previous cases, not including actinides. The largest differences are for cases with small uncertainties, and in the cases of larger uncertainties (above 100 pcm), the differences range from 7 to 25 %. In all these last cases, the elastic cross section is a large contributor to the total uncertainty and the studied isotope is part of the moderator or reflector.

2. Random pointwise/groupwise vs. TMC

TMC can also be compared with a hybrid version of the uncertainty propagation, using both covariance and random files. These methods are now used by different groups, as presented in Refs. [158, 159, 160]. The hybrid method is as follows:

1. Existing covariance files are used as the starting point. In general, cross section covariances are considered, sometimes with $\bar{\nu}$ covariances.
2. From the covariance files, random cross sections are generated according to a given probability distribution. Depending on the approximations, cross correlations between channels are considered or not. In general, correlations for a given reaction are considered. Random cross sections are then generated in pointwise or groupwise format.
3. From the random cross sections, a simulation is repeated a large number of times, each time with a different random cross section file.

Recently, a new method has been developed at the Paul Scherrer Institute (PSI), Switzerland, where covariance information is used to perturb ACE files (in a similar way as in Ref. [160]). A set of ACE files is then generated based on a covariance file (from ENDF/B-VII.1 or TENDL) and MCNP (or MCNPX) calculations are repeated to extract the effect of the perturbed quantities. These approaches are very close to the original TMC method, but starting one step away from theoretical model parameters. A few approximations are inherent to this approach, compared to the TMC method (such as the choice of the probability distribution or limitations due to the covariance formalism), but in practice, both results are equivalent.

Comparisons have been performed for different systems (thermal, fast) and on different quantities (k_{eff} , inventory after burn-up). Results for two systems are presented in Table XII: (1) a unit cell model based on a MOX fueled 3600 MWth Sodium-cooled Fast Reactor (SFR) concept and (2) a credit burn-up calculation for the OECD Phase 1-B benchmark. The method used by the Gesellschaft fuer Anlagen und Reaktorsicherheit (GRS) is to generate grouped cross section from existing covariance files. In a similar way, the AREVA method uses covariance files to generate random nuclear data libraries with pointwise cross sections. In the two following examples, the ^{238}U nuclear data were varied. Both covariance and random files were produced by NRG in a consistent manner. As seen in Table XII, the total uncertainty agrees quite well between the two methods. It comes certainly from the fact that a single reaction (capture in the fast neutron range) plays a key-role. For other contributions, the agreement is less noticeable, possibly due to different cross-correlation between reactions.

In the case of the AREVA method, called Nuclear Data Uncertainty Analysis (NUDUNA), comparisons for the k_{eff} and inventory were performed. The test case is the Phase 1B benchmark (burn-up credit calculations [162]). NUDUNA samples randomly ENDF-6 files

TABLE XII: Comparison between the TMC and grouped cross section uncertainty propagation methods for k_{eff} for a pin cell of a Sodium Fast Reactor, varying ^{238}U nuclear data. Results from GRS are obtained from Ref. [161].

Type Nucl. Data	GRS results (pcm)		NRG results (pcm) TMC
	TSUNAMI	XSSUSA/XSDTN	
All	1348	1328	1358 ± 40
$\bar{\nu}$	504	500	650 ± 50
(n,inl)	708	706	470 ± 50
(n, γ)	1025	1032	1050 ± 40

based on the nominal ENDF-6 information and the covariance information contained in files MF31 to 34 of ENDF-6 type files, *i.e.* it fully includes uncertainties of multiplicities, resonance parameters, fast neutron cross sections and angular distributions. In the same spirit as TMC, each random ENDF-6 file is then transformed with the help of NJOY and PUFF into transport code inputs, and for each such input a specific transport calculation is initiated. Since the method makes use of the full information contained in the ENDF-6 covariance files, it thus maps the uncertainty information contained in ENDF-6 files without further simplifications or approximations onto uncertainty estimates for transport code observables [164, 165]. Contrary to the previous comparison, this system is thermal and the impact of resonance range is important. Therefore, the treatment of the resonance parameter uncertainties has a large impact on the results. Results of the comparisons for k_{eff} are presented in Table XIII.

TABLE XIII: Comparison between the TMC and pointwise cross section uncertainty propagation methods for k_{eff} for the Phase 1B credit burn-up benchmark, varying ^{238}U nuclear data. Results from AREVA are obtained from Ref. [163].

Type Nucl. Data	AREVA results (pcm)		NRG results (pcm) TMC
	NUDUNA		
All	412 ± 42		390 ± 22
$\bar{\nu}$	245 ± 17		259 ± 25
Resonance range	219 ± 31		211 ± 11
Fast neutron range	167 ± 17		134 ± 30

In this case, the agreement between both methods is very good, giving confidence that both approaches provide reasonable results.

As seen in Fig. 34, the agreement between both methods for the isotope inventory is rather good. There is a slight trend of discrepancies for higher burn-up, but the differences stay small.

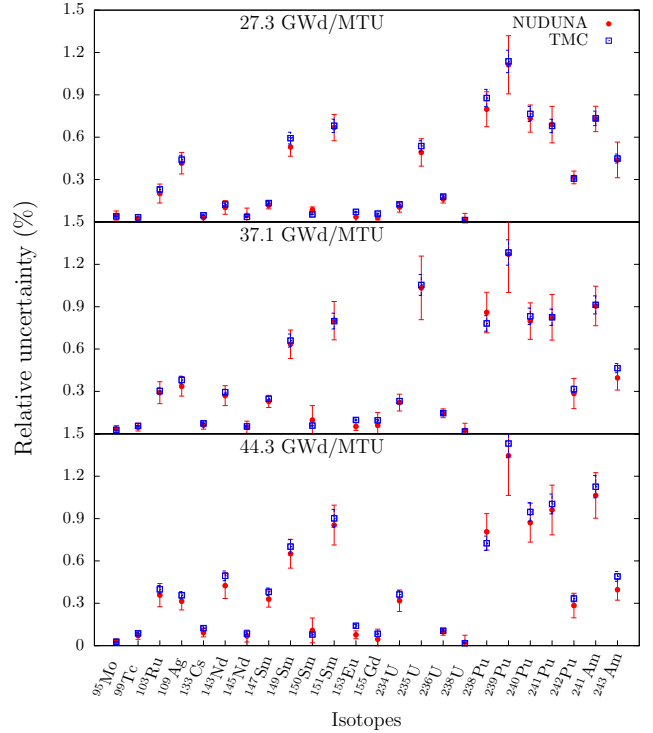


FIG. 34: Comparisons of the calculated uncertainties for the inventory after different burn-up, changing the ^{238}U nuclear data with two different methods. The system is the credit burn-up benchmark Phase 1-B.

C. Polynomial Chaos and TMC

A different way to propagate uncertainties (not only from nuclear data) can be realized with the Polynomial Chaos Technique (PCE). Three applications to nuclear data can be found in Refs. [166, 167, 168].

In Ref. [168], the non-intrusive PCE technique is applied by collecting a finite set of realizations of the stochastic output (the multiplication factor) corresponding to a predefinite set of realizations of the stochastic inputs. The non-intrusive spectral method is applied to the criticality benchmark *pst1-1* included in the Handbook of Criticality calculations with MCNP5. To illustrate the advantages of the method, the influence of a set of the 6.9 eV resonance of ^{239}Pu is studied. A total of 4 widths are assumed to be normally distributed with an associated 5 % relative standard deviation. The final 4 dimensional sparse grid is then obtained by progressively adding subgrids and by arresting this procedure once the contribution to the third order spectral coefficients was below a specified tolerance. At the end of this operation the final grid contains 49 points corresponding to a total of 65 realizations (including the ones used to

perform the parameter ranking) required to evaluate the spectral expansion. The values of the first three statistical moments obtained with the 4-dimensional PCE are compared in Table XIV, for different expansion orders. It can be seen in the Table that the PCE predictions of

TABLE XIV: Comparison between the TMC and the Polynomial Chaos (PCE) methods for k_{eff} for the ps1-1 benchmark [163].

	TMC	PCE		
		1 st order	2 nd order	3 rd order
k_{eff}	$1.0078 \pm 64 \text{ pcm}$	1.0081	1.0081	1.0081
std. deviation	0.0169	0.0169	0.0171	0.0172

the statistical moments are well in agreement with the TMC method. The probability density function of the multiplication factor obtained with a third order PCE is presented in Fig. 35 together with the distribution from the TMC calculations.

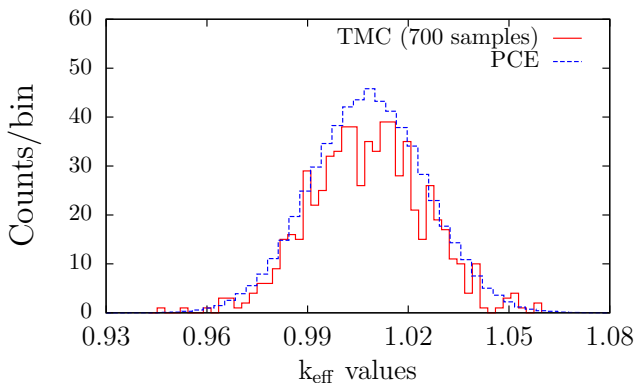


FIG. 35: Comparison of the probability density functions obtained by sampling the full calculation route (red line, 700 samples) and by sampling the Polynomial Chaos Expansion (blue line).

In Ref. [167], the PCE method was applied to show quantitatively how the uncertainty of each basic parameter, namely the radiation and neutron line widths, influence the resonance escape probability. The main conclusion is that this can amount, at least for the 21 thorium resonances considered, to around 75–130 pcm in units of reactivity. It is also noted that a non-Gaussian probability distribution function can be obtained in the case of large parameter uncertainties [169], as in the case of the TMC method [3].

D. TENDL Application for Heating Calculation

The use of the TENDL library can present numerous advantages compared to regular libraries. One important example is related to the photon production included in existing evaluations and their impact on heating calculations [170].

For a research reactor a sizable amount of heat is deposited. Unlike the situation in a fuel assembly in a power reactor, this process is not dominated by fission, but by photons (referred to as gamma heating, even though neutrons do contribute to it as well). It is difficult to calculate the amount of gamma heating in an experiment, even though the required accuracy is only 10 %. This is because photon production has never received the same sort of attention as neutron reactions typically have: fission product decay photons are not part of neutron transport data in JEFF-3.1.2, JENDL-4.0 or ENDF/B-VII.1, and there are photon production data for almost none of the fission products (even for the most notorious neutron capturing isotopes, ^{135}Xe , ^{149}Sm , or ^{151}Sm , there is no photon production). Also, for none of the Cd isotopes photon production data are available from either JEFF or ENDF/B. For research reactor with cadmium control rods and cadmium burnable poison, this has a non-negligible impact.

The impact of the extra photon production can be quantified by calculations for the High Flux Reactor in Petten, the Netherlands. For details of the calculations, see Ref. [170]. The reference run is performed with the nuclear data from the JEFF or ENDF/B library and a second run with the TENDL nuclear data for fission products is performed. In total, it is found that there is an effect on gamma heating of up to 7 % from fission products and ^{28}Al , and 5 % for cadmium, showing the advantage of the TENDL library compared to other libraries.

E. Adjustment: The Petten Method

A last application of the stochastic approach to nuclear data is presented in this section. The evaluation of neutron induced reactions can be seen as a combination of differential experimental results, theoretical calculations and *a posteriori* adjustments to integral measurements. The widely spread procedure to create a nuclear data library is to separate the evaluation part (mixture of theoretical calculations and educated adjustments to differential data) from the adjustment procedure (clever modifications of the evaluations to better fit a set of benchmarks with a specific simulation tool). In the case of important isotopes, the second step can be as long as many decades. As a part of grand effort to ease nu-

clear data evaluation, NRG has developed a method *re-combining* the two described stages into a single one, driven by ready-to-use software, referred as the *Petten method*. The efforts and cleverness of evaluators can now be focused on the choice of nuclear theory, parameters, and selection of differential and integral data, instead of manually running formatting and simulation programs. It was recently presented in Refs. [13, 148] that a Monte Carlo method can be used to perform adjustment on the nuclear quantities of neutron-induced reactions of ^{239}Pu and $^{63,65}\text{Cu}$. The adjusted cross sections, angular distributions and other quantities showed improved comparisons with integral criticality benchmarks, shielding benchmarks and differential data.

1. Method

As part of the traditional evaluation work (slow and tedious search of the right theoretical nuclear reaction parameters with the inclusion of high-precision experimental data), an additional step based on Monte Carlo adjustment can be used. Built on already tuned model parameters (called “*stage 0*”), it basically consists of searching by Monte Carlo the best set of model and resonance parameters compared to differential and integral experimental data. If properly performed, the results are adjusted nuclear data and model parameters for a nucleus (or a few of them, simultaneously), called “*stage 1*”, in better agreement with experimental data than the ones from the stage 0. This process could even become iterative (similar to a simulating-annealing procedure), where new Monte Carlo searches can be performed based on “*stage i*”. After a number of iterations, convergence should in principle be obtained. In the following, we are exploring the Monte Carlo adjustment up to stage 1, but higher iterations are possible.

The adjustment is an important step in the evaluation procedure. It is not always performed and is often subject of discussion within the nuclear data community. In simple terms, it consists to modify the nuclear data (*e.g.* cross sections) to obtain better agreement with integral experiments. Depending on the choice of integral experiments, different adjustments can be found. In general, it is always better to select simple, well-understood and clean experiments to avoid unwanted compensation. An important boundary condition is of course that the adjusted result is still in agreement with differential data.

The present *Petten method* of evaluation/adjustment was partly presented in Refs. [121, 123, 127], with a full original description in Ref. [13] and will be summarized below.

We believe that as long as experimental cross sections (and other nuclear data) are not perfectly known, it is perfectly acceptable to envisage a large number of eval-

uated curves to simulate our imperfect knowledge, and to guide us towards the best possible choice for applications. This random variation of course takes place inside the uncertainty bands associated with each cross section. A complete schematic approach is presented in Fig. 8. The full nuclear data file production relies on a small number of codes and programs, automatically linked together. The output of this system is either one ENDF-6 formatted file, including covariance data generated by random sampling, or a large number of random ENDF-6 files. The central evaluation tool is the TALYS code. A few other satellite programs are used to complete missing information and randomize input files. At the end of the calculation scheme, the formatting code TEFAL produces the ENDF files.

The next step is to select a set of integral and differential data. This selection will vary from one application group to another, simply because of different expertise, purpose of the evaluation and accessibility to benchmarks. But independently of this choice, the present procedure can be applied to any number of benchmarks, and any kind (criticality, dosimetry, fusion, activation and others). For instance, in Ref. [148] where Cu isotopes were studied, a few benchmarks from the ICSBEP database [140] were selected and as copper is of importance for fusion application, the Cu Oktavian benchmark [144] was also selected, with neutron and gamma leakages. Many ICSBEP benchmarks include copper, but it is expected that copper will not affect k_{eff} results by a large amount (contrary to Ref. [13] where ^{239}Pu was chosen). In the case of ^{239}Pu [13], we have selected a few benchmarks from the ICSBEP database [140]. The benchmarks highly sensitive to plutonium (denominated by “pst”, “pmf”, “pmm”, “pci” or “pmi”) are selected for the random search. We thus calculate *all* these benchmarks, with MCNP, for *one random ^{239}Pu library at the time*. As a large number of benchmarks are considered, it is easier to compare the performances of different libraries with a unique number such as the χ^2 -statistic, defined as

$$\chi^2 = \sum_{i=0}^n \left(\frac{(C_i - E_i)}{C_i} \right)^2, \quad (201)$$

with C_i the calculated value for the i benchmark and E_i the benchmark value. Depending on the considered nuclear data library, a specific value of χ^2 is obtained. A different goodness of fit estimator can be chosen, such as F , defined as

$$F = 10^{\sqrt{\frac{1}{N} \sum (\log(E_i) - \log(C_i))^2}}, \quad (202)$$

with C_i the calculated value for the benchmark i and E_i the benchmark value. Depending on the considered nuclear data library, a specific value of F is obtained. From

Eq. (202), the smaller F becomes, the better the agreement between calculations and experiments is. It should be mentioned that there exists other methods of minimizing a function, such as the grid search, the Rosenbrock's method, the simplex method and many others.

2. How to adjust a library, method 1

Detailed examples can be found in Refs. [13, 148]. In the case of ^{239}Pu , the adjustment can be performed in the following manner: all the isotope evaluations are kept constant and equal to the JEFF-3.1 library with the exception of ^{239}Pu .

Following this present evaluation method, a large number of evaluated files is produced, the number being limited by the production time (on average, the production of a single evaluation for ^{239}Pu takes about 1 to 2 hours on a typical 3 GHz personal computer while its validation with all selected benchmarks takes 12 hours). Fig. 36 presents the results of the benchmarks of the random files in terms of χ^2 as defined in Eq. (201). All single random evaluations are represented by a χ^2 value, and to compare with existing evaluations, results from other libraries are plotted as bands. The uncertainties on the dots (and the widths of the bands) are the statistical uncertainties coming from the MCNP calculations together with the benchmark uncertainties.

In Fig. 36, the results for 630 random ^{239}Pu libraries are presented. It is rather *unconventional* to visualize a library for which an isotope is represented by a set of evaluations (corresponding to probability distributions for different types of nuclear data), and Fig. 36 is a collapsed way of looking at n random evaluations applied to m benchmarks. As expected from a simple random approach, a large number of the evaluations performs quite poorly compared to other libraries, but a small set (about 6 % of the total number) outperforms all other traditional libraries. A different way of representing the same results is shown in Fig. 37, where χ^2 values of Fig. 36 are projected onto the y -axis and counted as histograms. In Fig. 37, each *random* χ^2 (for each *random* ^{239}Pu evaluation) is represented by a step of height 1 in the histograms. The four traditional libraries have a single step at their χ^2 value. This distribution is not symmetric, and has a large tail towards high χ^2 values. The four traditional libraries are in the low- χ^2 part of the graph, reflecting the amount of knowledge and time that have been invested in them. Again, we note that several of the *random* χ^2 are smaller than the ones from JEFF-3.1, ENDF/B-VII.0, ENDF/BVI.8 or JENDL-3.3, while the corresponding cross sections are all generated with a consistent method and lie inside the experimental uncertainties.

According to this probability distribution, it would be

interesting to know if the probability to obtain $\chi^2 \simeq 0$ is theoretically possible (meaning that even if its probability is small, it could be reached by having enough random evaluations). In the hypothesis that the variable C_i of Eq. (201) is independent and normally distributed, Pearson's chi-square test used above follows a chi-square distribution with k degrees of freedom [171]. It is defined in the interval $[0, +\infty)$ and governs a non-zero probability for $\chi^2 = 0$. It is then theoretically possible to "continuously" improve the agreement with a set of benchmarks by using more random evaluations. However, we do realize that in practice it will not be possible to obtain a perfect fit for all included benchmarks simultaneously. Additionally, the C_i 's are not fully independent, and a Log-Normal distribution seems to represent better the probability distribution of Fig. 37 (which is also defined at $\chi^2 = 0$). Nevertheless, figures like Fig. 37 are important to get an idea of how much room for improvement is left, even for conventional methods.

In the case of Cu adjustment, Fig. 38 presents the results of the benchmarks of the random files in terms of χ^2 as defined in Eq. (201). All single random files are represented by a χ^2 value, and to compare with existing evaluations, the result from the JEFF-3.1 library is plotted as a band. The uncertainties on the width of the band are the statistical uncertainties coming from the MCNP calculations together with the benchmark uncertainties.

At the top of Fig. 38, the results for 1500 random $^{63,65}\text{Cu}$ libraries are presented. A different way of representing the same results is shown at the bottom of Fig. 38, where χ^2 values in the top of Fig. 38 are projected onto the y -axis and counted in histograms. In this representation, each *random* χ^2 (for each *random* $^{63,65}\text{Cu}$ file) is represented by a step of height 1 in the histograms. The traditional JEFF-3.1 library has a single step for their χ^2 value. This distribution is not symmetric, and has a large tail towards high χ^2 values.

3. How to adjust a library, method 2

Alternatively, the ENDF file can be kept constant, except some parts of it. Again, in the case of ^{239}Pu , the following nuclear data sections can then modified:

- Prompt fission neutron spectrum: An important quantity with relatively large uncertainties is the fission neutron spectrum. It has been recently advocated that the fission neutron spectrum might deviate a bit stronger from the Madland-Nix model, especially for neutron emitted with low energy [172]. It was generally accepted that the fission neutron spectra follow a Maxwellian distribution as indicated in the Madland-Nix model [99].

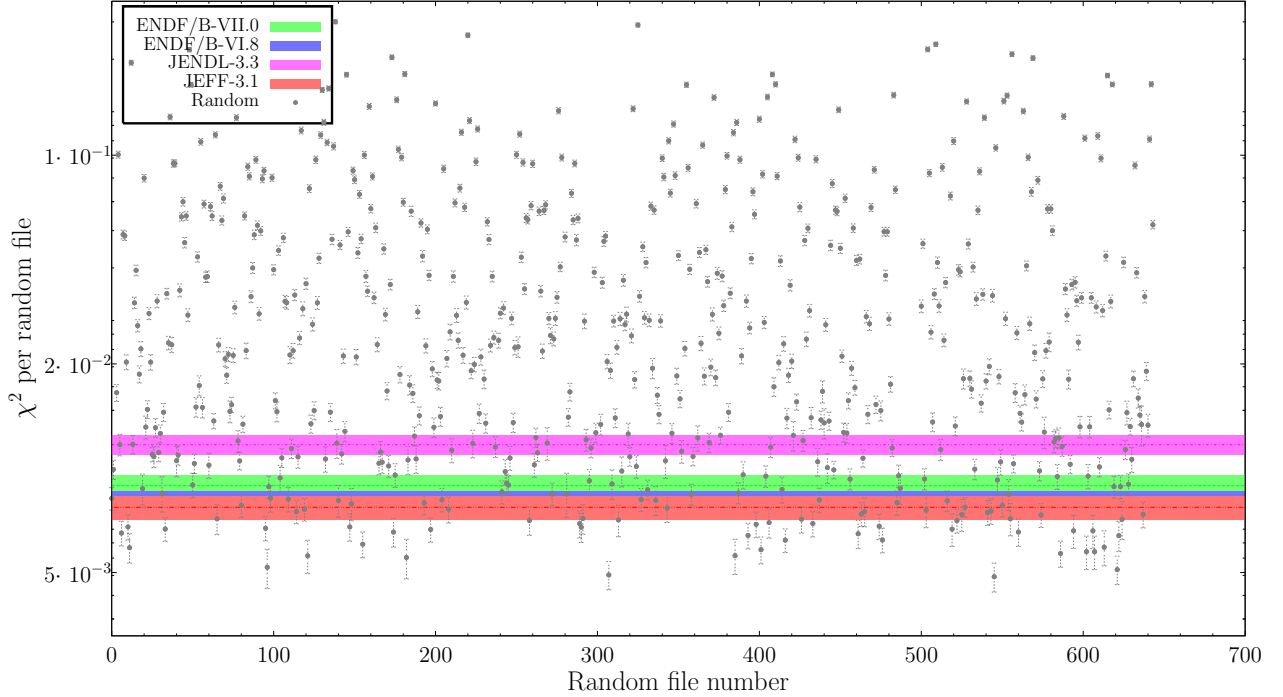


FIG. 36: Pearson χ^2 values for random ^{239}Pu evaluations (dots), compared to χ^2 for existing libraries (bands). One can see that for the selected benchmarks, the ^{239}Pu evaluation from the JEFF-3.1 library performs better than other “conventional” libraries, whereas about 6 % of our random ^{239}Pu evaluations perform better than any other library.

The experimental data for ^{239}Pu are relatively scarce (see Fig. 39) and leave some freedom of adjustment. We have followed the representation of Ref. [99] for the prompt fission neutron spectra (pfns) of ^{239}Pu , and the comparison of the adjusted pfns with that of JEFF-3.1 is presented in Fig. 39. The adjusted pfns have a higher tail at low energy for the emitted neutrons and a lower probability of emission above $E_{\text{out}} = 1$ MeV. The direct consequence of this change in shape for the pfns at all incident neutron energies is to globally lower the k_{eff} values of the fast and thermal benchmarks.

- $\bar{\nu}$: With the fission neutron spectrum modified, the number of emitted neutron per fission ($\bar{\nu}$) was adjusted mainly in the fast neutron region. As shown in Fig. 40 top, the ratio to the JEFF-3.1 evaluation is very close to one, with a constant positive bias from 0 to 1 MeV (about 0.3 %) and a slightly weaker change above 1 MeV. Even though $\bar{\nu}$ has an important effect on k_{eff} , it is believed to be well known, with an uncertainty smaller than 1 % for the whole energy range. The changes used in this work are well below this 1 % maximum uncertainty.

- Inelastic cross section: As $\bar{\nu}$ is strongly correlated with the fission cross section, the next sensitive cross section is the inelastic cross section. The resulting new cross section is presented in Fig. 40. As large experimental uncertainties are assigned for the inelastic measurements, there is a larger room for adjustment than for the fission cross section. The new cross section is lower than other evaluations, but still within experimental uncertainties.

4. Monte Carlo sensitivity

One of the possible outcome of using a Monte Carlo method for nuclear data evaluation is that a series of correlations can be extracted from the previous results. At this point, it is helpful to remember that for each calculated quantity, thousands of values are obtained. These quantities can be differential nuclear data (such as cross sections), but also integral nuclear data, such as a k_{eff} value for a given criticality benchmark, or a leakage flux from a fusion benchmark.

An example of two random calculated quantities is presented in Fig. 41. In this figure, the random leakage neutron fluxes of the Oktavian benchmark for copper at

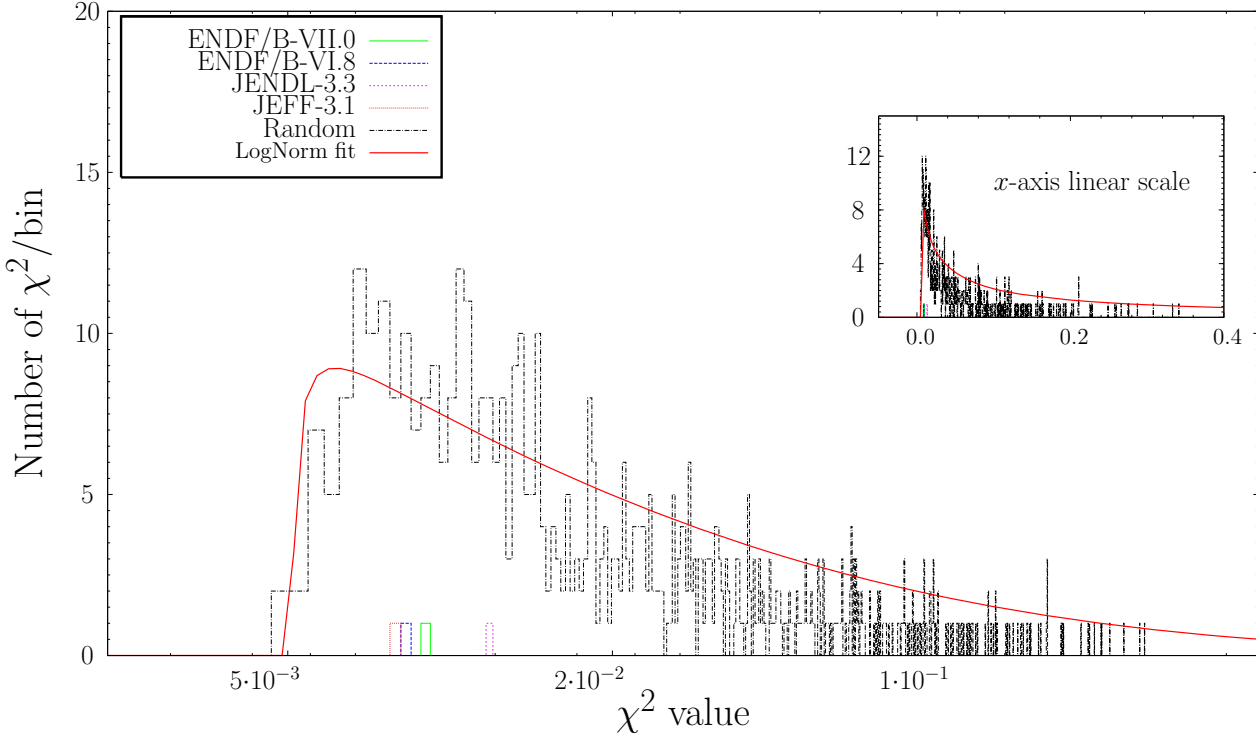


FIG. 37: χ^2 values for each random ^{239}Pu evaluations per bin, compared to χ^2 values for JEFF-3.1, ENDF/B-VII.0 and JENDL-3.3. This figure is the projection on the y -axis of Fig. 36. Note that the x -axis for the large plot is in log scale. The insert is the same plot with the x -axis in linear scale.

7 MeV (outgoing energy) are presented as a function of the random inelastic cross sections of ^{63}Cu at 2.4 MeV (incident energy). This type of presentation of data can be done for all Oktavian energies, all cross sections (and other nuclear data), and also all criticality benchmarks. It is then difficult to extract useful information from such a large amount of data. To avoid this difficulty, the data presented in Fig. 41 can be reduced to their correlation ρ_{xy} , defined as

$$\rho_{xy} = \frac{\sum_{i=1}^n (x_i - \bar{x})(y_i - \bar{y})}{(n-1)s_x s_y}, \quad (203)$$

with x_i the random inelastic cross sections, \bar{x} the average inelastic cross section, y_i the random neutron leakages, \bar{y} the average neutron leakage and s_x and s_y their standard deviations. The ρ_{xy} factor for the previous data is also presented in Fig. 41 as a slope of the spline fit to the data. It is then relatively easy to generalize the calculation of ρ_{xy} for different cases. As for the case of Fig. 41, different correlation factors can be calculated between the Cu Oktavian benchmark and nuclear data. As examples, Tables XV and XVI present the correlation

ρ_{xy} for different cases.

TABLE XV: Correlation factors between the Cu Oktavian neutron leakage benchmark and nuclear data (at given incident and outgoing energies).

E_{out}	Oktavian	Reaction	E_{in} neutron	ρ_{xy}
7 MeV		$^{63}\text{Cu}(\text{n,inl})$	2.4 MeV	-0.13
7 MeV		$^{63}\text{Cu}(\text{n,inl})$	13 MeV	-0.35
7 MeV		$^{63}\text{Cu}(\text{n,2n})$	20 MeV	-0.13
7 MeV		$^{63}\text{Cu}(\text{n,el})$	7 MeV	0.17
7 MeV		$^{65}\text{Cu}(\text{n,inl})$	14 MeV	0.01
7 MeV		$^{65}\text{Cu}(\text{n,2n})$	11 MeV	0.01
7 MeV		$^{65}\text{Cu}(\text{n,el})$	10 MeV	0.03
7 MeV		$^{65}\text{Cu}(\text{n,}\gamma)$	2 MeV	0.00

As expected, only a few reactions are correlated with the Oktavian neutron leakage benchmark. An example of correlation between the inelastic cross section of ^{63}Cu and the neutron leakage is presented in Fig. 42. Fig. 42 is an extension of Table XV for the $^{63}\text{Cu}(\text{n,inl})$ reaction at different incident neutron energies. This correlation plot

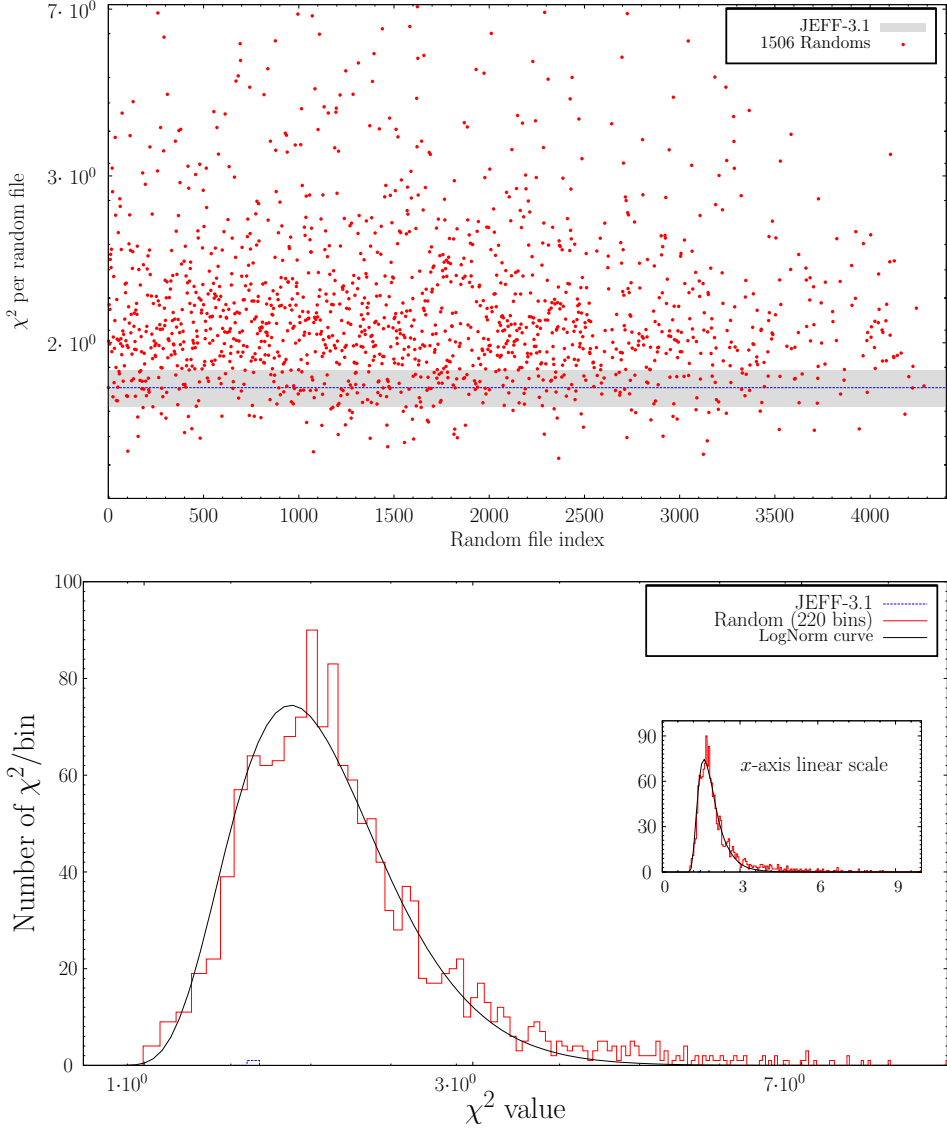


FIG. 38: Top: χ^2 values as defined in Eq. (201) for random $^{63,65}\text{Cu}$ files (dots), compared to χ^2 for the JEFF-3.1 library (band). Bottom: χ^2 values for each random $^{63,65}\text{Cu}$ files per bin, compared to χ^2 values for JEFF-3.1. This figure is the projection on the y -axis of the top part. Note that the x -axis for the large plot is in log scale.

indicates which part of the inelastic cross section of ^{63}Cu should be changed in order to adjust the neutron leakage of the Cu Oktavian. Of course this correlation plot is not unique: it is a reflection of the method used to obtain the ^{63}Cu random files. For instance, the negative correlation for E_{in} below 4 MeV and the positive correlation for E_{in} above 12 MeV come from the theoretical models within TALYS (it has already been noticed that there exists an anticorrelation for the inelastic cross section between its low and high energy parts). Based on this approach,

other type of correlations can be easily extracted:

- Nuclear data vs. neutron or gamma leakage: Fig. 42 can be reproduced for any kind of nuclear data: cross sections, emission spectra, neutron/gamma multiplicity and others.
- Nuclear data vs. criticality benchmarks: as for the previous case, similar studies can be done for criticality benchmarks. In practice, copper is not a good example to obtain correlation plots simply

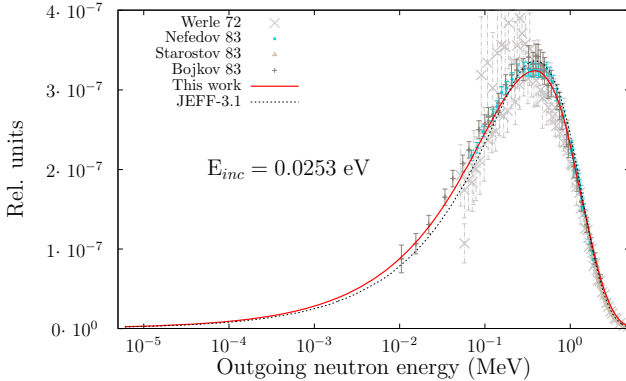


FIG. 39: Comparison of the measured and calculated ^{239}Pu fission neutron spectrum at the thermal incident neutron energy.

TABLE XVI: Correlation factors between different quantities, obtained from random nuclear data.

random nucl. data	Quantity 1	Quantity 2	correlation
H in H ₂ O scatt.	hst32-1	hst42-3	-0.01
H in H ₂ O scatt.	hst32-1	hst42-6	0.60
H in H ₂ O scatt.	hst42-1	lct7-4	-0.71
$^{239}\text{Pu} \bar{\nu}$	mcf1	mcf2	0.68
$^{239}\text{Pu} \bar{\nu}$	pst3-1	mcf2	-0.13
^{16}O	hst37-6	lct17-14	0.33
^{16}O	hmf78-2	lct17-14	0.16
^1H	hst37-6	lct17-14	0.01
^1H	hmf78-2	lct17-14	0.15

because copper does not have a large effect on criticality benchmarks. But this type of study is fully relevant for ^{238}U , ^{235}U or ^{239}Pu .

- Neutron or gamma leakage vs. criticality benchmarks: this type of correlation, never presented yet, can be of importance for important material like iron or light materials (carbon).
- Criticality benchmarks vs. criticality benchmarks: this type of correlation can be of importance for nuclear data adjustment, and general studies of criticality benchmarks. It is quite common in the ICS-BEP community that benchmark evaluators provide an educated guess on the correlations existing between benchmarks of the same type (for instance between two identical systems where the thickness of the reflector was changed). Studies as presented here for copper can be done for other important materials, providing correlation between criticality benchmarks for a given isotope. To obtain a unique

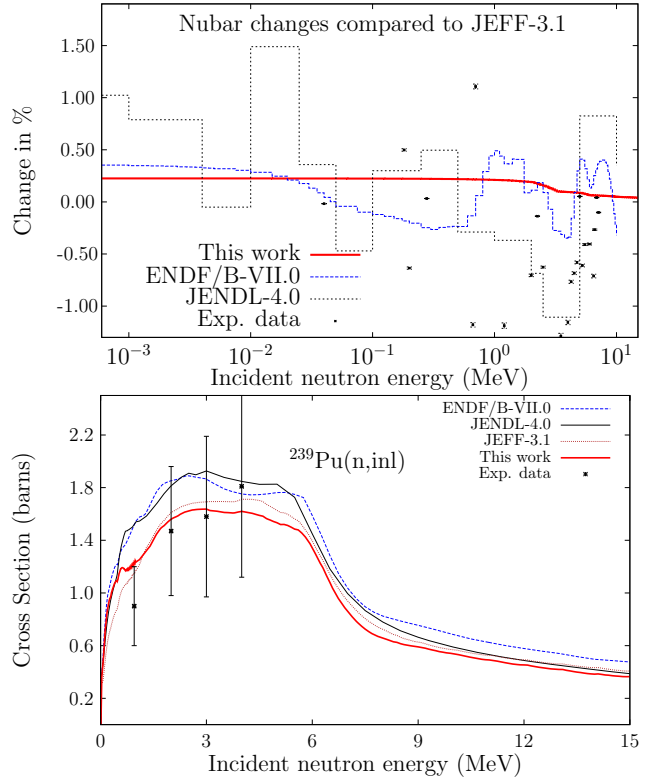


FIG. 40: Top: Changes from JEFF-3.1 in prompt $\bar{\nu}$ for ^{239}Pu (in %). At lower neutron energy, the ratio to JEFF-3.1 is constant and equal to 0.227 %. Bottom: Inelastic cross section for ^{239}Pu from this work and other libraries.

correlation due to all nuclear data, not only a single isotope can be varied, but all relevant isotopes.

- Neutron leakage vs. neutron leakage.
- Neutron leakage vs. gamma leakage.

In the case of ^{239}Pu , similar correlation vectors can be calculated between criticality benchmarks, due to the variations of a given nuclear data quantities. For the same benchmarks, different correlations can be found if different nuclear data quantities are considered. Examples are presented in Tables XVII and XVIII.

Similarly, it is possible to obtain the correlation factors (proportional to the sensitivity factors) by randomly changing a cross section as a function of the neutron energy. In the case of ^{56}Fe and the pmi2 benchmark (see Table VII for the explanation of "pmi"), the resonance parameters and the capture cross section in the fast neutron range were randomly varied and grouped capture cross sections were extracted. Only part of the capture cross section of ^{56}Fe is importance for the pmi2 benchmark. But using the random resonance parameters and

TABLE XVII: Correlation between selected benchmarks due to ^{239}Pu fission neutron spectrum (all incident and outgoing energies).

	pmf1	pmf2	pmf5	pmf6	pmf8	pmf12	pci1	pmi2	pmm1-1	mcf1	pst1-1	pst2-1
pmf1	1	0.95	0.92	0.94	0.95	0.90	0.04	-0.19	-0.22	0.46	0.02	0.02
pmf2		1	0.90	0.93	0.94	0.89	0.03	-0.18	-0.22	0.47	0.02	0.02
pmf5			1	0.92	0.93	0.89	0.02	-0.21	-0.22	0.51	0.03	0.03
pmf6				1	0.97	0.95	0.06	-0.25	-0.28	0.62	0.01	0.01
pmf8					1	0.94	0.05	-0.24	-0.26	0.57	0.01	0.01
pmf12						1	0.06	-0.25	-0.28	0.63	0.01	0.01
pci1							1	-0.63	-0.83	0.54	-0.91	-0.91
pmi2								1	0.72	-0.62	0.67	0.67
pmm1-1									1	-0.76	0.90	0.89
mcf1										1	-0.52	-0.52
pst1-1											1	0.99
pst2-1												1

TABLE XVIII: Correlation between the same benchmarks (see Table XVII), but due to $^{239}\text{Pu}(n,\text{inl})$.

	pmf1	pmf2	pmf5	pmf6	pmf8	pmf12	pci1	pmi2	pmm1-1	mcf1	pst1-1	pst2-1
pmf1	1	0.84	0.77	0.76	0.87	0.56	0.02	0.11	0.07	-0.07	0.01	-0.04
pmf2		1	0.72	0.69	0.78	0.49	0.04	0.12	0.07	-0.09	0.05	0.00
pmf5			1	0.62	0.73	0.44	0.01	0.08	0.02	-0.04	0.01	-0.02
pmf6				1	0.72	0.43	-0.04	0.07	0.06	-0.07	0.03	0.01
pmf8					1	0.54	0.01	0.14	0.09	-0.03	0.03	-0.02
pmf12						1	0.08	0.08	0.04	-0.03	0.05	0.02
pci1							1	0.03	0.01	-0.01	-0.06	-0.03
pmi2								1	-0.07	-0.02	0.01	-0.04
pmm1-1									1	-0.02	0.02	-0.04
mcf1										1	-0.07	0.08
pst1-1											1	0.09
pst2-1												1

the random k_{eff} values with Eq. (203), it is possible to extract the correlation between k_{eff} and the (n,γ) cross section in a given energy range, as presented in the top of Fig. VI F. The obtained correlation is proportional to the sensitivity used in perturbation methods.

The Monte Carlo approach of producing covariances and performing adjustment have a lot of ramifications. With the possibility to calculate correlations (proportional to sensitivities) between many different quantities, it answers the needs of traditional reactor physics studies and goes beyond. One of the only drawbacks of this method is the required time to obtain adjusted data and correlation matrices, but this is only computer time, which is considerably more abundant than human time.

F. Faster TMC

It can be argued that using TMC with a Monte Carlo code is applying a Monte Carlo method twice. Once with random nuclear data, and once with random transported particles. As presented in Ref. [3], the TMC method is highly time consuming because of the necessity to obtain a small $\sigma_{\text{statistics}}$ value used in Eq. (198). The $\sigma_{\text{statistics}}$ value is directly derived from the statistical uncertainties provided by the Monte Carlo code.

We can imagine that the “ultimate” uncertainty propagation tool can be achieved by merging both a Monte Carlo transport and a nuclear reaction code. At the moment, Monte Carlo transport codes are reading once and for all a nuclear data library containing all necessary information (cross sections and other). One could envision that for each new emitted particle from the source, a new nuclear data library is generated by using a nu-

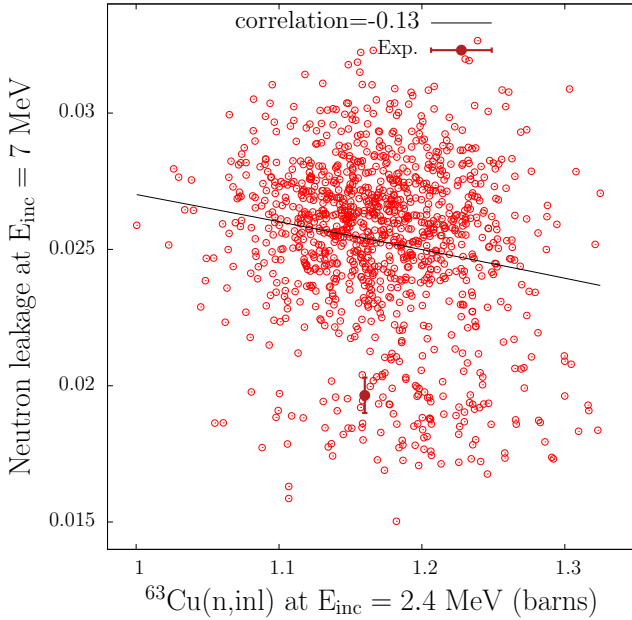


FIG. 41: Oktavian neutron leakage at $E_{\text{out}} = 7 \text{ MeV}$ as a function of the inelastic cross section of ^{63}Cu at $E_{\text{in}} = 2.4 \text{ MeV}$ for a thousand calculation with random copper files. The line approximates the data with a “natural smoothing spline” and the slope is the correlation between data.

clear reaction code. This would of course slow down the performance of the transport code, but a different (reactor) parameter would be obtained for each single particle emitted from the source (such as neutrons), not only due to the random particle, but also due to the random nuclear data. Another possibility would be to directly include random nuclear data at each new particle interaction, *i.e.* to hardwire the cross section generator. Then, two calculations, one with random nuclear data and one without, would provide the effect due to nuclear data.

This solution would be the most practical one for the end user, because it would hide the random nuclear data inside the transport code and relegate them at the same level as random source particles. In a simulation time very close to the present one (theoretically just twice larger), a parameter could be provided with their uncertainties (due to nuclear data, or if other quantities are varied, due to any input parameter). This approach is nevertheless not suitable for the time being with existing Monte Carlo transport codes because of technical burdens and slowness of the nuclear reaction codes (necessary to produce random nuclear data).

Starting from these observations, other solutions are however achievable. A first step toward a faster TMC was taken by Zwermann *et al.* as presented in Ref. [173].

In their approach, nuclear data uncertainty can be propagated by performing, instead of n long runs, $2 \times n$ individual short runs with two different seeds of the random number generator of the Monte Carlo transport code. This clever approach is easy to apply and is the first development towards speeding up the uncertainty propagation with a Monte Carlo transport code. This method, called “GRS method” in the following is summarized in Table XIX.

Parallel to this approach, we have developed an alternative fast TMC method, also allowing to propagate uncertainties with a Monte Carlo transport code in very short time compared to the TMC method. A summary can be found in Table XIX and the method can be explained as follows. If a single Monte Carlo simulation requires m histories to achieve meaningful results, the uncertainty due to an input parameter (nuclear data, temperature, dimensions,*etc*) with n random occurrences can be obtained by repeating the same calculation in two series:

1. Series 1

- (a) performing n calculations,
- (b) with m/n histories,
- (c) (randomly) changing each time the quantity of interest ND_i ($i = 1$ to n),
- (d) using a random seed s_i for the transport random number generator for each of the n runs.

2. Series 2

- (a) performing n calculations,
- (b) with m/n histories,
- (c) without changing each time the quantity of interest,
- (d) using a random seed s'_i (different from the first series) for each of the n new runs.

From the first series of calculation, an average quantity of interest is obtained with its standard deviation ($\bar{k} \pm \sigma_1$)

$$\begin{cases} \bar{k} = \frac{1}{N} \sum_{i=1}^N k_i \\ \sigma_1^2 = \frac{1}{N} \sum_{i=1}^N (k_i - \bar{k})^2, \end{cases} \quad (204)$$

different from the ones obtained from the second series of calculations ($\bar{k}' \pm \sigma_2$). The first series includes the variations of (a) random numbers in the Monte Carlo transport (due to the changing seed s_i) and (b) the random data to propagate, whereas the second series includes only the variations of random numbers in the Monte Carlo transport. Similar to Eq. (198), the uncertainty

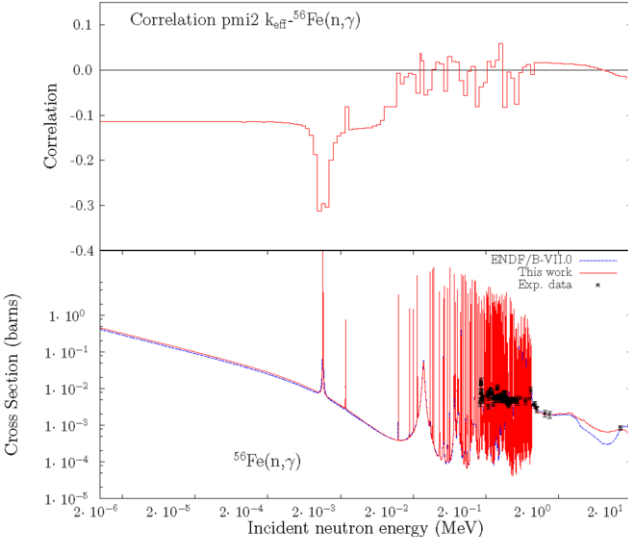
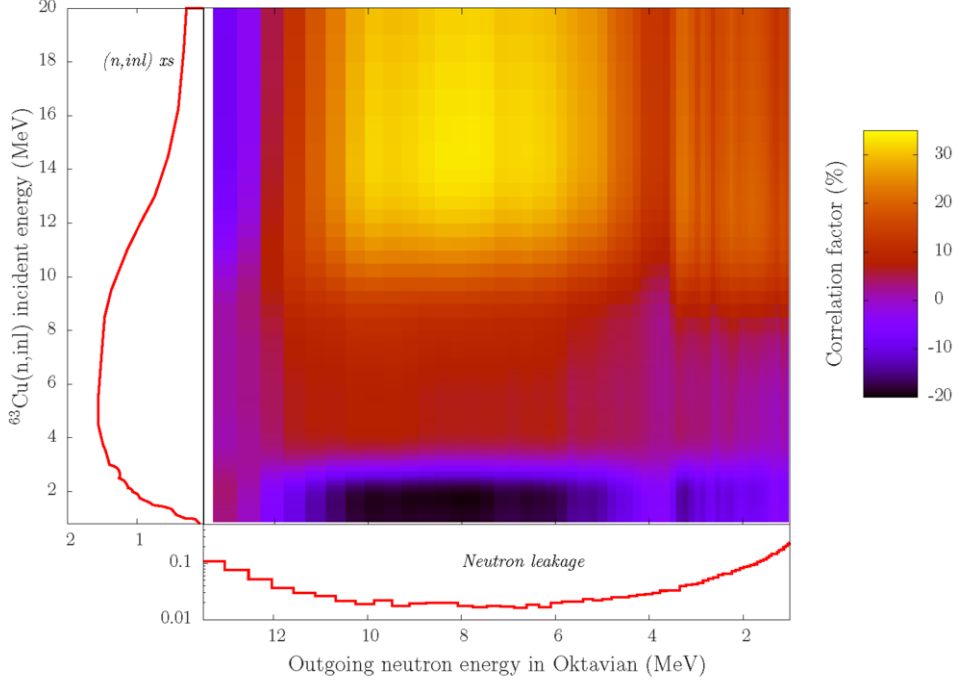


FIG. 43: Top: Correlation between the ^{56}Fe capture cross section and the k_{eff} of the pmi2 benchmark. Bottom: Capture cross sections for ^{56}Fe from this work and other libraries.

due to the varied quantity (such as nuclear data) can be obtained by

$$\sigma_{\text{series } 1}^2 = \sigma_{\text{series } 2}^2 + \sigma_{\text{nuclear data.}}^2. \quad (205)$$

The main advantage of this approach is the gain of calculation time compared to the normal TMC (a factor $n/2$, n being the number of random runs), being theoretically twice a “regular” Monte Carlo transport calculation time (by “regular” it is meant the needed time to obtain significant results in a Monte Carlo transport calculation). We have studied results for three methods: TMC, fast TMC and the GRS method for criticality-safety systems, showing the different performance of the fast methods compared to the slower one.

To test the performance of the fast uncertainty propagation methods, these results are compared to the ones from the regular TMC, the last considered as the most exact answer. The comparisons of calculated uncertainties can be easily done, since the same transport and depletion codes are used, as well as the same random nuclear data. Two types of calculations are realized: with criticality-safety benchmarks (k_{eff} calculations) from the ICSBEP collection ([140]) and with a simple model of a pin-cell burn-up ([132]).

In the case of criticality-safety benchmarks, k_{eff} is calculated, together with the uncertainties due to statistics and the random data. The random nuclear data (in the ENDF-6 format, read as ACE files by MCNP) for six isotopes are used: $^{239,240,241}\text{Pu}$, $^{235,238}\text{U}$ and ^{56}Fe , taken from the TENDL-2012 library. This gives the flexibility to investigate small uncertainties (less than 100 pcm) to large ones (above 1000 pcm) by selecting a given bench-

TABLE XIX: Comparison of computational effort of normal and fast Total Monte Carlo.

TMC

	neutron histories	running time	seed s ₀	Nuclear data ND ₁	Observed k ₁
run 1	m	T	s ₀	ND ₁	k ₁
run 2	m	T	s ₀	ND ₂	k ₂
:	:		⋮		⋮
run n	m	T	s ₀	ND _n	k _n
Total	m	nT			$\bar{k} \pm \sigma_1$
Method				$\sigma_1^2 = \sigma_{\text{statistics}}^2 + \sigma_{\text{nucl.data}}^2$	

Fast TMC

	neutron histories	running time	seed s ₀	Nuclear data ND ₁	Observed k ₁
run 1	m/n	T/n	s ₁	ND ₁	k ₁
run 2	m/n	T/n	s ₂	ND ₂	k ₂
:	:		⋮		⋮
run n	m/n	T/n	s _n	ND _n	k _n
subTotal					$k^* \pm \sigma_1$
run $n+1$	m/n	T/n	s' ₁	-	k' ₁
run $n+2$	m/n	T/n	s' ₂	-	k' ₂
:	:		⋮		⋮
run $2n$	m/n	T/n	s' _n	-	k' _n
subTotal					$k' \pm \sigma_2$
Total	$2 \times m$	$2T$			σ_1, σ_2
Method				$\sigma_1^2 = \sigma_2^2 + \sigma_{\text{nucl.data}}^2$	

mark in combination with random nuclear data for selected isotopes. Results are presented in Fig. 44.

In this figure, the k_{eff} uncertainties from the fast methods (fast TMC and the GRS method) are plotted as a function of the "normal" TMC method. The considered benchmarks are all fast and intermediate, allowing reasonable calculation time (less than one hour for a single calculation, with 30 to 60 pcm statistical uncertainties with 10^6 neutrons).

If the fast methods would yield the same answer as the "normal" TMC, all Δk_{eff} values could be represented on a single $y = x$ line. It can be seen that the results are very close to the $y = x$ line for both the fast TMC and GRS methods. Significant deviations start to be noticeable for small Δk_{eff} values (below 300 pcm), but results still present a good agreement, considering the statistical

uncertainties on the TMC and fast methods (presented as x and y error bars in Fig. 44, respectively). A linear fit through the data gives a slope of 0.98 ± 0.01 for each of the fast methods. These results confirm the good agreement for the GRS method presented in Ref. [173], where the studied systems provided uncertainties from 500 to 1400 pcm.

One should nevertheless notice that for small nuclear data uncertainties, a difference up to a factor 2 can be observed in some cases. This can be of importance for calculations of large systems, such as real nuclear reactors, where the effect of nuclear data on k_{eff} is believed to be rather small (less than 500 pcm).

Similar calculations were performed for spectral indexes, presenting good agreement between methods, given the higher level of uncertainties on these quantities (at the percent level). In the future, the fast methods will be tested by burn-up benchmarks and the results will be presented in a dedicated publication.

Also other accelerations of stochastic methods are welcome for this computer-expensive approach, such as variance reduction techniques, correlated sampling, Metropolis algorithm instead of "brute force" Monte Carlo, and the use of quasi-random numbers instead of pseudo-random numbers. All these more efficient routes to exact uncertainty propagation need to be explored.

VII. CONCLUSIONS

In this paper it has been advocated that nuclear data evaluation can be performed much more efficiently, and can have a much larger impact, if more disciplined working methods are adopted. It is clear that there are limits in our knowledge of nuclear physics:

- It is not possible to measure everything and the precision of those processes we can measure is finite.
- Theoretical nuclear structure and reaction models are not yet at the level where they should be.

While both aspects of nuclear physics require and deserve everlasting support, it is important to let nuclear technology benefit as soon as possible from any progress made. Therefore, it is important to provide *all* nuclear physics knowledge that is available *up to now* in a form ready for applications. In that process, we should aim to maximize completeness, *i.e.* no unnecessary omissions, and quality, *i.e.* no unnecessary approximations, while including a quantitative measure about our knowledge, also known as uncertainty information.

In this paper, we have shown the advantages of breaking with the tradition of incrementally improving data files one by one. Thanks to a system built around

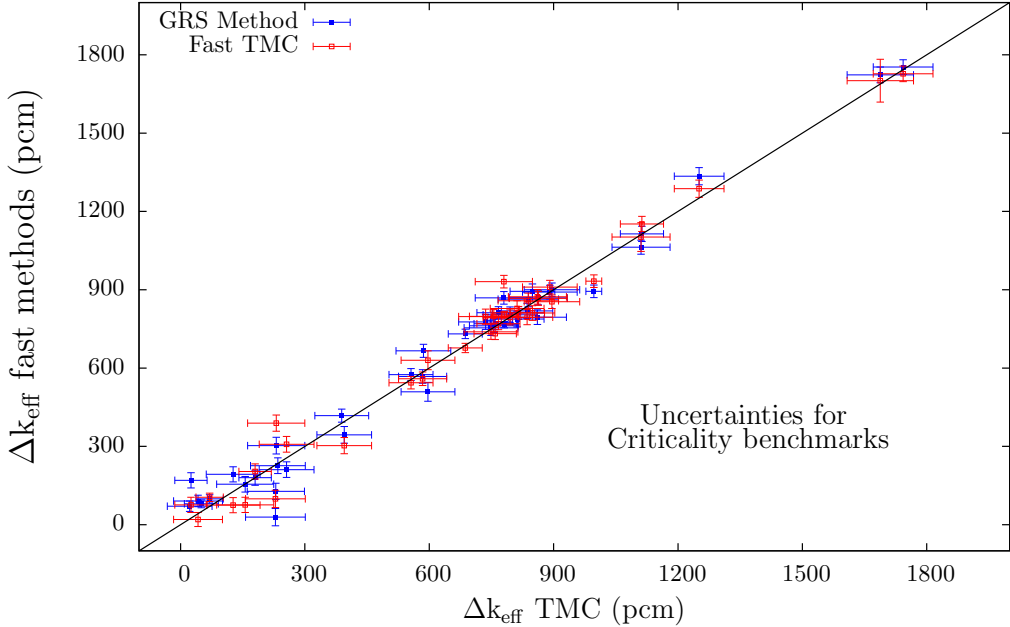


FIG. 44: Top: Ratio of calculated k_{eff} of the fast methods over the “normal” TMC method. The results are presented as function of the impact of the nuclear data. Bottom: Uncertainties of k_{eff} for different criticality-safety benchmarks in pcm. The results of the fast methods are plotted as a function of the results of the “normal” TMC method.

TALYS, a nuclear data library is not made at a certain moment in time for one isotope, or for all isotopes of an element, but rather for the whole nuclide chart at once, whereby all specific evaluation info per nuclide is kept from a previous version, or updated. A large step in efficiency and quality can be accomplished with this approach. In other words, we advocate a system in which nuclear data knowledge is no longer assembled at the level of an ENDF-6 nuclear data library, but rather one level deeper, while the ENDF-6 data library is just one of many possible outlets of this system. The necessary prerequisites for this are:

- An all-in-one nuclear model code, in our case TALYS.
- An internationally maintained Reference Input Parameter Library (RIPL).
- A verified and validated set of resonance parameters and their uncertainties.
- A renormalized and corrected selection of experimental data that could be automatically produced from a raw experimental database (EXFOR).
- For important/measured nuclides: A set of adjusted TALYS input parameters *and* their uncertainties.

- If needed: per nuclide a script with actions to take to produce the nuclear data library (running TALYS, if necessary copying parts of other libraries, direct inclusion of experiment, *etc.*).

The idea is then to store the above compact information in a database, and make sure that ENDF formatting, processing and integral validation become close to trivial. We have described two possible spin-offs of this system.

The TENDL library:

- This is currently the only existing large scale nuclear data library for transport, activation, *etc.* calculations created with one consistent approach.
- The number of data libraries with complete covariance data is unprecedented and allows for large scale testing of covariance data in applied calculations.
- For TENDL, the evaluations for all isotopes are mutually consistent in terms of completeness, global quality and formatting.
- The quality of both the central value data points and the covariance matrices will improve year after year through adjustment of TALYS input parameters per individual nuclide.

Total Monte Carlo:

- An uncertainty propagation method which is exact.
- A method which requires only the “main” software, *i.e.* the standard processing, transport and reactor physics codes.
- Can lead to automatic optimization, *i.e.* search for the best random library using differential and integral data.

We are thus approaching the situation in which the production of a complete ENDF-6 file is standard, quality assured and reproducible. When this is indeed accomplished, the main challenges are:

- Better physics models and parametrization of the nuclear models.
- Selecting and measuring good experimental data.
- Further development of uncertainty methodology.

Any improvement in these fields will be directly visible in the applied result. Note however, that the pure art

of nuclear data evaluation will probably always remain manual. It is just that once we have done it for a nuclide, we do not want to repeat it, so we store it, and we do not want to waste time with ad hoc ENDF-6 editing actions. Next, computer power does the rest.

Acknowledgments

We wish to warmly thank a few of our colleagues who made this work possible: Jean-Christophe Sublet for his deep knowledge of nuclear data processing and for his contagious enthusiasm, Jura Kopecky for his extensive help and vast knowledge as an experienced evaluator, and Steven van der Marck, Stephan Pomp, Robin Forrest, Eric Bauge for their immediate and unconditional belief in our working methodology. Finally, we would like to thank the rest of the nuclear data community for their challenging criticism.

-
- [1] A.J. Koning, S. Hilaire and M.C. Duijvestijn, “TALYS-1.0”, Proceedings of the International Conference on Nuclear Data for Science and Technology, April 22-27, 2007, Nice, France, Editors O. Bersillon, F. Gunsing, E. Bauge, R. Jacqmin, and S. Leray, EDP Sciences, 211 (2008). www.talys.eu.
- [2] A. Koning and D. Rochman, “Modern nuclear data evaluation: Straight from nuclear physics to applications (plenary presentation),” in *proceedings of the International Conference on Nuclear Data for Science and Technology, April 26-30, 2010, Jeju, Korea, Jour. of Korean Phys. Soc.*, **59**, 773 (2011).
- [3] A. Koning and D. Rochman, “Towards sustainable nuclear energy: Putting nuclear physics to work”, *Ann. Nucl. En.* **35**, 2024 (2008).
- [4] M. Uhl and B. Strohmaier, “STAPRE”, IRK-Vienna Report IRK-76/01, 1976, (Upd. 1978).
- [5] C.Y. Fu, ”Approximation of Precompound Effects in Hauser-Feshbach Codes for Calculating Double Differential (n , xn) Cross Sections”, *Nucl. Sci. Eng.* **100**, 61 (1988).
- [6] M. Blann, A.Y. Konobeev, W.B. Wilson, and S.G. Mashnik, ”Manual for Code Alice”, unpublished (2008).
- [7] P.G. Young, E.D. Arthur, M.B. Chadwick, ”Comprehensive Nuclear Model Calculations: Introduction to the Theory and Use of the GNASH Code”, Los Alamos National Laboratory report LA-12343-MS (1992).
- [8] M. Herman, R. Capote, B. Carlson, P. Obložinský, M. Sin, A. Trkov, H. Wienke, and V. Zerkin, ”EMPIRE: Nuclear Reaction Model Code System for Data Evaluation”, *Nucl. Data Sheets* **108**, 2655 (2007).
- [9] M.B. Chadwick, M. Herman, P. Obložinský, M.E. Dunn, Y. Danon, A.C. Kahler, D.L. Smith, B. Pritychenko, G. Arbanas, R. Arcilla, R. Brewer, D.A. Brown, R. Capote, A.D. Carlson, Y.S. Cho, H. Derrien, K. Guber, G.M. Hale, S. Hoblit, S. Holloway, T.D. Johnson, T. Kawano, B.C. Kiedrowski, H. Kim, S. Kuniedaa, N.M. Larson, L. Leal, J.P. Lestone, R.C. Little, E.A. McCutchan, R.E. MacFarlane, M. MacInnes, C.M. Mattoon, R.D. McKnight, S.F. Mughabghab, G.P.A. Nobre, G. Palmiotti, A. Palumbo, M.T. Pigni, V.G. Pronyaev, R.O. Sayer, A.A. Sonzogni, N.C. Summers, P. Talou, I.J. Thompson, A. Trkov, R.L. Vogt, S.C. van der Marck, A. Wallner, M.C. White, D. Wiarda, P.G. Young, ”ENDF/B-VII.1 Nuclear Data for Science and Technology: Cross Sections, Covariances, Fission Product Yields and Decay Data”, *Nuclear Data Sheets* **112**, 2887 (2011).
- [10] K. Shibata, O. Iwamoto, T. Nakagawa, N. Iwamoto, A. Ichihara, S. Kunieda, S. Chiba, K. Furutaka, N. Otuka, T. Ohsawa, T. Murata, H. Matsunobu, A. Zukeran, S. Kamada, and J. Katakura, ”JENDL-4.0: A New Library for Nuclear Science and Engineering”, *J. Nucl. Sci. Technol.* **48**, 1 (2011).
- [11] A.J. Koning, M. Avrigeanu, V. Avrigeanu, P. Batistoni, E. Bauge, M.-M. Be, P. Bem, D. Bernard, O. Bersillon, A. Bidaud, O. Bouland, A. Courcelle, C.J. Dean, P. Dos-Santos-Uzarralde, B. Duchemin, I. Duhamel, M.C. Duijvestijn, E. Dupont, U. Fischer, R.A. Forrest, F. Gunsing, W. Haeck, H. Henriksson, A. Hogenbirk, T.D. Huynh, R. Jacqmin, C. Jouanne, J. Keinert, M.A. Kel-

- lett, I. Kodeli, J. Kopecky, H. Leeb, D. Leichtle, J. Leppanen, O. Litaize, M.J. Lopez-Jimenez, M. Mattes, E. Menapace, R.W. Mills, B. Morillon, C. Mounier, A.L. Nichols, G. Noguere, C. Nordborg, A. Nouri, R.L. Perel, P. Pereslavtsev, R.J. Perry, M. Pescarini, M. Pillon, A.J.M. Plomp, D. Ridikas, P. Romain, Y. Rugama, P. Rullhusen, C. de Saint Jean, A. Santamaria, E. Sartori, K. Seidel, O. Serot, S. Simakov, J.-Ch. Sublet, S. Tagesen, A. Trkov, S.C. van der Marck, H. Vonach, "The JEFF evaluated nuclear data project", Proceedings of the International Conference on Nuclear Data for Science and Technology, April 22-27, 2007, Nice, France, editors O.Bersillon, F.Gunsing, E.Bauge, R.Jacqmin, and S.Leray EDP Sciences, 721 (2008).
- [12] Z.G. Ge, Y.X. Zhuang, T.J. Liu, J.S. Zhang, H.C. Wu, Z.X. Zhao, H.H. Xia, "The Updated Version of Chinese Evaluated Nuclear Data Library (CENDL-3.1)", Proc. International Conference on Nuclear Data for Science and Technology, Jeju Island, Korea, April 26-30, (2010).
- [13] D. Rochman and A. Koning, "How to randomly evaluate nuclear data: a new method applied to ^{239}Pu ", Nucl. Sci. and Eng. **169**, 68 (2011).
- [14] J. Raynal, "Notes on ECIS94", CEA Saclay Report No. CEA-N-2772, (1994).
- [15] A. Koning and J. Delaroche, "Local and global nucleon optical models from 1 keV to 200 MeV", Nucl. Phys. **A 713**, 231 (2003).
- [16] J.M. Quesada, A. Molina, M. Lozano, R. Capote, and J. Raynal, "Analytical expressions for the dispersive contributions to the nucleon-nucleus optical potential", Phys. Rev. **C 67**, 067601 (2003).
- [17] T. Tamura, "Analyses of the Scattering of Nuclear Particles by Collective Nuclei in Terms of the Coupled-Channel Calculation", Rev. Mod. Phys. **37**, 679 (1965).
- [18] J.P. Delaroche, in Proceedings of the International Symposium on "Nuclear Data Evaluation Methodology", ed. C.L. Dunford, October 12-16 1992, Brookhaven, USA, p. 347 (1992).
- [19] N. Olsson, E. Ramström, and B. Trostell, "Neutron elastic and inelastic scattering from Mg, Si, S, Ca, Cr, Fe and Ni AT $E_n = 21.6$ MeV" Nucl. Phys. **A 513**, 205 (1990).
- [20] B.V. Carlson, "Optical Model Calculations with the Code ECIS95", in the Workshop on Nuclear Reaction Data and Nuclear Reactors: Physics, Design and Safety, edited by N. Paver, M. Herman and A. Gandini, March 13 - April 14 2000, Trieste Italy, p. 61 (2001).
- [21] E. Sh Soukhovertskii, S. Chiba, J.-Y. Lee, O. Iwamoto and T. Fukahori, "Global coupled-channel optical potential for nucleon?actinide interaction from 1 keV to 200 MeV" J. Phys. G: Nucl. Part. Phys. **30**, 905 (2004).
- [22] P.P. Guss, R.C. Byrd, C.R. Howell, R.S. Pedroni, G. Tungate, R.L. Walter, and J.P. Delaroche, "Optical model description of the neutron interaction with ^{116}Sn and ^{120}Sn over a wide energy range", Phys. Rev. **C 39**, 405 (1989).
- [23] G.R. Satchler, "Direct Nuclear Reactions", Oxford University Press, New York, 1983.
- [24] P.E. Hodgson, "Nuclear Reactions and Nuclear Structure", Clarendon Press, Oxford, 1971.
- [25] E. Bauge, J.P. Delaroche, M. Girod, "Lane-consistent, semimicroscopic nucleon-nucleus optical model", Phys. Rev. **C 63**, 024607 (2001).
- [26] R. Capote, M. Herman, P. Obložinský, P. Young, S. Goriely, T. Belgya, A. Ignatyuk, A. Koning, S. Hilaire, V. Plujko, M. Avrigeanu, O. Bersillon, M. Chadwick, T. Fukahori, Z. Ge, Y. Han, S. Kailas, J. Kopecky, V. Maslov, G. Reffo, M. Sin, E. Soukhovitskii, and P. Talou, "RIPL- Reference Input Parameter Library for Calculations of Nuclear Reactions and Nuclear Data Evaluations", Nucl. Data Sheets **110**, 3107 (2009).
- [27] F. Maréchal, T. Suomijärvi, Y. Blumenfeld, A. Azhari, E. Bauge, D. Bazin, J.A. Brown, P.D. Cottle, J.P. Delaroche, M. Fauerbach, M. Girod, T. Glassmacher, S.E. Hirzebruch, J.K. Jewel, J.H. Kelley, K.W. Kemper, P.F. Mantica, D.J. Morrissey, L.A. Riley, J.A. Scarpaci, H. Sheit, M. Steiner, "Proton scattering by short lived sulfur isotopes", Phys. Rev. **C 60**, 034615 (1999).
- [28] H. Sheit, F. Maréchal, T. Glassmacher, E. Bauge, Y. Blumenfeld, J.P. Delaroche, M. Girod, R.W. Ibbotson, K.W. Kemper, J. Libert, B. Pritychenko, T. Suomijärvi, "Proton scattering by the unstable neutron-rich isotopes $^{42,44}\text{Ar}$ ", Phys. Rev. **C 63**, 014604 (2000).
- [29] E. Khan, T. Suomijärvi, Y. Blumenfeld, Nguyen Van Giai, N. Alamanos, F. Auger, E. Bauge, D. Beaumel, J.P. Delaroche, P. Delbourgo-Salvador, A. Drouart, S. Fortier, N. Frascaria, A. Gilibert, M. Girod, C. Jouanne, K.W. Kemper, A. Lagoyannis, V. Lapoux, A. Lépine-Szily, I. Lhenry, J. Libert, F. Maréchal, J.M. Maison, A. Mussumara, S. Ottini-Hustache, P. Piatelli, S. Pita, E.C. Pollaco, P. Roussel-Chomaz, D. Santonocito, J.E. Sauvestre, J.A. Scarpaci, T. Zerguerras, "Proton scattering from the unstable nuclei ^{30}S and ^{34}Ar : structural evolution along the sulfur and argon isotopic chains", Nucl. Phys. **A 694**, 103 (2001).
- [30] E. Bauge, J.P. Delaroche, M. Girod, G. Haouat, J. Lachkar, Y. Patin, J. Sigaud, J. Chardine, "Neutron scattering from the $^{155,156,157,158,160}\text{Gd}$ isotopes: Measurements and analyses with a deformed, semimicroscopic optical model", Phys. Rev. **C 61**, 034306 (2000).
- [31] J.P. Jeukenne, A. Lejeune, and C. Mahaux, "Many-body theory of nuclear matter", Phys. Rep. **C 25**, 83 (1976).
- [32] J.P. Jeukenne, A. Lejeune, and C. Mahaux, "Optical-model potential in nuclear matter from Reid's hard core interaction", Phys. Rev. **C 10**, 1391 (1974).
- [33] J.P. Jeukenne, A. Lejeune, and C. Mahaux, "Microscopic calculation of the symmetry and Coulomb components of the complex optical-model potential", Phys. Rev. **C 15**, 10 (1977).
- [34] J.P. Jeukenne, A. Lejeune, and C. Mahaux, "Optical-model potential in finite nuclei from Reid's hard core interaction", Phys. Rev. **C 16**, 80 (1977).
- [35] E. Bauge, J.P. Delaroche, M. Girod, "Semimicroscopic nucleon-nucleus spherical optical model for nuclei with $A > \simeq 40$ at energies up to 200 MeV", Phys. Rev. **C 58**, 1118 (1998).
- [36] R.R. Scheerbaum, "Spin-orbit splitting in nuclei near

- closed shells: (I). Contribution of the two-body spin-orbit interaction”, Nucl. Phys. **A 257**, 77 (1976).
- [37] S. Goriely and J.-P. Delaroche, ”The isovector imaginary neutron potential: A key ingredient for the r-process nucleosynthesis”, Phys. Lett. **B 653**, 178 (2007).
- [38] A. van der Woude, in ”Electric and Magnetic Giant Resonances in Nuclei”, edited by J. Speth (World Scientific, Singapore), p. 99-232 (1991).
- [39] C. Kalbach, ”Surface and collective effects in preequilibrium reactions”, Phys. Rev. **C 62**, 44608 (2000).
- [40] S. Watanabe, ”High energy scattering of deuterons by complex nuclei”, Nucl. Phys. **8**, 484 (1958).
- [41] D.G. Madland, in ”Proceedings of a Specialists’ Meeting on preequilibrium nuclear reactions”, Semmering, Austria, February 10-12, 103 (1988).
- [42] W.W. Daehnick, J.D. Childs, Z. Vrcelj, ”Global optical model potential for elastic deuteron scattering from 12 to 90 MeV”, Phys. Rev. **C 21**, 2253 (1980).
- [43] J. Bojowald et al, ”Elastic deuteron scattering and optical model parameters at energies up to 100 MeV”, Phys. Rev. **C 38**, 1153 (1988).
- [44] Y. Han, Y. Shi and Q. Shen, ”Deuteron global optical model potential for energies up to 200 MeV”, Phys. Rev. **C 74**, 044615 (2006).
- [45] Haixia An and Chonghai Cai, ”Global deuteron optical model potential for the energy range up to 183 MeV”, Phys. Rev. **C 73**, 054605 (2006).
- [46] P. Demetriou, C. Gramo and S. Goriely, ”Improved global α -optical model potentials at low energies”, Nucl. Phys. **A 707**, 253 (2002).
- [47] A. Koning, S. Hilaire, and S. Goriely, ”Global and local level density models”, Nucl. Phys. **A 810**, 13, (2008).
- [48] S. Goriely, S. Hilaire and A.J. Koning, ”Improved microscopic nuclear level densities within the Hartree-Fock-Bogoliubov plus combinatorial method”, Phys. Rev. **C 78**, 064307 (2008).
- [49] A. Ignatyuk, M. Itkis, V. Okolovich, G. Smirenkin, and A. Tishin, ”Anomalous Influence of the Angular Momentum on the Fission of Light Nuclei by Protons and α Particles”, Sov. Jour. Nucl. Phys. **21**, 255, (1975).
- [50] W. Myers and W. Swiatecki, ”Nuclear masses and deformations”, Nucl. Phys. **81**, 1 (1966).
- [51] A.V. Ignatyuk, K.K. Istekov, and G.N. Smirenkin, ”The Role of Collective Effects in the Systematics of Nuclear Level Densities”, Sov. Jour. Nucl. Phys. **29**, 450 (1979).
- [52] A.V. Ignatyuk, J.L. Weil, S. Raman, and S. Kahane, ”Density of discrete levels in ^{116}Sn ”, Phys. Rev. **C 47**, 1504 (1993).
- [53] O.T. Grudzhevich, A.V. Ignatyuk, V.I. Plyaskin, A.V. Zelenetsky, in Proc. Nuclear Data for Science and Technology (Mito, JAERI), p. 187 (1988).
- [54] A.S. Iljinov, M.V. Mebel, N. Bianchi, E. De Sanctis, C. Guaraldo, V. Lucherini, V. Muccifora, E. Polli, A.R. Reolon, and P. Rossi, ”Phenomenological statistical analysis of level densities, decay widths and lifetimes of excited nuclei”, Nucl. Phys. **A 543**, 517 (1992).
- [55] A.R. Junghans, M. de Jong, H.-G. Clerc, A.V. Ignatyuk, G.A. Kudyaev, and K.-H. Schmidt, ”Projectile-fragment yields as a probe for the collective enhancement in the nuclear level density”, Nucl. Phys. **A 629**, 635 (1998).
- [56] G. Hansen and A.S. Jensen, ”Energy dependence of the rotational enhancement factor in the level density”, Nucl. Phys. **A 406**, 236 (1983).
- [57] S. Goriely, F. Tondeur, J.M. Pearson, ”A Hartree-Fock Nuclear Mass Table”, Atom. Data Nucl. Data Tables **77**, 311 (2001).
- [58] D.M. Brink, ”Individual particle and collective aspects of the nuclear photoeffect”, Nucl. Phys. **4**, 215 (1957); P. Axel, ”Electric Dipole Ground-State Transition Width Strength Function and 7-Mev Photon Interactions”, Phys. Rev. **126**, 671 (1962).
- [59] J. Kopecky and M. Uhl, ”Test of Gamma-Ray Strength Functions in Nuclear Reaction Model Calculations”, Phys. Rev. **C 41**, 1941 (1990).
- [60] J. Kopecky, M. Uhl and R.E. Chrien, ”Radiative strength in the compound nucleus ^{157}Gd ”, Phys. Rev. **C 47**, 312 (1993).
- [61] D.G. Gardner, in ”Neutron Radiative Capture”, OECD/NEA Series on Neutron Physics and Nuclear Data in Science and Technology, eds. A. Michaudon et al., p. 62 (1984).
- [62] J. Kopecky, private communication, (2003).
- [63] M.B. Chadwick, P. Obložinský, P.E. Hodgson, and G. Reffo, ”Pauli-blocking in the quasideuteron model of photoabsorption”, Phys. Rev. **C 44**, 814 (1991); Handbook on ”Photonuclear data for applications: Cross sections and spectra”, IAEA-TECDOC-1178 (2000).
- [64] S. Hilaire, Ch. Lagrange, and A.J. Koning, ”Comparisons between various width fluctuation correction factors for compound nucleus reactions”, Ann. Phys. **306**, 209 (2003).
- [65] E.V. Gaï, A.V. Ignatyuk, N.S. Rabotnov, G.N. Smirenkin, 1969. *Physics and Chemistry of Fission*, IAEA, Vienna, p. 337.
- [66] A. Mamdouh, J.M. Pearson, M. Rayet and F. Tondeur, ”Fission barriers of neutron-rich and superheavy nuclei calculated with the ETFSI method”, Nucl. Phys. **A 679**, 337 (2001).
- [67] A. J. Sierk, ”Macroscopic model of rotating nuclei”, Phys. Rev. **C 33**, 2039 (1986).
- [68] S. Cohen, F. Plasil, and W. J. Swiatecki, ”Equilibrium Configurations of Rotating Charged or Gravitating Liquid Masses with Surface Tensor. II.”, Ann. of Phys. **82**, 557 (1974).
- [69] M. Sin, R. Capote and A. Ventura, ”Fission of light actinides: $^{232}\text{Th}(\text{n},\text{f})$ and $^{231}\text{Pa}(\text{n},\text{f})$ reactions”, Phys. Rev. **C 74**, 014608 (2006).
- [70] A. D’Arrigo *et al.*, ”Semi-Empirical Determination of the Shell Correction Temperature and Spin Dependence by Means of Nuclear Fission”, Jour. Phys. **G 20**, 365 (1994).
- [71] M. Ernebjerg and M. Herman, ”Assessment of approximate methods for width fluctuation corrections”, *Proceedings of the International Conference on Nuclear Data for Science and Technology - ND2004*, AIP vol. 769, eds. R.C. Haight, M.B. Chadwick, T. Kawano, and P. Talou, Sep. 26 - Oct. 1, 2004, Santa Fe, USA, p. 1233

- (2005).
- [72] P.A. Moldauer, "Statistics and the average cross section", Nucl. Phys. **A 344**, 185 (1980).
- [73] A.J. Koning and M.C. Duijvestijn, "A global pre-equilibrium analysis from 7 to 200 MeV based on the optical model potential", Nucl. Phys. **A 744**, 15 (2004).
- [74] C. Kalbach, "Two-component exciton model: Basic formalism away from shell closures", Phys. Rev. **C 33**, 818 (1986).
- [75] J. Dobeš and E. Běták, "Two-Component Exciton Model", Zeit. Phys. **A 310**, 329 (1983).
- [76] C. Kalbach, "Surface effects in the exciton model of preequilibrium nuclear reactions", Phys. Rev. **C 32**, 1157 (1985).
- [77] J.M. Akkermans and H. Gruppelaar, "Analysis of continuum gamma-ray emission in precompound-decay reactions", Phys. Lett. **B 157**, 95 (1985).
- [78] C. Kalbach, "Preequilibrium reactions with complex particle channels", Phys. Rev. **C 71**, 034606 (2005).
- [79] C. Kalbach, private communication, (2007).
- [80] C. Kalbach, "Systematics of continuum angular distributions: Extensions to higher energies", Phys. Rev. **C 37**, 2350 (1988).
- [81] J.M. Akkermans and H. Gruppelaar, "Random-Walk Model of Precompound Decay: Dynamics and multi-particle emission", Z. Phys. **A 300**, 345 (1981)
- [82] M. Blann and H. Vonach, "Global test of modified precompound decay models", Phys. Rev. **C 28**, 1475 (1983)
- [83] E. Gadioli and P.E. Hodgson, "Pre-equilibrium nuclear reactions", Oxford University Press, New York (1992).
- [84] M.B. Chadwick, P.G. Young, D. George, Y. Watanabe, "Multiple preequilibrium emission in Feshbach-Kerman-Koonin analyses", Phys. Rev. **C 50**, 996 (1994).
- [85] G. Audi and A.H. Wapstra, "The Ame2003 atomic mass evaluation: (I). Evaluation of input data, adjustment procedures", Nucl. Phys. **A 729**, 129 (2003).
- [86] S. Goriely and J.M. Pearson, "Skyrme-Hartree-Fock-Bogoliubov Nuclear Mass Formulas: Crossing the 0.6 MeV Accuracy Threshold with Microscopically Deduced Pairing", Phys. Rev. Lett. **102**, 152503 (2009).
- [87] E. Khan, S. Goriely, D. Allard, E. Parizot, T. Suominen, A.J. Koning, S. Hilaire, and M.C. Duijvestijn, "Impact of the giant dipole resonance on the photodisintegration of ultrahigh energy cosmic rays", Astroparticle Phys. **23**, 191 (2005).
- [88] S. Goriely, S. Hilaire and A.J. Koning, Astron. Astrop. Jour. **487**, 767 (2008).
- [89] J.A. Holmes, S.E. Woosley, W.A. Fowler, B.A. Zimmerman, "Tables of thermonuclear-reaction-rate data for neutron-induced reactions on heavy nuclei", At. Data Nucl. Data Tables **18**, 306 (1976).
- [90] D. Smith, "Covariance matrices for nuclear cross sections derived from nuclear model calculations", Tech. Rep. ANL/NMD-159, Argonne National laboratory, (2004).
- [91] D. Rochman, M. Herman, P. Obložinský, S. Mughabghab, M. Pigni, and T. Kawano, "Neutron cross section covariances from thermal energy to 20 MeV", in Proceedings of the International Conference on Nuclear Data for Science and Technology, (Nice, France), p. 265, April 23-27 (2007).
- [92] E. Bauge, S. Hilaire, and P. Dossantos-Uzarralde, "Evaluation of the covariance matrix of neutronic cross sections with the backward-forward Monte Carlo method", in Proceedings of the International Conference on Nuclear Data for Science and Technology, (Nice, France), p. 259, April 23-27 (2007).
- [93] D. Neudecker et al., "Comparison of Covariance Matrices Obtained by Different Methods", Jour. Kor. Phys. Soc. **59**, 1272 (2011).
- [94] H. Henriksson, O. Schwerer, D. Rochman, M. Mikhaylyukova, and N. Otuka, "The art of collecting experimental data internationally: EXFOR, CINDA and the NRDC network", in Proceedings of the International Conference on Nuclear Data for Science and Technology, (Nice, France), p. 197, April 23-27 (2007).
- [95] M. Chadwick, P. Obložinský, M. Herman, N. Greene, R. McKnight, D. Smith, P. Young, R. MacFarlane, G. Hale, S. Frankle, A. Kahler, T. Kawano, R. Little, D. Madland, P. Moller, R. Mosteller, P. Page, P. Talou, H. Trellue, M. White, W. Wilson, R. Arcilla, C. Dunford, S. Mughabghab, B. Pritychenko, D. Rochman, A. Sonzogni, C. Lubitz, T. Trumbull, J. Weinman, D. Brown, D. Cullen, D. Heinrichs, D. McNabb, H. Derrien, M. Dunn, N. Larson, L. Leal, A. Carlson, R. Block, J. Briggs, E. Cheng, H. Huria, M. Zerkle, K. Kozier, A. Courcelle, V. Pronyaev, and S. van der Marck, "ENDF/B-VII.0: Next generation evaluated nuclear data library for nuclear science and technology," Nuclear Data Sheets **107**, 2931 (2006).
- [96] S. Mughabghab, *Atlas of Neutron Resonances: Thermal Cross Sections and Resonance Parameters*. Elsevier, Amsterdam (2006).
- [97] D. Rochman and A. Koning, "Pb and Bi neutron data libraries with full covariance evaluation and improved integral tests," Nucl. Inst. and Meth. **A 589**, 85 (2008).
- [98] P. Talou, "Prompt fission neutrons calculations in the madland-nix model", Tech. Rep. LA-UR-07-8168, Los Alamos National Laboratory, Los Alamos, NM, USA, December 2007.
- [99] D. Madland and J. Nix, "New Calculation of Prompt Fission Neutron Spectra and Average Prompt Neutron Multiplicities", Nucl. Sci. and Eng. **81**, 213 (1982).
- [100] A. Wahl, "Systematics of fission-product yields", Tech. Rep. LA-13928, Los Alamos National Laboratory, Los Alamos, NM, USA, May (2002).
- [101] A. Koning and D. Rochman, "TENDL-2011: Consistent talys-based evaluated nuclear data library including covariance data", NRG Petten, the Netherlands, Tech. Rep. (2011), www.talys.eu/tendl-2011.
- [102] J. Kopecky, M. Delfini, H. van der kamp, and D. Nierop, "Revisions and extensions of neutron capture cross sections in the european activation file EAF-3," Tech. Rep. ECN-C-952-051, ECN, Petten, the Netherlands, July (1992).
- [103] J. Kopecky and D. Nierop, "The european activation file EAF-4, summary documentation", Tech. Rep.

- ECN-C-95-075, ECN, Petten, the Netherlands, December (1995).
- [104] R. Brissenden and C. Durston, "The calculation of neutron spectra in the doppler region", Tech. Rep. ANL-7050, Argonne National Laboratory, (1965).
- [105] J. Sublet, P. Ribon, and M. Coste-Delcaux, "CALENDF-2010: User manual", Tech. Rep. CEA-R-6277, Commissariat à l'Energie Atomique, Saclay, France, (2011).
- [106] P. Ribon, "The resonance self-shielding calculation with regularized random ladders", Annals of Nucl. En. **13**, 209, (1986).
- [107] A.J. Koning, M.C. Duijvestijn, S.C. van der Marck, R. Klein Meulekamp, A. Hogenbirk, "New nuclear data evaluations for Ca, Sc, Fe, Ge, Pb, and Bi isotopes", Proceedings of the International Conference on Nuclear Data for Science and Technology - ND2004, AIP vol. 769, eds. R.C. Haight, M.B. Chadwick, T. Kawano, and P. Talou, Sep. 26 - Oct. 1, 2004, Santa Fe, USA, p. 422 (2005).
- [108] Y. Watanabe et al. "Nuclear data evaluations for JENDL high-energy file", Proceedings of the International Conference on Nuclear Data for Science and Technology - ND2004, AIP vol. 769, eds. R.C. Haight, M.B. Chadwick, T. Kawano, and P. Talou, Sep. 26 - Oct. 1, 2004, Santa Fe, USA, p. 326 (2005).
- [109] A. Yu. Konobeyev, U. Fischer, A.J. Koning, H. Leeb, S. Leray and Y. Yariv, "What can we expect from the use of nuclear models implemented in MCNPX at projectile energies below 150 MeV- Detailed comparison with experimental data", Proceedings of the International Conference on Nuclear Data for Science and Technology, April 26-30, 2010, Jeju, Korea, Jour. Kor. Phys. Soc. **59**, 927 (2011).
- [110] F. Wrobel, "Nucleon induced recoil ions in microelectronics", in Proceedings of the International Conference on Nuclear Data for Science and Technology, (Nice, France), p. 339, April 23-27 (2007).
- [111] M.B. Chadwick, P.G. Young, S. Chiba, S.C. Frandle, G.M. Hale, G. Hughes, A.J. Koning, R.C. Little, R.E. Macfarlane, R.E. Prael, and L.S. Waters, "Cross-Section Evaluations to 150 MeV for Accelerator-Driven Systems and Implementation in MCNPX", Nucl. Sci. Eng. **131**, 293 (1999).
- [112] A. Trkov, M. Herman and D.A. Brown (ed.), "ENDF-6 formats manual: Data Formats and procedures for the evaluated nuclear data file ENDF/B-VI and ENDF/B-VII", Brookhaven National Laboratory report BNL-90365-2009 Rev. 2 (2011), available at www.nndc.bnl.gov.
- [113] Bob Macfarlane's webpages on the ENDF-6 format: <http://t2.lanl.gov/tour/tourbus.html>.
- [114] D. Rochman, "TAFIS-1.0: Generation of fission yields, nu-bar and covariances", User manual, NRG unpublished (2012).
- [115] D. Rochman, "TARES-1.1: Generation of resonance data and their uncertainties", User manual, NRG unpublished (2012).
- [116] A.J. Koning, "Requirements for an Evaluated Nuclear Data File for Accelerator-Based Transmutation", NEA Data Bank Report NEA/NSC/DOC(93) 6 (1993).
- [117] A.J. Koning and A. Hogenbirk, "High-energy nuclear data files: From ENDF-6 to NJOY to MCNP", NEA Data Bank Report NEA/NSC/DOC(97) 8 (1997).
- [118] A. Trkov, private communication. W evaluation, (2009).
- [119] D. Rochman, "TANES-1.0: Generation of fission neutron spectra and their uncertainties", User manual, NRG unpublished (2012).
- [120] J-Ch Sublet, A.J. Koning, R.A. Forrest, and J Kopecky "The JEFF-3.0/A Neutron Activation File - New Features, Validation and Usage", Proceedings of the International Conference on Nuclear Data for Science and Technology - ND2004, AIP vol. 769, eds. R.C. Haight, M.B. Chadwick, T. Kawano, and P. Talou, Sep. 26 - Oct. 1, 2004, Santa Fe, USA, p. 203 (2005).
- [121] D. Rochman, A. Koning, and S. van der Marck, "Uncertainties for criticality-safety benchmarks and k_{eff} distributions", Ann. Nucl. En. **36**, 810 (2009).
- [122] D. Rochman, A. Koning, and S. van der Marck, "Uncertainties for criticality-safety benchmarks and consequences for nuclear data measurements", in Proceedings of the 4th international workshop on nuclear fission and fission-product spectroscopy, CEA Cadarache, France, 13-16 May 2009, vol. AIP 1175, p. 95 (2009).
- [123] D. Rochman, A. Koning, and S. van der Marck, "Exact nuclear data uncertainty propagation for fusion neutronics calculations", Fus. Eng. Des. **85**, 669, (2010).
- [124] D. Rochman, A. Koning, and S. van der Marck, "Exact nuclear data uncertainty propagation for fusion design," in Proceedings of the International Conference on Nuclear Data for Science and Technology, April 26-30, 2010, Jeju, Korea, Jour. of Korean Phys. Soc. **59**, p. 1386 (2011).
- [125] D. Rochman, A. Koning, D. daCruz, and S. van der Marck, "Nuclear data uncertainty propagation for a sodium fast reactor", in Proceedings of the International Conference on Nuclear Data for Science and Technology, April 26-30, 2010, Jeju, Korea, Jour. of Korean Phys. Soc. **59**, p. 1191 (2011).
- [126] D. Rochman, A. Koning, and D. da Cruz, "Uncertainties for the kalimer sodium fast reactor: void coefficient, k_{eff} , β_{eff} , burn-up and radiotoxicity", Jour. Nucl. Sci. Tech. **48**, 1193 (2011).
- [127] D. Rochman, A. Koning, D. da Cruz, P. Archier, and J. Tommasi, "On the evaluation of ^{23}Na neutron-induced reactions and validations", Nucl. Inst. Meth. **A 612**, 374 (2010).
- [128] C. Gustavsson, S. Pomp, H. Sjostrand, G. Wallin, M. Osterlund, A. Koning, D. Rochman, K. Beijmer, and H. Henriksson, "Massive computation methodology for reactor operation (macro)", in Proceedings of the European Nuclear Conference (ENC 2010), Barcelona, Spain, 30 May - 2 June (2010).
- [129] D. Rochman, A. Koning, S. van der Marck, A. Hogenbirk, and D. van Veen, "Nuclear data uncertainty propagation: Total Monte Carlo vs. covariance (invited presentation)", in Proceedings of the International Conference on Nuclear Data for Science and Technology, April 26-30, 2010, Jeju, Korea, Jour. of Korean Phys. Soc. **59**,

- p. 1236 (2011).
- [130] D. Rochman, A. Koning, S. van der Marck, A. Hogenbirk, and C. Sciolla, "Nuclear data uncertainty propagation: Monte Carlo vs. perturbation", *Ann. Nucl. En.* **38**, 942 (2011).
- [131] D. Rochman, A. Koning, S. van der Marck, A. Hogenbirk, and D. van Veen, "Propagation of nuclear data uncertainty: Exact or with covariances", *Eur. Phys. Jour. Web of Conferences* **8**, 04003 (2010).
- [132] D. Rochman and A. Koning, "Propagation of $^{235,236,238}\text{U}$ and ^{239}Pu nuclear data uncertainties for a typical PWR fuel element", accepted in *Nucl. Technology* (2012).
- [133] J. Briesmeister, "MCNP - a general Monte Carlo n-particle transport code, version 4c", tech. rep. LA-13709-M, Los Alamos National Laboratory, Los Alamos New Mexico, USA (2000).
- [134] J. Leppanen, "PSG2 / serpent - a continuous-energy Monte Carlo reactor physics burnup calculation code", tech. rep., VTT Technical Research Centre of Finland, Finland (2010). <http://montecarlo.vtt.fi>.
- [135] G. Marleau, R. Roy, and A. Hébert, "DRAGON: A collision probability transport code for cell and super-cell calculations", tech. rep., Institut de génie nucléaire, École Polytechnique de Montréal, Montréal, Québec, (1994). Report IGE-157.
- [136] R. McFarlane, "NJOY99 - code system for producing pointwise and multigroup neutron and photon cross sections from endf/b data", Tech. Rep. RSIC PSR-480, Los Alamos National Laboratory, Los Alamos, NM, USA, (2000).
- [137] A.C. Kahler and R.E. MacFarlane, "Methods for Processing ENDF/B-VII with NJOY", *Nuclear Data Sheets* **111**, 2739-2890 (2010).
- [138] T. Takeda, N. Hirokawa, and T. Noda, "Estimation of error propagation in Monte Carlo burnup calculations", *Jour. of Nucl. Sci. and Technol.* **36** 738 (1999).
- [139] D. Rochman and C. Sciolla, "Total Monte Carlo uncertainty propagation applied to the phase i-1 burnup calculation, (a report for the pin-cell physics of tmi-1 pwr unit cell of the oecd/uam working group)", Tech. Rep. to be obtained, Nuclear Research and Consultancy Group (NRG), Petten, The Netherlands, (2012).
- [140] J.B. Bricks. et al., "International handbook of evaluated criticality safety benchmark experiments", Tech. Rep. NEA/NSC/DOC(95)03/I, Nuclear Energy Agency, Paris, France (2004).
- [141] D. Rochman and A. Koning, "Improving the H in H_2O thermal scattering data using the Petten method", accepted in *Nucl. Sci. and Eng.*, April (2012).
- [142] C. de Saint-Jean et al., "Assessment of existing nuclear data adjustment methodologies", Tech. Rep. NEA/NSC/WPEC/DOC(2010)429, Nuclear Energy Agency, Paris, France, (2011).
- [143] D. Rochman and C. Sciolla, "Total Monte Carlo uncertainty propagation applied to the phase i-1 burnup calculation, a report for the pin-cell physics of tmi-1 pwr unit cell of the oecd/uam working group", Tech. Rep. 113696, Nuclear Research and Consultancy Group (NRG), Petten, the Netherlands,
- ftp://ftp.nrg.eu/pub/www/talys/bib_rochman/tmc.nrg.pdf, (2012).
- [144] A. Takahashi, "Integral neutronics experiments at OKTAVIAN", Tech. Rep. OKTAVIAN Report B-83-01, <http://www-nds.iaea.org/fendl2/validation/benchmarks/jaerim94014/oktavian/n-leak/>, (1983).
- [145] I. Kodeli, H. Hunter, and E. Sartori Tech. Rep. Radiation Protection Dosimetry 116 (2005) 558, <http://www-nds.iaea.org/fendl2/validation/benchmarks/jaerim94014/fns-tof>, (2005).
- [146] C. Wong, J. Anderson, P. Brown, L. Hansen, J. Kammerdiener, C. Logan, and B. Pohl, "Livermore pulsed sphere program: Program summary through July 1971", Tech. Rep. UCRL-51144, Rev. 1, Lawrence Livermore National laboratory, (1972).
- [147] K. Ivanov and O. Cabellos, "Benchmark for uncertainty analysis in modelling (UAM) for design, operation and safety analysis of LWRs, volume 1: specification and support data for neutronics cases (phase 1)", Tech. Rep. version 1.0, <http://www.oecd-nea.org/science/wprs/egrsltb/UAM/>, (2011).
- [148] D. Rochman and A. Koning, "Evaluation and adjustment of the neutron-induced reactions of $^{63,65}\text{Cu}$ ", *Nucl. Sci. and Eng.* **170**, 265 (2011).
- [149] R. Forrest, "The European activation system: EASY-2001 overview", Tech. Rep. UKAEA FUS 449, UKAEA, Culham, UK (2001).
- [150] R. Meulekamp and S. van der Marck, "Calculating the Effective Delayed Neutron Fraction with Monte Carlo", *Nucl. Sci. Eng.* **152**, 142 (2006).
- [151] R. Capote and D. Smith, "An investigation of the performance of the Unified Monte Carlo method of neutron cross section data evaluation", *Nucl. Data Sheets* **109**, 2768 (2008).
- [152] R. Capote and D.L. Smith, "Unified Monte Carlo and Mixed Probability Functions", *Journal of the Korean Physical Society* **59**, 1284 (2011).
- [153] A. Hogenbirk, "An easy way to carry out 3d uncertainty analysis", in the Proceedings of the Joint International Topical Meeting on Mathematics and Computation and Supercomputing in Nuclear Applications (M&C +SNA 2007) (I. American Nuclear Society, LaGrange Park, ed.), (2007). Monterey, California, April 15-19, 2007, on CD-ROM.
- [154] A. Hogenbirk, F. Charpin, and S. van der Marck, "A novel method to carry out uncertainty analyses for iter shielding calculations: a useful tool in engineering and design phase", in the Proceedings of the Joint International Conference on Supercomputing in Nuclear Applications and Monte Carlo 2010 (SNA + MC2010), (2010). Hitotsubashi Memorial Hall, Tokyo, Japan, October 17-21.
- [155] Y. O. K. Furuta and S. Kondo, "SUSD: A computer code for cross section sensitivity and uncertainty analysis including secondary neutron energy and angular distributions", tech. rep., University of Tokyo, (1986). report UTNL-R0185, Nucl. Eng. Res. Lab, NEA Data Bank package n. 1151.
- [156] E. Bauge, R. Capote, U. Fisher, M. Herman,

- T. Kawano, I. Kodeli, A. Koning, A. Konobeyev, H. Leeb, D. Neudecker, P. Obložinský, P. Pereslavtsev, M. Pigni, D. Rochman, D. Smith, P. Talou, and A. Trkov, "Covariance data in the fast neutron region", Tech. Rep. WPEC Subgroup 24 final report, OECD/NEA Nuclear Data Bank, Paris, France, (2010).
- [157] R. Capote, D. Smith, and A. Trkov, "Nuclear data evaluation methodology including estimates of covariances", in the proceedings of the EFNUDAT Measurements and models of nuclear reactions workshop, Paris, May 25-27 (2010). Eur. Phys. Jour. **8**, 04001 (2010).
- [158] W. Zwermann, B. Krzykacz-Hausmann, L. Gallner, A. Pautz, and M. Mattes, "Uncertainty analyses with nuclear covariance data in reactor core calculations", in the proceedings of the International Conference on Nuclear Data for Science and Technology, April 26-30, 2010, Jeju, Korea, Jour. of Korean Phys. Soc. **59**, 1256 (2011).
- [159] A. H. O. Buss and J.-C. Neuber, "Nuduna: Nuclear data uncertainty analysis in criticality safety", in the Workshop on Nuclear Data and Uncertainty Quantification, Culham Centre for Fusion Energy, (2012). available at www.ccfef.ac.uk/easy2011/Nduq/talks/O_Buss.pdf.
- [160] W. Wieselquist, A. Vasiliev, and H. Ferroukhi, "Nuclear data uncertainty propagation in a lattice physics code using stochastic sampling", in the proceedings of the PHYSOR-2012 Advances in Reactor Physics conference, Knoxville, TN, April 15-20, (2012).
- [161] W. Zwermann, "Uncertainty propagation for the fuel pin model based on the european sodium-cooled fast reactor", Gesellschaft fuer Anlagen- und Reaktorsicherheit (GRS) mbH Forschungszentrum, Garching, Germany, private communication, (2011).
- [162] M. D. DeHart, M. C. Brady, and C. V. Parks, "OECD/NEA burnup credit calculational criticality benchmark phase 1-b results", Tech. Rep. NSCDOD(96)-06 and ORNL-6901, Oak Ridge National Laboratory, (1996).
- [163] O. Buss, "Comparison of burn-up uncertainties in phase 1b benchmark". AREVA NP GmbH, Offenbach am Main, Germany, private communication, (2011).
- [164] O. Buss, A. Hoefer, J.-Ch. Neuber, "NUDUNA - Nuclear Data Uncertainty Analysis", Nuclear Data Week, Santa Fe, Nov. (2010), Available online:<http://www.nndc.bnl.gov/proceedings/> 2010csew-gusndp/Tuesday/CSEWG/
- [165] O. Buss, A. Hoefer, J.-Ch. Neuber, "NUDUNA - Nuclear Data Uncertainty Analysis", ICNC 2011 Proceedings, Edinburgh, Sept. (2011).
- [166] P. Dossantos-Uzarralde and A. Guittet, "A polynomial chaos approach for nuclear data uncertainties evaluations", Nuclear Data Sheets **109**, 2894 (2008).
- [167] M.M. Williams, Annals of Nucl. Energy, (2012). to be submitted, private communication.
- [168] L. Gilli, "Uncertainty propagation in criticality benchmarks using a non-intrusive polynomial chaos technique". Delft Technical University, private communication, (2012).
- [169] M.M. Williams private communication, (2012).
- [170] S. van der Marck, A. Koning, and D. Rochman, "Photoproduction data for heating calculations", in the proceedings of the International conference on the Physics of Reactors (PHYSOR-2008), Interlaken, Switzerland, September 14-19, (2008).
- [171] M. Abramowitz, I.A. Stegun eds. (1965), Chapter 26 in "Handbook of Mathematical Functions with Formulas, Graphs, and Mathematical Tables", New York: Dover, pp. 940, MR0167642, ISBN 978-0486612720.
- [172] V.M. Maslov and N.A. Tetereva and V.G. Pronyaev and A.B. Kagalenko and K.I. Zolotarev and R. Capote and T. Granier and B. Morillon and F.J. Habsch and J.C. Sublet, " $^{235}\text{U}(\text{n},\text{f})$ $^{233}\text{U}(\text{n},\text{f})$ and $^{239}\text{Pu}(\text{n},\text{f})$ prompt fission neutron spectra", Jour. Korean Phys. Soc. **59**, 1337 (2011).
- [173] W. Zwermann, B. Krzykacz-Hausmann, L. Gallner, A. Pautz, K. Velkov, "Aleatoric and epistemic uncertainties in sampling based nuclear data uncertainty and sensitivity analyses", in the proceedings of the PHYSOR-2012 conference, Knoxville, TN, USA, American Nuclear Society, April 15-20 (2012).